

# **Flax NLRs and the Equilibrium-Switch Model**

by

**Hayden Burdett**

*Thesis  
Submitted to Flinders University  
for the degree of*

**Doctor of Philosophy**  
College of Science and Engineering  
November 2018

---

# Table of Contents

<b>Table of Contents</b>	<b>1</b>
<b>Summary</b>	<b>5</b>
<b>Declaration</b>	<b>7</b>
<b>Acknowledgments</b>	<b>8</b>
<b>Table of Abbreviations</b>	<b>9</b>
<b>Chapter 1 – Introduction to Plant innate Immunity</b>	<b>13</b>
<b>The Plant Innate Immune System</b>	<b>13</b>
Non-Host Resistance (NHR)	13
Pathogen Associated Molecular Patterns (PAMPs)	14
PAMP Recognition Receptors (PRRs)	14
PAMP Triggered Immunity (PTI)	15
Effectors	15
Nucleotide Binding, Leucine Rich Repeat Receptors (NLRs)	16
Effector Triggered Immunity (ETI)	17
<b>Plant NLRs and Effectors</b>	<b>19</b>
NLRs: the artists formerly known as R proteins	19
TIR domain	21
NB-ARC domain	26
LRR domain	34
Effectors	35
<b>NLR/Effector interactions</b>	<b>37</b>
Direct interaction model	37
Indirect interaction model	41
Integrated decoy model	43
<b>NLR regulatory interactions</b>	<b>44</b>
Domain-domain interactions in NLRs	45
<b>Plant NLR domain-domain interactions</b>	<b>49</b>
TIR domain responsible for signalling	49
Some NB-ARC domains can abrogate signalling	50
Some TIR-NB-ARC/CC-NB-ARC proteins are autoactive	50
Interactions between LRR domain and ARC domain are important for inhibition and activation	51
<b>Current Model of NLR induced ETI</b>	<b>52</b>
<b>Aims and Objectives</b>	<b>54</b>
<b>Chapter 2 - Materials &amp; Methods</b>	<b>55</b>
<b>General Procedures</b>	<b>55</b>
Agarose gel electrophoresis	55
Sodium Dodecyl Sulphate-Polyacrylamide Gel Electrophoresis (SDS-PAGE)	55
Western Blot	55

SYPRO® Ruby stain	56
<b><i>Pichia pastoris</i> protocols</b>	<b>56</b>
Mutation and transformation of L6 and L7 constructs into <i>P. pastoris</i>	56
<i>Pichia pastoris</i> transformations	57
<i>Pichia pastoris</i> Test Expression	58
<b>NLR Protein Expression and Purification</b>	<b>58</b>
Expression of NLRs in <i>Pichia pastoris</i>	58
Preparation of Cleared Lysate	59
Immobilised Metal Affinity Chromatography (IMAC)	59
StrepTactin Affinity Chromatography (SAC)	60
<b>NLR ATP and ADP Occupancy Determination</b>	<b>60</b>
Sample Preparation	60
Nucleotide Quantification	61
Protein Quantification using SYPRO® Ruby stain	61
<b>Effector Expression and Purification</b>	<b>61</b>
Plasmids	61
Expression of Effector proteins by autoinduction	62
Preparation of Cleared Lysate and IMAC	62
Cleavage of Histidine Tag and Size exclusion chromatography	62
<b>Surface Plasmon Resonance (SPR)</b>	<b>63</b>
<b>Chapter 3 – Residues in the TIR domain of flax NLRs L6 and L7 influence their nucleotide binding properties</b>	<b>64</b>
<b>Introduction</b>	<b>64</b>
Flax NLR genes	64
L6 and L7	66
<b>Results</b>	<b>70</b>
Test expressions of transformed <i>P. pastoris</i>	72
Purifications of L6, L7 and mutants for Nucleotide binding assays	74
Nucleotide Binding Calculations	76
<b>Discussion</b>	<b>82</b>
Differences in elicitor-dependent HR may be explained by differing nucleotide binding for L6 and L7	82
Amino acids in the $\alpha$ A helix of the TIR domain of L6 and L7 are responsible for differences in elicitor-dependent HR	82
Polymorphic residues within the TIR domains of L6 and L7 are also responsible for differences in the nucleotide binding of the proteins	83
A residue in the Nucleotide Binding domain of L7 promotes autoinhibition?	84
L6 and L7 effector interaction – ADP as a negative regulator?	85
L6 MHV and L7 MHV - autoactive mutations?	87
MHV and the L6/L7 polymorphisms: on again off again	89
How does L6 and L7 nucleotide binding data compare to other nucleotide binding proteins?	90
Inhibited NLRs are ADP bound, active forms of NLRs are ATP bound	91
Some NLRs are capable of ATP hydrolysis, and this may play a role in resetting an active NLR to the inactive state?	93

Presenting the Equilibrium-Switch Model	94
Future work and conclusions	98
<b>Chapter 4 - Improved purification of flax NLRs M, L6 and L7</b>	<b>100</b>
<b>Introduction</b>	<b>100</b>
<b>Methods</b>	<b>101</b>
Constructs	101
Expression and Purification	102
ATP/ADP Assays	102
<b>Results</b>	<b>102</b>
M IMAC purification vs M SAC purification	102
Comparison of purity of M from IMAC, IMAC-SAC and SAC	109
L6 and L7 can also be purified using the SAC method	111
Western blots of M L6 and L7 SAC purified protein	115
ATP/ADP binding of M IMAC and SAC purified protein	117
Purification of other NLRs	121
<b>Discussion</b>	<b>121</b>
SAC purification is an improvement on IMAC purification	121
SAC purification is an improvement on IMAC/SAC tandem purification	124
Purification of other NLRs may require some optimisation	126
Other methods of plant R protein purification focus on domains, and not full-length protein	128
Purification of full-length APAF-1 and NLRC4	129
New possibilities for analysis of more pure NLR protein	131
Conclusion	136
<b>Chapter 5 - Surface plasmon resonance to measure NLR-effector interaction</b>	<b>137</b>
<b>Introduction</b>	<b>137</b>
Surface plasmon resonance (SPR)	137
M and AvrM: Direct interaction in the innate immune pathway	138
AvrM	138
The molecular basis for M/AvrM interaction remains elusive	140
<b>Methods</b>	<b>144</b>
Sensor chip NTA surface preparation	144
Sensor chip SA surface preparation	145
<b>Results</b>	<b>147</b>
AvrM, avrM, EA2 and a3 purification	147
Ni-NTA Immobilisation	151
SA-biotin-trisNTA Immobilisation	154
Ni-NTA AvrM experiments	158
M and AvrM on SA-biotin-trisNTA surface	165
Multi-cycle kinetics for AvrM interaction with M	169
M and avrM Multi-cycle kinetics	173
Single cycle kinetics	177
AvrM and avrM Mutants	180
<b>Discussion</b>	<b>182</b>

M immobilisation method	182
Kinetics of the M/AvrM interaction	186
M/avrM interaction	187
M interaction with AvrM and avrM mutants	187
M complex formation and effector binding?	188
Direct binding not so uncommon?	191
Future work	191
Microscale thermophoresis to measure protein-protein interactions?	192
Conclusions	192
<b>Chapter 6 - General Discussion</b>	<b>194</b>
<b>Equilibrium-Switch Model for plant NLRs</b>	<b>194</b>
Nucleotide exchange and ATP hydrolysis	196
What comes first, effector binding or nucleotide exchange?	196
Complex formation; a plant apoptosome?	197
<b>Small GTPases and third party interactors</b>	<b>198</b>
<b>Still waiting for a structure</b>	<b>198</b>
<b>Direct effector interaction NLRs for robust resistance!</b>	<b>199</b>
<b>Conclusion</b>	<b>199</b>
<b>Chapter 7 - Appendices</b>	<b>200</b>
<b>Appendix 1 – Vector Maps and L6 and L7 Site Directed Mutagenesis Gels</b>	<b>200</b>
Vectors	200
Mutagenesis	201
<b>Appendix 2 – Sample IMAC purification of NLR</b>	<b>208</b>
<b>Appendix 3 – Calculation of Protein Concentration</b>	<b>209</b>
<b>Appendix 4 - Purification of Sr33, a CC-containing NLR from <i>Aegilops tauschii</i> and RUN1, a TIR-containing NLR from <i>Muscadinia rotundifolia</i></b>	<b>211</b>
<b>Appendix 5 - Kinetic models for M/AvrM and M/avrM interactions</b>	<b>213</b>
<b>References</b>	<b>218</b>

## Summary

Plants are susceptible to pests and disease. Unlike animals, each plant cell is required to defend itself against pathogen invasion. A two-tiered innate immune system allows plants to combat pathogens. The role of the first tier is to deter common, non-specialised pathogens from infecting the host, whilst the role of the second tier is to defend against pathogens able to bypass the first, which pathogens achieve by secretion of effector proteins.

Plants can detect and respond to secreted effectors through proteins known as Nucleotide Binding (NB) Leucine-Rich Repeat (LRR) domain Receptors (NLRs). Plant NLRs induce a robust immune response, characterised by localised cell death around the site of infection, known as a hypersensitive response. Despite extensive work, the mechanism by which plant NLRs are regulated, how they perceive effectors, and how they signal a hypersensitive response are still unclear.

These questions can be probed by examination of the full-length plant NLRs *in vitro*, which, to date, has proven difficult. Here, the nucleotide binding of L6 and L7, NLRs from flax purified from *Pichia pastoris*, are reported. Flax NLRs able to induce effector-dependent cell death were found to be bound with low levels of ADP, whilst those that induced a weaker, slower immune response were found to be bound with high levels of ADP. Previous published data demonstrated that other auto-active plant NLRs preferentially bind ATP over ADP. Collectively, these data, combined with the results of *in planta* and yeast-2-hybrid assays on L6, L7 and mutants created by collaborators, suggests an equilibrium-switch model of activation, where a plant NLR cycles between ADP/ATP bound states, only detecting an effector when in an ATP-bound state.

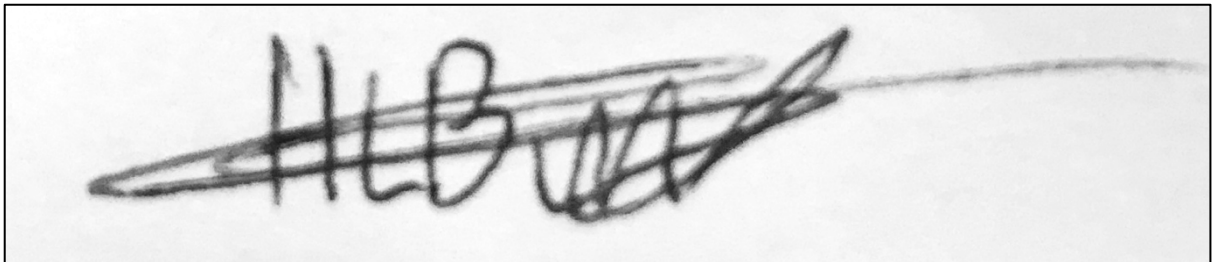
To further interrogate this model NLRs protein of higher purity and yield were required. Modification of existing techniques allowed for increased purity and yields of three flax NLRs. Using StrepTactin Affinity Chromatography, M, L6 and L7 were purified to >90% purity, whilst maintaining yields suitable for both biochemical and biophysical experiments.

Purified M, AvrM and avrM proteins was used in the analysis of the interaction between a full-length NLR and effector *in vitro*, utilising Surface Plasmon Resonance (SPR). The results showed that M interacts weakly with AvrM *in vitro*, but that no interaction was detected between M and avrM. The interaction of M with various gain-of-function and loss-of-function mutants of AvrM and avrM was also investigated, but interaction kinetics were not able to be calculated.

The results presented answer questions about the activation, and interaction with effectors, of flax NLRs. However, how the difference in nucleotide binding of flax NLRs influences their interaction with their cognate effectors remains to be answered. Improved purification of plant NLRs will enable more diverse experiments to be conducted, such as the structural characterisation of full-length plant NLRs, and further analysis of NLR/effector interaction in the presence and absence of nucleotides using SPR. These experiments will be critical if we are to completely unravel the function of these important class of plant proteins.

## Declaration

'I certify that this thesis does not incorporate without acknowledgment any material previously submitted for a degree or diploma in any university; and that to the best of my knowledge and belief it does not contain any material previously published or written by another person except where due reference is made in the text.'

A rectangular box containing a handwritten signature in black ink. The signature is stylized and appears to read 'H. Burdett'.

Hayden Burdett

## Acknowledgments

I would like to thank Peter Anderson for supervising my project, reading many drafts of thesis, posters, presentations, emails and everything else. I think you have been an excellent supervisor, always looking out for my best interests, and being incredibly supportive throughout.

I would like to thank both Emma de Courcy-Ireland and Nick Warnock, who helped me so much throughout my PhD with lab work, new techniques, old protocols, literature and presentations, I would never have been able to finish without you two, thank you so much!

I would also like to thank the members of the Anderson and Soole lab and School of Biology, past and present, including Kathleen Soole, Colin Jenkins, Yuri Shavrukov, My-my Huynh, Motiur Rahman, Crystal Sweetman, Jai Strempe, Dave Kennedy, Alex McDonald, Adam Bentham, Carrie-Anne Lewis, Chevaun Smith, Vajira Wanniarachchi, Lam Nyugen, Georgia Guild, Jason Smith, Chris Waterman, Lette Dametto, Barry Rainbird, Arif Malik and anyone else I have forgotten, you all made the lab a fun place to work!

I would also like to thank Simon Williams, Maud Bernoux, Peter Dodds and Bostjan Kobe for their help as well, for helping with direction and collaboration on manuscripts.

I would like to thank my family and friends for supporting me through the last few years and would like to especially thank my parents for their love and support (I remembered to acknowledge them this time ☺).

Lastly, I'd like to thank Ella, who has been the most important person throughout my entire PhD, without whom I would never have got this far. Always there to support me when things got tough, you are truly the best!

## Table of Abbreviations

<b>Abbreviation</b>	<b>Meaning</b>
<b>AAA+</b>	ATPases Associated with diverse Cellular Activities
<b>AAP</b>	ATPase activating proteins
<b>ADI</b>	Adenine Nucleotide Dissociation Inhibitor
<b>ADP</b>	Adenosine-Diphosphate
<b>AEF</b>	Adenine Nucleotide Exchange Factor
<b>ANOVA</b>	Analysis of variance
<b>APAF-1</b>	Apoptotic Protease Activating Factor 1
<b>ARC</b>	shared between APAF-1, some R proteins and CED-4
<b>ATP</b>	Adenosine-Triphosphate
<b>ATR1</b>	Arabidopsis Thaliana Recognised 1
<b>AtTIR</b>	Arabidopsis thaliana TIR-containing protein
<b>AVR</b>	Avirulence
<b>BED</b>	named after the Drosophila proteins BEAF and DREF
<b>BMGY</b>	Buffered Glycerol-Complex Medium
<b>BMMY</b>	Buffered Methanol-Complex Medium
<b>BSA</b>	Bovine serum albumin
<b>CARD</b>	Caspase Activation and Recruitment Domain
<b>CC</b>	Coiled-Coil
<b>CED-4</b>	Cell Death protein 4
<b>CED-9</b>	Cell Death protein 9
<b>CIEX</b>	Cation Exchange Chromatography
<b>CNL</b>	CC-NB-ARC-LRR
<b>co-IP</b>	Co-immunoprecipitation
<b>CP</b>	Coat protein
<b>Cryo-EM</b>	cryo-Electron Microscopy
<b>CV</b>	Column Volume
<b>DAMP</b>	Damage Associated Molecular Pattern
<b>DARK</b>	Death-associated APAF1-related killer
<b>dATP</b>	Deoxyadenosine triphosphate
<b>DNA</b>	Deoxyribo Nucleic Acid
<b>dNTP</b>	Deoxyribonucleotide-Triphosphate
<b>DTT</b>	Dithiothreitol
<b>EDS1</b>	Enhanced Disease Susceptibility 1
<b>EDTA</b>	Ethylenediaminetetraacetic acid
<b>ETI</b>	Effector-triggered Immunity
<b>FF</b>	Fast Flow
<b>FPLC</b>	Fast protein liquid chromatography
<b>FRET</b>	Fluorescence Resonance Energy Transfer
<b>GAP</b>	GTPase activating proteins

<b>GDI</b>	Guanidine Nucleotide Dissociation Inhibitor
<b>GDP</b>	Guanosine-Diphosphate
<b>GEF</b>	Guanidine Nucleotide Exchange Factor
<b>GFP</b>	Green Fluorescent Protein
<b>GTP</b>	Guanosine-Triphosphate
<b>HABA</b>	2-[4 -hydroxy-benzeneazo]benzoic acid
<b>HD1</b>	Helical Domain 1
<b>HD2</b>	Helical Domain 2
<b>HEPES</b>	4-(2-hydroxyethyl)-1-piperazineethanesulfonic acid
<b>HETHS</b>	HElical Third Domain of STAND
<b>HMA</b>	Heavy-Metal Associated
<b>HP</b>	High Performance
<b>HR</b>	Hypersensitive Response
<b>HSD</b>	Honest Significant Difference
<b>IB</b>	Immunoblot
<b>IMAC</b>	Immobilised Metal Affinity Chromatography
<b>ITC</b>	Isothermal Titration Calorimetry
<b>LHD</b>	Leucine-Histidine-Aspartate
<b>LRR</b>	Leucine-Rich Repeat
<b>MALS</b>	Multi-Angle Light Scattering
<b>MAPK</b>	Mitogen-Activated Protein Kinase
<b>MHD</b>	Methionine-Histidine-Aspartate
<b>MHV</b>	Methionine-Histidine-Valine
<b>MLA</b>	Mildew A locus
<b>MS</b>	Mass Spectrometry
<b>MST</b>	Mircoscale Thermophoersis
<b>mV</b>	milliVolt
<b>MWCO</b>	Molecular Weight Cut-Off
<b>NACHT</b>	NAIP (neuronal apoptosis inhibitor protein), C2TA (MHC class 2 transcription activator), HET-E (incompatibility locus protein from Podospora anserina) and TP1 (telomerase-associated protein)
<b>NAD</b>	NACHT-Associated Domains
<b>NB/NBD</b>	Nucleotide Binding/Nucleotide Binding Domain
<b>NHR</b>	Non-Host Resistance
<b>NLR</b>	NB-LRR Receptor
<b>NLRC4</b>	NLR family CARD domain-containing protein 4
<b>NMR</b>	Nuclear Magnetic Resonance
<b>NOD</b>	Nucleotide Binding -Oligomerisation Domain
<b>NRIP</b>	N receptor-interacting protein 1
<b>NTA</b>	Nitilotriacetic acid
<b>PAD4</b>	PhytoAlexin Deficient 4

<b>PAMP</b>	Pathogen Associated Molecular Pattern
<b>PCR</b>	Polymerase Chain Reaction
<b>PMSF</b>	Phenylmethane Sulfonyl Fluoride
<b>PRR</b>	PAMP Recognition Receptor
<b>PTI</b>	PAMP-triggered Immunity
<b>PVX</b>	Potexvirus Potato virus X
<b>RanGAP2</b>	Ran GTPase-activating protein
<b>RATX1</b>	related to ATX1
<b>RGA</b>	Resistance Gene Analogues
<b>RIN4</b>	RPM1 interacting protein 4
<b>RLK</b>	Receptor-like Kinase
<b>RLP</b>	Receptor-like Protein
<b>RNBS</b>	Resistance Nucleotide Binding Site
<b>ROQ1</b>	Recognition of XopQ 1
<b>ROS</b>	Reactive Oxygen Species
<b>RPM1</b>	Resistance to <i>Pseudomonas syringae</i> pv. <i>maculicola</i> 1
<b>RPP1</b>	Recognition of <i>Peronospora Parasitica</i> 1
<b>RPS2</b>	Resistance to <i>Pseudomonas syringae</i> 2
<b>RPS4</b>	Resistance to <i>Pseudomonas syringae</i> 4
<b>RPS5</b>	Resistance to <i>Pseudomonas syringae</i> 5
<b>RPV1</b>	Resistance to <i>Plasmopara viticola</i>
<b>RRS1</b>	Resistance to <i>Ralstonia solanacearum</i> 1
<b>RU</b>	Response Units
<b>RUN1</b>	Resistance to <i>Uncinula necator</i> 1
<b>SA</b>	StrepAvidin
<b>SAC</b>	StrepTactin Affinity Chromatography
<b>SAG101</b>	Senescence-Associated Carboxylesterase 101
<b>SAXS</b>	Small Angle X-ray Scattering
<b>SDM</b>	Site-directed Mutagenesis
<b>SDS-PAGE</b>	Sodium Dodecyl Sulphate-Polyacrylamide Gel Electrophoresis
<b>SEC</b>	Size Exclusion Chromatography
<b>SNC1</b>	Suppressor of <i>npr1-1</i> , Constitutive 1
<b>SPL6</b>	Squamosa Promoter Binding Protein-Like 6
<b>SPR</b>	Surface Plasmon Resonance
<b>SR</b>	SYPRO Ruby Stain
<b>STAND</b>	Signal Transduction ATPases with Numerous Domains
<b>TAE</b>	Tris Acetate EDTA
<b>TBS-T</b>	Tris-Buffered Saline and Tween 20
<b>TEV</b>	Tobacco etch virus
<b>TIR</b>	Toll/Interleukin-1 Receptor
<b>TNL</b>	TIR-NB-ARC-LRR
<b>UV</b>	Ultraviolet

<b>WHD</b>	Winged Helical Domain
<b>WRKY</b>	Tryptophan-Arginine-Lysine-Tyrosine domain
<b>XopQ</b>	Xanthomonas euvesicatoria type III effector, XopQ
<b>YPD</b>	Yeast extract Peptone Dextrose

# Chapter 1 – Introduction to Plant innate Immunity

## The Plant Innate Immune System

Unlike mammals, plants do not have specialised cells for fighting disease. Consequently, each plant cell needs to be able to detect and respond to pathogenic invaders. Each cell must also differentiate between different classes of invaders; necrotrophs, which kill the host cell and feed off the nutrients; and biotrophs which do not kill the host cell, but rather re-direct nutrients to the pathogen to survive and complete their lifecycle. These two types of pathogens elicit different immune responses and it is important for the plant to be able distinguish them and respond accordingly. Plants must also not waste energy and resources by having constitutively active immune responses; regulation is crucial for longer-term plant survival. So how do plants do all of this? The first layer of the plant immune system is to keep the pathogens out of the host cells.

### Non-Host Resistance (NHR)

NHR prevents non-specialised pathogens from entering plant cells. Most plant cells have cell walls that act as a barrier to pathogen infection. Others combine barriers with the release of antimicrobial compounds to aid in defence. Furthermore, plant leaves combine waxy cuticles, callose deposition to infection sites, and closing of stomata and other entry points, to limit access of the pathogen to nutrient filled host cells. There is no single NHR strategy *per se*, it is a complex passive system of defence, consisting of a combination of barriers and antimicrobials designed to keep a large range on non-specialised pathogens and other organisms at bay. Bettgenhaeuser et al. (2014) provide a comprehensive review into NHR of a variety of plants, against rust pathogens.

Pathogens that have evolved to bypass host-specific defence strategies are termed adapted pathogens (Dodds and Rathjen, 2010). They have evolved in concert with the host plant, continually adapting to continue to subvert the NHR mechanisms in place. To deal with specialised pathogens, plants have, in turn, developed more specialised

defence systems. These specialised defence systems define the plant innate immune system and it is the innate immune system that helps protect against pathogens that can bypass NHR mechanisms. There are two levels of plant innate immunity, PAMP-Triggered-Immunity (PTI) and Effector-Triggered-Immunity (ETI). The plant innate immune system is summarised in Figure 1.1.

### **Pathogen Associated Molecular Patterns (PAMPs)**

To signal immune responses, a plant must first discern whether a pathogen has breached any preformed barriers. There is no sense in signalling defence responses in the absence of pathogens; it is a waste of resources, and thus damaging to the plant. To determine the presence of a pathogen, plants have evolved to detect highly conserved pathogen molecules, without which the pathogen would be unable to survive or maintain pathogenicity. These molecules are termed Pathogen Associated Molecular Patterns, or PAMPs.

Bacterial flagellin, or its active epitope flg22 (Zipf et al 2004), is the best-known example of a PAMP. Other PAMPs include the bacterial elongation factor Tu (epitope elf18) (Gunze et al 2004), bacterial peptidoglycan (Willmann et al., 2011), fungal xylanase (Ron and Avni, 2004) and fungal chitin (Miya et al., 2007). Host derived compounds that are produced as a direct result of pathogen infection can also induce PTI, and these compounds are known as Damage Associated Molecular Patterns, or DAMPs. Known DAMPs include peptides (Krol et al., 2010, Yamaguchi et al., 2010) and cell-wall derived oligogalacturonides (Brutus et al., 2010). Newman et al. (2013) provide an excellent review on known PAMPs, whilst Choi and Klessig (2016) discuss some of the more common DAMPs. Plants can recognise and respond to these PAMPs/DAMPs through a set of proteins known as PAMP Recognition Receptors, or PRRs.

### **PAMP Recognition Receptors (PRRs)**

All known plant PRRs are located on the plasma membrane and are either receptor-like kinases (RLKs) or receptor-like proteins (RLPs). Both types contain an extracellular domain, a transmembrane domain, and an intracellular domain, but whilst RLKs have an intracellular kinase domain, RLPs have a short cytosolic domain

(Monaghan and Zipfel 2012). The extracellular domain of many known PRRs binds to the target PAMP; FLS2 binds to the flagellum epitope flg22 (Chinchilla et al 2006); EFR binds to Ef-Tu epitope elf18 (Zipfel et al 2006); and XA21 binds Ax21 (Lee et al 2009). PRRs are covered extensively in a review by Zipfel (2014), whilst regulation of PRRs is covered by Couto and Zipfel (2016).

Upon PAMP/DAMP binding, PRRs complex with a downstream signalling partner, and causing a signal cascade resulting in immune responses, known as PAMP triggered immunity, or PTI.

### **PAMP Triggered Immunity (PTI)**

PTI involves ion fluxes, protein phosphorylation, increased cytosolic  $Ca^{2+}$ , multiple transcription changes (thousands reported in Arabidopsis upon detection of flg22 (Denoux et al., 2008)); and the accumulation of  $Ca^{2+}$  dependent protein kinases, mitogen activated proteins kinases (MAPKs), ATP and Reactive Oxygen Species (ROS) (Chisolm et al 2006). These responses prevent the pathogen penetrating the cell wall or plasma membrane, and make unfavourable living conditions for the pathogen. The PTI response and many of the signalling mechanisms and expression changes are covered in reviews by Bigeard et al. (2015) and Li et al. (2016).

Successful biotrophic pathogens need to inhibit, silence, or subvert the PTI response, providing favourable living conditions on the plant host and enable the resupply of nutrients. To achieve pathogenicity, they secrete of a cocktail of proteins called effectors.

### **Effectors**

Effector proteins are a diverse and enigmatic group of proteins. Whilst there is no 'archetypal' effector, they are often characterised as small, secreted, cysteine rich proteins. Most effector proteins need to be able to enter the plant cytosol, and once secreted from the pathogen, must pass through the host plasma membrane. Effectors which are detected by dominant resistance proteins in the host plant cell and induce a defence response are known as avirulence effectors, or factors. Effectors which avoid detection are referred to as virulence effectors or factors.

Effectors have a diverse variety of functions. *Avr2* from *Cladosporium fulvum* inhibits a least four different cysteine proteases in tomato plants, subverting some of the host's important immune responses (Shabab et al 2008), whilst *ATR13* from *Hyaloperonospora arabidopsidis* can suppress callose deposition triggered in the PTI response (Sohn et al 2007).

The biochemical function of most effectors is unknown, especially those secreted by biotrophic fungi. Part of the reason for this is the extreme difficulty in researching many phytopathogenic fungi, as they cannot be cultured in the absence of the host and thus are difficult to genetically transform. Some effectors that have been identified have a similar protein structure to known host proteins, e.g. *AvrP123* from the flax rust, *Melampsora lini*, is related to kazal-like protease inhibitors (Catanzariti et al 2007), and *AVR-Pita* from *Magnaporthe oryzae*, which shares homology with some metalloproteases (Orbach et al 2000). Effectors, especially those from rust fungi, will be discussed in further detail below.

In summary, effector proteins enable pathogens to suppress the PTI response and enable infection; however, plants have evolved a mechanism to detect and respond to these proteins, in the form of NLRs.

### **Nucleotide Binding, Leucine Rich Repeat Receptors (NLRs)**

NLRs can detect either the effector, or changes induced by the effector, and induce appropriate immune responses. The mechanisms behind this detection and regulation of the signalling response are the focus of both this thesis, and a large body of research reported in the plant disease literature. There are two major classes of plant NLRs, defined by their N-terminal signalling region; Coiled-coil NB-ARC-LRRs (or CNLs) and the Toll/Interleukin-1 Receptor NB-ARC LRRs (or TNLs). Both types of NLR have the similar function; to detect the presence of a pathogen, and to signal the effector-triggered-immune responses.

## **Effector Triggered Immunity (ETI)**

The ETI immune response is a stronger iteration of PTI, and whilst there are a diverse number of responses occurring, its hallmark is a localised cell death that is commonly referred to as a Hypersensitive Response (HR). It prevents biotrophic pathogens from further colonising the infected cell or neighbouring cells. Some necrotrophic pathogens have been shown to exploit HR to expand zone of dead plants cells at the infection sites (Govrin and Levine, 2000). However, how the signal is transmitted from plant NLR protein downstream to defence signalling elements in the cell is unknown.

Salicylic acid, nitric oxide, and various reactive oxygen species all are important in the ETI response, as are MAP Kinases (and their kinases and their kinase kinases). The gene products of SAG101, PAD4 and EDS1 are also implicated in the downstream signalling of ETI (Wagner et al., 2013). Reviews including Cui et al. (2015), Zhang et al. (2014), Seybold et al. (2014), Meng and Zhang (2013) and Wiermer et al. (2005) discuss these elements of ETI in much more detail than is provided in this introduction. Downstream signalling of ETI lies outside the scope of this thesis, which will focus more on NLR protein structure and function. That said, knowing what occurs downstream of plant NLRs is very important for determining their function and regulation, as well as identifying potential binding partners or signalling molecules.

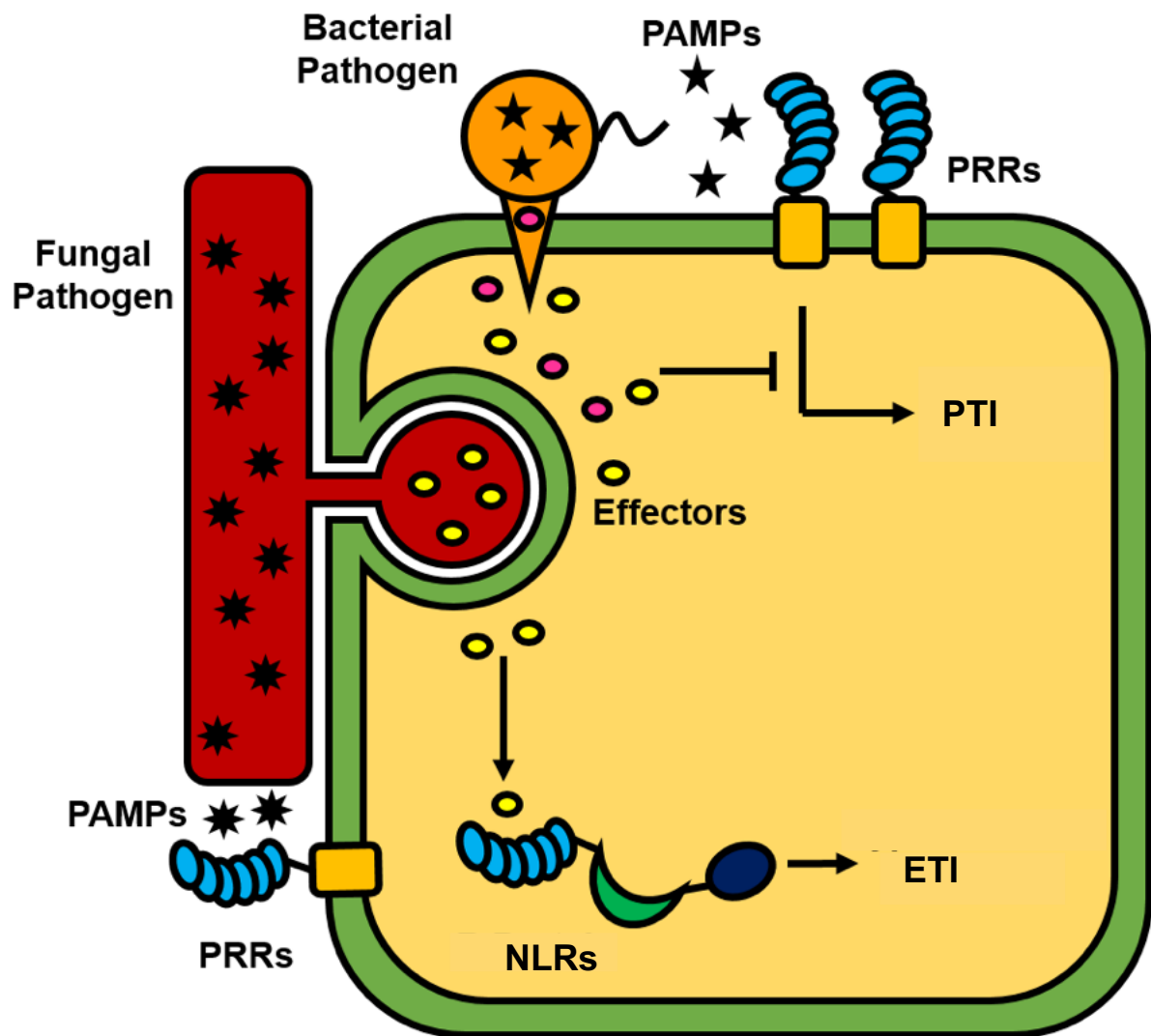


Figure 1.1 Simplified schematic of plant innate immunity adapted from Dodds and Rathjen (2010). Pathogen Associated Molecular Patterns (PAMPs) are detected by PAMP Recognition Receptors (PRRs). Interaction between the PAMPs and PRRs is known as PAMP Triggered Immunity (PTI). PTI includes a variety of changes within the cell, aimed at preventing pathogen entry to the cell, destroying the pathogen, or making unfavourable living conditions for the pathogen. Some pathogens can evade PTI through secretory proteins called effectors. Effectors can manipulate the host cell to provide favourable living conditions for the pathogen and one of the ways they do this is to inhibit PTI. Through evolution, plants have developed mechanisms to combat effectors, called Nucleotide Binding, Leucine Rich Repeat Receptors (NLRs). NLRs detect effectors, in what is commonly referred to as Effector Triggered Immunity (ETI). ETI results in a wide range of immune response but is often characterised by a programmed cell death event called the Hypersensitive Response (HR).

## Plant NLRs and Effectors

### **NLRs: the artists formerly known as R proteins**

NLRs belong to a larger group of proteins known as STANDs (signal transduction ATPases with numerous domains) which are important in various cellular functions, including plant disease resistance and inflammation and apoptosis in mammals. STANDs are a group of proteins related to the similar AAA+ proteins (ATPases Associated with diverse cellular Activities), involved in a diverse range of activities, including protein degradation and DNA replication, thermotolerance, and membrane fusion and microtubule motor movement in eukaryotes (Hanson and Whiteheart, 2005). STAND proteins often contain a central nucleotide-binding oligomerization domain (NOD). NLRs (nucleotide binding [NB], leucine-rich repeat [LRR]/nucleotide-binding oligomerization domain [NOD]-like receptors) can be found in both animals and plants. Domain architecture of other STAND members can be found in Figure 1.2.

Most NLRs contain a sensor domain, a nucleotide binding domain, and a signalling domain. Characterisation of the interactions between these domains, and with other proteins is limited. These interactions can differ vastly between plant species, and sometimes even within the same group of plant NLRs. Structural insights will be crucial in identifying regions of biochemical activity and interaction interfaces, and the next part of this introduction will focus on some structural elements, biochemical properties and intra- and inter-NLR interactions for each of the domains.

As mentioned previously, plant NLRs are often divided into two classes, CNLs and TNLs. Whilst CNLs are found throughout the plant kingdom, TNLs are found exclusively in dicots, with no TNLs discovered in any monocot species.

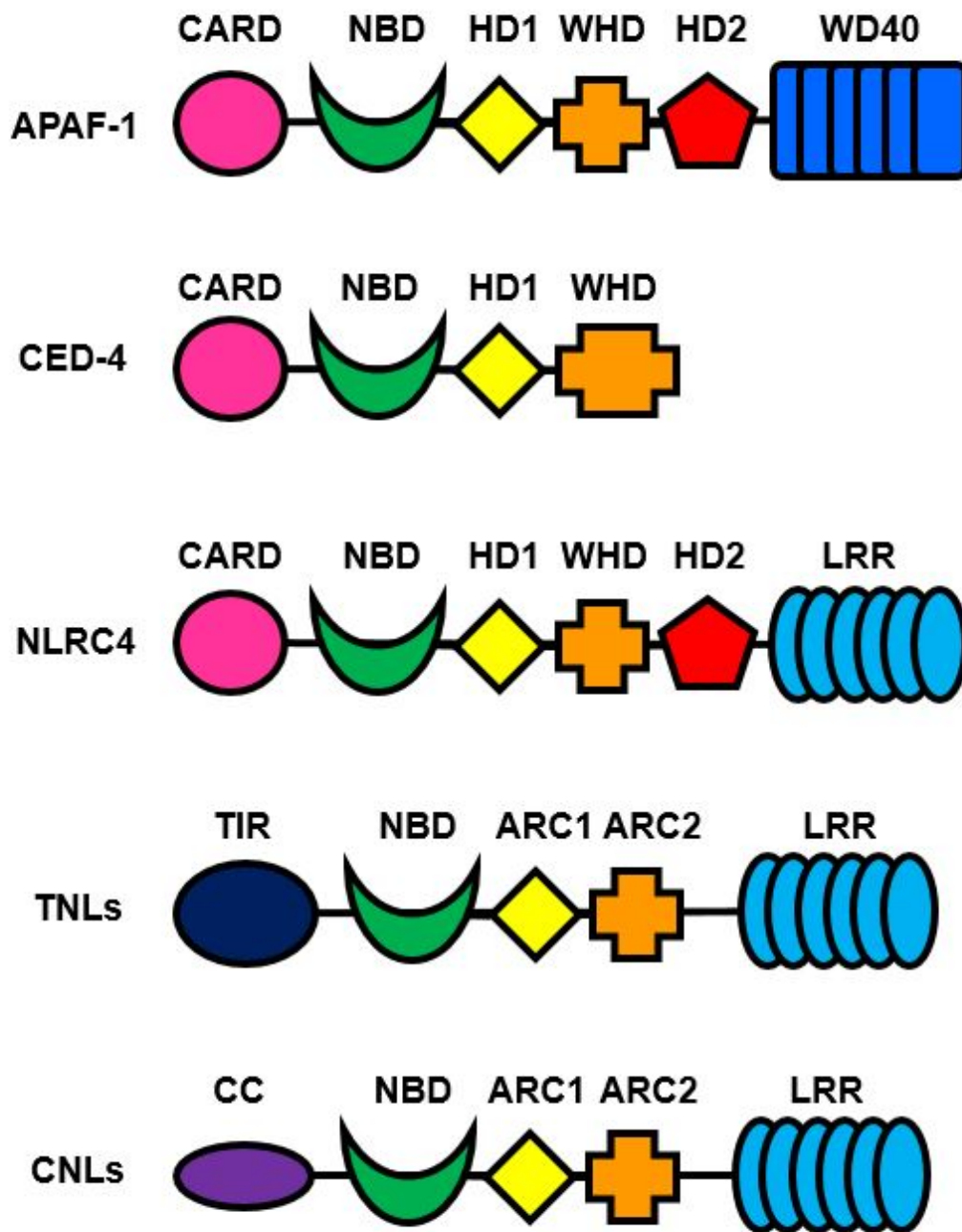


Figure 1.2 Architecture of select members of the STAND family adapted from Bentham et al. (2017). Each has a variable N-terminal signalling domain, and a nucleotide binding domain, with APAF-1, CED-4, NLRC4 and the TNLs/CNLs all containing ARC domains (also known as the HD1/WHD domains). All but CED-4 have a C-terminal ligand binding domain, with APAF-1 containing WD40 repeats, and NLRC4, TNLs and CNLs containing LRR domains.

Jacob et al. (2013) provides a great review on the evolution and divergence of the NLR types in plant species. Whilst this thesis will touch on aspects of CNLs, the focus will be on TNLs, starting with the TIR domain.

## **TIR domain**

The TIR domain was named after the cytoplasmic region of the Toll protein from *Drosophila melanogaster* and Human Interleukin-1 Protein (Gay and Keith 1991) and is found across plant, animal and bacterial species. The TIR domain is often found linked with other domains, however there are examples of TIR-only containing proteins in some dicotyledonous plants. The TIR domain has been shown to interact with other proteins and may form a scaffold enabling interaction with other proteins or protein domains (Ve et al., 2015). The TIR domain is a useful identifier for isolating resistance gene analogues (RGAs), in conjunction with various NB-ARC motifs, and is found amongst many different dicotyledonous species. This section will address some of the known functions of the TIR domain in plants, as well as structural data and known protein-protein interactions involving plant TIR domains.

### ***TIR domain autoactivity in planta***

The TIR domain has been shown to be the signalling component in many plant NLR proteins. Various *in planta* expression studies have demonstrated that the TIR domain is necessary and sufficient for HR signalling in many plants. Frost et al. (2004) demonstrated that the TIR domain of the flax rust allele, L10, was sufficient to signal effector-independent HR *in planta*. Expression of the L6 TIR domain removed from its NB-ARC and LRR domains, results in an autoactive resistance phenotype in both flax and tobacco (Bernoux et al., 2011). By creating various truncations of the flax rust resistance allele, L6, and visualising the cell death in flax leaves, it was found that the L6<sup>1-233</sup> fragment defined the smallest functional unit of the TIR signalling domain *in planta*. Similar results have also been shown for truncations of the *A. thaliana* bacterial-resistance gene, RPS4, (Swiderski et al., 2009). SNC1 TIR can also induce effector-independent HR in *N. benthamiana* (Zhang et al., 2017).

In contrast, some TIRs require additional C-terminal or N-terminal extensions, as shown by various RPP1 NLRs (Michael Weaver et al., 2006, Schreiber et al., 2016).

RPP1-WsA requires a portion of the NB-ARC domain to signal HR, whilst RPP1-NdA TIR requires an N-terminal extension. RPP1-WsB TIR cannot induce HR with either of the above extensions, however, expression of the RPP1-WsB TIR with a GFP tag does induce HR *in planta* (Krasileva et al., 2010). GFP can form dimers (Phillips, 1997), which, as will become clear in the next section, may explain why the RPP1-WsB TIR domain can signal with a dimerising tag, but not without.

Plant TIR domains are necessary and sufficient to signal HR in many cases, however there are clear exceptions. Other domains of the NLR are involved in activation and regulation of TIR domain signalling, and understanding these interactions will be crucial to understanding how plant NLRs function.

### ***Structural elements***

The *Arabidopsis thaliana* TIR-containing protein, AtTIR, was the first plant TIR protein to have its crystal structure solved (Chan et al. 2010). The structure shares similar features to that of mammalian and bacterial TIR domains, with a five-stranded parallel  $\beta$ -sheet, surrounded by a tight cluster of  $\alpha$ -helices, with the exception that it has two additional exposed  $\alpha$ -helical domains. These exposed  $\alpha$ -helices contain a cluster of positively charged residues, which are thought to be important for plant TIR domain function.

The crystal structure for the L6 TIR domain has also been solved and it shows around 40% sequence homology to that of AtTIR (Ve et al 2010; Bernoux et al. 2011). Like AtTIR, the L6 TIR structure also comprises a five-stranded parallel  $\beta$ -sheet, surrounded by five  $\alpha$ -helices. Like AtTIR, the L6 TIR has the same conserved unique third  $\alpha$ D helix.

The L6 TIR crystal structure, seen in Figure 1.3, was solved with two predicted dimer interfaces, with important residues required for homodimerization and function (Bernoux et al 2011). Crystal structures for both RPS4 and RRS1 from *Arabidopsis* have also been solved, and they have considerable structural homology to L6 and AtTIR, particularly RPS4. The RRS1 and RPS4 crystals were solved both in homodimer and heterodimer conformations and is the first and only structurally defined

TIR heterodimer (Wan et al. 2013; Williams et al. 2014). The interfaces between the TIR domains of RPS4 and RRS1, as well as the L6 TIR homodimer show some conserved function between plant species.

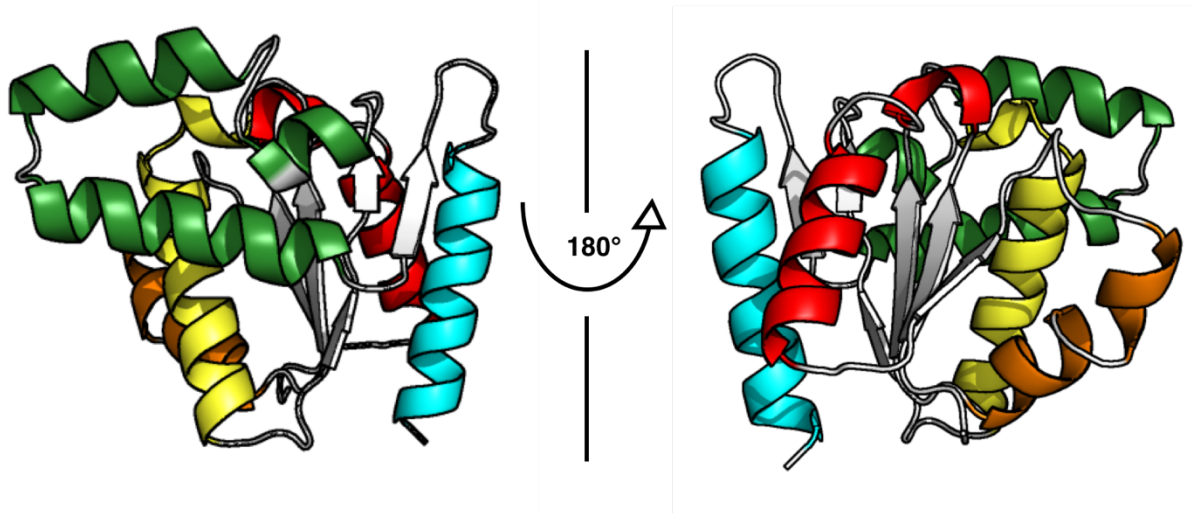


Figure 1.3 Structure of the L6 TIR domain. Crystal structure solved by Bernoux et al. (2011).  $\alpha$ -helices coloured Red ( $\alpha$ A), Orange ( $\alpha$ B), Yellow ( $\alpha$ C), Green ( $\alpha$ D), Blue ( $\alpha$ E), with loops and  $\beta$ -sheets coloured white. TIR domain is rotated  $180^\circ$  on y-axis.

Some TIRs utilise only one of the two interfaces, whilst others require both in order to signal HR. The interfaces are named for the secondary structure elements predominantly involved in the interaction, and hence are called the AE interface and the DE interface. The AE interface, involving the  $\alpha$ A and  $\alpha$ E helices, was first reported by Williams et al. (2014), demonstrating the interface between RPS4 homodimers, and RPS4/RRS1 heterodimers. A highly-conserved intercalating histidine pair forms at the core of this interface. Mutations of residues in this interface impair dimerization, autoactivity and effector dependent activity in L6/RPS4/SNC1.

The DE interface was first reported by Bernoux et al. (2011), and formed one of two interfaces in the crystal structure of the L6 TIR domain. Extensive mutagenesis, *in planta* experiments, yeast-2-hybrid assays and SEC-MALS (Size Exclusion Chromatography coupled with Multi-Angle Light Scattering) identified the DE interface as the important interface (Bernoux et al., 2011). An extensive network of hydrogen bonds and electrostatic interactions form the DE interface, with residues from the  $\alpha$ D and  $\alpha$ E helices, as well as residues from the  $\beta$ E strand and DE and EE loops all facilitating the dimerization. Mutation of R164, K200, G201, W202, D208 and K216 all disrupt yeast-2-hybrid assay dimerisation, and mutations to P160, R164, K200, D208 and K216 disrupt self-association when examined by MALS.

Zhang et al. (2017) further demonstrated the importance of these dimeric interfaces by introducing mutations in both interfaces into full-length L6. Mutations to the AE interface (F79A and K209E) and DE interface (R164A, R164E, K200E and W202A) both knocked-out effector-dependent HR in flax and tobacco, as well as effector-independent HR induced by autoactive mutants. Similar results were seen for the RPS4/RRS1 heterodimeric complex (Williams et al., 2014), with mutations in both interfaces impairing immune function in full-length proteins.

These two interfaces seem conserved across plant TIRs, with SNC1 TIR and RPP1 both functionally impaired by mutations to these interfaces (Zhang et al., 2017). Interestingly, the TIR domain of RPP1, from *Muscadinia rotundifolia*, does not appear to dimerise in solution, but requires conserved residues in the AE interface in order to

function (Williams et al., 2016). These insights show the necessity of the TIR domain to interact with other TIR domains to function, demonstrating that a dimeric or higher order structure formation is required for TNL function. It is crucial then that TIR domains are prevented from dimerising in the absence of pathogen effectors, and it is thought that the NB-ARC domain and LRR domain play this role.

### **NB-ARC domain**

The NB-ARC domain is the central domain of an NLR. It has roles in activation and in regulation of TIR domain signalling. The plant NB-ARC domain has demonstrated nucleotide binding capabilities and possesses ATP hydrolysis activity reminiscent of animal NLR nucleotide binding domains (Tameling et al., 2002, Tameling et al., 2006, Williams et al., 2011, Sornaraj, 2013, de Courcy-Ireland, 2015). The nucleotide binding site of the NB-ARC has several well conserved motifs (Maekawa et al., 2011, Meyers et al., 2005, Meyers, 2003, Meyers et al., 1999). It has been proposed by many, including Dodds and Rathjen (2010), that the NB-ARC domain may act as a platform for oligomerisation, given the sequence conservation between plant and animal NB domains. It is clearly an important regulatory domain for plant NLRs.

### ***NB-ARC domain Nomenclature, a sea of acronyms***

The NB-ARC domain shares sequence and structural homology to the mammalian intracellular NLR family's NACHT-NAD domain (NACHT - NAIP (neuronal apoptosis inhibitor protein), C2TA (MHC class 2 transcription activator), HET-E (incompatibility locus protein from *Podospora anserina*) and TP1 (telomerase-associated protein), NAD - NACHT-associated-domains) (Koonin and Aravind, 2000). To date, the only structural information on plant NLR NB-ARC domains comes from homology modelling based on the APAF-1 and CED-4 NB-ARC domains, as there is no structure of a plant NB-ARC domain. The NB-ARC domain is comprised of three distinct subdomains; the nucleotide binding (NB) domain, which shares homology with the mammalian NLRs NACHT domain; the ARC1 (shared between APAF-1, some R proteins and CED-4) domain (also known as the GxP module), which shares homology with mammalian NLRs NAD1 domain; and the ARC2 domain (also known as the HETHS domain) which shares homology with the NAD2 domain in mammalian NLRs (Takken and Goverse, 2012).

Many studies have shown conserved motifs of these subdomains that are crucial for NLR function and regulation, validated by structural data from related proteins APAF-1 and CED4. The next part of the introduction will go into more detail regarding the key motifs of the NB, ARC1 and ARC2 subdomains, as well as discussing their roles in regulation of TIR signalling, from a structural, biochemical and functional perspective. It will also highlight the interactions of both of these domains, both within the NLR protein itself, as well as with other proteins, involved in protein regulation and activation.

### ***Structural elements from other species***

As stated above, much of the understanding of the role of the plant NB-ARC domain is derived from functional data from *in planta* experiments, and biochemical data on truncated NLR protein. Invaluable structural information has been inferred from the structures of related but distantly evolved proteins, including APAF-1 (Riedl et al., 2005, Reubold et al., 2009, Reubold et al., 2011) CED-4 (Yan et al., 2005, Qi et al., 2010) and NLRC4 (Hu et al., 2013, Hu et al., 2015, Zhang et al., 2015). These studies demonstrated the important role that nucleotide plays in determining the conformation of the NB and ARC domains. ATP-bound CED-4 has a vastly different conformation to ADP-bound APAF-1 (Yan et al., 2005, Qi et al., 2010). Structures of the NB-ARC domains of APAF-1, CED-4 and NLRC4 can be seen in Figure 1.4.

Riedl et al. (2005) provided the first crystal structure of an NB-ARC domain, from APAF-1, and found it to be structurally similar to related mammalian NACHT-NAD domains. In APAF-1, four distinct subdomains were identified; the NB, ARC1, ARC2 and ARC3 subdomains, each containing conserved structural features to that of NACHT and NAD domains, found in animal NLRs. Overlay of the NB-ARC domain of plant NLR proteins on the structure of APAF-1, combined with sequence alignments, shows that the ARC3 subdomain is missing completely from plant NLR proteins, and is instead replaced with a flexible loop region connecting to the LRR domain (van Ooijen et al., 2008).

Yan et al. (2005) solved the crystal structure of CED-4, the third member of the NB-ARC containing family. It has a similar structure to APAF-1 and NLRC4, with distinct NB, ARC1 and ARC2 domains. The structure shows CED-9 binding to an asymmetric CED-4 dimer, with an ATP buried deep within each CED-4 molecule. This is in contrast to NLRC4 and APAF-1, both of which were purified with an ADP buried within a NB-ARC1/HD1-ARC2/WHD interface.

The structure of the mammalian NLR protein NLRC4 has also been solved (Hu et al., 2013, Hu et al., 2015, Zhang et al., 2015). Unlike structures solved for APAF-1 and CED-4, the NLRC4 structure was solved without its N-terminal domain, and unlike the APAF-1 structure, did contain the C-terminal extension. The structure of NLRC4 is similar to that of APAF-1, showing four distinct subdomains comprising the NB domain, a Helical Domain (HD1) equivalent to ARC1, a Winged Helical Domain (WHD) equivalent to ARC2 and a second Helical Domain (HD2) equivalent to the APAF-1 ARC3 domain, as well as the aforementioned LRR unit.

The APAF-1, NLRC4 and CED-4 structures enable generation of homology models of plant NLR NB-ARCs, allowing experiments to be designed around conserved motifs and important amino acids. Without the structure of a plant NB-ARC domain, homology models from APAF-1, CED-4 and NLRC4 would have to suffice.

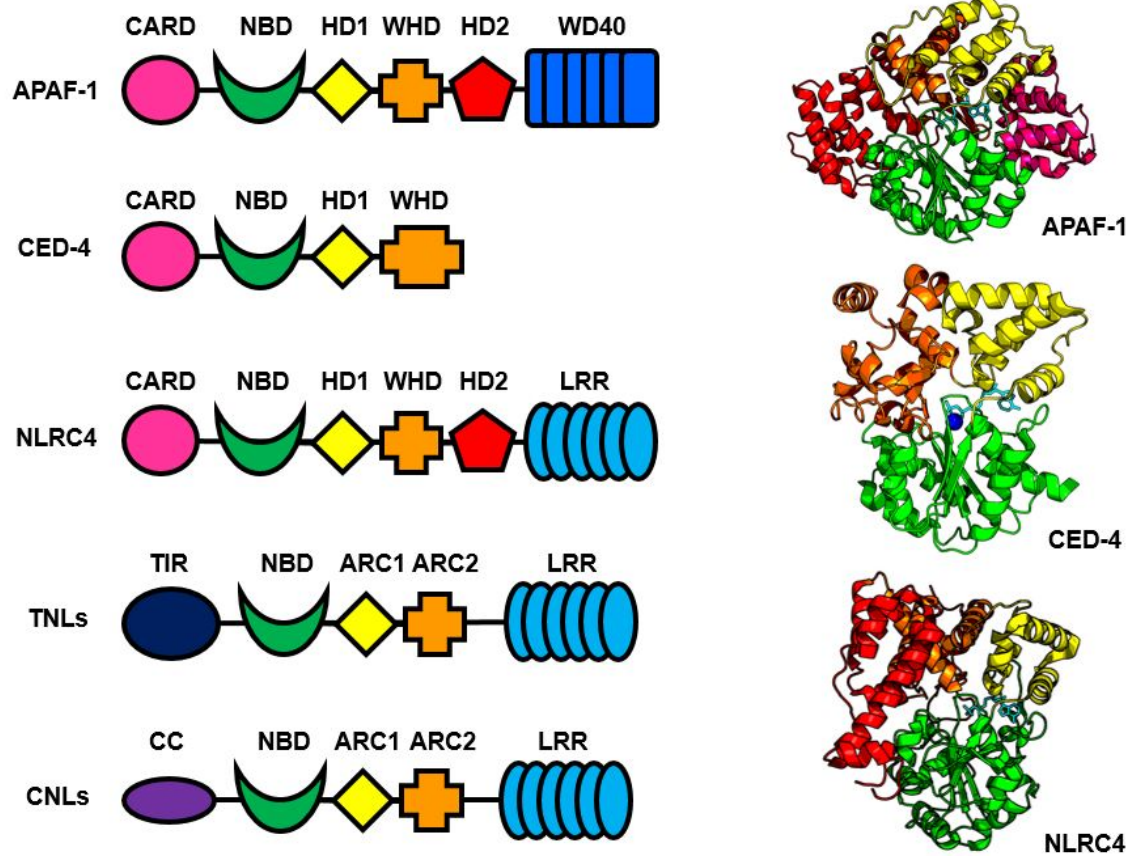


Figure 1.4. Domain architecture of APAF-1, CED-4, NLRC4, and two classes of plant NLRs, TNLs and CNLs. Partially adapted from Bentham et al. (2017) Right, the structures of the NB-ARC domains of APAF-1, CED-4 and NLRC4, highlighted by subdomains (Pink – CARD, Green NBD, Yellow HD1/ARC1, Orange WHD/ARC2 and Red HD2/ARC3).

Overall the region of the ADP-binding pocket and ARC2 subdomain of plant NLRs is more similar to APAF-1 than CED-4, and for this reason most structures generated for plant NLR NB-ARC domains are based on the APAF-1 crystal structure rather than the CED-4 crystal structure. Given that the CED-4 molecule is found to be bound to ATP in its 'inactive' state, rather than the ADP found for both APAF-1, and plant NLRs based on nucleotide binding data from Williams et al. (2011), the APAF-1 model is more appropriate for modelling plant NLR NB-ARC domains than CED-4. Comparison of the structure of I-2 to APAF-1 and CED-4 revealed that many of the critical motifs of the NB-ARC domain are conserved throughout the three proteins (van Ooijen et al., 2008).

The motifs crucial for plant NLR function are well conserved throughout the family of NLR proteins, and as well as STANDs and the AAA+ class of proteins. This high conservation of sequence and structure suggests commonality of function of NLRs throughout the plant kingdom. In the next section some of the key motifs of the NB-ARC domain in plant NLRs will be considered.

### ***NB-ARC domain motifs***

The NB-ARC domain is involved in the regulation and activation of the defence signalling response, transducing effector detection into TIR domain signalling at the appropriate moment. To understand how it performs its regulatory functions, it is necessary to first examine the functions of the subdomains and key motifs. The P-loop motif and the MHD motif are the most extensively studied, however there are a few other motifs that are conserved in the NB-ARC domain. I refer the reader to reviews by (Takken et al., 2006) and Bentham et al. (2017).

The P-loop motif of NB-ARC domain is the perhaps the most critical motif and is seen in red in Figure 1.5. The P-loop is a flexible, glycine-rich loop containing a highly conserved lysine responsible for binding a phosphate of a nucleotide (consensus sequence for the P-loop is GXXXXGK(T/S)). The structure of APAF-1 reveals that nucleotide binding is coordinated by various interactions between the conserved lysine and the  $\beta$ -phosphate of ADP (Riedl et al., 2005). In plant NB-ARC domains, it is likely that the conserved lysine of the P-loop interacts with  $\beta$ - and  $\gamma$ -phosphates of a bound

nucleotide. Hypersensitive response phenotypes are suppressed by mutation of this conserved lysine in many different NLRs (Dinesh-Kumar et al., 2000, Bendahmane et al., 2002, Tameling et al., 2002, Bernoux et al., 2011). Autoactive HR phenotype mutants of many different plant NLRs are also abrogated by mutation of the conserved lysine (Bendahmane et al., 2002, Moffett et al., 2002, Howles et al., 2005, Tameling et al., 2006, Gabriels et al., 2007, Sueldo et al., 2015, Wang et al., 2015). From this point on, P-loop mutation will refer to mutation of the conserved lysine in the P-loop, unless stated otherwise.

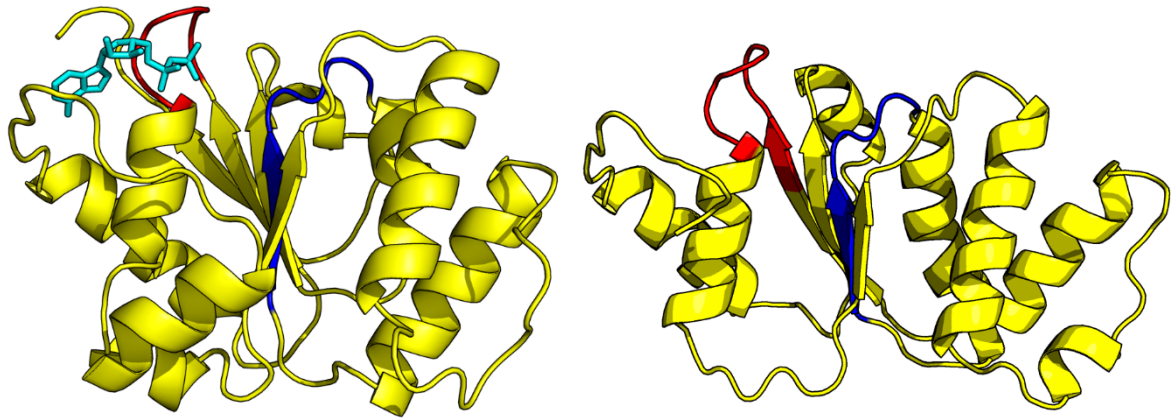


Figure 1.5 Comparison of APAF-1 nucleotide binding domain structure (left) and L6 nucleotide binding domain homology model structure (right), generated using the Phyre2 server (Kelley et al., 2015) using APAF-1 NB-ARC as a model. The ADP molecule highlighted in cyan, P-loop motif in red and Walker B motif in blue.

The second of the best characterized motifs in plant NLRs is the highly conserved methionine-histidine-aspartate (MHD) motif. Located in the ARC2 sub-domain, and found in NB-ARC and NACHT domains, mutation of the conserved histidine or aspartate typically results in an autoactive phenotype *in planta* (Bendahmane et al., 2002, Howles et al., 2005, de la Fuente van Bentem et al., 2005, Tameling et al., 2006, Williams et al., 2011). The ARC2 domain of APAF-1 is brought into contact with the NB domain by interactions between the histidine in the analogous LHD motif and the  $\beta$ -phosphate of ADP, and this interaction thought to maintain APAF-1 in a a closed conformation (Riedl et al., 2005). MHD mutations are thought to release these autoinhibitory interactions, and concurrently reduce the affinity for ADP, facilitating a preference for ATP binding and therefore an active conformation of the protein.

### ***Measurement of Nucleotide Binding in plant NLRs***

Few NLRs have had their ability to bind nucleotides directly examined. This is likely due to difficulties in purification of full length NLRs suitable for biochemical analysis (Schmidt et al., 2007). The NB-ARC domain of tomato NLRs I-2 and Mi-1 were the first to have their nucleotide binding properties assessed (Tameling et al., 2002, Tameling et al., 2006). The first full-length NLR to be assessed was barley CNL MLA27. When purified from insect cells, MLA27 was shown to be predominately purified in an ADP-bound state. (Maekawa et al., 2011). ADP and ATP binding has also been measured in the flax NLRs, M and L6 purified from *Pichia pastoris* (Williams et al., 2011).

Different nucleotide bound states of the proteins were found to correlate with their HR phenotype. The wild type M and L6 proteins were purified bound to ADP, and were in an inactive state *in planta*, unless challenged by effector AvrM. P-loop mutations of M that were found purified with negligible nucleotide were non-functional *in planta*, and a mutation in the MHD motif, found to be bound with ATP, was active *in planta*, even in the absence of the effector AvrM (Williams et al., 2011).

Apart from its observed biochemical functions, the NB-ARC domain interacts with other domains across many NLRs. These interactions can be autoinhibitory, or

involved in the activation of the NLR. Interactions between the domains of NLRs will be discussed in a separate section.

## **LRR domain**

The C-terminal LRR domain is the largest domain of the canonical plant NLR. Whilst it does not have a clear singular defined role throughout plant NLRs, it has been shown to be involved in effector detection (Dodds et al., 2006), autoinhibition and even activation of NLRs (Moffett et al., 2002, Wang et al., 2015).

The LRR domain consists of series of LxxLxLxxNxL repeats, with L being a leucine residue, and x being any other amino acid. LRR domains are present among a variety of different proteins, with the LRR family making up one of the biggest classes of proteins. Despite LRR containing proteins having vastly different roles, the structure and modularity of the LRR make them suitable for varying protein interactions.

The LxxLxLxxNxL motif forms a  $\beta$ -sheet, and is followed by a variable region, before repeating again. The repeats form a horseshoe/solenoid like structure, with loops and  $\alpha$ -helices on the outside and  $\beta$ -sheets inside (Kobe and Kajava, 2001). This produces a high surface area-volume ratio, making it an effective platform for protein-protein interaction.

Solved structures of LRRs have come mostly from proteins from the animal kingdom. The LRR forms a horseshoe-like structure in NLRC4, a mammalian TLR protein involved in inflammasome signalling. Hu et al. (2013) described the structure of NLRC4, with the LRR domain making contacts with the NB domain and key residues in the WHD, equivalent to the ARC2 subdomain in plants, involved in autoinhibition of the NLRC4 protein.

Sequence alignments show the most variable component in plant NLRs is generally the LRR domain, likely because of diversifying selection pressures. Studies have shown that differences in the LRR domain confer difference in pathogen specificity to some plant NLRs (Ravensdale et al., 2012, Wulff et al., 2009, Dodds et al., 2001, Ellis

et al., 1999). One of the best illustrations of this is shown by domain swapping experiments of the LRR domains of the flax NLRs, L10 and L6, with that of L2, resulting in a modification of the resistance specificity of the chimeric L10 and L6 proteins to that of the L2 allele (Ellis et al., 1999).

Moffett et al. (2002) showed also that the LRR domain of Rx is involved in regulation of signalling. The LRR domain can enable effector-dependent signalling when expressed together with the CC-NB-ARC fragment, either together or separately, whereas expression of the CC-NB-ARC domain on its own is unable to induce a HR, even in the presence of the effector CP (Coat Protein).

In an autoactive form of Rp1, a CNL from Maize, designated Rp1-D21, the LRR domain appears to destabilise the interaction between the CC and NB-ARC domains, releasing the autoinhibition and resulting in an autoactive phenotype. Wang et al. (2015) propose that the CC domain interacts with the ARC2 domain to maintain a ready signal inactive state. Upon effector or elicitor binding, the LRR domain perturbs the interaction between the NB-ARC and CC, allowing conformational changes to take place to allow the CC domain to signal downstream HR responses.

The diverse functions of LRRs in plant NLRs are yet to be fully unravelled, with different functions of LRRs occurring within related alleles. The structure of the LRR lends itself to protein-protein interaction, making it a probable target for binding of effectors, and also an autoinhibitory and regulatory domain for the signalling components of the protein.

## **Effectors**

Effector proteins are secreted into the host to subvert immune responses to make for a more pathogen-hospitable environment. Effector proteins are hugely variable, and there is not as yet universal effector motif, apart from the RxLR motif commonly found in oomycete effectors, and the RxLR-like motif found in some fungal effectors (Rehmany et al., 2005, Kale et al., 2010). While all effectors have signal peptides for export from the pathogen, they are highly variable in many other characteristics. For

example they may be cysteine-rich (Liu et al., 2012), form dimers (Ve et al., 2013), be highly divergent and rapidly changing (Jiang et al., 2008), mimic host peptides (Petre et al., 2016), act as proteases (Roden et al., 2004) and disrupt host gene function (Kong et al., 2017).

Until recently, effectors from only a few fungal pathogens had been identified, but thanks to new methods more are being identified. Selin et al. (2016) described over 80 effector proteins that have been cloned and characterized from crop-infecting fungi and oomycetes. Of these, 43 had been matched to a cognate NLR. Here I will describe a few fungal effectors in more detail.

The effector protein, *Avr<sub>a10</sub>*, from *Blumeria graminis sp hordei*, is thought to be detected by the NLR MLA10 from barley. *Avr<sub>a10</sub>* does not have a signal peptide, which whilst not unique amongst known effectors is uncommon, as most effectors discovered to date have a signaling peptide to facilitate secretion out of the pathogen. *Avr<sub>a10</sub>* is thought to target components of the PTI pathway in barley, specifically involved in gene-regulation. (Shen and Schulze-Lefert, 2007). This makes sense as MLA10 is nuclear localized and when co-expressed with *Avr<sub>a10</sub>*, elicits a HR (Ridout et al., 2006).

*Avr2* is an effector protein from *Fusarium oxysporum f. sp. Lycopersici* and is perceived by the NLR I-2 from tomato (Houterman et al., 2009). *Avr2* is coded by an intronless gene and is a 15.7 kDa protein upon expression, with some N-terminal proteolysis likely occurring before or during infection. *Avr2* was originally identified in xylem of infected tomato plants (Houterman et al., 2009), and I-2 is expressed in the parenchyma cells which are adjacent to xylem cells (Mes et al., 2000). A single point mutation at R45H in *Avr2* can knockout recognition by I-2 and maintain virulence and this effect was seen across both tomato and tobacco hosts.

*Avr2* needs to be translocated to the nucleus in order to trigger I-2-mediated HR. *Avr2* can also form homodimers *in planta* and in yeast-2-hybrid assays, but it is unknown what role this dimerization might play in avirulence or virulence. *Avr2* has also been shown to bind Six5, a related effector protein from the same pathogen, and both *Avr2*

and Six5 are required for I-2 mediated resistance in tomato (Ma et al., 2015). This is unique as it demonstrates a requirement of two effector genes to initiate resistance in a host from one NLR gene.

So how can plants possibly be able to cope with such a diversity of pathogen effectors? They can do this by diversifying the ways in which they detect pathogens. These will be explored further in the next section.

## **NLR/Effector interactions**

There are three models of NLR activation by effectors; direct, indirect, and the integrated decoy model, with some common features between them.

### **Direct interaction model**

In the direct interaction model, the effector protein directly interacts with the NLR, however examples of this are limited (Jia et al., 2000, Dodds et al., 2006, Wang et al., 2007, Catanzariti et al., 2010, Krasileva et al., 2010, Ve et al., 2013). This interaction is thought in some cases to cause a conformational change in the NLR, releasing autoinhibitory domain-domain interactions, enabling the NLR to signal. Examples of direct NLR/effector interaction are presented below, and are summarised in Figure 1.6.

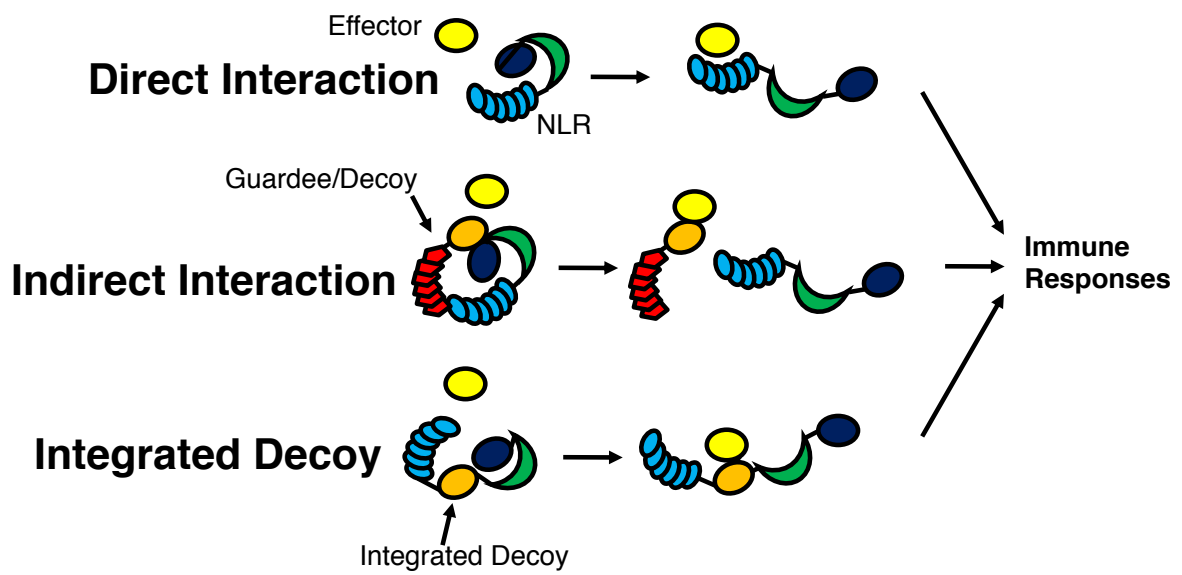


Figure 1.6 The three models of NLR/effector interaction, the Direct Interaction Mode, the Indirect Interaction Model, and the Integrated Decoy Model. In the direct model the effector binds directly to the NLR, causing conformational changes leading to downstream immune signalling. In the indirect model, the NLR senses changes caused by an effector on a guardee or decoy protein. The integrated decoy model combines both Direct and Indirect interaction, with decoy domains located within the NLR itself.

### ***Pi-ta and the effector AVR-Pita***

Pi-ta is a rice NLR that gives resistance to rice blast fungus *Magnaporthe grisea*. Pi-ta detects the avriuelnce gene product AVR-Pita to induce disease resistance. AVR-Pita binds directly to the LRR of Pi-ta. Yeast-2-hybrid assays demonstrated that the LRR domain of Pi-ta is necessary for AVR-Pita binding, and a single mutation in either the Pi-ta LRR domain (alanine to serine 918) or AVR-Pita (glutamate to Aspartate 177) is sufficient to knock out this interaction and any HR response (Jia et al., 2000). This interaction between NLR and effector was the first reported example of the direct NLR/effector model of interaction.

### ***L5, L6, L7 and the effector AvrL567***

*AvrL567* was the first rust fungal pathogen effector gene to be cloned (Dodds et al., 2004). AvrL567 proteins are small (147aa) secreted proteins and those that induce an immune response also directly interact with their NLR pair in yeast-2-hybrid assays (Dodds et al., 2006). There is a family of AvrL567 proteins, each recognised differently by L5, L6 and L7 NLRs. Of note are AvrL567s –A –B –C and – D. AvrL567A is recognised by L5, L6 and L7, whilst AvrL567B is induces strong HR in the presence of L5, weak HR in the presence of L6, and no HR in the presence of L7. AvrL567C does not induce an immune response with any of the three NLRs (Dodds et al., 2004) and AvrL567D is detected by L6 and L7, but not by L5.

Effector mutations of AvrL567 variants reveal various contact points between L5/L6 and AvrL567s at different positions, and the changes have additive effects (Ravensdale et al., 2012). L5 and L6 interact at similar positions with AvrL567, but have different amino acid requirements at certain positions, suggesting some difference in binding or disruption of autoinhibition caused in the two NLRs.

Chimeric L5 and L6 proteins showed that the TIR, NB, ARC1 and ARC2 subdomains also influence effector resistance specificity. Presence of a hybrid L5-L6 TIR-NB junction prevented interaction with any L6-interacting AvrL567 mutants, despite the presence of the required polymorphisms elsewhere in the protein (Ravensdale et al.,

2012). This indicates that interactions between the TIR-NB may be important in effector detection and consequential downstream signalling.

### ***M and the effector AvrM***

Another flax NLR and flax rust effector pair that interacts in yeast-2-hybrid assays is M and AvrM (Catanzariti et al., 2010). AvrM-A triggers the strongest response *in planta*, followed by AvrM-D, with AvrM-B and –C significantly weaker, whilst AvrM-E and avrM do not elicit a response. avrM differs from the other AvrM genes in the cluster, in that it contains a large internal deletion. It was found that only the C-terminus of the AvrM protein was required to induce a HR, and that most of the polymorphisms between the proteins occurred in this region. Changing each of the polymorphisms individually in avrM to those found in AvrM had no effect on the immune response, thus a combination of changes was expected to be responsible for the difference in HR between the two effector proteins (Ve et al., 2013).

Mutational analysis performed by Ve et al. (2013) showed that like L6/AvrL567, the M/AvrM interaction has multiple contact points, at key charged residues throughout the dimer of the AvrM protein. The amino acid residues involved in this interaction will be discussed further below and the interaction will be explored further in chapter five of this thesis.

### ***RPP1 and the effector ATR1***

RPP1, an NLR from Arabidopsis, is activated by direct binding of *Hyaloperonospora arabidopsidis* effector ATR1 to the LRR domain and co-expression of the ATR1 protein and RPP1 induces HR in tobacco (Krasileva et al., 2010). The ATR1 protein also co-IPs with RPP1, in correlation with HR, however the binding of the effector to the LRR is not sufficient to induce HR, as demonstrated by a P-loop mutant of RPP1 that was able to retain its ATR1 binding ability but was not able to induce HR, indicating further changes need to occur post-effector binding to trigger HR. The TIR domain of RPP1 was sufficient to induce effector-independent HR, but only when fused to a GFP-tag, whilst the TIR-NB construct could not induce HR, which suggests that the NB domain of RPP1 can obstruct TIR dimerization.

Similar to L5/L6 and AvrL567 and M and AvrM, there are likely multiple contact points between ATR1 and RPP1. Chimeras and mutations of various ATR1 variants and RPP1 allelic variants describe various contact points required to change HR specificity (Steinbrenner et al., 2015). As with L5/L6 and AvrL567, the substitutions are additive, as confirmed by HR, co-IP and bacterial growth inhibition assays. The interactions between NLR and effector are complex, and likely involve disruption of intra-domain interactions within the NLR, allowing activation.

Direct interaction of NLR and effector proteins provide a clear and logical path to resistance activation, however it is a very limited system, with the plant having to produce an NLR for each new virulent effector. Other models of interaction enable plants to provide resistance to multiple pathogens through one or two NLRs. Such efficiency is provided by the decoy/guardee model, or the indirect model of activation.

### **Indirect interaction model**

In the indirect model of NLR/effector interaction, a plant NLR senses changes to a host protein caused by an effector. This mode is advantageous, as it can allow a single NLR to provide resistance to multiple effector proteins, given that they target the same host protein that the NLR monitors. This is exemplified by the RPM1/RPS2/RIN4 system in *Arabidopsis thaliana* (Belkhadir et al., 2004). It is also harder for the effectors to break this resistance, especially if the host protein is a vital target to maintain virulence. Below are some examples of the indirect model of activation.

#### ***N, NRIP and p50: localisation***

N, a TNL from Tobacco (*Nicotiana tabacum*), provides resistance to Tobacco mosaic virus (TMV) by indirect association of the N-TIR domain with the helicase domain of TMV's replicase (p50) (Burch-Smith et al., 2007). Interaction of the N-TIR and p50 effector is mediated by a third protein, the appropriately named N receptor-interacting protein 1 (NRIP1) (Caplan et al., 2008). The NRIP1 protein is normally localised within the chloroplasts, but is moved to the cytoplasm and nucleus by the p50 effector, and this complex is perceived by the TIR domain (Caplan et al., 2008). N is then localised to the nucleus, and associates with SPL6 (SQUAMOSA PROMOTER BINDING PROTEIN-LIKE 6) to trigger downstream immune responses (Padmanabhan et al.,

2013). This highlights the requirement of both an additional protein and a change in localisation of a host protein to induce an NLR mediated immune response, demonstrating the diverse range of functions involved in the indirect model of interaction.

### ***Prf/Pto, AvrPto and AvrPtoB: Kinase Bait Trap***

Prf is an NLR from tomato (*Solanum lycopersicum*), that provides resistance to *Pseudomonas syringae* pv. *tomato* (Pst) (Tang et al., 2007). Resistance occurs when the effectors AvrPto or AvrPtoB interact with the Serine/Threonine Kinase, Pto. Prf and Pto exist in a complex, with Pto negatively regulating Prf activity (Mucyn et al., 2006, Mucyn et al., 2009). Interaction of Pto with AvrPto/AvrPtoB disrupts this regulation (Mucyn et al., 2009), allowing Prf to oligomerise and recruit further downstream binding partners (Gutierrez et al., 2010). Various autophosphorylation and transphosphorylation events of Pto bound to Prf enable the autoinhibitory interactions of Prf to be released (Ntoukakis et al., 2013). This highlights the regulation of NLR signalling by self and by binding partners, and is a perfect demonstration of the indirect NLR/effector interaction model.

### ***Rx, RanGAP2 and CP: indirect or transient interaction?***

Rx is a CNL from potato (*Solanum tuberosum*) that provides resistance to potato virus X (PVX) (*Potexvirus Potato virus X*) expressing the viral coat protein, CP (Bendahmane et al., 1999). Rx interacts with Ran GTPase-activating protein (RanGAP2) through its CC domain. Over-expression of RanGAP2 leads to an Rx-dependent activation of defense response, whilst Rx-containing *Nicotiana benthamina* plants with silenced RanGAP2 expression can no longer provide resistance to PVX (Sacco et al., 2007). It is not yet known how the CP triggers Rx/RanGAP2-mediated resistance, but it is speculated that a transient or indirect interaction with RanGAP2 may enable transient or direct interaction with Rx (Hao et al., 2013). This highlights some of the ambiguity in one of the better characterized pathosystems in plant innate immunity, and is an example where a third party is involved in the interaction between an NLR and an effector.

These three examples of indirect NLR/effector activation are but a sample of the many characterised interactions between a bait/decoy protein, effector and NLR. Recently,

it has been discovered that some NLRs themselves have additional domains that function as a bait for effector proteins. These NLRs have an integrated decoy domain, usually at the N-terminus or C-terminus, but also be between canonical domains. This model blurs the lines between direct and indirect interaction models of NLR/effector activation.

### **Integrated decoy model**

The third model of NLR/effector interaction represents a combination of the previous two models. In the integrated decoy model, often a pair of NLRs give resistance to effectors, with each protein having a specific role, either effector detection or defence signalling. The NLR involved in effector detection contains a domain mimicking the target of the effector, or an integrated decoy domain. Binding of the effector to the decoy domain releases the other member of the pair for signalling (Cesari et al., 2014, Maqbool et al., 2015, Le Roux et al., 2015, Sarris et al., 2015).

#### ***RPS4, RRS1 and AvrRPS4, PopP2***

RPS4 and RRS1 provide resistance in *A. thaliana* to *P. syringae* pv. *pti* and *R. solanacearum* variants expressing AvrRPS4 and PopP2, respectively. This pair of NLRs also provide resistance to a third pathogen, *Colletotrichum higginsianum* expressing an as yet unidentified effector (Narusaka et al., 2009). RPS4 function requires RRS1 co-expression, and the proteins directly interact in the plant cell. AvrRPS4 can interact with the RRS1 WRKY domain, triggering conformational changes enabling RPS4 signalling (Sarris et al., 2015), and likewise, PopP2 acetylates the WKRY domain of RRS1, again enabling RPS4 to induce immune responses (Le Roux et al., 2015). It is unknown if the RRS1 WRKY domain is functional but is clearly acting as a bait domain for the two effector proteins.

#### ***RGA4 & RGA5 and AVR1-CO39 & AVR-PIA, Pikp-1 & Pikp-2 and Avr-Pik***

RGA4 and RGA5 are CNLs from rice (*Oryza sativa*), that provide resistance to the rice blast fungus (*Magnaporthe oryzae*) expressing effectors AVR1-CO39 and AVR-Pia. Like RPS4 and RRS1, RGA4 and RGA5 provide resistance as a pair, with RGA4 constitutively active in the absence of RGA5, and RGA5 suppressing RGA4 signalling. RGA5 also contains a decoy domain directly targeted by AVR1-CO39 and AVR-Pia (Cesari et al., 2014). The decoy domain of RGA5 is at the C-terminus, and shares

sequence homology with ATX1, a copper chaperone containing a heavy metal-associated domain (Cesari et al., 2013). The RATX1 (related to ATX1) provides another example of a decoy integrated into one member of an NLR pair.

Pikp-1 and Pikp-2, like RGA4 and RGA5, are a CNL pair that also provides resistance to rice blast fungus, by detection of effector AVR-Pik (Ashikawa et al., 2008, Yoshida et al., 2009). Detection of AVR-Pik also occurs through an integrated HMA domain, but instead of being located at the C-terminus, is located between the CC domain and the NB-ARC domain of Pikp-1. AVR-Pik allele, AVR-PikD, directly interacts with the Pikp-1 HMA domain, presumably disrupting the Pikp-1/Pikp-2 complex interaction, enabling signalling of immune responses (Maqbool et al., 2015). The HMA domain, apart from effector binding, is non-functional, and highlights the effectiveness of the integrated decoy domain in NLR/effector interactions.

Integrated decoy domains appear to be common within the plant kingdom, with Kroj et al. (2016) observing that all plants they tested had NLRs with atypical integrated protein domains. They also identified a Zinc Finger-BED type protein domain as another potential decoy domain, and suggest that there may be many different types of decoy domain in NLRs.

Effector binding or modification, be it to the NLR or to a decoy/guardee, likely causes conformational changes within the NLR enabling signal transduction. What are the conformations that keep signalling in check? It is crucial that NLR signalling be triggered only when required. Other domains of the NLR keep the TIR domain in an inactive state in the absence of the pathogen. In the next section, some of the intra-domain interactions of NLR involved in autoinhibition of signalling, and how their disruption can lead to NLR activation will be examined.

## **NLR regulatory interactions**

Given that most plant NLRs induce cell death upon activation, it is crucial that they are tightly regulated. Constitutively active plant NLR phenotypes range from stunted growth to unviability. The N-terminal TIR or CC domain induces HR, and as the TIR

and CC make up a small proportion of the plant NLR, the NB-ARC and LRR domains control the switch from inactive to active and ensure signalling only when appropriate. To further reinforce an early point, there is no structural information of either the NB-ARC or LRR domains of plant NLRs, and thus all inferences on molecular interactions and structural changes must be made using homology models based on structural data from APAF-1, CED-4 and NLRC4.

## **Domain-domain interactions in NLRs**

### ***APAF-1, CARD blocks nucleotide exchange?***

As shown by Riedl et al. (2005) the N-terminal CARD domain of APAF-1 interacts with the NBD and WHD domains. The interfaces involve one of the CARD domain's  $\alpha$ -helices important for caspase recruitment. ADP co-ordinates interaction between the CARD domain, NBD, WHD and HD1 domains. Release of these interactions by exchange of ADP for ATP allows caspase recruitment. However, the stacking of the CARD domain is such that it restricts the access of ADP to the solvent, making nucleotide exchange impossible. In order for the CARD domain to fulfil its role it also needs the  $\alpha$ -helix involved in caspase recruitment to be solvent exposed, thus there needs to be a conformational change.

This suggests either a need for an exchange of nucleotide to release the CARD domain, or disruption of the interactions of the CARD and NBD by ligand binding to enable oligomerisation formation and downstream signalling. Given the CARD domain associates with ADP and blocks the only channel toward the bound nucleotide, it is possible that the CARD domain effects the capacity of the APAF-1 protein to bind exchange and hydrolyse ATP. It remains unclear which process occurs first; ligand binding to APAF-1, or exchange in nucleotide.

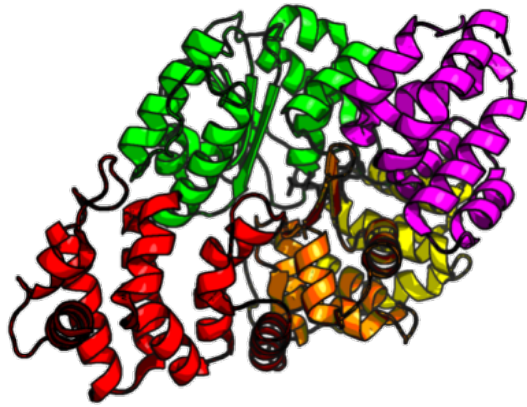
### ***Oligomerisation to the active signalling complex: APAF-1 apoptosome***

The cryoEM structure of the APAF-1 apoptosome shows the formation of heptameric complex, with a central hub and seven spokes (Zhou et al., 2015). The central hub is comprised of NBD, WHD and HD1 domains, with the spokes comprised of WD40 repeats, connected to the central hub via the HD2 domain. No density was reported for the CARD domains, likely reflecting their flexibility in the heptamer, and suggesting

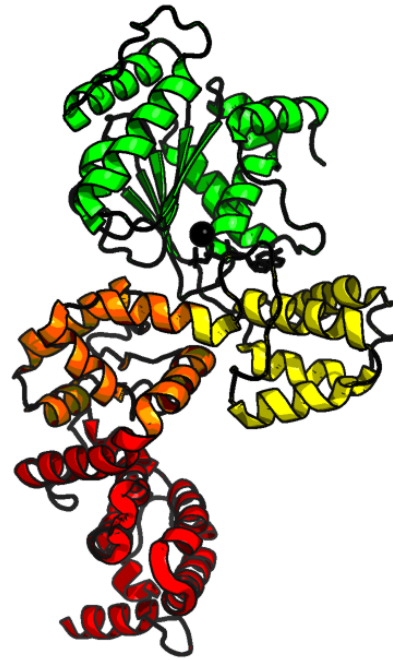
that they have been released from binding to the NB domain. A dATP molecule is found bound to each APAF-1 member of the apoptosome.

To switch from an inactive monomer to an active apoptosome complex, extensive conformational changes in the APAF-1 monomer are required. The most prominent change is the position of the WHD domain relative to the NBD/HD1 domains, as seen in Figure 1.7. The change involves repositioning the WHD away from the buried ADP molecule, exposing it to the solvent, allowing nucleotide exchange to occur.

This shifting of the WHD moves the histidine in the MHD motif from direct contact with the ADP in the auto-inhibited state, to a position distant from the nucleotide binding pocket in the active apoptosome. The sensor-1 motif, a conserved motif in the NB domain involved in sensing ATP in many AAA+ proteins (Miller and Enemark, 2016), interacts with an arginine in the auto-inhibited monomer and moves to directly interact with the  $\gamma$ -phosphate of the bound dATP/ATP in the apoptosome complex. The Walker B motif moves from an idle position in the auto-inhibited structure to direct contact with the  $\gamma$ -phosphate in the active state.



APAF-1 ADP bound



APAF-1 dATP apoptosome monomer

Figure 1.7 Comparison of the domain structure of the APAF-1 monomer in inactive state and active state. Inactive APAF-1 bound to ADP from Riedl et al. (2005) active APAF-1 monomer bound to dATP from Zhou et al. (2015). CARD domain shown in pink, the NB domain in green HD1 in yellow, WHD in orange and HD2 in red.

Intra-domain and inter-domain interactions therefore play an extensive role in nucleotide exchange, oligomerisation, and signalling in APAF-1, and similar interactions are possible in plant NLRs given the structural and functional similarities between the proteins. APAF-1 provides good structural information for modelling plant NLR activation, however the C-terminal extension of APAF-1 is a WD40 repeat, different the LRR of most plant NLRs. Roles of the LRR domain, as well as more functions of the NB-ARC domain, can be inferred from the structural data of a mammalian NLR, NLRC4.

***NLRC4 structure, inactive monomer bound to ADP, kept in check by intramolecular interactions***

The crystal structure of NLRC4 bound to an ADP molecule was solved by Hu et al. (2013). The NBD-WHD domain and NBD-HD2/NBD-LRR interactions plays a role in autoinhibition of NLRC4. These interactions are mediated by a bound ADP molecule. The WHD motif contains a histidine at position 438 (likely part of the MHD motif) that, along with the P-loop motif, interact with the phosphate groups of ADP. Mutation of this histidine to leucine results in a constitutively active protein, which also forms higher order oligomeric structures, consistent with mutations shown in APAF-1. The oligomeric structures of CED-4, DARK and APAF-1 all have a similar mode of organisation, with one side of the NBD domain stacking against the opposite side of another NBD domain (Qi et al., 2010, Yuan et al., 2011, Zhang et al., 2015, Zhou et al., 2015).

Hu et al. (2013) superimposed their inactive NLRC4 crystal structure into an oligomeric structure of CED-4 and found that the LRR domain overlapped with another CED-4 molecule. This shows the LRR domain of NLRC4 blocks binding of another NLRC4 monomer to the NBD, demonstrating that the LRR domain may play a role in autoinhibition. A mutation of Y617A at the interface between the LRR and NBD results in a constitutively active NLRC4 protein. Deletion of the LRR domain also leads to a constitutively active protein. Removal of the HD2 domain results in an even more autoactive protein.

Disruption of key residues between the HD2 and NBD domains of NLRC4 also results in a constitutively active protein, and addition of a mutation that perturbs NBD-LRR interaction increases the strength of this autoactivity. Altogether, the interactions between the HD2-NBD and LRR-NBD domains cooperatively inhibit the NLRC4 protein from signalling. The LRR-NBD and NBD-HD2 interaction sites are close to the proposed ligand binding site of NLRC4, and it is thought that upon ligand binding these interactions are somehow disrupted, and downstream signalling can progress, probably by dimerization of the NBD domains of the NLRC4 proteins. Exchange of nucleotide from ADP to ATP is also required, but it is not known if the rearrangements due to ligand binding preclude nucleotide exchange, or if nucleotide exchange enables the conformational changes to occur.

### ***Conformational changes lead to active oligomer***

From the various structures of related NLRs, a basic model of activation of plant NLR activation can be hypothesised. The signalling component is kept in check by interactions with the NB and ARC domains, and an ADP molecule coordinates these interactions. The sensor domain (LRR or WD40) detects a signal and causes conformational changes. These changes are perceived in the ARC2 subdomain, enabling exchange of nucleotide and release of the signalling domain. In the case of APAF-1 and NLRC4 this activated protein is then able to oligomerise and recruit the binding of downstream signalling molecules.

How might this model be applied to plant NLRs? This is considered in the next section. Given the evolutionary separation between APAF-1, NLRC4 and plant NLRs, there will no doubt there will be differences, but any similarities could be invaluable to help guide research.

## **Plant NLR domain-domain interactions**

### **TIR domain responsible for signalling**

In many NLRs, the TIR domain is constitutively active, kept in check by the other domains of the full-length protein (Krasileva et al., 2010, Bernoux et al., 2011, Williams et al., 2014, Schreiber et al., 2016). These interactions need to be sufficiently strong

to prevent auto-activation, but weak enough that they can be disrupted when required, be that by direct effector binding or modification of the guardee/decoy protein. As a result, the interactions between domains of an NLR are very finely tuned, with domain swaps between similar NLRs often 'breaking' resistance (Qi et al., 2012, Steinbrenner et al., 2015). Some of the interactions between the domains of NLRs, studied by point mutation, co-IPs, domain swaps and co-infiltration experiments are outlined below.

### **Some NB-ARC domains can abrogate signalling**

The interactions between the TIR domain and NB-ARC domain can be inhibitory, as shown by TIR domains losing autoactivity when expressed with the NB-ARC domain (Bernoux et al., 2011, Wang et al., 2015). In attempts to establish the minimal functional unit of L6 TIR domain, Bernoux et al. (2011) found that the more of the NB-ARC domain included in the infiltrated NLR construct, the less chlorosis was observed in transient expression assays. Put another way, the NB-ARC domain could abrogate L6 TIR dimerization, and thus prevent signalling from occurring. This correlated with a reduction in self-association as shown by yeast-2-hybrid assays, demonstrating that the NB-ARC prevented L6 TIR dimerization and thus TIR-domain autoactivity.

This inhibitory effect was also observed by Krasileva et al. (2010), with RPP1-WsB TIR-GFP fusion protein able induce effector-independent HR in tobacco, in contrast to the inhibited RPP1-WsB TIR-NB-ARC-GFP fusions. Wang et al. (2015) also demonstrated inhibitory interactions with the signalling domain and NB-ARC domain, with inclusion of the NB-ARC domain preventing the CC domain of Rp1 from inducing HR.

### **Some TIR-NB-ARC/CC-NB-ARC proteins are autoactive**

In contrast, some TIR domains can only signal effector-independent HR when expressed with the NB-ARC, suggesting both autoinhibitory and activation-inducing interactions. The NB-ARC likely plays a role in TIR domain activation by providing a platform for dimerization or oligomerisation. Deletions of the LRR domain results in autoactivity in RPS5 (Ade et al., 2007), RPP1A (Michael Weaver et al., 2006) and RPS2 (Tao et al., 2000). Why do some TIRs require NB-ARC to signal and why are some abrogated by inclusion of NB-ARC? Many TIR domains have been shown to

require dimerization to signal, and it may be that some TIRs require a small extension to enable dimerization to occur, whilst others are completely inhibited from dimerising by even the smallest inclusion of the NB-ARC domain. What is clear is that there are extensive interactions between TIR and other domains of the NLR, each sensitively tuned and controlled, to be released when required.

### **Interactions between LRR domain and ARC domain are important for inhibition and activation**

Apart from its role in ligand sensing, the LRR domain also interacts with other domains of the NLR, causing inhibition and activation. Interactions between the LRR and ARC1 and ARC2 subdomains are crucial for NLR function. Using domain swaps between Rx and Gap2, Moffett (2006) and Sloatweg et al. (2013) demonstrated that physical association of charged residues on the ARC2 and LRR domain could facilitate activation and autoinhibition. They suggest these electrostatic interactions at the interface of the two domains likely hold the protein in an ADP bound off state. Upon disruption of this interaction, by an effector for example, the protein switches to an open conformation. The electrostatic nature of the interaction also means it can be disrupted and reassociated quickly, enabling multiple 'rounds' of activation. Various chimeric Rx/Gap2 proteins demonstrated the need for compatibility between the interactions between ARC2 and LRR domains for correct function NLR.

Interactions between the LRR and other domains are also important for function of the maize NLRs Rp1 and D12. Chimeric domain swaps of these two proteins by Wang et al. (2015) demonstrated interactions between the NB-ARC and LRR domains, and CC and ARC2 domains. The authors suggested that the CC domains of the proteins are inhibited by interactions with the ARC2 subdomain, and upon activation by the as yet unknown elicitor, the LRR domain disrupts this autoinhibition, releasing the CC domain for signalling. Incompatibility between these domain interactions resulted in autoactive or inactive NLRs, again demonstrating the importance of domain-domain interactions in function.

As shown by various chimeric NLRs, point mutation experiments, co-IP and co-infiltration experiments, the interactions between the domains of NLRs are crucial for their function. Studies of these interactions, combined with the properties of the domains, and the various activation mechanism have led to many models of NLR activation, however there are still many questions to be answered.

## **Current Model of NLR induced ETI**

TIR domain signalling is kept in check by intra-domain interactions with the NB-ARC and LRR domains that are coordinated by an ADP molecule. Interactions are strong enough to prevent effector-independent signalling, but not so strong that they require large changes in order to be broken. Upon effector activation, either through direct binding of the effector to the LRR domain or integrated decoy domain, or modification of the guard/decoy protein, there are large-scale conformation changes of the NLR. Interactions between LRR and NB-ARC are disrupted and changed, enabling exchange of the bound ADP to an ATP molecule.

Upon ATP binding, the TIR domains are free to interact with other TIR domains. This results in the formation of a dimer or oligomer, that can signal necessary downstream immune responses, through currently unknown mechanisms. There are many questions still to be answered about how NLRs function. It is implied that effector recognition occurs before nucleotide exchange, but this has yet to be shown experimentally. Even with structural data on the active and inactive forms of APAF-1 and NLRC4 it is not clear whether the nucleotide exchange releases autoinhibition and enables ligand binding, or if ligand binding of the elicitor enables nucleotide exchange, and then subsequent downstream signalling through oligomerisation. The formation of large multimeric NLR structures is also inferred from domain interactions, co-IPs and mammalian structural studies. Interaction between effector and NLR has only been studied in static *in vitro* experiments.

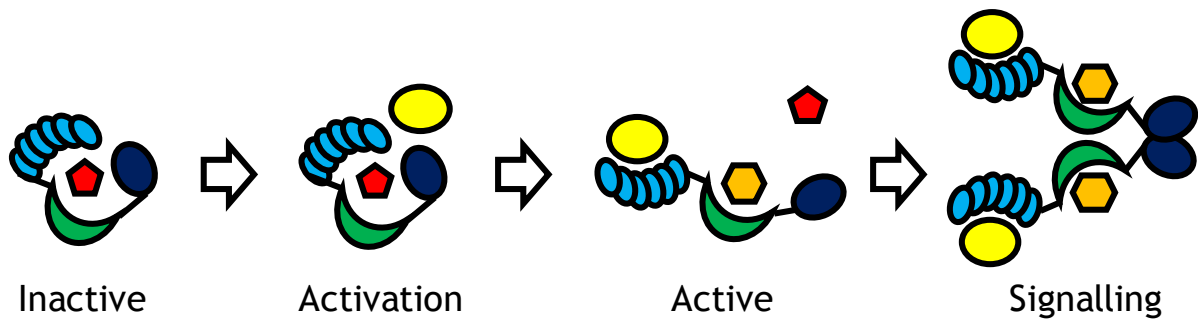


Figure 1.8 Schematic of the switch model of NLR activation. The NLR is kept in an inactive, auto-inhibited state by an ADP molecule (red pentagon). The NLR is activated by and elicitor (yellow), and undergoes conformational changes, allowing nucleotide exchange to ATP (orange hexagon). In the active state, the NLR can form a multimeric signalling complex, allowing signalling of HR.

## Aims and Objectives

In this thesis I hope to answer some of these questions regarding regulation and activation of NLRs. To do this, I look at the role of nucleotide binding in flax NLRs L6 and L7, using recombinant purified full-length proteins. I also try to purify other NLRs and devise a modified method to produce purer flax NLRs. Finally, I provide preliminary results of an experimental system to observe the interaction between a full-length NLR and effector *in vitro* in real time using Surface Plasmon Resonance.

### Chapter 3 Aims and Objectives

- Aim of chapter three is to determine the biochemical cause of the difference between L6 and L7 HR phenotype.
- This is to be done by purifying L6 and L7 and determining the amount of nucleotide bound to the proteins, as performed for M by Williams et al. (2011).
- Mutagenesis of residues known to affect the HR phenotype will also be introduced in the recombinantly expressed protein, and the effect of these mutations will be observed.

### Chapter 4 Aims and Objectives

- Aim of chapter four is to improve the purity of flax NLRs recombinant protein purifications, as current purity and yield is insufficient for more sensitive assays and structural studies.
- This is to be done by optimising the purification strategy by exploiting the high affinity of the Strep-II tag already used in NLR purification.

### Chapter 5 Aims and Objectives

- Aim of chapter five is to develop a method to measure the kinetics of the interaction between full length NLR and effector *in vitro*, as current methods used to assess NLR-effector interactions are not sensitive enough.
- This is to be done by developing a SPR-based method for assessing interaction of flax NLR M, and flax rust effectors AvrM and avrM. Assessing interaction of wild-type proteins and mutants should provide some insight into the requirements of AvrM-induced M activation, and the activation of NLRs by direct interaction with effectors in general.

## **Chapter 2 - Materials & Methods**

### **General Procedures**

#### **Agarose gel electrophoresis**

1% (w/v) agarose gels were made with 1X TAE buffer (40 mM Tris Acetate Buffer, 1 mM EDTA pH 8.0) and 1:10,000 Gel Red Nucleic Acid Gel Stain. Gels were run at 90 V for 60 min and bands were visualised using a Chemi-Doc (Bio-Rad).

#### **Sodium Dodecyl Sulphate-Polyacrylamide Gel Electrophoresis (SDS-PAGE)**

SDS-PAGE was performed as described by Laemmli (1970). Prior to gel separation, protein samples were denatured by mixing with a 3 x sample buffer (62.5 mM Tris-HCl pH 6.8, 20% Glycerol, 2% SDS, 5% B-mercaptoethanol, 0.5% Bromophenol Blue) and boiled at 95°C for 5 min. Proteins were run using a 10% acrylamide resolving gel and 4% acrylamide stacking gel SDS-PAGE in a 'Tetra Cell' gel electrophoresis unit (Bio-Rad); Electrophoresis was conducted at 170 V for 1 h in 1 x Running buffer (125 mM Tris pH 8.3, 960 mM Glycine 0.5% SDS)

#### **Western Blot**

Western blots were conducted post SDS-PAGE, as described by Towbin et al. (1979) with proteins transferred to a HyBond-ECL nitrocellulose membrane (Amersham Biosciences) using a 'mini trans-blot' apparatus (Bio-Rad) at 60 V for 90 min. The membranes were then incubated with Blotto (5 mM Tris, 0.1% Tween, 150 mM NaCl, 5% Skim milk powder) at 25°C for 1 h and then washed with fresh Blotto at 25°C for 15 min. To confirm the presence of purified proteins, membranes were incubated with monoclonal mouse anti-6xHis-tag antibody diluted 1:1000 in Blotto or a polyclonal rabbit anti-Strep-tag II antibody diluted 1:1000 in Blotto overnight at 4°C. After incubation with the primary antibody, membranes were washed by 2 x 15 min Blotto wash steps at 25°C, followed by incubation with goat anti-mouse horseradish peroxidase conjugated purified antibody (Rockland) diluted 1:1000 in blotto or goat anti-rabbit horseradish peroxidase conjugated purified antibody diluted 1:1000 in blotto at 25°C for 1 h. Incubation with secondary antibody was followed by 2 x 10 min

wash steps with TBS-T (5 mM Tris, 0.1% Tween, 150 mM NaCl) and a 2 min incubation with Amersham ECL Select Western Blotting Detecting Reagent (GE Healthcare). Membranes were imaged using a Chemi-Doc (Bio-Rad).

### **SYPRO® Ruby stain**

Following SDS-PAGE, proteins were stained using SYPRO® Ruby stain (Invitrogen), according to manufacturer's instructions. Gels were added to 35 ml of SYRPO Ruby and microwaved on high for 30 s. Gels were then incubated at 25°C for 30 s, and then microwaved on high for a further 30 s. Gels were then incubated at 25°C for 30 min. Gels were then washed using 50 ml wash solution (10% ethanol, 7% acetic acid) for 30 min. Two more wash steps using Milli-Q water were performed before gels were imaged with a Chemi-Doc (Bio-Rad).

### ***Pichia pastoris* protocols**

#### **Mutation and transformation of L6 and L7 constructs into *P. pastoris***

L6 (29-1294) and L7 (29-1294) in pPICZ constructs were obtained from Emma de Courcy-Ireland and used as template DNA to generate mutations. Mutations were introduced by site-directed mutagenesis using the Phusion™ Site Directed Mutagenesis protocol, using primers with the desired mutation. Primers contained the desired change in the central codon and spanned nine base pairs (three codons) either side of the target codon.

Site-directed mutagenesis was performed using methods described in the Phusion™ SDM manual. Reactions containing 10x HF buffer, 10 mM dNTPs, 50 ng forward primer, 50 ng reverse primer, 100 ng of template and 0.1 U Phusion™ were made up to 20 µL or 50 µL volumes. The PCR conditions used were 98°C for 30 s initial denaturation; 30 cycles at 98°C for 30 s denaturation, variable annealing temperature according to the T<sub>m</sub> of the primer for 30 s, and 72°C for 6 min extension, with an additional 72°C for 7 min final extension and 4°C hold.

Reactions were treated with *Dpn1* at 37°C for 1 h to remove template DNA and transformed into *E. coli* strain DH10B by electroporation using the Bio-Rad gene-

pulser II, according to manufacturer's instructions. Transformants were selected and used for plasmid purification using a commercial plasmid purification kit (Wizard Promega). Plasmids were sent for sequencing (AGRF) and those with the desired mutation were used for *P. pastoris* transformation. Vector map, gels, and primer sequences can be found in Appendix 1. All changes were successfully integrated into L6 and L7 in pP6H3C.

### ***Pichia pastoris* transformations**

*P. pastoris* strain x33 was used for all expression and purification in this study. Transformation of *P. pastoris* was performed as described in Williams et al. (2011) and according to the manufacturer's instructions (Invitrogen). Electro-competent *P. pastoris* were prepared fresh for each transformation. Untransformed *P. pastoris* was grown overnight in 2 mL YPD (1% (w/v) yeast extract, 2% (w/v) peptone, 2% (w/v) dextrose) at 30°C. The following day, the overnight culture was used to inoculate 100 mL 2xYPD (2% (w/v) yeast extract, 4% (w/v) peptone, 4% (w/v) dextrose). The 2xYPD culture was grown at 30°C until an OD<sub>600</sub> of 0.6-0.8. Cells were harvested by centrifugation at 1000 x *g* at 4°C for 5 min, then resuspended in 50 mL iced cold H<sub>2</sub>O. Cells were harvest by centrifugation at 1000 x *g* 4°C and resuspended in 25 mL ice cold H<sub>2</sub>O. Cells were harvested by centrifugation at 1000 x *g* 4°C and resuspended in 2 mL ice cold 1 M sorbitol. Cells were harvested a final time at 1000 x *g* at 4°C and resuspended in 200 µL ice cold sorbitol and immediately used for transformation.

Before transformation, pPICZ plasmids containing L6, L7 and mutants were linearized using *Sac1* restriction endonuclease, according to manufacturer's instructions (New England Biolabs, Ipswich, Massachusetts, United States). Briefly, 5.5 µL of CutSmart™ buffer was added to 10-20 µg of plasmid DNA in 50 µL of water, followed by 1 µL of U.mL<sup>-1</sup> of *Sac1*. Reactions were incubated at 37°C for 1 h, then at 60°C for 20 min to deactivate the *Sac1* enzyme. Linearization was confirmed by agarose gel, as seen in Appendix 1, Figure 7.5, then DNA was purified and concentrated by ethanol precipitation (Sambrook et al., 1989). Ten microlitres of at least 1 µg.mL<sup>-1</sup> linear DNA was used for transformation in *P. pastoris*.

Constructs were transformed in *P. pastoris* as described previously by Williams et al. (2011), but transformants were plated on YPD plates supplemented with either 1000  $\mu\text{g}\cdot\text{mL}^{-1}$  or 100  $\mu\text{g}\cdot\text{mL}^{-1}$  Zeocin. Higgins and Cregg (1998) and Williams (2010) reported that higher zeocin concentrations select for multiple integration events into the *P. pastoris* genome and that this leads to greater yield of recombinant protein. After 2-3 days incubation at 30°C, characteristically creamy *P. pastoris* colonies appeared, and were selected for test expressions.

### ***Pichia pastoris* Test Expression**

Single colonies from YPD with 1000  $\mu\text{g}\cdot\text{mL}^{-1}$  Zeocin selection plates were used to inoculate 10 mL of BMGY (Buffered Glycerol-Complex Medium (1% Yeast Extract, 2% Peptone, 100 mM Potassium Phosphate buffer (pH 6.0), 1.34% YNB, 4 x 10<sup>-5</sup>% Biotin, 1% Glycerol)) media and grown for 48 h at 30°C. Cultures were harvested by centrifugation and resuspended in 10 mL BMMY (Buffered Methanol-Complex Medium (1% Yeast Extract, 2% Peptone, 100 mM Potassium Phosphate buffer (pH 6.0), 1.34% YNB, 4<sup>^</sup>10<sup>-5</sup>%, 0.5% Methanol)) media. Cultures were grown for a further 48 h at 15°C, with addition of methanol to 0.5% v/v every 24 h. Cells were harvest by centrifugation again, before being resuspended in 1 ml lysis buffer.

Glass beads washed in lysis buffer were then added to the cell resuspension, to a 1:1 volume ratio of cells to glass beads. Resuspended cell pellets were vortexed for 2 min before debris and beads were pelleted by centrifugation. Ten microlitres of supernatant was run on SDS-PAGE for Coomassie stain and anti-6xHis-tag immunoblot to determine both successful integration of the linearized plasmid into the *P. pastoris* genome, and for expression of soluble NLR proteins.

## **NLR Protein Expression and Purification**

### **Expression of NLRs in *Pichia pastoris***

*Pichia pastoris* cell growth and harvest of was conducted as described by Williams et al. 2011. *P. pastoris* expressing the desired protein was used to inoculate 10 mL BMGY with 100  $\mu\text{g}\cdot\text{mL}^{-1}$  Zeocin (Invitrogen). This culture was grown overnight at 30°C with 200 rpm shaking and used as an inoculum for a 100 mL BMGY with 100  $\mu\text{g}\cdot\text{mL}^{-1}$

ampicillin culture. This culture was grown at 30°C for 72 h with 200 rpm shaking. The *P. pastoris* cells were harvested by centrifugation at 3000 x *g* for 10 min. The supernatant was discarded, and the pellet resuspended in 100 mL BMMY media with 100 µg.mL<sup>-1</sup> ampicillin. This culture was incubated at 15°C for 72 h with 200 rpm shaking, with the addition of 0.5% methanol every 24 h. Cells were harvested by centrifugation at 3000 x *g* for 10 min and washed once by resuspension in 50 mL of 20 mM Tris, pH 7.5, 150 mM NaCl, 5 mM EDTA, before centrifugation at 3000 x *g* for 10 min. Cells were then snap frozen in liquid nitrogen and stored at -80°C until required.

### **Preparation of Cleared Lysate**

Purification of NLR proteins from *P. pastoris* was conducted as described in Williams et al. (2011). *Pichia pastoris* cells expressing the desired NLR were resuspended in three times the volume of cell lysis buffer (50 mM Tris pH 8.0, 150 mM NaCl, 10 mM imidazole 10% glycerol, 0.25 mM TritonX-100, 20 mM β-mercaptoethanol, if purifying by StrepTactin Affinity Chromatography only, imidazole was omitted). Following resuspension, protease inhibitors (1 mM PMSF, 1 mM Benzamide, 1 mM Benzamide-HCl and 5 mM ε-amino-n-caproic acid) and 20 mM β-mercaptoethanol were added, then cells were lysed by three sequential passes through a French Press (Aminco), precooled to 4°C, at 2,000 to 5,000 psi. Unlysed cells and cell debris were removed by centrifugation at 4,500 x *g* for 15 min at 4°C. The supernatant was centrifuged at 100,000 x *g* for 45 min at 4°C. Cell lysates were titrated to pH 7.7-7.8 and protease inhibitors were re-added.

### **Immobilised Metal Affinity Chromatography (IMAC)**

Immobilised Metal Affinity Chromatography (IMAC) was conducted as described by Williams et al. (2011). Cell lysates were loaded onto a 3 mL IMAC column (Ni-Sepharose 6 Fast Flow, Amersham Biosciences, Piscataway, NJ, U.S.A.) that had been pre-equilibrated with equilibration buffer (20 mM Tris pH 8, 130 mM NaCl, 0.25 mM Triton X-100, 10 mM imidazole). The column was washed with 10 column volumes of wash buffer (20 mM Tris pH 8, 130 mM NaCl, 0.25 mM TritonX-100, 55 mM imidazole). Two 15 mL fractions were eluted into 35 mL of gel filtration buffer (20 mM Tris pH 7.5, 150 mM NaCl, 10% glycerol, 10 mM Magnesium Acetate, 1 mM DTT) with

5 column volumes of elution buffer (20 mM Tris pH 8, 130 mM NaCl, 0.25 mM Triton X-100, 250 mM imidazole). Protein samples were concentrated to 1 mL using a 30,000 MWCO concentrator (Millipore) in preparation for ATP/ADP quantification studies, or to 20 mL for further purification using a StrepTactin Column.

### **StrepTactin Affinity Chromatography (SAC)**

Prior to use, a 1 mL StrepTactin Superflow (Fischer Biotech) column was regenerated by running 10 to 20 column volumes of Strep-tag II regeneration buffer (Fischer Biotech) over the column. The column was then washed with an excess of 2-[4 - hydroxy-benzeneazo]benzoic acid (HABA) in Strep Buffer (100 mM Tris-HCl pH 8.0, 150 mM NaCl). Protein samples from either IMAC purification or *P. pastoris* lysates were loaded onto the column and washed with 20 column volumes of Strep Buffer. If performing the IMAC-SAC tandem purification method, protein samples were eluted into 40 mL assay buffer (50 mM Tris-HCl pH 7.5, 50 mM NaCl, 10 mM Magnesium Chloride, 10% Glycerol) using the same assay buffer at pH 8.0 containing 2.5 mM d-desthiobiotin. Eluates were then concentrated to 500  $\mu$ L using a 30,000 MWCO concentrator (Millipore) and frozen at -80°C until required. If purifying using the SAC purification method, proteins samples were eluted using a 0-10 mM d-desthiobiotin gradient over 25 mL. Fractions were assayed by SYPRO® Ruby stain, and those containing NLR protein were pooled and flash frozen in liquid nitrogen and stored at -80°C until required.

## **NLR ATP and ADP Occupancy Determination**

### **Sample Preparation**

Nucleotide occupancy assays were conducted as described by Williams et al. (2011), using a ATP Bioluminescent Assay Kit (Sigma-Aldrich) and IMAC purified protein samples. Protein samples were boiled at 95°C for 5 min to release any bound ATP/ADP and then centrifuged at 14,000 rpm for 1 min using a bench-top centrifuge. Samples were then split into two reactions; one to measure ATP and the other to measure ADP. ATP samples were mixed with a pyruvate kinase buffer (125 mM Tris-Acetate pH 7.4, 5 mM Phosphoenolpyruvic acid, 2.5 mM Magnesium Sulphate) and left on ice for 30 min. ADP samples were mixed with a pyruvate kinase buffer that

contained pyruvate kinase (125 mM Tris-Acetate pH 7.4, 5 mM Phosphoenolpyruvic acid, 2.5 mM Magnesium Sulphate, 125 U.mL<sup>-1</sup> Pyruvate Kinase (Sigma-Aldrich)) and left to incubate at RT for 30 min. ADP samples were boiled at 95°C for 1 min and centrifuged at 14,000 rpm for 1 min using a bench-top centrifuge.

### **Nucleotide Quantification**

All readings were recorded in mV using a 1250 luminometer (BioOrbit) connected to a QM1240 True RMS Multimeter (Digitech). The luminometer was blanked using 100 µL of ATP assay mix (Sigma-Aldrich Kit). To measure NLR sample ATP or ADP, 10 µL of the ATP or ADP reaction was then added to the ATP assay mix, and an mV reading was taken. An internal standard was then used, with 10 µL of a 2x10<sup>-8</sup> M or 2x10<sup>-7</sup> M ATP standard added to the protein sample. Readings of both ATP and ADP reactions, and internal standards were done in triplicate. Readings were converted from mV to M using the internal standard as a reference, and nucleotide binding was expressed as a percentage of moles of nucleotide per mole of protein. The equation used to calculate moles of nucleotide can be seen in chapter 3.

### **Protein Quantification using SYPRO® Ruby stain**

Protein samples were run on 10% SDS-PAGE before being stained with SYPRO® Ruby stain as described above. To quantify the amount of protein used in the nucleotide quantification assays BSA standards were also loaded into the gels and used to generate a standard curve. All bands were quantified using ImageLab software (Bio-Rad). An example of protein concentration quantification can be seen in Appendix 3.

## **Effector Expression and Purification**

### **Plasmids**

AvrM (103-343), avrM (46-280), and mutants in pMCSG7 were obtained from the Kobe Lab, University of Queensland, identical to plasmids used in (Ve et al., 2011a). Approximately 50-100 ng of plasmid DNA was mixed with electrocompetent BL21 (DE3) cells, and transformed by electroporation using the Bio-Rad genepulser II, as per manufacturer's instructions for *E. coli*. After electroporation, 200 µL of LB media

was added to the cells and left to recover at 37°C for 1 h, before being plated on LB agar plates containing 100 µg.mL<sup>-1</sup> of ampicillin. Plates were left to grow overnight at 37°C.

### **Expression of Effector proteins by autoinduction**

Expression of *AvrM* and *avrM* was performed as previously described in Ve et al. (2011a). Six colonies of transformed BL21 were used to inoculate 10 mL of LB media containing 100 µg.mL<sup>-1</sup> of ampicillin, and were grown overnight at 37°C with shaking at 225 rpm. The overnight cultures were used to inoculate 1 L of autoinduction media (Studier, 2005) containing 100 µg.mL<sup>-1</sup> of ampicillin, which were allowed to grow at 37°C with 225 rpm shaking to an OD<sub>600</sub> of 0.6-0.8, before lowering the temperature to 20°C and allowing the cells to grow overnight. The next day cells were harvested by centrifugation in a JLA 9.1 rotor (Beckman) at 7,446 x *g* for 20 min at 4°C. Cells were then resuspended in lysis buffer (50 mM HEPES pH 8, 500 mM NaCl, 30 mM Imidazole) and flash frozen in liquid nitrogen and store at -80°C until required.

### **Preparation of Cleared Lysate and IMAC**

Cells were thawed, and 1 mM DTT and 1 M PMSF was added. Lysis of *E. coli* cells was performed using a French Press (Aminco) precooled to 4°C, with two passes at 2,000 to 3,000 psi. Lysed cells and cell debris was removed by centrifugation in a Ti-70 rotor (Beckman) at 15,000 x *g* for 40 min at 4°C. Clarified lysate was then passed through a 0.22 µm, filter, and loaded onto a 5 mL HisTrap column using an AKTA Pure FPLC (GE Healthcare). Column was washed with 20 CV of lysis buffer, and effectors were eluted using elution buffer (50 mM HEPES pH 8, 500 mM NaCl, 250 mM Imidazole). Fractions were analysed by SDS-PAGE and Coomassie stain, and those containing the target effector were pooled.

### **Cleavage of Histidine Tag and Size exclusion chromatography**

Effector proteins were dialysed into a TEV protease buffer (50 mM Tris-HCl pH 8.0, 500 mM NaCl, 1 mM DTT, 0.5 mM EDTA) using SnakeSkin™ Dialysis Tubing 10,000 MWCO (ThermoFischer) for 30 min at ambient temperature, before addition of 500 µL of 3 mg.mL<sup>-1</sup> TEV protease. Samples was left to dialyse overnight at 4°C. TEV protease and uncleaved effector protein was removed by passing the sample over a

re-equilibrated 5 mL HisTrap column. The cleavage of the 6xHis-tag was confirmed by SDS-PAGE, Coomassie stain and anti-6xHis-tag western blot. Effector protein with the 6xHis-tag cleaved off was then concentrated to ~1mL using a 15,000 MWCO concentrator (Millipore). Effectors were further purified by size exclusion chromatography using a Superdex 200 HiLoad 26/60 column (GE Healthcare) pre-equilibrated with 10 mM HEPES pH 7.4, 150 mM NaCl. Fractions were analysed by SDS-PAGE, and those corresponding to the target effector protein were concentrated using a 15,000 MWCO concentrator (Millipore) to 10 mg.mL<sup>-1</sup>, before being flash frozen in liquid nitrogen, and stored at -80°C until required.

## **Surface Plasmon Resonance (SPR)**

All SPR experiments were conducted using a BIACORE 2000 (Biacore AB), using Sensor chip NTA (GE healthcare) and Sensor chip SA (GE Healthcare). Biotin-trisNTA was purchased from BiotechRabbit and diluted in H<sub>2</sub>O. Protein was purified as described above, with M purified by SAC and AvrM/avrM mutants purified by IMAC and SEC. Running buffer used contained 50 mM Tris-HCl pH 8 and 150 mM NaCl, , the conditioning buffer was running buffer with 3 mM EDTA added, and the regeneration buffer was running buffer with 350 mM EDTA added. Specifics of SPR experiments can be found in Chapter five. All statistical analysis was performed in the BIAevaluation software (GE Healthcare), and curves were exported to Microsoft Excel to produce figures.

# **Chapter 3 – Residues in the TIR domain of flax NLRs L6 and L7 influence their nucleotide binding properties**

## **Introduction**

Data from this chapter is part of the published work *Bernoux, M., Burdett, H., Williams, S. J., Ellis, J. G., Newell, K., Anderson, P., Dodds, P. N., Kobe, B., Lawrence, G., Zhang, X. & Chen, C. 2016. Comparative analysis of the flax immune receptors L6 and L7 suggests an equilibrium-based switch activation model. The Plant Cell. 28:146-59*

Written text in this chapter is my own, however some figures are the work of other authors of the paper. Data by others is clearly indicated, work done with *P. pastoris* purified protein and nucleotide measurements was performed by me.

## **Flax NLR genes**

Flax and flax rust are used as a model for plant innate immunity, with numerous NLRs and effectors cloned and characterised. The genes encoding the NLRs were the first to be identified, with at least 30 different alleles mapping to 5 loci, titled K, L M, N and P (Islam and Mayo, 1990). L6 was the first of these genes to be cloned (Lawrence et al., 1995) and was found to be similar to other cloned resistance genes at the time, RPS2 from Arabidopsis (Mindrinis et al., 1994) and N from tobacco (Whitham et al., 1994). All contain a central nucleotide-binding domain and leucine rich repeat domain. The L alleles have since been well characterised, and are extensively used to study NLR function, due to their combination of overlapping effector specificity and high sequence homology. In this study, L6 and L7, two alleles with extremely high sequence similarity, but very different phenotypes, as highlighted in Figure 3.1, are used to probe NLR function further.

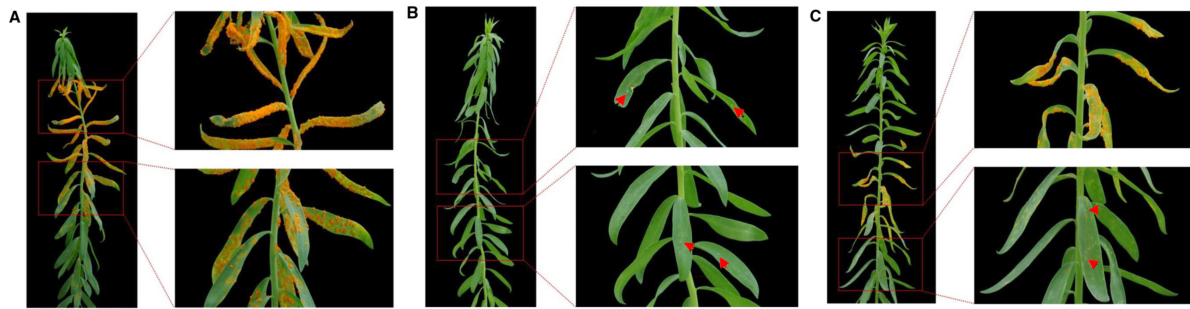


Figure 3.1 Resistant and susceptible phenotypes of flax, 14 days after inoculation by AvrL567 allele carrying flax rust strain CH5F2-138. **(A)** Flax cultivar **Bison** **(B)** a Bison backcross line (x12) containing the L6 gene from **Birio**, and **(C)** a Bison backcross line (x12) containing the L7 gene from **Barnes**. Zoomed regions of upper leaves and lower leaves of each plant show differences in leaf resistance and susceptibility, with orange 'rust' an indicator of disease and red arrows indicating HR flecks.

Work of others, adapted Figure 2 from Bernoux et al. (2016).

## L6 and L7

The L locus is a multi-allelic flax rust resistance locus, with 13 different TIR containing NLRs, each with differing functional characteristics and effector targets. There are only 10 polymorphic residues between L6 and L7 (Figure 3.2), all of which reside in or near the predicted TIR domain (Bernoux et al., 2011). Both proteins signal HR after recognition of flax rust strains carrying the effector AvrL567. L6-induced HR is stronger and more robust than that of L7-induced HR, when co-expressed in tobacco with an AvrL567 background (Bernoux et al., 2011). Given their near homologous sequence, the same cognate effector and yet a different resistance phenotype, they make good candidates to study the effects of subtle changes to the N-terminal signalling domain on the biochemical and functional aspects of the plant innate immune response.

Interestingly, despite the polymorphisms, L6 and L7 TIR domains produce comparable effector-independent HR, and both are able to self-associate *in planta*, in contrast to the resistance phenotypes of the full-length proteins (Bernoux et al., 2011). In solution, the purified TIRs both scatter light in a MALS assay consistent with a molecular weight of a dimer, and yet in yeast-2-hybrid assays full-length L7 has a weaker interaction with AvrL567 than L6, (Dodds et al., 2006, Bernoux et al., 2011). One explanation for these data is that the TIR imparts an inhibitory effect of the activation of the NB domain and that the L7 TIR has a more inhibitory influence than that of the L6 TIR domain.



When reciprocal changes in the L6 and L7 TIRs are expressed in planta in a AvrL567 background, no single residue is found to be responsible for the differing resistance phenotype. Rather, a series of three residues on an  $\alpha$ -helix are responsible for the differing in HR response. S83, R85 and R86 are all located on the  $\alpha$ A helix of the TIR domain and are not part of either of the two interfaces described by Bernoux et al. (2011).

Interestingly, L5 and L10 have the same residues in the  $\alpha$ A helix of the TIR domain as L7 (Figure 3.2) and yet still produce a robust L6-like HR response when expressed in transgenic AvrL567 containing tobacco leaves. Both L5 and L10 produce a very robust HR in the presence of AvrL567, despite having the same L7  $\alpha$ A helix amino acids. Examining other amino acids polymorphisms between L7 and L5, in combination with mutational analysis seen in Figure 3.3, revealed a cysteine to arginine mutation in the nucleotide binding domain could provide L7 with near L6 like HR in the presence of AvrL567. Interesting, this mutation in the L6 SRR/FCY mutant would allow the return of the L6 phenotype.

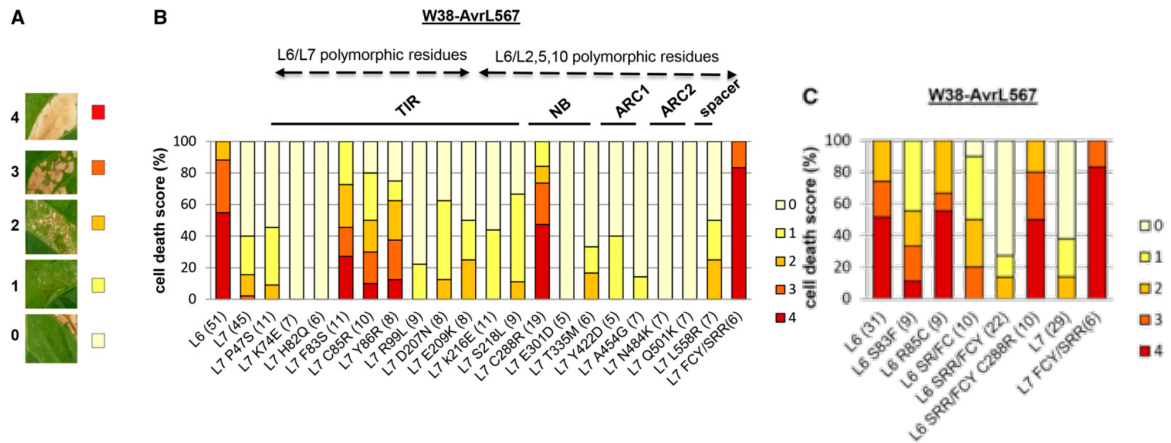


Figure 3.3 Reciprocal mutations in the TIR(83,85,86) and NB(288) regions of L7 and L6 have complementary effects on effector-dependent signalling activity. HR scoring of L6 and L7 mutants infiltrated and expressed in transgenic tobacco W38 expressing AvrL567. **A** Representatives of severity of HR in tobacco leaves, 4 being complete necrosis/chlorosis of the infiltrated leaf tissue, and 0 being no HR observed. **B** L7 and **C** L6 mutants' HR scoring in tobacco W38 expressing AvrL567. Figure in brackets indicate number of replicates, with the bars representing to portion of replicates that fall into each HR score. Domains of mutations are indicated above **B**.

Work of others, adapted from Bernoux et al. (2016)

These data, when considered with the fact that L6 and L7 TIRs are both capable of signalling a strong HR when expressed alone in planta, indicates that the TIR domain of these flax NLRs is involved of regulation of the HR. Rather than being a weaker signalling resistance protein, L7 is more tightly regulated than L6, to an extent that the regulation impedes its ability to signal a HR even in the presence of AvrL567. The positions of the polymorphisms in the TIR domain and nucleotide binding suggests that there may be an interaction between the two domains that causes this tighter regulation.

Given the importance of nucleotide binding in regulation of the NLRs, particularly its coordination of nucleotides, the nucleotide binding profiles of L6, L7 and the reciprocal mutants introduced above were measured. This chapter presents *in planta* (Maud Bernoux, CSIRO Canberra), AvrL567 interaction in yeast-2-hybrid assays (Maud Bernoux, CSIRO Canberra) and biochemical data (presented for examination in this thesis) of L6, L7 and reciprocal polymorphic residues between L6 and L7, to explore how differences in the TIR domain effect regulation and activation of an NLR.

## **Results**

L6 (29-1294) and L7 (29-1294) cDNA in pPICZ were used to generate mutations in the P-loop (K271M), MHD motif (D541V, henceforth referred to as MHV), L6 to L7 (SRR/FCY), L7 to L6 (FCY/SRR) and L7 C288R. Mutation was performed by site-directed mutagenesis and mutants were confirmed by sequencing. The positions of mutations in the full-length proteins can be seen in Figure 3.4.

## L6 and L7 mutations

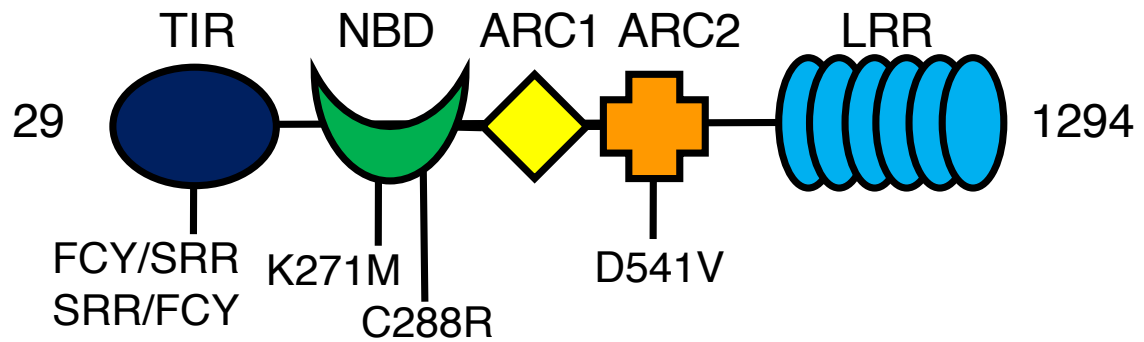


Figure 3.4 Positions of mutations in L6 and L7 proteins used in this study. Numbers indicate residue numbers of the full length protein, the amino acid single letter code and amino acid position of each mutation listed on bottom of schematic of NLR.

### **Test expressions of transformed *P. pastoris***

Test expression was performed as described in Williams et al. (2011) and the *P. pastoris* user manual (Invitrogen). As shown by Figure 3.5A, there are visible bands at the expected molecular weights for each of the mutants generated. Weaker expression was observed for L6 K271M, L7 K271M and L6 MHV, compared to expression of L7 MHV, as shown by western blot in Figure 3.5A. There also appear to be other bands reacting with the anti-6xHis-tag antibody, which may indicate N-terminal breakdown products, or non-specific binding of host *P. pastoris* proteins to either primary or secondary antibodies. If they are N-terminal breakdown products, they are likely the result of the harsh glass bead lysis conditions used in the test expression, compared with the controlled lysis used in large scale purifications.

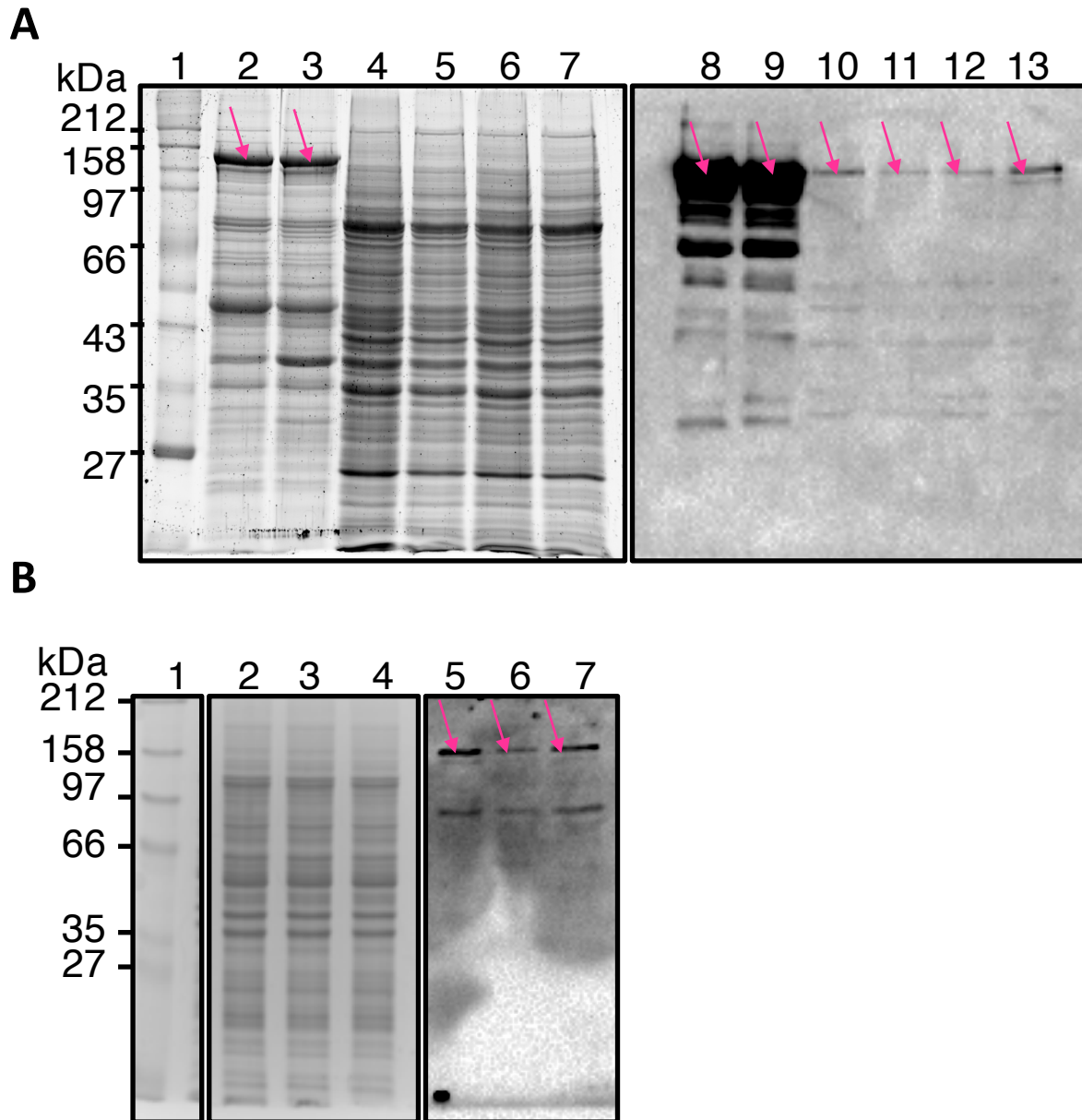


Figure 3.5 **A** Test expression of L6 K271M, L7 K271M, L6 MHV and L7 MHV proteins in *P. pastoris*. **1** Molecular Weight Marker, **2** IMAC Purified L6 **3** IMAC Purified L7, **4** L6 K271M test expression cell lysate, **5** L7 K271M test expression cell lysate, **6** L6 MHV test expression cell lysate, **7** L7 MHV test expression lysate. **8-13** contain the same samples in the sample order as **2-7**, showing an immunoblot probed with an anti-6xHis-tag antibody. **B** Test expression of L6 SRR/FCY, L7 FCY/SRR and L7 C288R. **1** Molecular weight marker, **2** L6 SRR/FCY test expression cell lysate, **3** L7 FCY/SRR test expression lysate, **4** L7 C288R test expression cell lysate. **5-7** contain the same samples in the sample order as **2-4**, but instead show an immunoblot with an anti-6xHis-tag antibody. Bands corresponding to full length NLRs indicated with pink arrows

Stronger expression of L6 SRR/FCY and L7 C288R compared to L7 FCY/SRR can be seen by anti-6xHis-tag antibody western blot in Figure 3.5B. Again, there appear to be other bands on the western blot, indicating either N-terminal breakdown products, or contaminating host proteins. With all mutants successfully expressed, albeit to varying expression levels in test expression conditions, larger scale purifications were performed for nucleotide binding analysis.

### **Purifications of L6, L7 and mutants for Nucleotide binding assays**

L6, L7 and mutants were purified from *P. pastoris* using a protocol previously described in Williams et al. (2011). A summary of the purification at each step can be seen in appendix 2, Figure 7.7. Figure 3.6 shows a representative sample of L6 and L7 wild type and mutants used for nucleotide binding studies. As shown by the SYPRO® Ruby stains and anti-6xHis-tag immunoblot, there are still both significant co-purifying bands, as well as N-terminal breakdown products. The effects of these proteins on nucleotide binding is accounted for using negative controls, however optimising and improving the purity will be addressed in chapter four.

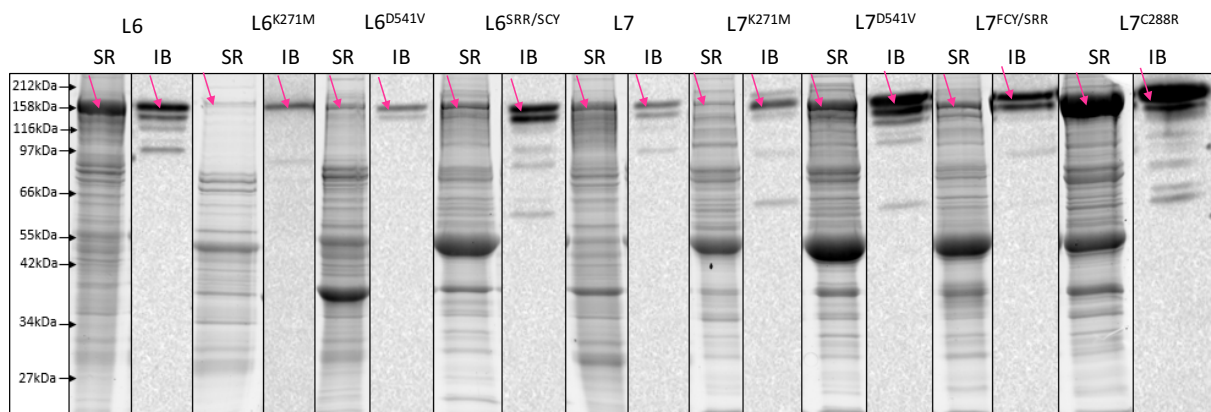


Figure 3.6 My work, adapted from Bernoux et al. (2016) Supplemental Figure 8: SYPRO® Ruby stain (SR) and Immunoblot (IB) analysis of L6 and L7 mutant protein purified by IMAC. Proteins were transferred and probed with an anti-6xHis-tag antibody. Molecular weight size markers are shown with arrows, and bands corresponding to full length NLRs indicated with pink arrows.

Concentrations of purified protein varied from 300-400 nM for the P-loop mutations, and up to 2-3  $\mu$ M for the wild type proteins, with other mutations falling in between. Low expression of the P-loop mutants may be due to the proteins inability to bind nucleotide, as expression of P-loop mutation NLRs *in planta* also results in reduced protein (Williams et al., 2011), presumably due to the instability caused by absence of the nucleotide. Similar low levels of protein expression were also found for a P-loop mutation in the M protein (Williams, 2010). Each protein was purified at least in triplicate, and samples were then used to measure levels of bound nucleotide.

### **Nucleotide Binding Calculations**

ATP and ADP concentrations were calculated using Equation 1. The mV readings included an internal standard that was used to calculate the sample concentration. Three replicates were performed for each purified sample. Blanks were used to account for background nucleotide levels. The averaged blank ATP concentration was subtracted from the average ATP concentration to give the final ATP concentration. ADP was calculated in the same manner, with subtraction of the final ATP concentration from the ADP concentration to calculate the final ADP concentration. Nucleotide occupancy was calculated by dividing the number of moles of ATP and ADP by the number of moles of protein in the assay, calculated as described in Appendix 3, and was expressed as a percentage.

Equation 1 Calculation of nucleotide concentrations from mV readings. ATP mV = mV reading from luminometer for ATP sample, ATP&Standard mV = mV reading for ATP sample + internal standard, [Standard] M = concentration of the internal ATP standard, [ATP] M = concentration of ATP sample, Blank mV = mV reading from blank sample, Blank&Standard = mV reading for blank sample + internal standard, [Blank] M = concentration of blank sample, Mean [ATP] M = average of ATP sample concentrations, Mean [Blank] M = average of blank sample concentrations, Final [ATP] M = concentration of ATP used for occupancy calculations, Mean [ADP] M = average of ADP sample concentrations, Final [ADP] M = concentration of ADP used for occupancy calculations.

$$\frac{ATP\ mV}{ATP\&Standard\ mV - ATP\ mV} \times [Standard]\ M = [ATP]\ M$$

$$\frac{Blank\ mV}{Blank\&Standard\ mV - Blank\ mV} \times [Standard]\ M = [Blank]\ M$$

$$Mean\ [ATP]\ M - Mean\ [Blank]\ M = Final\ [ATP]\ M$$

$$(Mean\ [ADP]\ M - Mean\ [Blank]\ M) - Final\ [ATP]\ M = Final\ [ADP]\ M$$

### ***L6 binds negligible ATP and low ADP***

Previous attempts had been made to purify L6 protein from *P. pastoris* and to measure bound nucleotide (Schmidt et al., 2007, Williams et al., 2011). The concentration of partially purified NLR protein was estimated by SYPRO® Ruby staining using a BSA standard curve. Protein concentrations of L6 ranged from 20-70  $\mu\text{g.g}^{-1}$  of *P. pastoris* cells. L6 nucleotide concentrations measured here of  $2.7 \times 10^{-7} \pm 2.9 \times 10^{-8}$  M are consistent with those described in Williams et al. (2011) of  $2.5 \times 10^{-7}$  M. L6 was found to be bound to  $0.2 \pm 0.1\%$  ATP and  $23.7 \pm 4.6\%$  ADP. This nucleotide binding occupancy is comparable but slightly lower to that of M ( $2 \pm 0.1\%$  ATP and  $35 \pm 3\%$  ADP (Williams et al., 2011)).

### ***L7 binds negligible ATP and much higher ADP than L6***

L7 protein was also purified successfully from *P. pastoris*, at similar concentration and purity to that of L6. Like L6, L7 was found to be bound with negligible ATP ( $0.5 \pm 0.1\%$ ). There was however a difference in the amount of ADP bound, with L7 having around double that of L6, at  $69.2 \pm 6.9\%$ . This contrasts with other purified flax NLR proteins, with both M and L6 having low ADP. Some M mutants have been shown to have a large amount of ADP bound (MD364E  $\sim 100\%$ ) (Williams et al., 2011), but L7 is the first wild-type NLR protein to have greater than 50% nucleotide occupancy post purification.

### ***L6 K271M binds negligible nucleotide***

Less protein was obtained during the L6 K271M purification, with  $2.17 \times 10^{-7}$  M, compared to the  $1.49 \times 10^{-6}$  M and  $9.56 \times 10^{-7}$  M seen for L6 and L7, respectively. As observed with P-loop mutants in other NLRs, L6 K271M has lost its ability to bind nucleotide, consistent with its inability to signal HR. L6 K271M bound  $0.6 \pm 0.2\%$  of ATP and  $2.5 \pm 0.7\%$  ADP, making its essentially empty from either ADP or ATP, comparable to what has been seen with M and other P-loop mutations in NLR proteins (Williams et al., 2011). The K271M mutants (both L6 and L7) were used as a negative control for each corresponding wild-type protein, as baseline ATP and ADP for what nucleotides are associated with co-purified *P. pastoris* proteins. The rationale behind using the P-loop mutant as a negative control, as opposed to the empty vector used by Williams et al. (2011), is the co-purified proteins associated L6 K271M are likely to

be more similar to the co-purified proteins found in the flax NLR purifications compared to the empty vector purifications.

***L7 K271M also binds negligible nucleotide***

L7 K271M, another P-loop mutation, was also purified, at similar purity to L6 K271M, but slightly lower concentrations. Unsurprisingly, L7 was also found to be bound to negligible amounts of ADP or ATP, ( $1.4 \pm 1.8\%$  ATP and  $6.6 \pm 3.9\%$  ADP), consistent with the resistance phenotypes typically associated with other P-loop mutations in a diverse range of plant NLRs, including L6. The higher variation in the occupancy values can be attributed to low nucleotide measurements, close to limits of detection of the assay.

***L6 SRR/FCY has nucleotide binding similar to that of L7, whilst L7 FCY/SRR binds less ADP than L7 but it similar to L6***

The reciprocal mutations in the L6 and L7  $\alpha$ A helix of the TIR domain resulted in reciprocal changes to the nucleotide binding of the NLR protein. Whilst ATP binding within the L6 SRR/FCY mutant ( $3.7 \pm 0.9\%$ ) remained relatively unchanged compared to the wild type protein, ADP binding increased to  $68.7 \pm 1.6\%$ , levels comparable to L7. This increase in ADP correlates with a decrease in HR scoring for the L6 SRR/FCY mutant, as seen in Figure 3.3. The reciprocal change in L7, L7 FCY/SRR, also changes the ADP binding, decreasing ADP occupancy to  $36.6 \pm 1.5\%$ , correlating with an increase in HR strength as seen in the *in planta* assays. L6 SRR/FCY and L7 FCY/SRR proteins were expressed and purified to higher concentrations and purity than the P-loop mutants, but slightly lower than the wild type L6 and L7 proteins.

***L7 C288R binds less ADP than L7, but more than L6 and L7 FCY/SRR***

The L7 C288R was expressed and purified in *P. pastoris* to a concentrations and purity similar to L6. Of all the mutants examined, this was the most highly expressed of all the flax NLR proteins analysed in this study. Nucleotide binding for this protein also correlated with the HR experiments, with negligible ATP ( $1.8 \pm 0.5\%$ ) and slightly decreased ADP ( $45.6 \pm 2.7\%$ ) relative to L7; although it did not quite equal the 30% ADP seen for L6, it is more similar to L6 in terms of nucleotide binding than L7.

### ***L6 MHV binds negligible nucleotides***

Based on the results of Williams et al. (2011) for the analogous M autoactive mutant MHV, the L6 MHV mutant was expected to bind ATP. M MHV mutant protein was found to have nucleotide occupancy of  $18 \pm 4\%$  ATP, and  $5.40 \pm 2\%$ , however the L6 MHV protein purified with  $0.4 \pm 0.2\%$  ATP and ADP  $6.0 \pm 1.3\%$ . This may be attributed to a decrease in stability of the L6 MHV protein, making it difficult to capture the protein in a native, stable form, bound to a nucleotide. Purifications of L6 MHV protein yielded 10-fold protein less than the wild-type L6 protein.

### ***L7 MHV ATP/ADP binding is very similar to L7***

In contrast with low yields of L6 MHV, L7 MHV could be purified to concentrations similar to that of that of L6 and L7 proteins. L7 MHV protein was purified with negligible bound ATP, but around  $79.2 \pm 6.7\%$  ADP, similar to that of L7. This correlates with the HR phenotypes observed for the L7 protein, with a high ADP occupancy correlating with weak tissue chlorosis, indicating a weaker HR response.

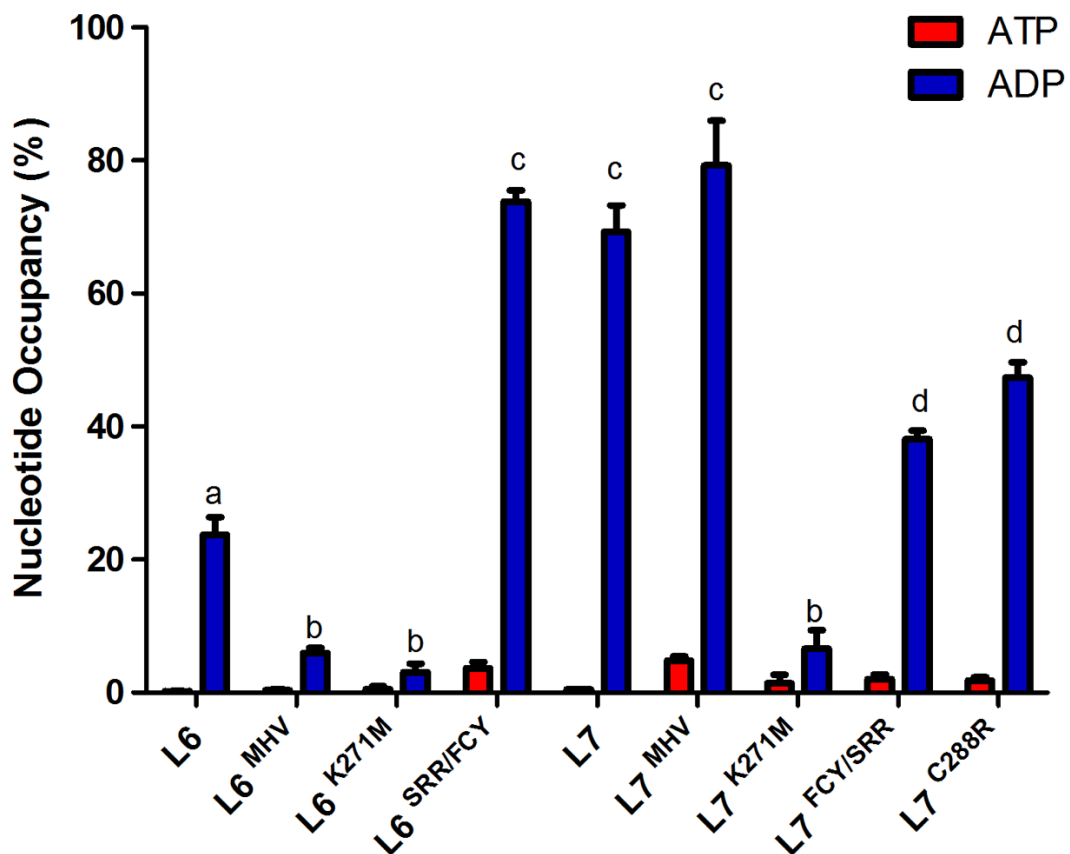


Figure 3.7. Nucleotide Occupancy of flax NLRs L6 and L7, and various mutants. ATP and ADP quantifications of L6, L7 and mutant proteins. Nucleotide occupancy is expressed as the number of moles of ATP or ADP per moles of NLR protein purified by Nickel affinity chromatography. L6 K271M and L7 K271M proteins were used as a negative control and confirmed that other co-purifying proteins did not contribute to measurements of ATP and ADP. Nucleotide occupancy measurements of all proteins were done in triplicate and recorded with error bars representing 1 SD from the mean. One-way ANOVA, Tukey's HSD post hoc test, and tests for normality and equal variances were run and revealed the presence of four statistically different groups for ADP values (a to d). ATP occupancy was negligible in all samples and not significantly different from each other.

My work, adapted from Bernoux et al. (2016)

## Discussion

### Differences in elicitor-dependent HR may be explained by differing nucleotide binding for L6 and L7

Using previously described methods described by Williams et al. (2011), it has been demonstrated that L6 and L7, when expressed and purified from *P. pastoris*, both co-purify bound with endogenously derived nucleotides. Both L6 and L7 purified proteins had negligible levels of bound ATP, whereas L7 was purified with 69% of protein bound with ADP, and L6 purified with 23% of the protein bound with ADP. It was also shown that the P-loop mutants of L6 and L7 bind low to negligible levels of ADP, similar to that shown for the purified M protein (Williams et al., 2011).

The differences in HR phenotype observed with expression of the L6 and L7 proteins *in planta* (Figure 3.3) correlate with ADP binding. An NLR with less ADP bound may indicate a lower affinity for ADP than one with a more ADP bound. Based on this hypothesis, L6 is able to exchange an ADP for ATP more readily than L7. Nucleotide exchange has been shown to be crucial for both APAF-1 and NLRC4 activation, with ATP binding a requirement for conformational changes required for activation in both proteins (Reubold et al., 2009, Hu et al., 2013). The additional phosphate of the ATP molecule plays an important role in the restructuring of the domains involved in regulation of signalling, in both APAF-1 and NLRC4. The difference in strength of ADP binding may therefore explain the difference in HR strength between L6 and L7. The P-loop mutants highlight the need for a functional P-loop for correct NLR function, as both L6 and L7 are both non-functional *in planta* and unable to bind significant amounts of nucleotide with a defective P-loop.

### Amino acids in the $\alpha$ A helix of the TIR domain of L6 and L7 are responsible for differences in elicitor-dependent HR

There are 10 polymorphic amino acids between the flax rust resistance alleles, L6 and L7, and all lie within the TIR domain. Mutational analysis combined with *in planta* HR assays showed that residues 83, 85 and 86 are responsible for differences in HR between L6 and L7, as seen in Figure 3.3. These residues are all on the  $\alpha$ A helix,

and not involved in the dimer interface for L6 TIR-TIR interactions (Bernoux et al., 2011), and do not compromise the ability of the TIR domain to signal effector-independent HR.

The L6 SRR/FCY mutant reduced the L6 AvrL567-induced HR significantly, whilst the reciprocal change, L7 FCY/SRR, changed the HR phenotype of L7 to a significantly stronger resistance phenotype, comparable to that of wild type L6. Changing all three residues in either L6 or L7 had a pronounced effect, effectively knocking out L6 HR signalling whilst giving L7 a very robust HR phenotype. This suggests all three residues may play a cumulative role in autoinhibition of NLR signalling, likely through interaction with other domains of the NLR or with the effector, as the HR strength of the truncated TIR does not differ between L6 and L7 (Bernoux et al., 2011).

### **Polymorphic residues within the TIR domains of L6 and L7 are also responsible for differences in the nucleotide binding of the proteins**

The same TIR residues that alter the HR phenotype of L6 and L7, also effect the nucleotide binding of L6 and L7. As Figure 3.7 shows, the L6 SRR/FCY mutant has increased ADP binding compared to wild type L6. The L7 FCY/SRR mutant causes decreased ADP binding, to levels comparable to L6. This correlates with the HR phenotypes seen in Figure 3.3, with proteins that purify with lower levels of bound ADP having a stronger HR phenotype. Inversely, those with higher ADP binding have a weaker HR phenotype.

Given all these amino acid changes are located in the TIR domain, and not the nucleotide binding domain, it appears that the interaction between the two domains is different between the two proteins, and that this interaction is the likely cause of the differences in HR phenotype and nucleotide binding properties. Examining differences between the nucleotide binding domain sequences of strong and weak L alleles identified several residues of interest.

## **A residue in the Nucleotide Binding domain of L7 promotes autoinhibition?**

As Figure 3.3 shows, eight different residues in the NB-ARC domain of L7 were chosen to generate mutations and examine the HR phenotype in *N. benthamiana*. One residue (C288) stood out. As shown in Figure 3.2 this cysteine residue is not conserved between L6 and L7, and other L alleles with a strong HR phenotype, including L5, L10 and L2.

Changing the cysteine to an arginine in the L7 protein resulted in a significant change to the HR phenotype and the nucleotide binding properties, producing an HR phenotype and a reduced ADP binding protein equivalent to the L6 and L7 FCY/SRR proteins. The same change in L6 did not abrogate or enhance HR, and presumably did not affect the nucleotide binding properties in the wild type protein, however it did enable the L6 SRR/FCY mutant to regain a strong HR phenotype. Presumably this protein (L6 SRR/FCY+C288R) would purify with lower levels of bound ADP, although this protein was not analysed in this study.

These data further suggest that interaction between the TIR and NB domains is a key difference between the L6 and L7 proteins. Based on a comparison of the protein sequences of L6, L7 and other L alleles, it is tempting to speculate that the cysteine present in L7 is the major factor in its inhibition. L2, L5 and L10 all have the same amino acids in the  $\alpha$ A region of the TIR domain as L7, however, all three L2, L5 and L10 proteins produce a robust HR in both *N. benthamiana* and flax. The cysteine residue in the TIR domain of L7 could be interacting with the cysteine in the NB domain, forming a stronger bond to that that seen in L6, L2, L5 and L10, all of which have only a single cysteine in either of these positions. Structural studies of full-length proteins would reveal if a disulphide bond between the two cysteines in L7 prevents the release of auto-inhibitory interactions between the two domains.

Interaction experiments between the TIR domain and NB domains of each of these NLRs would provide more insight into this regulatory mechanism. There is a precedent for intra-molecular interactions between other NLR domains and the TIR domain that

contribute to the inhibition of plant TIR signalling (Moffett et al., 2002, Bernoux et al., 2011). The crystal structure of the inactive form of APAF-1 shows the CARD domain also obscures access of the ADP molecule to the solvent (Riedl et al., 2005) demonstrating some negative regulation by signalling domains in other related proteins. Structural information of L6 or L7 TIR and NB-ARC domains would provide some more details on this interaction.

### **L6 and L7 effector interaction – ADP as a negative regulator?**

Given that the TIR domains of L6 and L7 have no difference in their ability to signal when expressed without the NB-ARC and LRR domains, examining intra-molecular interactions between domains and with the effector are crucial. Yeast-2-hybrid assays provide some insights into the interaction between NLR and effector, and have been used extensively in the field (Catanzariti et al., 2010).

In yeast-2-hybrid assays L6 can interact with AvrL567, but the interaction between L7 and AvrL567 is much weaker (Bernoux et al., 2016). The interaction between L6 and AvrL567 is abrogated by the SRR/FCY mutations but can be returned to wildtype L6 levels by introducing the C288R mutation. AvrL567 can interact with both L7 FCY/SRR and L7 C288R, the two mutants to give a L6-like HR phenotype.

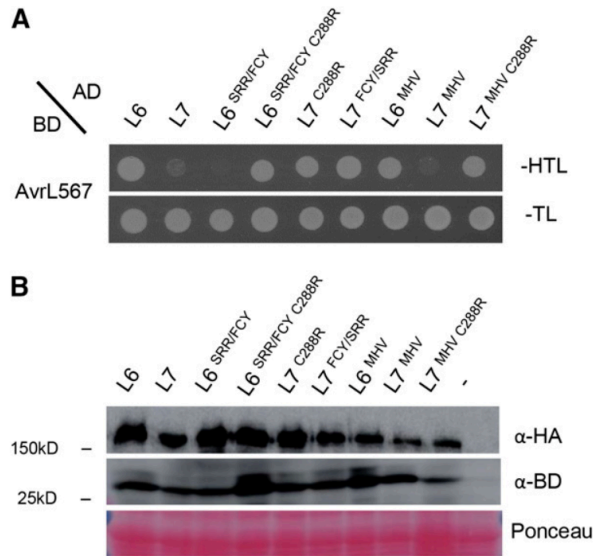


Figure 3.8 'R/Avr Physical Interaction in Yeast.'. **A** yeast-2-hybrid assay showing interaction between AvrL567 and L6/L7 and mutants. **B** Immunoblot showing expression of NLRs and effectors. A Ponceau stain was used as a loading control.

Work of others, adapted from Bernoux et al. (2016)

This yeast-2-hybrid assay interaction data correlates with both HR phenotypes and nucleotide binding data; a protein that can interact with the effector has low ADP binding and can signal HR, whereas proteins that have weak interaction with the effector also have high ADP binding, and cannot signal HR.

What comes first in this interaction? Is it the interaction with effector required for a change in the nucleotide binding properties of the protein that then enables signalling, or does the protein need to be in an ATP bound conformation to bind the effector, after which signalling can occur? To explore this, we observe some properties of the MHV mutations in both L6 and L7.

### **L6 MHV and L7 MHV - autoactive mutations?**

The MHD motif is a conserved region in the ARC2 subdomain of plant NLRs. Many studies have shown that mutation of this residue creates an autoactive form of the NLR, able to induce effector-independent HR. L6 is consistent with other NLRs, as shown in Figure 3.9A, with an MHV mutant able to induce AvrL567-independent cell death. In contrast, L7 MHV was unable to induce effector-independent HR.

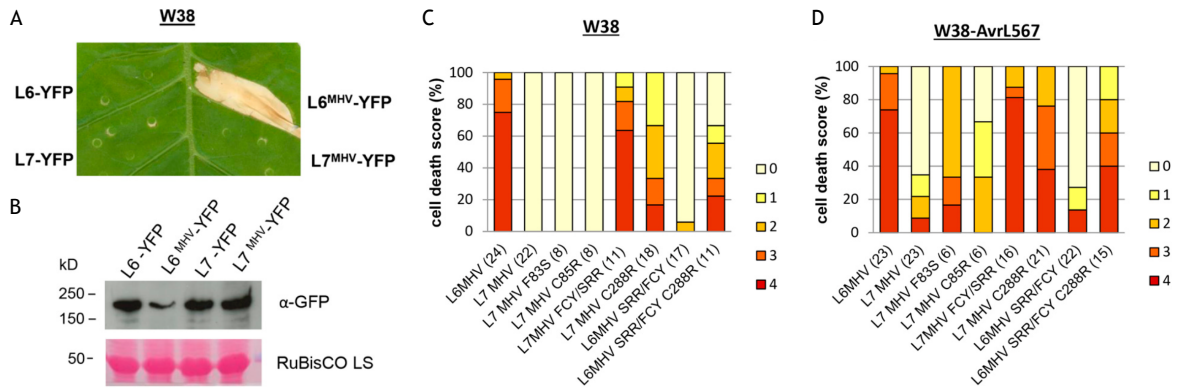


Figure 3.9 L7 MHV is unable to induce effector-dependent and -independent cell death activation, but reciprocal mutations in the TIR (83,85,86) and NB (288) regions of L7 and L6 have restorative and complementary effects on L7 MHV effector-independent signalling activity. **A** Sample of HR of L6, L7 and MHV mutants fused to YFP expressed in tobacco leaves in absence of effector protein. **B** Anti-GFP immunoblot showing expression of NLR proteins in A. RuBisCO is used as a loading control as visualised by Ponceau stain. HR scoring of mutants in **C** absence of effector AvrL567 and **D** presence of effector follows the same scoring as in Figure 3.3A.

Work of others, adapted from Bernoux et al. (2016).

Whilst L6 MHV is able to signal auto-activity *in planta*, like the M MHV mutant (Williams et al., 2011), L6 MHV was found to be purified with negligible ATP and ADP, in contrast to preference for ATP of M MHV measured by Williams et al. (2011). This may be attributed to a more flexible, less stable L6 MHV protein, losing structure during the purification process, as reflected by both lower yields from *P. pastoris*, and during agro-infiltration in *N. benthamiana*, shown by immune-blot analysis in Figure 3.9B. This loss of structure could be explained by a decrease affinity for ADP binding, key for co-ordinating the domains of an NLR in its inactive state, however more experiments are required to test this hypothesis. Work by Tameling et al. (2006) on the CC-NB-ARC domain of I-2 observed similar behaviour of the ATP binding domains. They were able to capture I-2 CC-NB-ARC in the ADP form with relative ease, however the ATP bound form was much more unstable and difficult to work with.

L7 MHV saw no change in bound ADP, having the same ADP occupancy as the wild type L7 protein. This again correlates with an ADP bound and inactive NLR. Additionally, unlike L6 MHV, L7 MHV was able to be purified to reasonably high yields, comparable to wild type, and showed similar expression levels during agro-infiltration, shown in Figure 3.9B. This result again highlights the importance on an ADP molecule in stabilising the NLR, and that nucleotide exchange is required for release of inhibitory interactions of the NB-ARC with the TIR domain. The ADP bound form is clearly inactive, whilst the ATP bound form is quite unstable. This suggests that there must be some balance between the two forms.

### **MHV and the L6/L7 polymorphisms: on again off again**

Introducing reciprocal changes in the TIR domains of L6 and L7 also changes the properties of the MHV mutant forms and their effector-independent (Figure 3.9C) and effector-dependent (Figure 3.9D) HR *in planta*. As Figure 3.9C shows, introduction of the SRR/FCY mutation into a L6 MHV full-length protein completely suppresses auto-activity in tobacco, and severely weakens AvrL567 induced HR. The reciprocal mutation, L7 FCY/SRR, enables the full-length L7 MHV to induce both effector independent HR and effector dependent HR. Introduction of the C288R mutation into L6 MHV SRR/FCY and L7 MHV also allowed for effector independent HR, but slightly

weaker than L6 MHV and L7 FCY/SRR MHV. This mutation also results in slightly stronger effector dependent HR in both L7 C288R MHV and L6 SRR/FCY C288R MHV proteins.

Nucleotide binding experiments were not performed for these particular mutant proteins, but it is likely, based on other mutations and *in planta* data, that the L6 SRR/FCY MHV mutation would bind ADP to similar levels as L7, L7 MHV and L6 SRR/FCY proteins. It is less clear whether the nucleotide binding capacity of the L7 FCY/SRR MHV mutant protein would resemble that of L6 MHV due to decreased stability of the protein, or an ATP bound state as described by Williams et al. (2011), but it is highly unlikely that the mutant would bind ADP levels comparable to the wild type protein and still induce effector independent HR. The nucleotide binding of the C288R mutations in the L7 MHV and L6 SRR/FCY MHV protein is also unknown. It is again likely that these proteins bind less ADP than the L7 MHV mutation, but whether they bind ATP or have negligible ATP or ADP bound due to instability is difficult to predict.

These mutations give some insight into the activation of NLRs, showing that there are two key changes required before signalling can be introduced: (a) exchange of nucleotides and (b) interaction with the Avr effector. Other NLRs with this MHV mutation have been shown to be bound to ATP and to be autoactive (Williams et al., 2011). Perhaps these proteins are more stable in solution than L6 MHV, and do not have strong affinity for ADP like L7 MHV.

### **How does L6 and L7 nucleotide binding data compare to other nucleotide binding proteins?**

The nucleotide binding data of L6 and L7 are similar to that of other expressed and purified NLR proteins, M (Williams et al., 2011), and MLA27 (Maekawa et al., 2011) and consistent with the idea that NLR proteins bind ADP in their native and inactive state. For example, refolded homodimeric MLA-27 was shown to be purified with approximately 43% of the protein bound to ADP, whilst natively purified full-length M was found to be purified with approximately 35% ADP.

Mi-1 and I-2 proteins were also found to bind nucleotides (Tameling et al., 2006), although it is difficult to directly compare nucleotide binding data obtained in these experiments to that of L6 and L7 presented here. This is because Mi-1 and I-2 full-length proteins could not be expressed and purified from *E. coli*, and therefore truncations of the protein were used to measure nucleotide binding. The authors also did not measure the nucleotide content of the proteins, but rather tested the proteins ability to bind exogenous radiolabelled ATP. Both Mi-1 and I-2 were shown to bind both ADP and ATP, whilst the P-loop mutation severely weakened this binding.

Overall, despite very limited studies measuring nucleotide binding of full-length NLRs, L6 ADP binding is consistent with other NLRs, whilst L7 binds more ADP than others reported in the literature. Across many studies, P-loop mutants reduce nucleotide binding, as was the case with L6 and L7. The MHV mutation in M results in an ATP bound state (Williams et al., 2011), in contrast to L6 MHV, which has negligible ATP bound, and L7 MHV, which has ADP binding similar to that of wild type L7.

### **Inhibited NLRs are ADP bound, active forms of NLRs are ATP bound**

There are a few examples of plant and animal NLRs binding ADP and ATP, and there is strong correlation between ADP bound inactive monomers and ATP bound active oligomers. The best characterised example is APAF-1, with ample structural and biochemical evidence to suggest nucleotide exchange is a key part of the formation of the apoptosome. NLRC4, also provides an example of an auto-inhibited NLR, but its activation remains less clear.

The inactive APAF-1 monomer crystal structure, missing the WD40 domain, was found bound to an ADP molecule (Riedl et al., 2005). The CARD domain, NB domain, ARC1 and WHD1 domains are all structured around the ADP molecule, which is buried deep within the protein. In all there are eight bonds between the ADP and APAF-1 monomer, six with the phosphate groups and two with the adenine rings. Exchange of nucleotide is crucial for activation of APAF-1, with the oligomeric apoptosome requiring dATP/ATP to form (Reubold et al., 2009). Although it is still unclear how precisely

nucleotide exchange occurs, some kinetic studies suggest that APAF-1 has a higher affinity for ATP, and higher cellular ATP/ADP ratios may mean that ATP outcompetes ADP for binding to the APAF-1 monomer. Cytochrome C, playing a role of an 'effector' for APAF-1, may enable binding of ATP to occur more quickly, in turn enabling formation of the apoptosome. APAF-1 therefore is a great example of the ADP-bound inhibited and ATP-bound active NLR, which forms the basis of many models of NLR function.

Fellow member of the STAND family, NLRC4, was also shown to bind ADP in its auto-inhibited form (Hu et al., 2013). The crystal structure of NLRC4 revealed that the phosphate groups of ADP gave structure to the flexible Walker A motif of NLRC4, where two more hydrogen bonds occur between the adenine ring and the NB domain, whilst the  $\beta$ -phosphate of the ADP molecule interacts with the histidine in the WHD domain of NLRC4. Interruption of this histidine  $\beta$ -phosphate interaction gives rise to an autoactive phenotype of NLRC4, showing the importance of interactions with an ADP molecule in regulation of protein activation. Unlike APAF-1 however, no ATP was observed in the active NLRC4 complex in the recent cryo-EM structure (Zhang et al., 2015), suggesting that ADP release alone, and not ATP binding is sufficient for NLRC4 signalling, but this remains untested. NLRC4 provides an interesting example for nucleotide binding, with an ADP bound inactive state, and an as yet unidentified active state.

There are obvious parallels between plant NLRs and the two-forementioned mammalian NLRs when it comes to ATP/ADP binding. It would seem the plant NLRs bind ADP in an inactive state, as evidenced here and by others, and that an active plant NLR requires ATP binding to function. The similarities between systems do not end at nucleotide binding, as both APAF-1, NLRC4 and some plant NLRs have been shown to possess ATPase activity, proposed as a means of regulation between the two nucleotide bound states.

## **Some NLRs are capable of ATP hydrolysis, and this may play a role in resetting an active NLR to the inactive state?**

The role of ATP hydrolysis in plant NLR activation is still unclear. It has been well established in APAF-1 that hydrolysis functions as a regulatory mechanism. Any APAF-1 that prematurely binds ATP can be 'reset' back into an ADP-bound form, preventing inappropriate apoptosome formation (Reubold et al., 2009). Some plant NLRs have also been shown to possess ATP hydrolysis activity (Tameling et al., 2006), and it is also thought to function as a regulatory mechanism, however more studies are required to confirm this.

Reubold et al. (2009) proposed that the hydrolysis activity of APAF-1 is purely regulatory, and not required for the formation of the signalling complex, or for signalling activity produced by the complex. This was demonstrated by using a non-hydrolysable ATP analogue, AppNHp, to form a stable, functional apoptosome. ATP (and AppNHp) is required for the formation of the multimeric apoptosome signalling complex, and it has also been shown that oligomerised APAF-1 can no longer hydrolyse ATP (Kim et al., 2005, Reubold et al., 2009). Both of these observations support a model of hydrolysis as a regulatory function, and not a source of energy for driving large conformation changes required to form the apoptosome. Despite the evolutionary distance between plants and animals, plant NLRs may also utilise hydrolysis activity to regulate the premature activation of NLRs.

Tameling et al. (2002) observed that the plant NLRs, I-2 and Mi-1, possess ATPase activity. I-2 and Mi-1 CC-NB-ARC proteins were fused to GST tags and expressed in *E. coli*. Conversion of [ $\alpha^{32}\text{P}$ ] ATP to [ $\alpha^{32}\text{P}$ ] ADP was measured after incubation at 25°C and a  $V_{\text{max}}$  of  $6.2 \pm 1.5$  pmol ATP hydrolyzed.min<sup>-1</sup>. $\mu\text{g}^{-1}$  protein was calculated for I-2. This ATPase activity was dependent on Mg<sup>2+</sup> and mutations to the P-loop prevented ATP hydrolysis from occurring. Mutations that impaired ATP hydrolysis activity, S233F (in the RNBS-A motif) and D283E (in the Walker B motif), created auto-active phenotypes of the I-2 protein (Tameling et al., 2006).

This lower activity was due to impairment in hydrolysis activity, and not nucleotide binding, as evident by the similar  $K_m$  values of the hydrolytic and impaired hydrolytic I-2 proteins. The I-2 S233F mutant was also found bound to significantly less ADP than the wild type counterpart, suggesting that ATP hydrolysis is the likely source of ADP for inactive NLRs. This is supported by empty I-2 protein having a similar affinity for both ADP and ATP (Tameling et al., 2002). Given high cellular ATP:ADP ratios, NLRs are likely to fold with and become associated with ATP. This suggests that hydrolysis, as proposed for APAF-1, play a role in maintaining NLRs in an ADP bound off-state.

M has also been shown to hydrolyse ATP (Sornaraj, 2013). Using [ $\alpha$ 32P] ATP, the ATP hydrolysis rates of M, M K268L (P-loop mutation) and M MHV proteins were measured. The wild type M protein had a  $V_{max}$  of  $2.4 \pm 0.1$  pmol ATP hydrolyzed.min<sup>-1</sup>. $\mu$ g<sup>-1</sup> protein, comparable to that of I-2. The MHV mutant had a faster rate of ATP hydrolysis with a  $K_{cat}$  of 2.63 mol ATP.min<sup>-1</sup> compared to the 0.39 mol ATP.min<sup>-1</sup> for wild-type M. This may be due to an increased binding affinity for ATP, however this is not reflected by a decreased  $K_m$  between wild-type ( $4.5 \pm 1.4$   $\mu$ M) and M MHV ( $9.4 \pm 1.4$   $\mu$ M). Perhaps a reduced affinity for ADP, as a result of faster release of bound ADP is responsible for the increased hydrolysis rate of M MHV. The ability of M MHV protein to both bind more ATP (Williams et al., 2011) and hydrolyse ATP more rapidly (Sornaraj, 2013) than wild-type M protein shows definitively that nucleotide exchange is required for activation of NLRs, and that NLRs are likely to cycle between an ADP and ATP bound form, as, despite the higher hydrolysis rates, M MHV is still found more commonly associated with ATP rather than ADP.

Nucleotide binding and hydrolysis are often presented as part of the switch model, but it is becoming apparent that NLRs are not as static as first thought. A new dynamic model of activation is therefore proposed, as described below.

### **Presenting the Equilibrium-Switch Model**

Plant NLRs are hypothesised to operate by the so-called 'switch' model; in that the NLR exists in two states, an ADP-resting state and an ATP-active state. An effector or elicitor can then trigger the NLR to switch from the ADP-bound resting state to the

ATP-bound active state and initiate downstream signalling events. ATP hydrolysis then returns the NLR back to its ADP-bound inactive state, ready to signal again. It has proven difficult to test this switch model *in vitro*, as recombinant full-length NLRs are hard to purify, there are few NLR/effector pairs that have both NLR and effector identified, and few that work by the direct interaction model. The results presented in this chapter, along with other published literature, hint at a different model of activation of NLRs.

Rather than being in a stasis, bound only to ADP, there is evidence that suggests that the NLR cycles between ATP- and ADP-bound forms in the absence of the Avr effector. I-2 and Mi-1 CC-NB-ARC domains have similar affinities for ADP and ATP (Tameling et al., 2002), CNL MLA27 and TNL M can bind ADP and ATP *in vitro* (Maekawa et al., 2011, Williams et al., 2011), and autoactive M mutant MHV protein preferentially binds ATP *in vitro*. I-2 and Mi-1, APAF-1, NLRC4 and M also possess ATPase activity (Tameling et al., 2002, Reubold et al., 2009, Hu et al., 2013, Sornaraj, 2013), even in absence of an elicitor, suggesting they cycle between their on and off states, rather than remain locked into an inactive ADP bound state.

Interaction with the effector may also not be favourable in the ADP-bound conformation. Yeast-2-hybrid assays identified a correlation between ADP binding and NLR/effector interaction. NLRs that could induce HR (L6, L6 MHV, L6 FCY/SRR C288R, L7 SRR/FCY, L7 C288R, L7 C288R MHV) were all able to interact with AvrL567 *in planta*, and those tested all had reduced ADP binding when purified from *Pichia pastoris* compared to NLRs that could not interact, or had weaker interaction, with AvrL567 (L7, L6 SRR/FCY, L7 MHV). This correlation suggests that the NLR must be in an ATP-bound form to bind an effector. NLRs presumably then cycle between an ADP-bound and ATP-bound state in the absence of the effector.

Hydrolysis of ATP is likely to return the NLR to an ADP bound state. This hydrolysis and nucleotide exchange represents an equilibrium of ADP and ATP bound states of the NLR within an uninfected plant cell. This equilibrium is then shifted to the active ATP bound form in the presence of an effector. There is evidence that active,

oligomeric NLRs in complex with their elicitor lose their ability to hydrolyse ATP (Reubold et al., 2009), and this loss of activity would result in a shift toward the ATP-bound side of the equilibrium. This slow accumulation of the ATP-bound state would also ensure a slow initiation of HR, and would presumably reach a point of no return, when there are sufficient ATP-bound NLRs in an activated, signalling state. Support for a threshold of HR activation is suggested in the literature (Morel and Dangl, 1997).

L6 presents a sufficient amount of the 'active' form for AvrL567 binding, enabling it to become activated and signal. L7, due to its increased retention of ADP caused by regions of the TIR domain and nucleotide binding domain, is unable to present as much ATP-bound NLR for AvrL567 binding, and thus cannot induce HR as quickly and robustly as L6. The reciprocal L6-L7 mutants in the TIR domain changes the ability of the NLR to retain ADP, and thus shift the ATP/ADP equilibrium away from the inactive ADP bound form to the active form. A schematic of the equilibrium-switch model of NLR activation is shown in Figure 3.10.

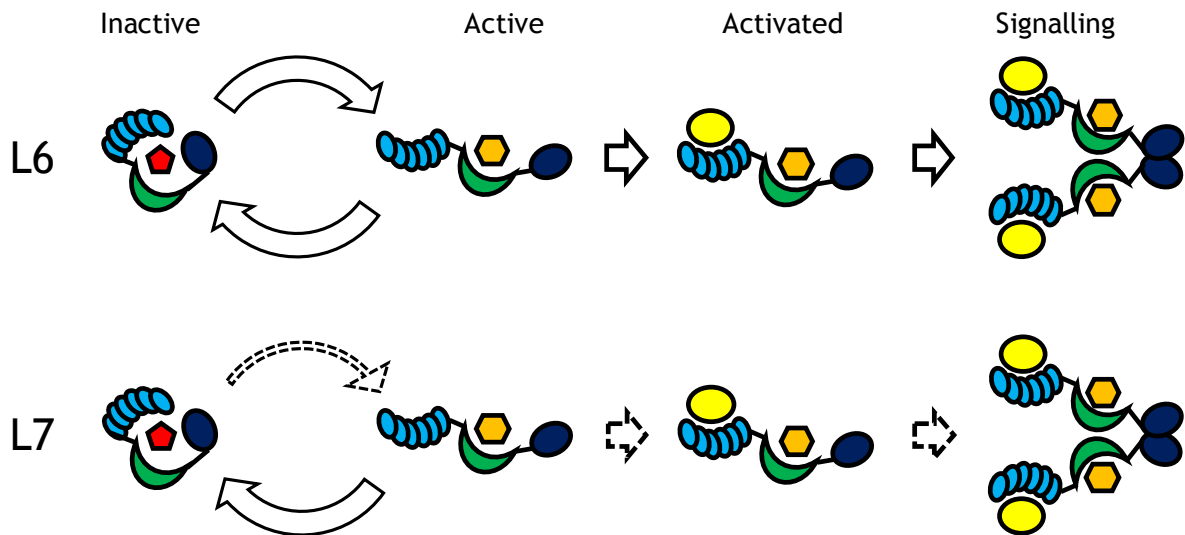


Figure 3.10 Equilibrium-Switch Model for plant NLR activation, joint work of others and I, adapted from Bernoux et al. (2011). Simplified graphical representation of activation of NLRs. The dark blue oval represents the TIR domain, green crescent the NB-ARC domain and the light blue chain of ovals the LRR. The red pentagon represents ADP, and orange hexagon ATP. The Avr effector is represented by a yellow oval. Arrows with solid line indicate normal response, whilst dashed arrows indicate a relatively weaker response. NLRs cycle between an inactive and active state in an uninfected plant cell. The inactive state is coordinated by binding of ADP. The NLR can shift into the active state by binding ATP. This nucleotide binding may occur due to higher ATP/ADP ratios in the cell, and upon the initial folding of the NLR. Hydrolysis of the bound ATP resets the NLR to an inactive ADP bound form. An infected plant cell will have NLRs interact with effector proteins. The ATP bound active form is able to recognise the effector. Effector binding could lock the NLR in the ATP bound state, thus enabling the TIR domains to self-associate and enable immune response signalling. L6 cycles more readily between its ADP and ATP bound state than L7, as evidenced by their differing phenotypes and their nucleotide binding properties. As more ATP form is presented for AvrL567 binding, more L6 is locked into the ATP-bound form and can signal. The is much less L7 in the ATP-bound form, and thus less able to bind AvrL567 and signal immune responses.

Other NLRs and STANDs are also thought to function by this equilibrium-switch model. APAF-1 can bind both ATP and ADP in the absence of cytochrome c and possesses slow steady hydrolysis to 'reset' the active protein. It is likely to be cycling between an ADP-bound and ATP-bound state. It is still not clear whether APAF-1 binds ATP before it binds cytochrome c or after, however upon binding of cytochrome c, APAF-1 forms an apoptosome, and loses the ability to hydrolyse ATP, in a similar manner to the model proposed for L6 and L7 activation.

An equilibrium-switch activation mechanism is also supported by the activity of MalT, a bacterial member of the STAND family of receptors. Danot (2015) found that the ARC2-equivalent domain in MalT was involved in intramolecular interactions holding the protein in a closed state. Crosslinking this region with the NB domain locked the protein in an ADP-bound off state. Measuring affinity for the elicitor, maltotriose, Danot (2015), found a reduced affinity for the crosslinked mutant than the wild type protein. This suggests that MalT needs to change conformation in order to present an active form for elicitor binding and signalling to occur, echoing the features of the NLR equilibrium-switch model.

## **Future work and conclusions**

Whilst the results reported in this chapter form the basis for the equilibrium-switch model of NLR activation, there remain numerous questions. How does the ATP hydrolysis activity of L6 and L7 compare to other plant NLRs, and other NLRs in general? These will be key experiments to test the validity of this model but were not possible to do considering the number of potential contaminating ATPases in the IMAC purified L6 and L7 proteins used in this chapter.

Is there difference in the interaction between the TIR domain and NB domain of L6 and L7? Does the TIR domain block access to the nucleotide binding domain, in a manner similar to the CARD domain blocking access to the nucleotide binding domain in the Apaf1 crystal structure solved by Riedl et al. (2005). Solving the structure of L6, or L7, or any plant NLR for that matter, would provide a wealth of knowledge on the

interplay of domains of these NLRs. The full-length structure of a plant NLR is still the holy grail for many in the field.

Interaction studies using domains may be a more realistic short-term approach, as domains of NLRs are more easily expressed and purified. There are a range of protein-protein interaction techniques that could be employed to measure such interactions, including SPR, ITC, and MST. Analysis of the kinetics of the interaction between the effector and NLR proteins would also be a good way to test the model, particularly in ATP/ADP bound forms. The limiting factor for many of these experiments with NLRs is the difficulty in producing soluble pure protein. In the next results chapter, I present a modified NLR purification protocol that is much faster and produces more protein of higher purity from *P. pastoris* cells. I also report attempts to purify two NLRs from other species and report the nucleotide binding properties of M from this modified purification protocol.

# Chapter 4 - Improved purification of flax NLRs M, L6 and L7

## Introduction

*'Do not waste clean thinking on dirty enzymes' - Efraim Racker*

*'Don't waste clean thinking on dirty protein' – Colin Jenkins*

Purification of plant NLRs has proven to be extremely challenging, with few full-length or near full-length NLRs expressed and purified. Even among purified full-length proteins, yields are low (Schmidt et al., 2007, Williams et al., 2011), and samples are far from homogenous (Bernoux et al., 2016). NLR research has been buoyed by the expression and purification of the mammalian proteins APAF-1 and NLRC4 with sufficient yield and purity to conduct structural and biochemical experiments, including enzyme assays, cryoEM, crystallography and protein-protein interaction assays (Riedl et al., 2005, Reubold et al., 2009, Reubold et al., 2011, Hu et al., 2013, Hu et al., 2015, Zhang et al., 2015).

Many of the biochemical studies to date have been conducted on truncated constructs of NLRs, and whilst hugely informative, often provides more questions than answers. An example of this is the conflicting data of Tameling et al. (2006) on I-2 and Mi and Ueda et al. (2006) on the tobacco N protein, where it is suggested that I-2 and Mi are bound to ADP in non-stressed conditions, and whilst N is postulated to bind to ATP in non-stressed conditions. Expression of full-length NLRs, of high purity and concentration, would enable a more robust investigation of NLR activation.

The first generation of full-length NLR purification resulted in low yields of impure protein. Schmidt et al. (2007) and Williams et al. (2011) presented methods for expression and purification of flax NLR expression, with expression in *Pichia pastoris*, and purification by immobilised metal affinity chromatography (IMAC). This method resulted in purity of M and L6 of ~70%, with protein yields of 10-40 µg.g<sup>-1</sup> of *P. pastoris*

cells. Such concentrations and yields made it difficult to perform biochemical experiments other than the nucleotide binding data presented by Williams et al. (2011).

Sornaraj (2013) reported a modification of the technique described in Williams et al. (2011) that included a second affinity-tag. The Strep-tag II on the C-terminus of M and L6 enabled purification of these NLRs to >90% purity, first by purifying by IMAC, then by StrepTactin affinity chromatography (SAC). The downside of this protocol was a significant increase in purification time and the subsequent decrease in yield and loss of nucleotide from the binding site. These problems made it difficult to perform many diverse experiments with sufficient replication from a homogenous batch of protein.

This chapter presents a modification to this method of NLR purification, that enables the rapid purification of flax NLRs M, L6 and L7, to much higher purity (>90%) than methods previously described. NLRs were expressed in *Pichia pastoris*, and lysates prepared as described by Schmidt et al. (2007), Williams et al. (2011) and in chapter 3 of this thesis. The purification employs the use of the Strep-tag II and SAC purification methods, as described by Sornaraj (2013), but with omission the IMAC step. This technique was also used to attempt to purify two other NLRs, Sr33 from *Aegilops taucshi* (Periyannan et al., 2013) and RUN1 from *Muscadinia rotundifolia* (Barker et al., 2005).

## **Methods**

### **Constructs**

Constructs coding for M, L6 and L7 containing an N-terminal 6xHis-tag and a C-terminal Strep-tag II were available in the laboratory (Sornaraj, 2011). Full-length Sr33 cDNA was cloned into pP6H3C by Adam Bentham and was transformed into *P. pastoris* by Stephanie Davis (Honours student, Flinders University). Full-length RUN1 cDNA was provided by Dr Ian Dry (CSIRO) in the pP6H3C vector and introduced into *P. pastoris* by Stephanie Davis. Both Sr33 and RUN1 constructs contained a N-terminal 6xHis-tag and C-terminal Strep-tag II.

## **Expression and Purification**

Expression and lysis of all NLR containing *P. pastoris* cells was performed as described in Williams et al. (2011) and Bernoux et al. (2016). Clarified lysates were prepared in the same manner as described in the chapter 2 section 'Preparation of Clarified Lysate', with a few changes. These changes were as follows; imidazole was removed from the lysis buffer (50 mM Tris pH 8.0, 150 mM NaCl, 10% glycerol, 0.25 mM Triton X-100, 20 mM  $\beta$ -mercaptoethanol), and lysates were filtered using sterile 0.22  $\mu$ m filters prior to adjustment to pH 8.0 using high pH Strep buffer (100 mM Tris pH 10, 150 mM NaCl).

Before use, StrepTrap HP columns were either washed with water and ten column volumes of Strep buffer (100 mM Tris pH 8, 150 mM NaCl) if unused, or regenerated using HABA and a high pH Strep Buffer (pH 10). Lysate was applied to a 1 mL StrepTrap HP column using a 50 mL superloop, before being washed with Strep buffer. Strep-tag II tagged proteins were eluted using a gradient of 0-10 mM d-desthiobiotin in Strep buffer. Fractions were analysed by SDS-PAGE and Immunoblot, and fractions containing NLR protein were pooled and either used immediately for ATP/ADP assays, or stored at -80°C until required.

## **ATP/ADP Assays**

Assays were conducted as described in chapter three. Additionally, another assay was setup at the same time as the first assay in order to measure change in ATP/ADP occupancy after incubation at 1 h at room temperature before boiling, so as to measure conversion rates of ATP to ADP (if any).

## **Results**

### **M IMAC purification vs M SAC purification**

In order to compare the SAC protein purification method to the IMAC protein affinity purification method, both purifications were performed using cells from the same expression. Lysates for IMAC purification were prepared as described by Bernoux et al. (2016), whilst SAC lysates were prepared without the imidazole in the lysis buffer. The clarified lysate, approximately 20 mL, was applied to a 5 mL HisTrap FF column,

and 15 mL of lysate applied to a 1 mL StrepTrap HP column. The HisTrap column was washed with 10 mM Imidazole, before a gradient elution from 10 mM to 250 mM imidazole. The StrepTrap HP column was washed with Strep buffer before a gradient elution from 0 mM to 10 mM d-desthiobiotin. UV traces of the two purifications be been seen in Figure 4.1.

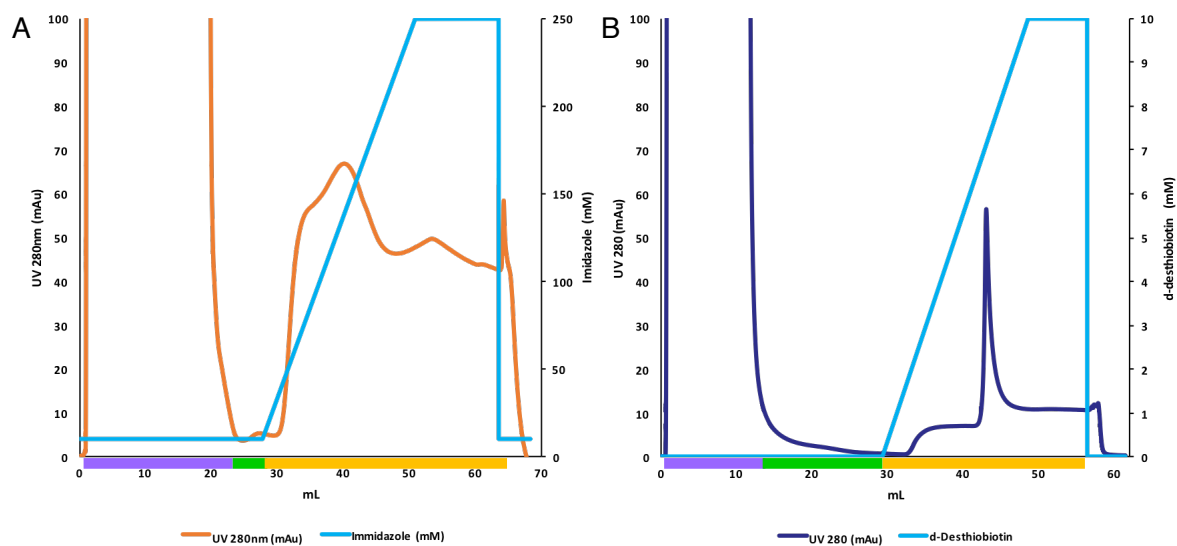


Figure 4.1 UV trace of M IMAC and SAC purifications. **A** UV trace of M IMAC purification, **B** UV trace of M SAC purification. Purple line corresponds to the flow through fractions, green line to the wash fractions and yellow line to the elution fractions.

Figure 4.1A shows an example UV trace for M IMAC purification. The elution peak for M, commencing at approximately 75 mM imidazole, is broad, with M protein visible in every fraction thereafter. Fractions containing M protein, as seen in Figure 4.2, were pooled and concentrated using a 30 kDa concentrator, giving a final concentration of  $375 \mu\text{g}\cdot\text{mL}^{-1}$  in 1 mL at ~30-40% purity, as assessed by Imagelab software, and a yield of  $33.5 \mu\text{g}\cdot\text{g}^{-1}$  of *P. pastoris* cells, from 10 g of frozen cells.

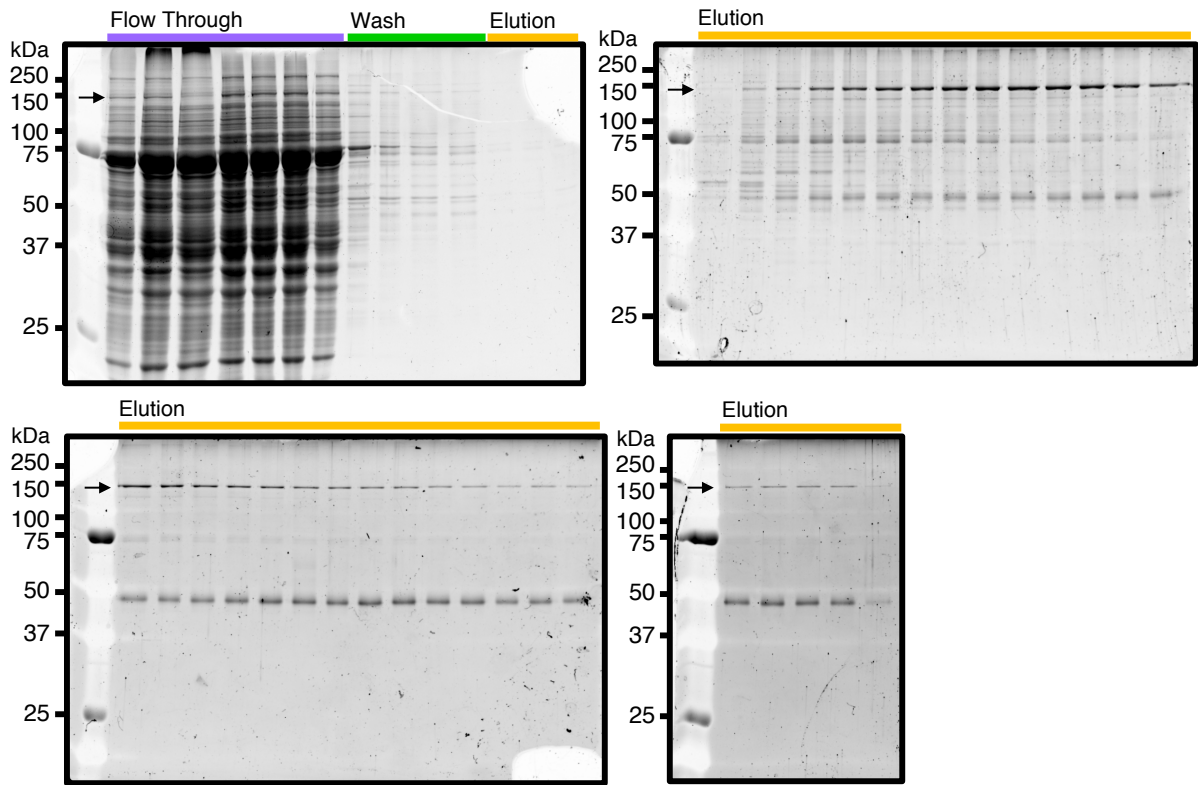


Figure 4.2 SYPRO® Ruby stain of fractions from M IMAC purification seen in Figure 4.1A. Arrows indicate the band corresponding to M protein, purple indicates the flow through fractions, green the wash fractions and yellow the elution fractions.

Figure 4.1B shows an example UV trace for M SAC purification. Compared to the IMAC purification elution profile, M eluted in a single, sharp peak at ~5 mM d-desthiobiotin. Analysis of the fractions from the purification in Figure 4.1B by SDS-PAGE can be seen in Figure 4.3, with bands corresponding to M visible across many of the wash and elution fractions. Intense bands corresponding to M can be seen on the third gel, corresponding to the UV peak in Figure 4.1B. The three fractions with the most intense bands were pooled, giving a final concentration of 31.88  $\mu\text{g}\cdot\text{mL}^{-1}$  in 3 mL at >90% purity, and a yield of 30.85  $\mu\text{g}\cdot\text{g}^{-1}$  of *P. pastoris* cells, from 3 g of frozen cells.

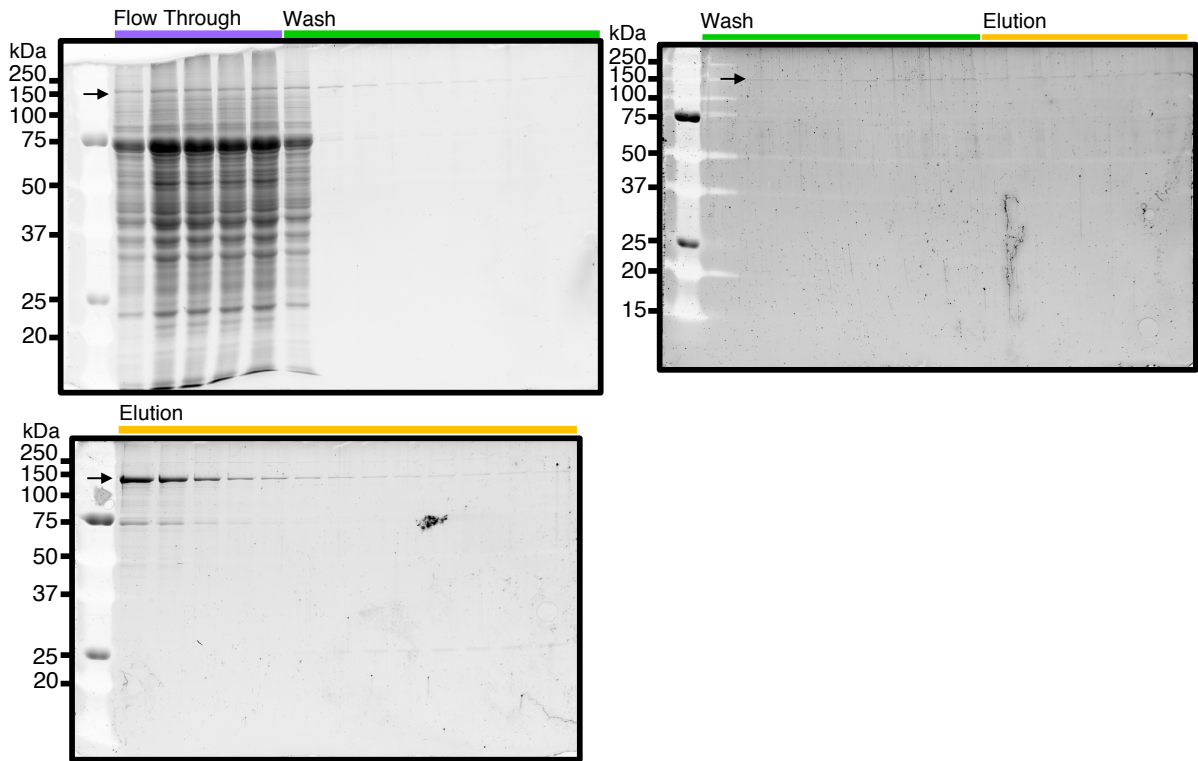


Figure 4.3 SYPRO® Ruby stain of fractions from M SAC purification seen in Figure 4.1. Arrows indicate the band corresponding to M protein, purple bars indicate the flow through fractions, green the wash fractions and yellow the elution fractions.

## **Comparison of purity of M from IMAC, IMAC-SAC and SAC**

The protein purity achieved by each method was assessed by SDS-PAGE and SYPRO® Ruby stain. After destaining, gels were imaged using a Chemi-Doc instrument (Bio-Rad) and resultant images were analysed using ImageLab software (Bio-Rad). Each lane was boxed, and an area for each band within the lane was assigned. Volume analysis of the lanes took the volume of all bands within a lane, and added them together, before giving a percentage contribution for each band to the total of the lane. This percentage contribution to the total volume was taken as the percentage purity of the protein and represents a more quantitative method than visual analysis done to measure purity in the past. An example of this measurement can be seen in Appendix 3.

As seen in Figure 4.4, the average purity of M IMAC purifications was ~30%, and for M IMAC-SAC and M SAC the average purity was ~85%. There is a clear increase in purity from using SAC compared to the IMAC purification. Whilst there is a decrease in M concentration from IMAC to SAC, the total yield between them is comparable, due to the greater volume of purified protein for SAC. The SAC purification method therefore is superior in purity to the IMAC method and provides higher yields than the combined IMAC-SAC method.

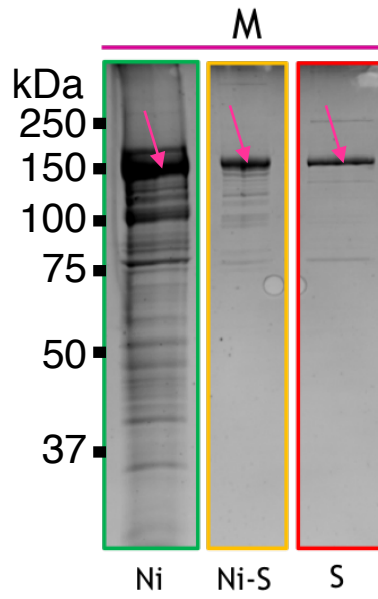


Figure 4.4 Comparison of different M purification techniques by SDS-PAGE and SYPRO® Ruby stain. Ni - IMAC only purification, Ni-S - IMAC purification, followed by SAC purification, and S - SAC purification only. Pink arrows indicate band corresponding to full length NLR

## **L6 and L7 can also be purified using the SAC method**

Given the success of the M SAC purification, attention was turned to L6 and L7 proteins. As seen in chapter 3, the IMAC purification method for L6 and L7 yielded low purity samples, unsuitable for many biochemical and biophysical experiments. Therefore L6 and L7 were also purified by SAC. A typical UV trace for L6 SAC purification can be seen in Figure 4.5, showing a sharp peak comparable to that observed for M, but reaching a much higher absorbance peak at 280 nm. The final concentration of the pooled fractions from the peak was  $141.3 \mu\text{g}\cdot\text{mL}^{-1}$  in 4 mL, with a yield of  $149 \mu\text{g}\cdot\text{g}^{-1}$  of *P. pastoris* cells. The yield of L6 protein was over three times that of IMAC ( $45.8 \mu\text{g}\cdot\text{g}^{-1}$ ) and almost 200 times that of IMAC-SAC ( $0.9 \mu\text{g}\cdot\text{g}^{-1}$ ). The purity was comparable to the L6 IMAC-SAC method. Collectively, these data indicate that the SAC purification method is applicable to other flax NLRs. Comparisons of all three methods for L6 purification can be seen in Figure 4.7.

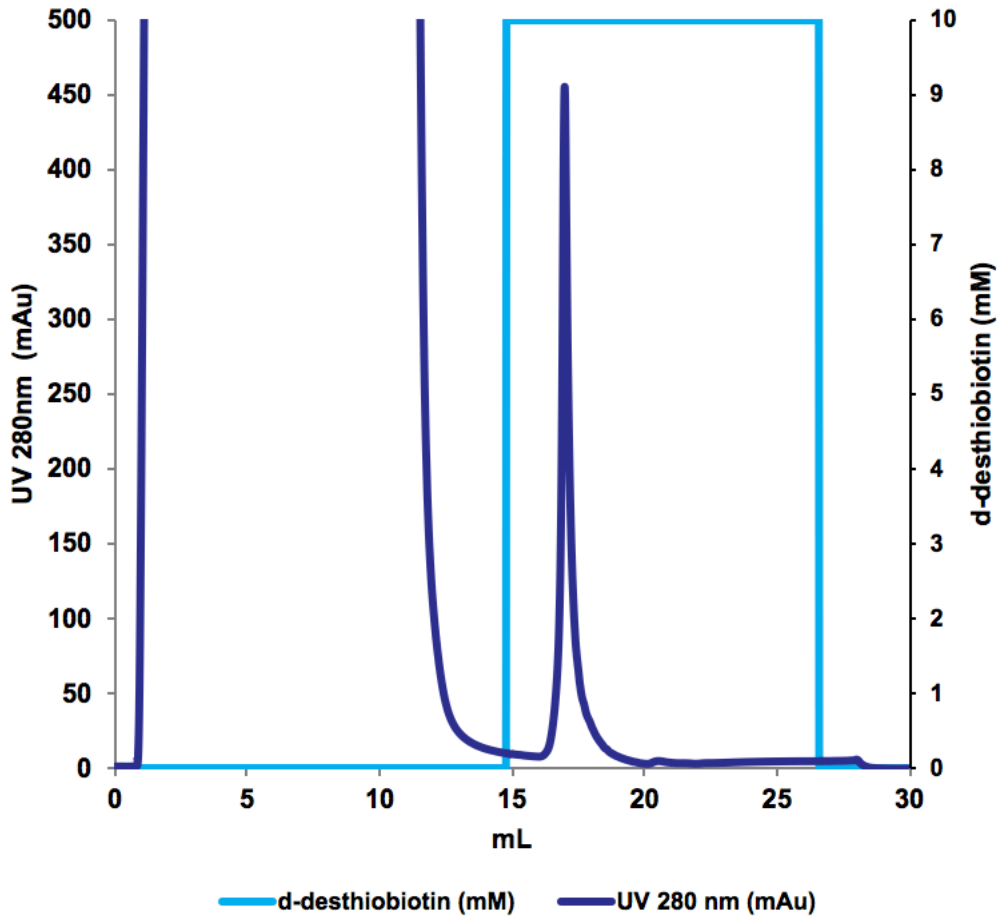


Figure 4.5 UV trace of L6 SAC purification. UV 280 is shown in dark blue, whilst the d-desthiobiotin concentration is shown in cyan. A large peak corresponding to L6 can be seen at the 17-18mL mark.

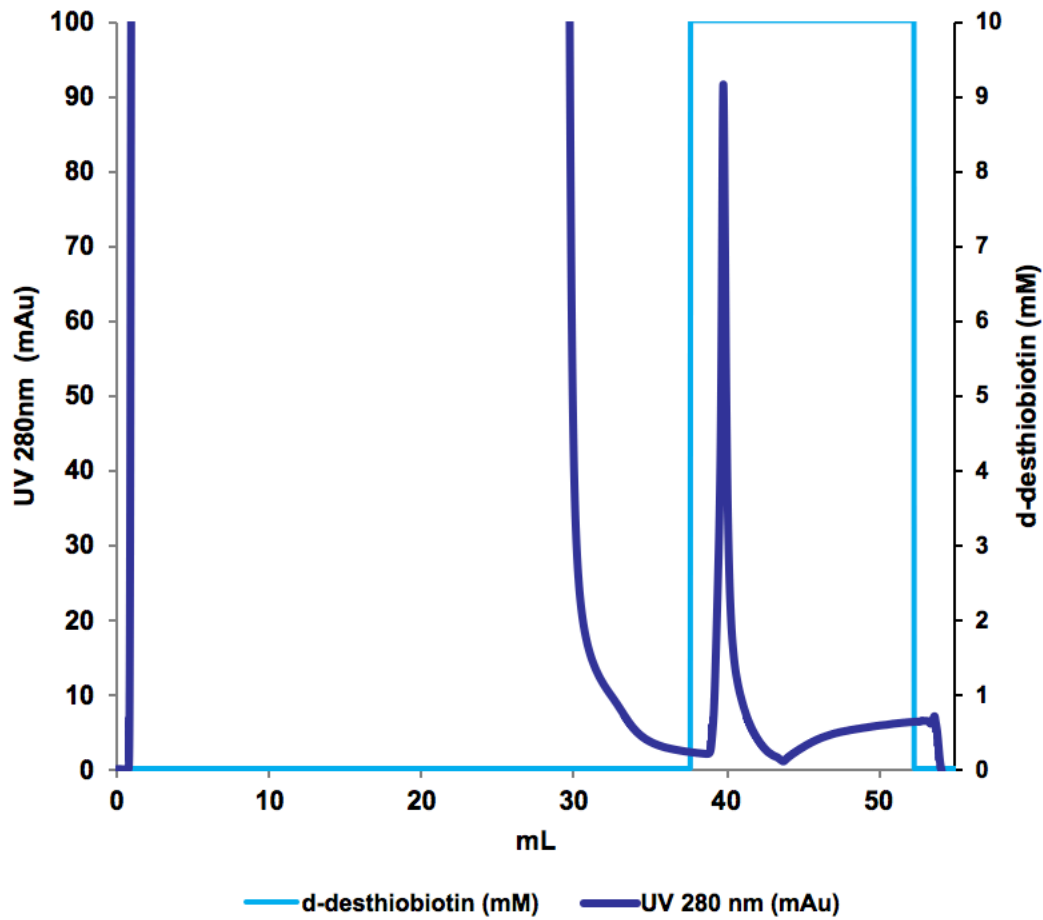


Figure 4.6 UV trace of L7 SAC purification. UV 280 is shown in dark blue, whilst the d-desthiobiotin concentration is shown in cyan. A large peak corresponding to L7 can be seen at the 40 ml mark.

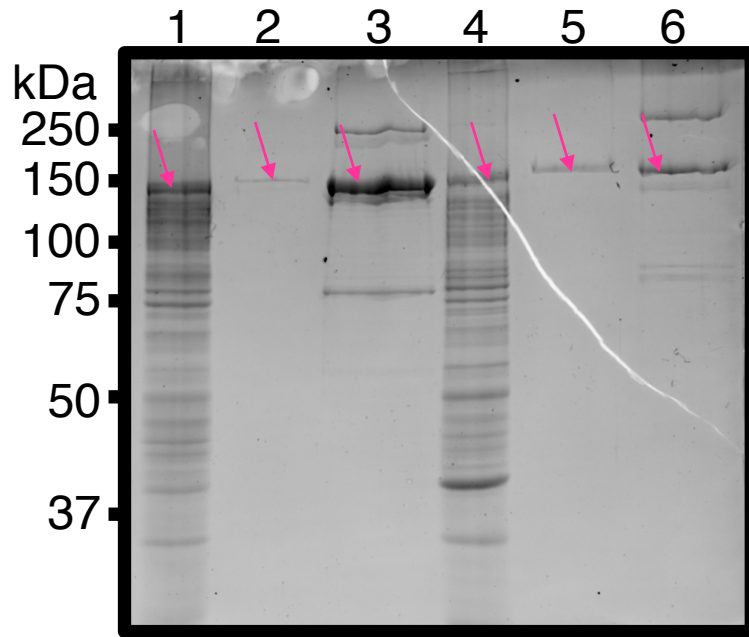


Figure 4.7 Comparison of different L6 and L7 purification techniques by SDS-PAGE and SYPRO® Ruby stain. Lane 1 L6 IMAC, Lane 2 L6 IMAC-SAC, Lane 3 L6 SAC, Lane 4 L7 IMAC, Lane 5 L7 IMAC-SAC Lane 6 L7 SAC. Pink arrows indicate band corresponding to full length NLR

L7 was also purified using the SAC method. A typical UV trace can be seen in Figure 4.6, showing a sharp elution peak comparable to M and L6. Fractions corresponding to the peak were pooled, with a final concentration of  $27.90 \mu\text{g.mL}^{-1}$  in 4 mL, with a yield of  $27.91 \mu\text{g.g}^{-1}$ , comparable to M SAC purification yields. The yield was comparable to L7 IMAC purified protein ( $39.49 \mu\text{g.g}^{-1}$ ) and much higher than L7 IMAC-SAC purified protein ( $0.28 \mu\text{g.g}^{-1}$ ), with the purity comparable to L7 IMAC-SAC purified protein. Comparisons of purity and concentration of L7 IMAC, L7 IMAC-SAC and L7 SAC purifications can be seen in Figure 4.7.

### **Western blots of M L6 and L7 SAC purified protein**

To confirm the presence of the purified NLRs, and to determine if any co-purifying proteins were N-terminal or C-terminal breakdown products, anti-6xHis-tag and anti-Strep-tag II western blots were performed on SAC purified and concentrated M, L6 and L7 proteins. As Figure 4.8 shows, the only immune reactive band seen for each of the purifications in both the anti-6xHis-tag and anti-Strep-tag II western blots was a band at  $\sim 145$  kDa, demonstrating the NLRs were purified without degradation.

In summary, the SAC method of purification is faster than IMAC and the IMAC-SAC method, provides higher yields and greater purity than the other two methods, and results in stable NLRs. To confirm that the proteins were still functional, and to compare the purification method to the IMAC purification method used in chapter 3, the level of ATP/ADP binding occupancy was measured.

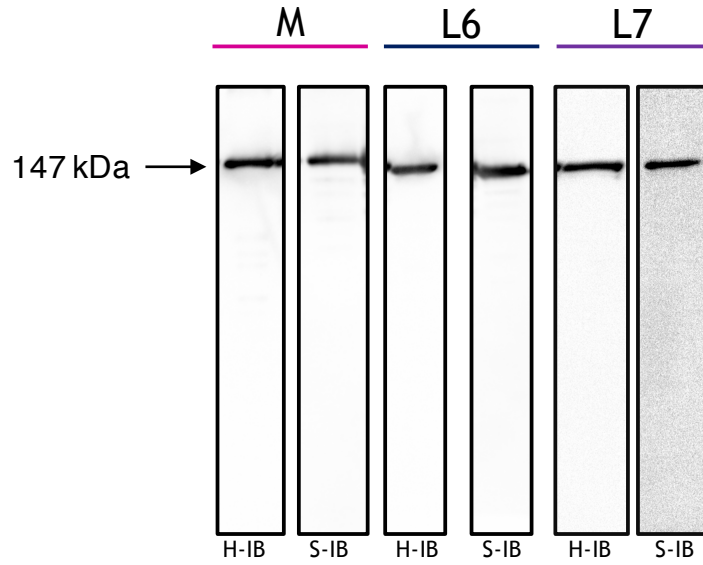


Figure 4.8 Western Blots of SAC purified M, L6 and L7. Anti-6xHis-tag (H-IB) and anti-Strep-tag II (S-IB) westerns blots of SAC purified M, L6 and L7 protein. Monoclonal mouse anti-6xHis-tag was used as the primary antibody, with a goat anti-mouse peroxidase conjugate as the secondary antibody, whilst a polyclonal rabbit anti-Strep-tag II was used as the primary, with a goat anti-rabbit conjugate used as the secondary. Both blots were developed using the Amersham ECL Select Western Blotting Detecting Reagent and imaged with a ChemiDoc (Bio-Rad).

### **ATP/ADP binding of M IMAC and SAC purified protein**

To measure the bound nucleotide in the SAC purified M protein, the same luminescent assay was used as described in chapter 3. As seen in Figure 4.9, M purified by IMAC was found bound with  $2 \pm 0.1\%$  ATP and  $35 \pm 3\%$  ADP, comparable to occupancy measured in Williams et al. (2011). In comparison, the M purified by SAC had an occupancy of  $15 \pm 1\%$  ATP and  $27 \pm 2\%$  ADP. This result shows that the M purified from SAC has a similar capacity to bind nucleotides compared with that of IMAC - purified M. It can therefore be safely assumed that the SAC-purified M protein is likely to be correctly folded.

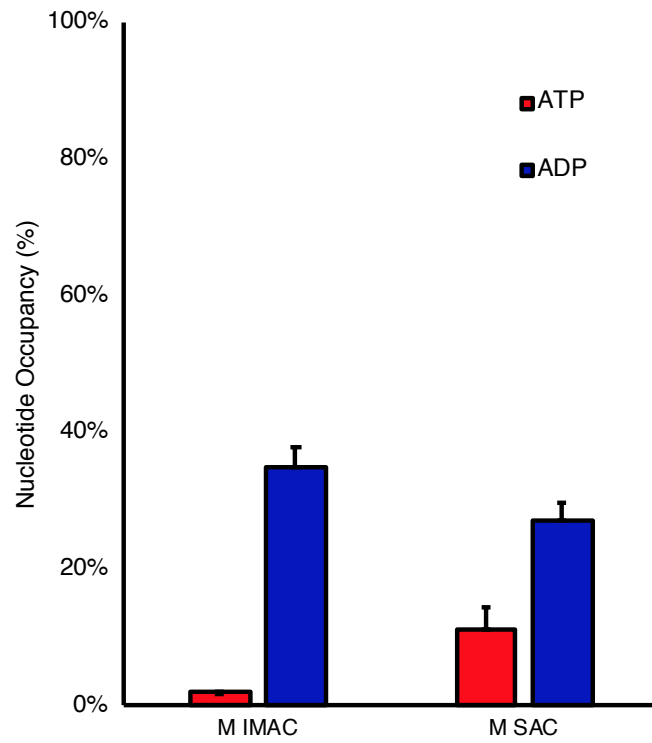


Figure 4.9 ATP/ADP occupancy of M IMAC protein and SAC purified protein. ATP/ADP occupancy is expressed as the number of moles of ATP or ADP per moles of NLR protein purified by either IMAC or SAC. Nucleotide occupancy measurements of both proteins were done from triplicate purifications and recorded with error bars representing the standard error from the mean.

Interestingly, despite having similar total nucleotide binding levels, there is an increase in the amount of ATP bound to the SAC purified M protein compared to the IMAC purified protein. Given the SAC purification method was faster than the IMAC method, it is plausible that more of the M protein has been captured in an ATP-bound form, than the IMAC purified samples due to the extended purification time during which the bound ATP may be hydrolysed to ADP.

To assess if incubation time would affect the change in nucleotide occupancy of the SAC purified sample, some protein was left to incubate at room temperature for 1 h, before nucleotide occupancy was measured again. As shown in Figure 4.10, the occupancy of M changed markedly after 1 h incubation. The ATP occupancy decreased from  $15 \pm 1\%$  to  $6 \pm 2\%$ , and the ADP occupancy increased from  $27 \pm 4\%$  to  $47 \pm 7\%$ . This is consistent with the hypothesis raised above that more SAC purified M protein is captured in ATP bound state because of the faster purification protocol. M could be hydrolysing ATP to ADP during the purification process, and the faster purification time in the SAC method allows some of the ATP bound state to be captured. Further testing of this hypothesis is warranted but was not able to be completed within the timeframe of this project.

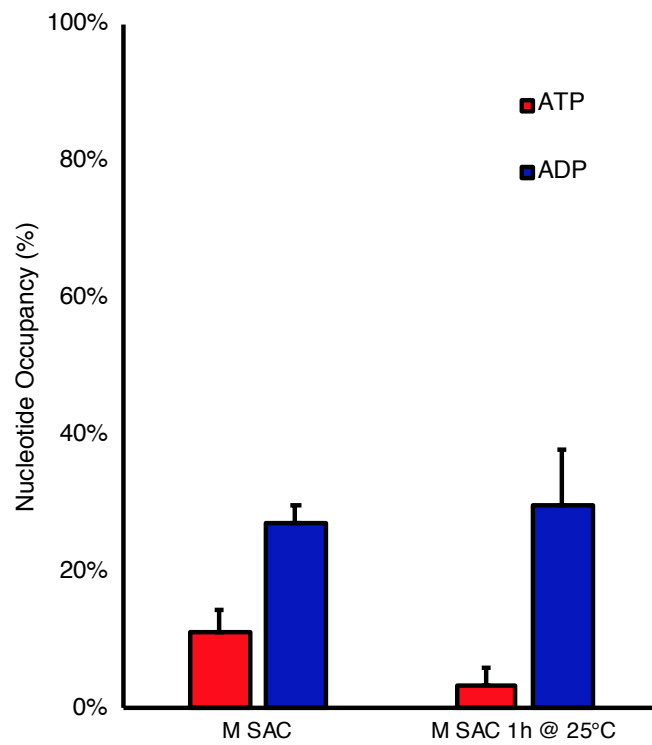


Figure 4.10 ATP/ADP occupancy of M SAC purified protein, before and after incubation at room temperature. ATP/ADP occupancy is expressed as the number of moles of ATP or ADP per moles of NLR protein purified by either IMAC or SAC. Nucleotide occupancy measurements of both proteins were done from triplicate purifications and recorded with error bars representing the standard error from the mean.

## **Purification of other NLRs**

Although this technique proved effective for flax NLRs M and L6, when applied to other NLRs Sr33 and RUN1 it was less successful (Appendix 4), though this was more likely a protein expression issue than an issue with the purification method used, as only weak bands could be seen in the crude lysate samples for both RUN1 and Sr33. Regardless, a method of producing flax NLRs at high purity than IMAC whilst maintaining the protein integrity has been achieved, opening the door to many potential experiments, some of which will be outlined in the discussion below.

## **Discussion**

Expression and purification of full-length NLRs has been difficult, with very few reported successes (Schmidt et al., 2007, Williams et al., 2011, Maekawa et al., 2011, Bernoux et al., 2016). In each instance, either poor yield, poor purity or both made experimentation with the purified protein difficult, with significant contaminants seen for flax NLRs purified from *Pichia pastoris*, (Schmidt et al., 2007, Williams et al., 2011, Bernoux et al., 2016), and low yields for MLA27 purified from insect cells (Maekawa et al., 2011). Whilst important negative controls were used in each case to extract biologically relevant information, the purity and yields have made further experiments, such as crystallisation and protein-protein interaction techniques, difficult or impossible. The SAC purification method described here for the flax NLRs M, L6 and L7 may enable such experiments to be undertaken in the future.

## **SAC purification is an improvement on IMAC purification**

The IMAC method of protein purification was first reported by Schmidt et al. (2007) and adapted for the measurement of nucleotide by Williams et al. (2011) and Bernoux et al. (2016). After optimisation of expression and solubility, Schmidt et al. (2007) were able to produce 3 mg of M protein from 250 g of *P. pastoris* cells ( $12 \mu\text{g}\cdot\text{g}^{-1}$ ), of reasonable purity when assessed by Coomassie stained SDS-PAGE, as seen in Figure 4.11.

In comparison, Williams et al. (2011) used a much lower initial *P. pastoris* cell mass when purifying M and L6 proteins for nucleotide binding assays, starting with just three grams of *P. pastoris* cells. The decreased starting material enabled Williams et al.

(2011) to apply the *P. pastoris* lysate directed to an IMAC column, rather than the CIEX/IMAC tandem approach required for the large amount of *P. pastoris* lysate required by Schmidt et al. (2007). This improved the yield to 20-40  $\mu\text{g}\cdot\text{g}^{-1}$ , and no doubt cut down the purification time dramatically, possibly at the cost of some purity, as visual comparison of the two purifications would suggest (Figure 4.11).

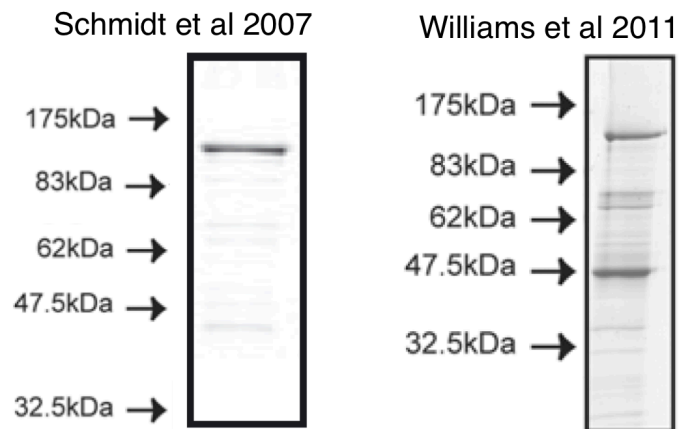


Figure 4.11 SDS-PAGE Coomassie stain of pooled, concentrated full-length M protein from *P. pastoris* reproduced from Schmidt et al. (2007) and Williams et al. (2011), Schmidt et al. (2007) used CIEEX, IMAC and SEC to obtain a yield of  $12 \mu\text{g.g}^{-1}$  from a cell mass used of 250 g. Williams et al. (2011) employed IMAC to obtain a yield of  $20\text{-}40 \mu\text{g.g}^{-1}$  from a cell mass of 3 g.

The SAC purification method reported in this thesis was able to improve both the protein yield and purity compared to other methods, with a yield of M protein of 30.85  $\mu\text{g}\cdot\text{g}^{-1}$  of *P. pastoris* cells produced from 3 g of *P. pastoris* cells, to >90% purity, when assessed by a more sensitive protein stain, SYPRO® Ruby stain. In addition to the increase in yield and purity, the time taken to purify the protein was also reduced, from 10 h with the method described in Williams et al. (2011) to just 3 h. This method was also applicable to L6 and L7, as shown in the Figures above. The SAC method therefore represents an improvement in purification of three flax NLRs. However, how it performs when scaled up to the cell mass used in Schmidt et al. (2007) will be of interest.

### **SAC purification is an improvement on IMAC/SAC tandem purification**

In order to measure the ability of M and L6 to hydrolyse ATP, Sornaraj (2013) and de Courcy-Ireland (2015) devised a tandem purification system, to remove some of the contaminants from IMAC purified M and L6 Figure 4.11. Purification of M using a tandem method involving both IMAC and SAC resulted in increased sample purity (50-70% up to >90%) as seen in Figure 4.12, but involved long purification times, and much lower yields, down to  $\sim 0.5 \mu\text{g}\cdot\text{g}^{-1}$  of cells, and sometimes even lower levels for some mutants of M.

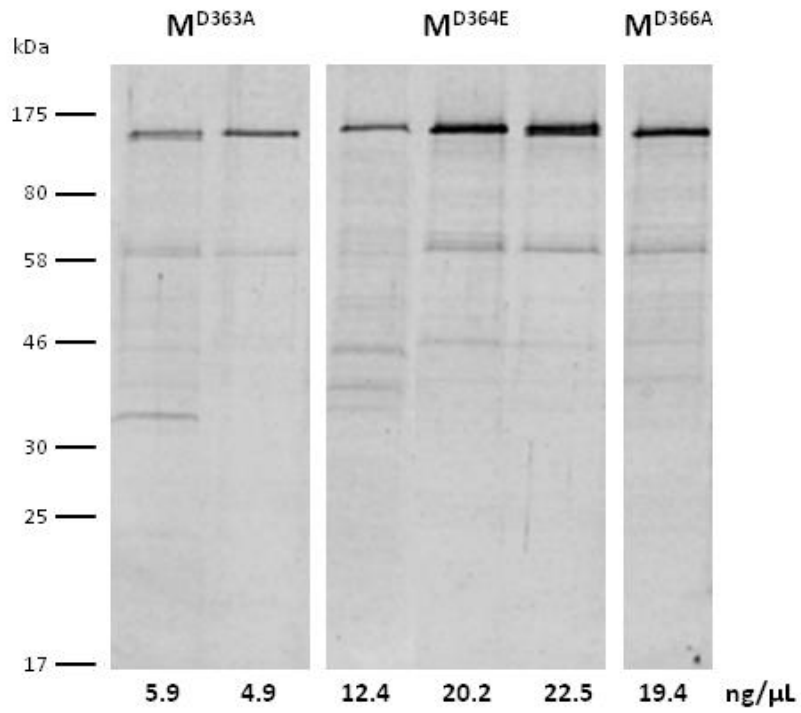


Figure 4.12 SYPRO® Ruby stain of IMAC-SAC purified M mutant proteins, reproduced from de Courcy-Ireland (2015).. Below each lane is the concentration of M for each mutant, determined using a BSA standard curve, in a total of 500 μL.

The SAC method retained the purity of the tandem-purification method, but with a comparable yield to the IMAC method. The nucleotide binding of SAC purified M also indicated that the protein was likely to be folded correctly. Interestingly, the SAC purified M protein was bound to more ATP than the IMAC purified samples, as seen in Figure 4.9. This was thought to be due to a faster purification time, with SAC requiring less time to purify than the IMAC method. This hypothesis was supported by the results of an experiment involving incubating the SAC purified protein at room temperature for one hour and re-measuring nucleotide occupancy. After one hour, the ATP binding was decreased, comparable to that seen for M IMAC purified samples, whilst the ADP binding had increased. This change in occupancy is supported the observations by Sornaraj (2013), that full-length M has the ability hydrolyse ATP into ADP.

The difference in nucleotide binding also provides evidence that supports the equilibrium-switch method presented in chapter 3, as here it is demonstrated that M can bind both ATP and ADP. Whether M can rebind ATP after hydrolysis is not yet known, and this needs to be tested to further validate the equilibrium-switch model. Overall, the M protein purified from SAC appears to be active, stable, and of high purity compared to IMAC and IMAC-SAC methods. The SAC method was also applied to two other NLRs.

### **Purification of other NLRs may require some optimisation**

The SAC method was also applied to two other NLRs, Sr33, an CC-containing NLR from *Aegilops tauschii*, and RUN1, a TIR containing NLR from *Muscadinia rotundifolia*. Sr33 provides resistance to a variety of stem rust races, including the Ug99 strain. RUN1 gives resistance to grapevine powdery mildew caused by the fungus *Uncinula necator*. Both Sr33 and RUN1 are of significant commercial importance and have been studied extensively and thus would be great candidates for further research.

Expression of RUN1 and Sr33 in *P. pastoris* was conducted in an identical manner to that of M, L6 and L7. Clarified lysates were also prepared in the same manner, and

purification using the SAC method was also identical. Unfortunately, no protein of the size expected of the full-length RUN1 protein was visible on either Coomassie or SYPRO® Ruby stain and immunoblot of both anti-6xHis and anti-Strep-tag II showed no visible bands at the predicted molecular size for RUN1. Interestingly, RUN1 has a nucleus localisation domain, which if recognised in *P. pastoris*, may interfere with its expression. Cloning of the RUN1 gene into pP6H3C vector without the C-terminal nuclear targeting domain may increase its expression in *P. pastoris*.

In contrast to RUN1, soluble protein of Sr33 was observed after purification by SAC, visible by SYPRO® Ruby stain, and immunoblot with both anti-6xHis-tag and anti-Strep-tag II antibodies. There are, however, significant breakdown products associated with purified Sr33, as evident by the results of the two immunoblots. One clear band at ~100kDa can be seen for Sr33 in the anti-6xHis-tag immunoblot, indicating no 6xHis-tagged breakdown products. In the anti-Strep-tag II immunoblot however, there are at least 7 bands smaller than the full-length Sr33 band, indicating several Strep-tag II containing breakdown products.

As the Strep-tag II was the only tag utilised in purification, it is probable the 6xHis-tagged breakdown products did not bind to the column, and the breakdown and degradation of Sr33 is occurring prior to affinity purification. Optimisation of expression and lysis therefore could improve the purification method for Sr33, be that different growth and induction temperatures, different growth and induction times, different methanol concentrations, or different lysis methods or additives.

Whilst the SAC method may not have been successful in attempts to purify other NLRs, the low expression and instability of RUN1 and Sr33 are the likely causes for poor to negligible protein yields, and are not due to a failure of the affinity purification step. It remains of upmost importance to optimise expression and preparation of clarified lysate in expression of NLRs for this technology to be applied across the spectrum of plant NLRs.

## **Other methods of plant R protein purification focus on domains, and not full-length protein**

Over the years, many research groups have tried to purify full-length plant NLRs, to varying degrees of success. As reported earlier, each of the flax NLRs were expressed and purified from *P. pastoris*, however MLA27 was purified from insect cells. Purification of MLA27 was performed by IMAC, and size exclusion chromatography, with the Maekawa et al. (2011) reporting the protein was purified to homogeneity, though their method of assessment of purity was not mentioned.

A direct comparison of MLA27 purification to that of flax NLRs is difficult, as no explicit yield of MLA27 is mentioned, nor are there any gels to assess protein concentration. Maekawa et al. (2011) also measured the nucleotide binding capabilities of MLA27, showing it binds proximately 61% ADP, comparable to L7. Maekawa et al. (2011) attempted to purify 19 other MLA proteins using the same method, but were unsuccessful, highlighting the difficulty in purifying full-length NLRs. Attempts have been made to purify flax NLRs from insect cells, however despite high yielding protein seen by SDS-PAGE, all the protein was insoluble and unusable in biochemical, biophysical and structural analysis (de Courcy-Ireland, 2015). Given the difficulty of purifying full-length NLRs, many have turned to expression and purification of truncated NLRs.

Seemingly the domain that has had the most success in purification is the TIR domain, with bacterial expression providing yields exceeding 40 mg.mL<sup>-1</sup> and purity often homogenous. AtTIR (Chan et al., 2010), L6 (Ve et al., 2011b), RPS4, RRS1, SNC1 (Wan et al., 2013), RPV1 (Williams et al., 2016) and RPP1\_NdA (Zhang et al., 2017) were all purified from *E. coli*, lysed by sonication, and purified using IMAC and size exclusion chromatography. There are now seven different crystal structures of plant TIR domains, each providing new insights into the function of NLRs. How TIRs interact with the rest of the NLR still remains unclear, demonstrating the need for structural data of a full-length NLR.

Other studies using purified protein to probe the molecular mechanisms of NLR activation and regulation have used truncated version of NLRs, from truncation of the N-terminal signalling domain (Ueda et al., 2006), truncation of the LRR domain (Tameling et al., 2002, Tameling et al., 2006, Ueda et al., 2006, Fenyk et al., 2016), and truncation of both domains, leaving just the NB-ARC domain (Fenyk et al., 2012, Fenyk et al., 2015). Methods of purification utilised *E. coli* or insect cells, and most used IMAC to purify the protein. It is hard to compare the purification of these truncated domains to the full-length NLRs produced in this study, as many do not report yields or purity. No other NLRs have been reported to be purified from *P. pastoris*, but there are reports of protein purified from *E. coli* and *Nicotiana benthamiana* using a Strep-tag II and StrepTactin columns (Fenyk et al., 2012, Fenyk et al., 2015).

### **Purification of full-length APAF-1 and NLRC4**

Despite the difficulty of purifying full-length plant NLRs, there is precedent for successful purification of full-length mammalian NLRs, NLRC4 and APAF-1, with APAF-1 of sufficient purity and concentration for crystallography studies (Reubold et al., 2011). For both NLRC4 and APAF-1, structures of the multimeric complexes formed were solved by cryoEM. Perhaps adaption of some of the purification techniques used for these two mammalian proteins could be applied to the purification of plant NLRs.

The APAF-1 crystal structure was first solved as a truncated protein, missing the WD40 repeats at the C-terminus (Riedl et al., 2005). APAF-1 1-591 was able to be purified from *E. coli*, and a straightforward IMAC and anion exchange protocol was used to purify the APAF-1 1-591 construct to 3 mg.mL<sup>-1</sup>, sufficient for crystallisation. Protein from this purification strategy was also used for ATP hydrolysis assays, and for measuring oligomeric state by size exclusion chromatography.

To purify the full-length protein, Reubold et al. (2009) had to express the full-length APAF-1 protein in insect cells, and cells were lysed in the presence of detergent Nonidet P-40, presumably to help improve solubility of the protein. The full-length protein was then purified to homogeneity using a combination of IMAC, anion-

exchange, TEV protease and SEC, to 15 mg.mL<sup>-1</sup>, sufficient for crystallography studies. Given that flax NLRs M, L6 and L7 are localised to membranes (Takemoto et al., 2012) and are likely to interact with said membranes, inclusion of different detergents in the lysis buffer may further aid in purification (Seddon et al., 2004). Zhou et al. (2015) also used insect cells for expression of full-length APAF-1, and also used IMAC and SEC techniques to purify protein for cryoEM. The authors used 5 µM of full-length APAF-1 complexes, and used ITC to measure interactions, requiring concentrations of 4 µM of full-length protein. Scaling up the *P. pastoris* and SAC method could also enable cryoEM and ITC studies to be done on full-length flax NLRs.

NLRC4 has also been purified to high concentrations and purity. Hu et al. (2013) were able to purify murine full-length NLRC4 from insect cells using a His-Sumo tag, a tag used to enhance protein expression and solubility (Butt et al., 2005). NLRC4 was purified by IMAC, the tags were cleaved using TEV PreScission protease, and NLRC4 was further purified using ion-exchange and SEC. The concentrations required for crystallisation were 5 mg.mL<sup>-1</sup>, with less required for CD and ATPase assays. Usage of solubility tags may also aid in the purification of M, L6 and L7, however removal of these tags may cause the full-length protein to precipitate or may prevent any oligomeric interactions between monomers from forming (Esposito and Chatterjee, 2006).

The His-SUMO or His-MBP tags on full-length NLRC4 did not appear to pose these problems for Zhang et al. (2015), as they were able to solve the structure of the NLRC4/NAIP2 complex by cryoEM after cleaving off the solubility tags. Using insect cells for expression, and purification by IMAC, ion exchange and SEC, Zhang et al. (2015) were able to produce sufficient NLRC4 and NAIP2 (3 mg.mL<sup>-1</sup>) for cryoEM studies of the inflammasome complex. Given the success of using solubility tags for NLRC4, using such tags for purification of full-length NLRs is something that should definitely be considered. Despite this, the flax full-length NLR yields achieved with the *P. pastoris* SAC method reported here are approaching those obtained using the above techniques, opening many new avenues for different protein assays and techniques to be applied.

## **New possibilities for analysis of more pure NLR protein**

With more pure protein, different experimental methods become viable, as contaminants can often cause false positives within biochemical experiments, cause major issues in biophysical experiments, and prohibit and obstruct attempts to solve protein structure.

*'Issues of low M-protein yield and purity made these experiments technically challenging, and at this stage, we cannot report on the capacity of purified M protein to rebind ATP, hydrolyse it, or whether the presence of purified AvrM has any impact on these biochemical properties.'* (Williams et al., 2011)

### **Nucleotide binding and hydrolysis assay redux?**

In chapter 3 of this thesis the nucleotide binding of wild type L6 and L7 and a variety of L6 and L7 mutants is reported. However, the purity of the protein samples used made it difficult to measure the ability of the full-length proteins to bind exogenously added nucleotides, similar to methods reported by Tameling et al. (2006). With the increased purity afforded by the SAC purification method, these experiments are more likely to succeed using full-length protein, than just using the IMAC method of purification. With more pure protein, the effect of external factors, such as addition of nucleotides to change bound state, and addition of effector proteins on nucleotide binding could also be measured, enabling testing of the equilibrium-switch model.

With more pure protein, the ability of full-length proteins to hydrolyse ATP could be revisited, with less chance of contaminants effecting the sensitive  $\alpha$ -P<sup>32</sup> ATP hydrolysis assays as performed by Sornaraj (2013) and de Courcy Ireland (2015). Increased protein concentrations may also enable high throughput ATPase assays to be used, such as the malachite green assay used by Hu et al. (2013) to measure ATPase activity of NLRC4. Measuring the hydrolysis activity of L6 and L7 and the mutants reported in chapter 3 would provide some more insight into the equilibrium-switch model presented.

Increased protein purity may also enable the discovery of other biochemical properties of full-length NLRs. Recently it has been shown that some NLRs can bind and bend DNA. Fenyk et al. (2015) demonstrated that the NB-ARC domain of Rx1 could bend and melt DNA *in vitro* in an ATP-dependent manner, and a follow up study by Fenyk et al. (2016) showed that the CC-NB-ARC domain of I-2 preferentially bound ssDNA and dsDNA over ssRNA. They also showed an ATP-dependent melting of DNA by I-2, and the addition of DNA increased ATP hydrolysis rates. Addition of ADP reduced the ability of the I-2 CC-NB-ARC to bind DNA. These experiments can now be attempted with full-length M, L6 and L7, as yields used in the assays were similar to those obtained for the full-length NLRs, at around  $\sim 100 \mu\text{g}\cdot\text{ml}^{-1}$  used for the assays reported in Fenyk et al. (2015) and Fenyk et al. (2016). As well as assays to determine other biochemical properties of full-length NLRs, protein-protein interaction assays can also be explored.

### ***Protein-protein interaction experiments***

Protein-protein interactions are very important in many signalling pathways, and plant NLR signalling is no exception. There are three different NLR/effector interaction models described, each with various well characterised examples. Despite extensive co-IP and yeast-2-hybrid assays, there are very few studies measuring the kinetics of the interactions. To date, there is one study that reports the kinetics of the interaction between members of the integrated-decoy class of NLR/effector interaction, with Maqbool et al. (2015) examining the interaction between AVR-PikD and the HMA domain of Pikp-1 using SPR.

Understanding the kinetics of the interaction is important for understanding how the interaction may occur within the host cell, enabling comparison between different NLR-effector pairs. Such information would also enable assessment of other factors, for example, whether a change in the nucleotide bound state can affect the interaction between L6 or L7 between AvrL567, and whether mutations might effect the interaction.

There are a number of methods that can be used to measure protein-protein interaction kinetics, including isothermal titration calorimetry (ITC), surface plasmon

resonance (SPR), microscale thermophoresis (MST), fluorescence resonance energy transfer (FRET) and nuclear magnetic resonance (NMR) (Acuner Ozbabacan et al., 2011), each with their own features and draw-backs. Surface plasmon resonance is of interest to this study, as it can be performed with low concentrations of high purity protein ( $\sim 25\text{-}50 \mu\text{g.mL}^{-1}$ ) (Rich and Myszka, 2007), and can be used in conjunction with tags already present on the purified L6 and L7 proteins. SPR will be discussed more in the next chapter. The SAC purification method can be used for protein-protein interaction experiments, but is it suitable for structural biology studies?

### ***Not so crystal clear? X-ray crystallography unlikely to structure of full-length NLR***

To date, the only structural models for canonical plant NLR domains are of the N-terminal signalling domains, the numerous aforementioned TIR structures (Chan et al., 2010, Bernoux et al., 2011, Williams et al., 2014, Williams et al., 2016, Zhang et al., 2017), and three CC domain structures, two solved by X-ray crystallography, MLA10 (Maekawa et al., 2011) and Rx (Hao et al., 2013), and one by solution NMR, Sr33 (Casey et al., 2016). NMR solution structure is unviable for full-length NLRs, as current methods have an upper protein size limit of  $\sim 25$  kDa (Billeter et al., 2008).

It is feasible to use X-ray crystallography to solve the crystal structure of a full-length NLR as demonstrated by Reubold et al. (2011), who reported solving the crystal structure of full-length APAF-1. Using protein concentrations of  $15 \text{ mg.mL}^{-1}$ , the structure was solved to  $3 \text{ \AA}$  resolution. This concentration is much higher than that reported here for plant NLRs, meaning that determining the structure of a plant NLR by X-ray crystallography with this purification method is unlikely. However there are cases in which proteins have been crystallized at  $2 \text{ mg.mL}^{-1}$  (McPherson and Gavira, 2014), which could be achieved by upscaling the SAC method of purification. A more feasible approach to solving the structure of plant NLRs lies in the field of electron microscopy.

### ***Cool! Structure of a plant NLR from cryoEM?***

The structure of a full-length NLR, especially in an oligomeric state or in complex with an effector or guard, would enable a better understanding of the mechanisms underpinning NLR activation and regulation. As mentioned above, X-ray

crystallography has so far yielded structures of only the N-terminal signalling domain, as well as some decoy domains (Maqbool et al., 2015), of NLRs. Recent advances in cryoEM, particularly the advent and utilisation of direct electron detection cameras (Li et al., 2013), have enabled researchers to capture near atomic models of large protein structures and complexes.

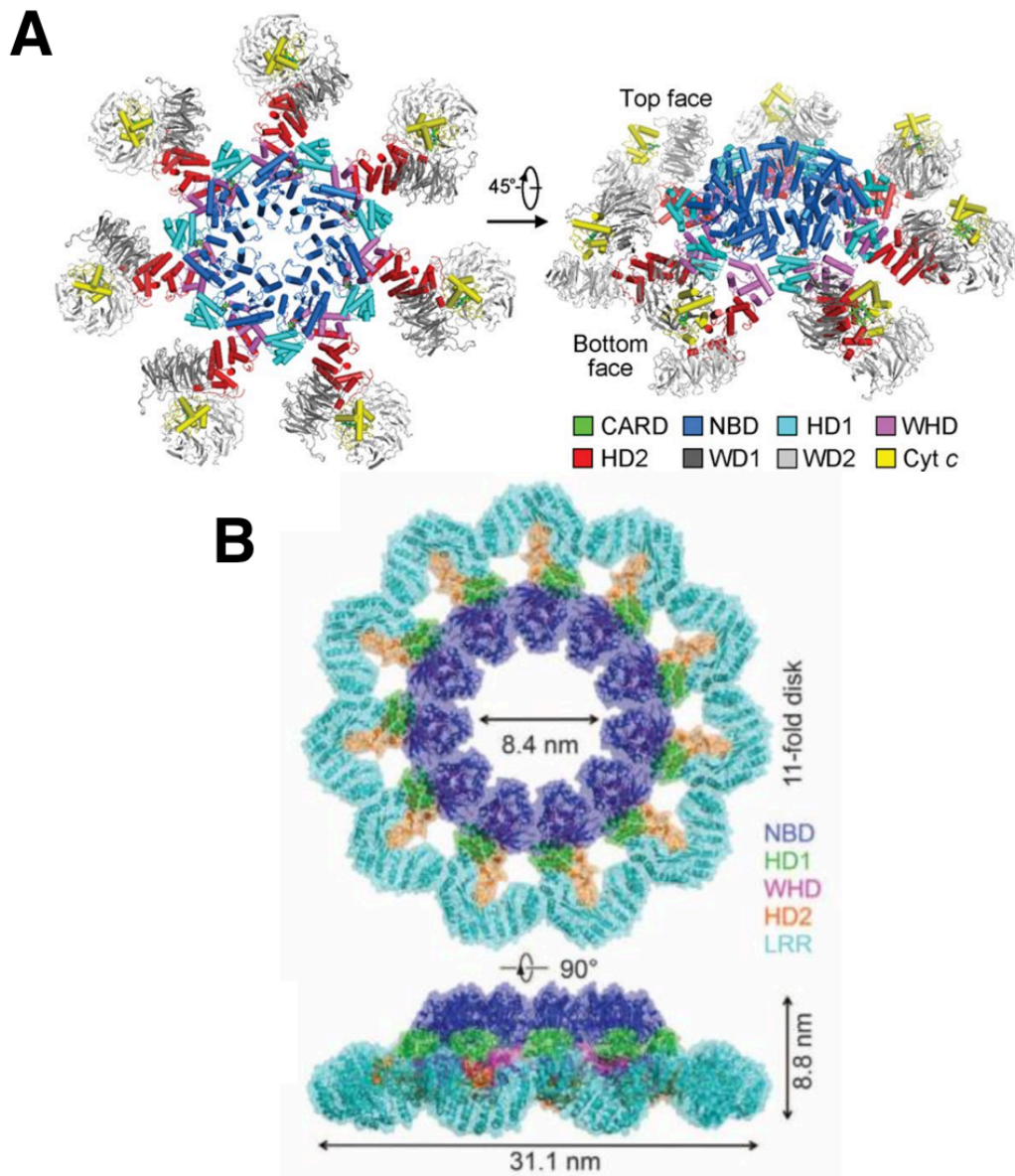


Figure 4.13 Oligomeric cryoEM structures of APAF-1 (A) and NLRC4 (B). Taken from (Li et al., 2013) and (Zhang et al., 2015). Full length plant NLRs may form a ring-like structure, enabling downstream signalling to occur.

Of particular interest, are the structures of the APAF-1 apoptosome (Zhou et al., 2015), and NLRC4 (Zhang et al., 2015). Protein concentrations required for cryoEM vary depending on the size of the protein, and the oligomeric state (Thompson et al., 2016), but for APAF-1 apoptosome and NLRC4 inflammasome, concentrations of 3.5 mg.mL<sup>-1</sup> and 3 mg.mL<sup>-1</sup>, respectively, were sufficient. It is possible that flax NLRs purified by the SAC method presented in this work would be suitable for cryoEM studies, due to the low yields and sample volumes required for cryoEM compared to protein X-ray crystallography.

## **Conclusion**

The work presented here demonstrates that M, L6 and L7 proteins can now be purified using a faster, more efficient purification strategy. With increased protein purity comes more opportunities to explore the activation, regulation and protein-protein interactions of full-length NLRs. Coupled with advances in structural biology techniques, we may also be closer to a structure of a full-length NLR. With purer M protein and that of both virulent and avirulent effectors, the interaction between these molecules at the plant-pathogen interface can now be probed *in vitro*. In the next chapter, the SAC purified M protein is used to measure interaction between the cognate effectors, AvrM and avrM, using SPR.

# Chapter 5 - Surface plasmon resonance to measure NLR-effector interaction

## Introduction

The ATP/ADP binding assays described in chapter one of this thesis led to the proposal of an equilibrium-switch model, whereby NLRs cycle between an ADP-bound inactive state and an ATP-bound active state. These ATP/ADP binding experiments were however static end-point readings, and may not be indicative of the dynamic, changing state in which NLRs exist. In order to further probe the equilibrium-switch model, it is necessary to examine the interaction of an NLR and effector in both an ATP- and ADP-bound states. To assess these interactions, a method to measure protein-protein interactions in real time, with control over the chemical environment is required. A method to measure interactions *in vitro* would also enable the interaction kinetics to be characterised, compared to static methods of protein-protein interaction experiments such as co-IPs and yeast-2-hybrid assays.

## Surface plasmon resonance (SPR)

One method of examining protein-protein interactions in real time is surface plasmon resonance (SPR). This technique exploits the phenomena of surface plasmon resonance on a gold surface struck with plane-polarized light under total internal reflection conditions (Liedberg et al., 1983). Changes to mass on the surface of the gold surface changes the energy or angular requirements of the plane-polarized light to maintain surface plasmon resonance, and light source angle or intensity is changed to maintain this (Liedberg et al., 1983). A change in the angle or intensity of the light is correlated linearly to the number of molecules on the gold surface.

It is possible to examine the interaction between essentially any two molecules, provided one can be immobilised to the surface of an SPR chip in a native, active state (Szabo et al., 1995) . By immobilising one of a pair of interactors to the surface and flowing the other over the chip, it is possible to derive accurate real-time interaction kinetics without labelling proteins or modification of their native state. This also gives

the ability to change buffer conditions and test how the interaction performs under various conditions, for example at different temperatures, pH, protein concentrations, and with various other molecules such as excess ADP and ATP in the case of the NLR/effector interaction. Before examining what changes the interaction however, it is first necessary to characterise the kinetics of the initial interaction. The work presented in this chapter describes the attempts to establish an assay for M/AvrM interaction in real-time using SPR.

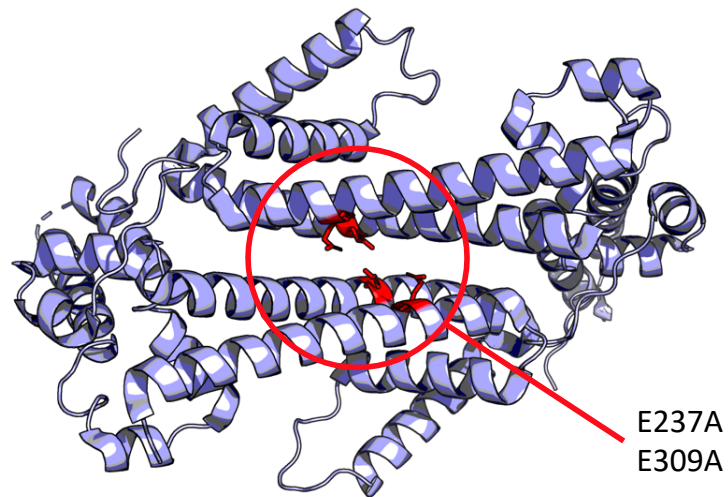
### **M and AvrM: Direct interaction in the innate immune pathway**

The M locus contains approximately 15 different genes, only one of which is required for resistance to *M. lini* carrying the AvrM-A gene. This gene is termed *M*, and was cloned by Anderson et al. (1997). It encodes a NLR protein with 86% sequence identity to L6. *M* has been the focus of many biochemical and functional studies (Williams et al., 2011, Ve et al., 2013) and remains one of the few full-length NLR proteins to be expressed in a recombinant system, and purified to sufficient yield to conduct biochemical analyses (Williams et al., 2011, Schmidt et al., 2007). It is also one of only a few NLRs with an identified virulence and avirulence effector that have been both cloned, expressed, purified and have structures solved (Ve et al., 2013). Furthermore, *M* protein has been shown to interact directly with its effector AvrM in yeast-2-hybrid assays and by co-IP (Catanzariti et al., 2010). It is therefore one of the few NLR/effector combinations that meets all the requirements to study the interaction *in vitro* and how this interaction is affected by biochemical changes.

### **AvrM**

Genes at the *AvrM* locus have also been cloned and characterised. There are four avirulent variants, *AvrM-A*, *-B*, *-C* and *-D* and one virulence variant, *avrM* (Catanzariti et al., 2006). Like AvrL567 AvrM proteins are haustorially expressed and expression of *AvrM-A*, *-B*, *-C* or *-D*, together with the *M* gene in flax result in HR, with *avrM* not inducing any immune response (Catanzariti et al., 2006). Expression in tobacco yields similar results, with *AvrM-A* giving strong HR, *AvrM-D* and *-C* giving slightly weaker HR and *AvrM-E* and *avrM* showing no HR.

**A** AvrM



**B** avrM

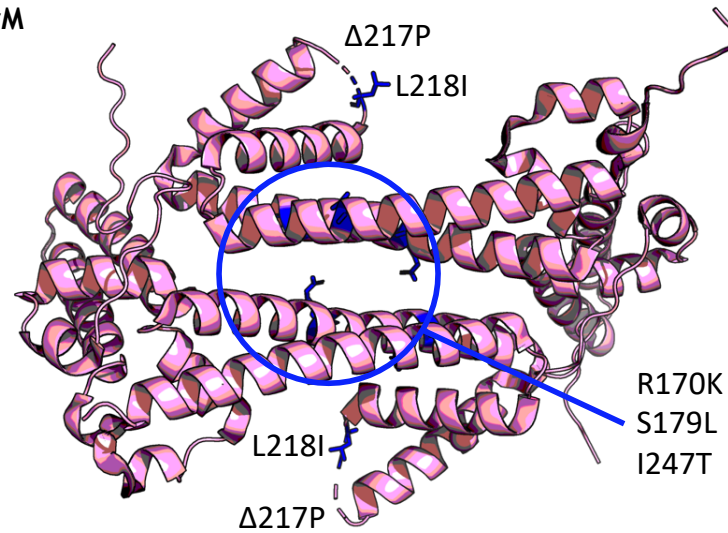


Figure 5.1 Crystal structures of AvrM and avrM. **A** The AvrM dimer is shown in blue, with mutations effecting HR shown in red. **B** The avrM dimer is shown in pink, with mutations effecting HR shown in blue. Figure made using Pymol.

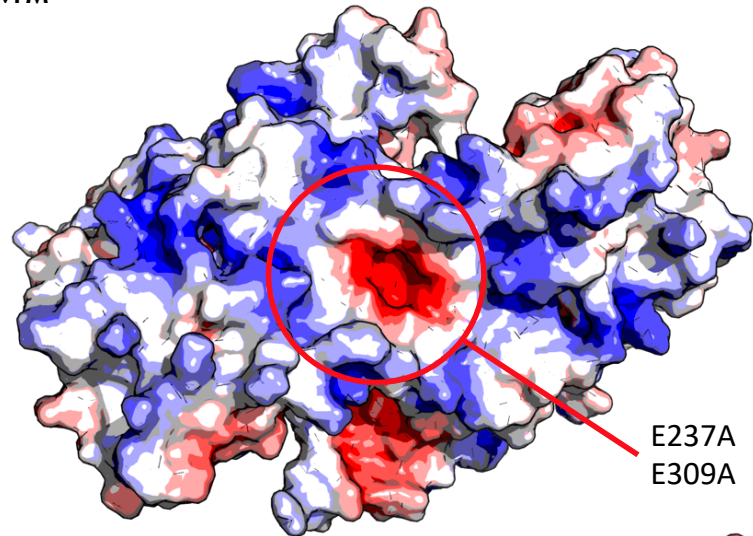
The C-terminal region of AvrM-A was also shown to form a dimer in yeast-2-hybrid assays and by co-IP, with avrM only weakly showing dimerization in co-IP experiments. Ve et al. (2013) crystallised and solved the structure of the C-terminal domains of AvrM-A and avrM, shown in Figure 5.1. AvrM forms a dimer, with no close structural similarity to other known proteins.

A hydrophobic surface patch was shown to be required for internalisation in plant cells, whilst a C-terminal coil-coiled domain was required for interaction with M (Ve et al., 2013). Much like AvrL567 and L5/L6 there are likely to be multiple contact points between the NLR and its Avr effector, as individual changes to the polymorphic residues impair or initiate a recognition event *in planta*. The exact interfaces that control the interaction between M and AvrM are as yet unknown.

### **The molecular basis for M/AvrM interaction remains elusive**

M and AvrM interact *in planta* to induce HR. M and AvrM interact directly, as demonstrated by yeast-2-hybrid assays (Catanzariti et al., 2010). AvrM appears to form a dimer in solution, in SEC-MALS experiments (Rahman, 2016). In contrast, avrM does not interact with M *in planta* or in yeast-2-hybrid assays and does not induce HR. avrM elutes at a volume that would constitute a dimer under SEC, but MALS and SAXS analysis indicate the protein exists as a monomer in solution (Williams, Casey, Zhang unpublished). AvrM has a negatively-charged patch at the dimer interface, whilst avrM has a positively-charged patch at the same position, as seen in Figure 5.2. A summary of the interaction and dimerization can be seen in Figure 5.3.

**A** AvrM



**B** avrM

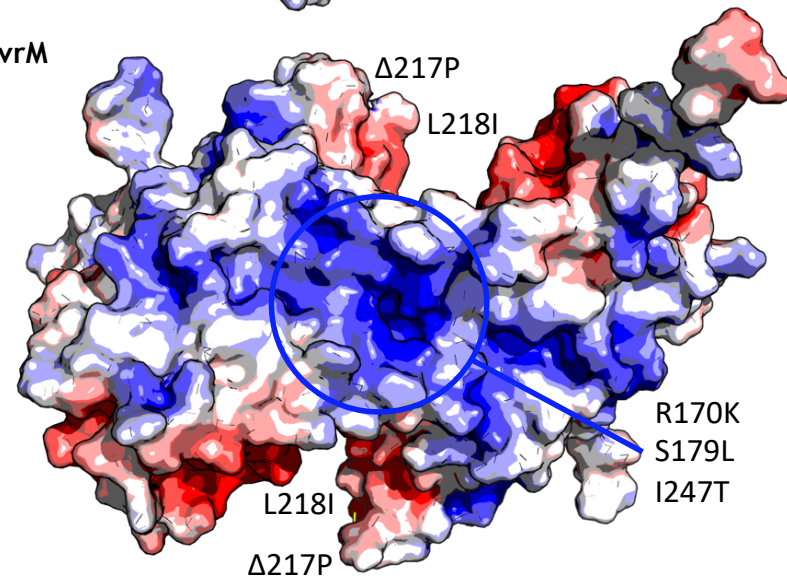


Figure 5.2 Electrostatics of AvrM and avrM structures. Both AvrM (A) and avrM (B) are shown with surface electrostatics, blue indicating a positive charge and red indicating a negative charge. Orientations of structures are the same as Figure 5.1, and residues in mutants AvrM<sup>E237A+E309A</sup> (EA2), avrM<sup>R170K+ S179L+I247T</sup> (a3) and avrM<sup>R170K+ S179L+I247T+Δ217P+L218I</sup> (a5) are indicated. Electrostatics were calculated using APBS (Baker et al., 2001), and figures made using Pymol.

Introducing mutations in the charged dimer interfaces of both AvrM and avrM led to some intriguing results (Rahman, 2016). In AvrM<sup>E237A+E309A</sup> (EA2), positions seen in Figure 5.1A, a change of two charged glutamates to alanines in the interface of the AvrM dimer, knocked out *in planta* recognition by M, as well as any interaction in yeast-2-hybrid assays. A difference in charge at the dimer interface of AvrM and avrM can be seen in Figure 5.2. However, the change did not cause a change in the biophysical properties of the protein under SEC or MALS, as it retained its ability to dimerise.

Mutants in the interface of avrM, avrM<sup>R170K+ S179L+I247T</sup> or avrM a3, positions seen in Figure 5.1B, caused a partial regain of HR *in planta*, but did not change their ability to interact with M in yeast-2-hybrid assays, but it did enable dimerization to reoccur. Further mutations to avrM, avrM<sup>R170K+ S179L+I247T+Δ217P+L218I</sup> or avrM a5, positions seen in Figure 5.1B, gave a full M/AvrM-like HR. But it did not appear to change the interaction of these avrM mutants with M in yeast-2-hybrid assays. These effects on *in planta* HR and in yeast-2-hybrid assay interaction with M, and dimerization state in solution can be seen in Figure 5.3.

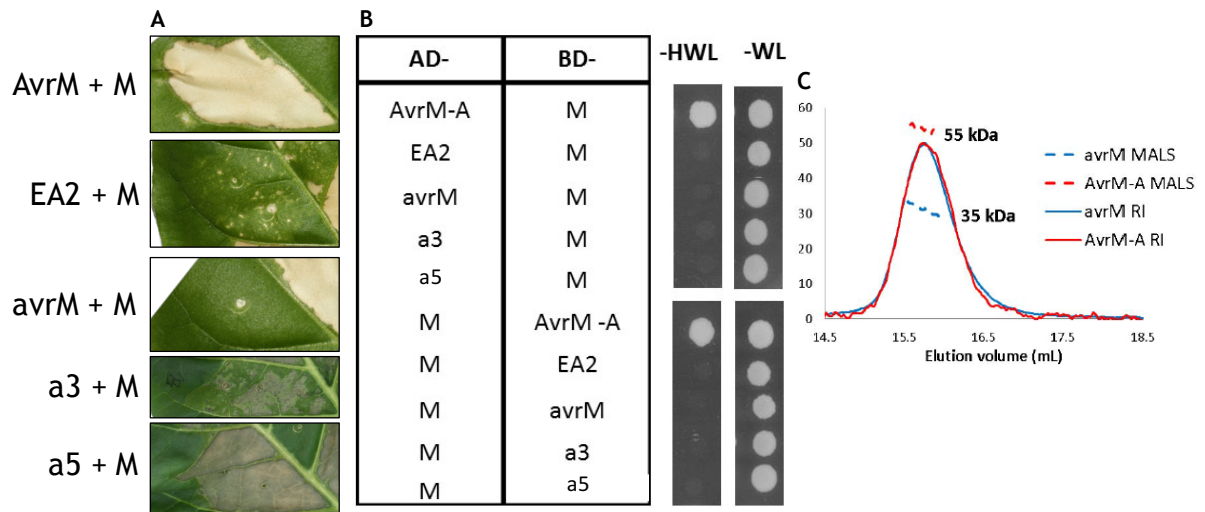


Figure 5.3 M and AvrM & avrM mutants phenotypes, interaction and behaviour in solution, adapted from figures of Rahman (2016). **A** Agrobacterium-mediated expression of AvrM and avrM mutants with M in *N. benthamiana* HR phenotypes. **B** Yeast-2-hybrid assays showing the interaction of M and AvrM and avrM mutants. **C** SEC-MALS data for avrM and AvrM, indicating the average molecular mass in solution of the two proteins.

This raises a number of questions regarding the interaction between M and AvrM/avrM. Is the dimerization of avrM a factor at all in the interaction M? The avrM mutants can form dimers and still not induce a response, and a dimeric AvrM can avoid detection. Is direct interaction required at all for the downstream immune response? avrM mutants a3 and a5 can both induce HR without demonstrating any binding with M in yeast-2-hybrid assays. To probe these questions further SPR was used to investigate the interaction of NLR and effector in real-time.

To measure the ability of both AvrM and avrM and mutants to bind M, interaction kinetics for each will be determined, with the goal to measure accurate, reproducible association and dissociation rate constants for each interaction. This information will provide a more detailed insight into the activation of M, whether a rapid association of AvrM to M triggers the response, or a slow dissociation of AvrM from M means it remains active for longer, or whether binding occurs at all. This technique may also allow binding stoichiometry to be determined, and how the interaction is affected by the presence of ATP and ADP, further probing the equilibrium-switch model of L6 and L7 activation. Kinetic information cannot be obtained from co-IPs or yeast-2-hybrid assays, which provide interaction data as a snapshot in time, thus giving a yes or no answer, rather than the strength or speed of the binding occurring during the interaction.

## **Methods**

### **Sensor chip NTA surface preparation**

The Nitrilotriacetic acid (NTA) surface is described by the manufacturer (GE Lifesciences) as a gold surface with a dextran matrix. NTA moieties are fused to the carboxymethyl-dextran matrix. Before use, the surface was conditioned with running buffer (50 mM Tris pH 8.0 150 mM NaCl) 3 mM EDTA, to remove any residual Ni, salts or metals from previous runs.

Surfaces were charged with 0.5 mM NiSO<sub>4</sub> for 60 s and 10  $\mu\text{L}\cdot\text{min}^{-1}$ . The sample channel, a channel referring to one of four microfluid channels in each chip, each able to be used independently, was injected with 6xHis-tagged ligand (M) before both

sample and reference channels were injected with analyte (AvrM, avrM) at varying concentrations, flow rates and injection times. After analyte injection, both channels were injected with a regeneration buffer (running buffer with 350 mM EDTA) to remove the nickel, as well as any M and AvrM retained on the surface. A schematic of the Ni-NTA immobilisation can be seen in Figure 5.4A.

### **Sensor chip SA surface preparation**

The Streptavidin (SA) surface is described by the manufacturer (GE Lifesciences) as a gold surface with a dextran matrix. Streptavidin molecules are immobilised on the carboxymethylated-dextran matrix. Before use, the surface was conditioned with three pulses of 1 M NaCl 50 mM NaOH, as per manufactures instructions. The sample surface was injected with 500 nM biotin-trisNTA for 60 s at 10  $\mu\text{l}\cdot\text{min}^{-1}$ . In some experiments, the reference surface was also injected with biotin-trisNTA, with the same injection conditions as the sample channel. A schematic of the SA-biotin-trisNTA immobilisation can be seen in Figure 5.4A.

Varying reference channels were used to accommodate non-specific binding, but the sample channel was always as follows: first an injection of Nickel, then ligand, followed by injections of the analyte. Concentrations, flow rates and injection times varied, as did the number of injections and regeneration conditions.

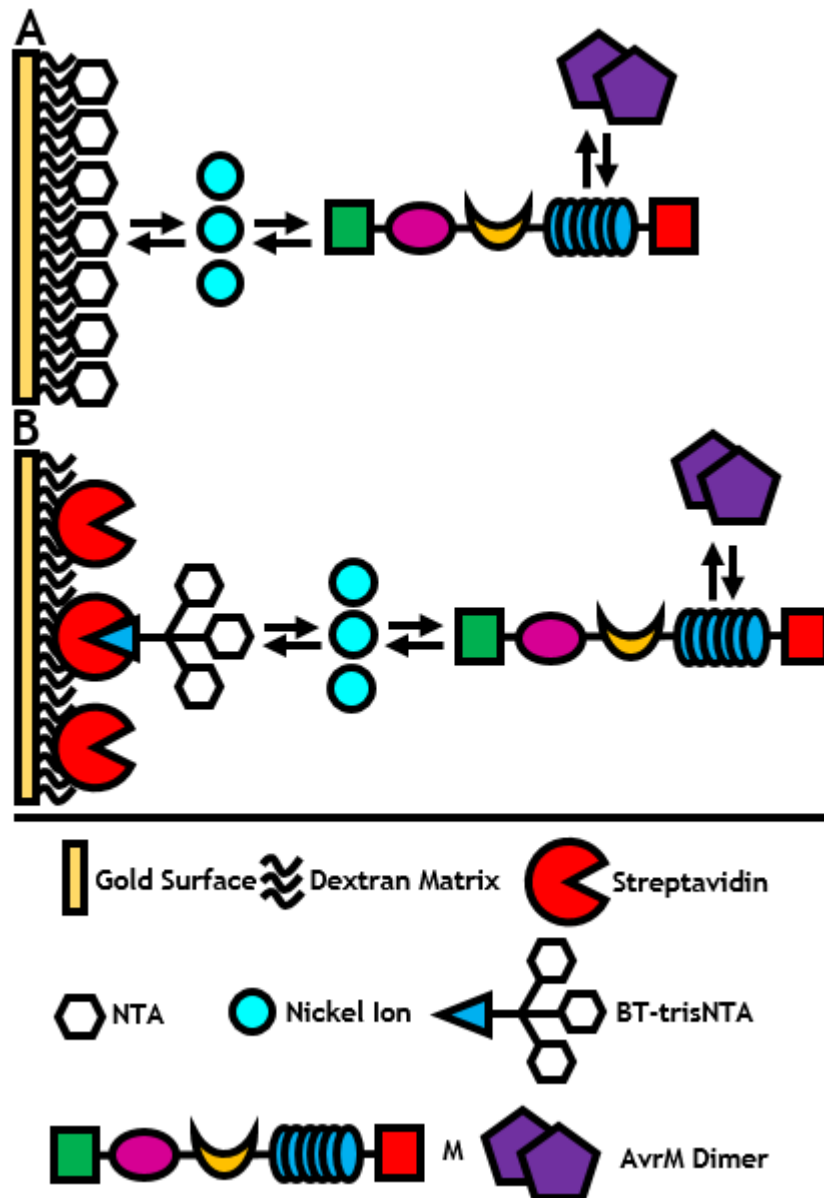


Figure 5.4 Representation of the two methods used for M immobilisation to the SPR Chip. **A.** A NTA chip is charged with nickel ions, followed by the injection of M. AvrM is then flowed over the immobilised M before regeneration with EDTA. **B.** An SA chip is first treated with biotin-trisNTA (BT-trisNTA) to saturate the SA molecules. Nickel is then injected over the surface, followed by M. AvrM is then flowed over, with regeneration using NaCl and NaOH.

## Results

### **AvrM, avrM, EA2 and a3 purification**

AvrM, avrM, AvrM EA2 and avrM a3 were expressed and purified as described in (Ve et al., 2013). Samples of each of the effectors can be seen in Figure 5.5. Each was concentrated to 10 mg.mL<sup>-1</sup> for use in assays.

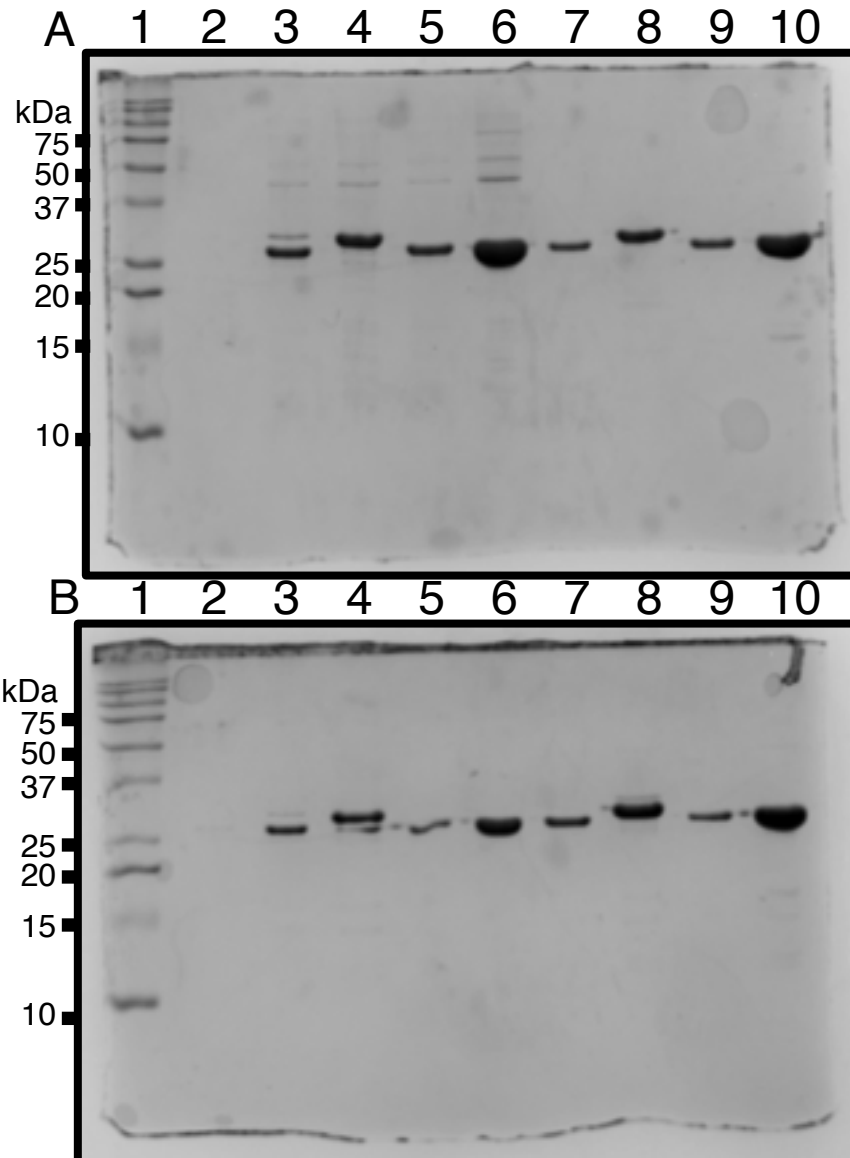


Figure 5.5 Examples of purified AvrM, avrM, AvrM EA2 and avrM a3 proteins. **A** SYPRO® Ruby stain of AvrM and avrM proteins. Lane 1 Ladder. Lane 2 Blank. Lane 3 AvrM+TEV protease. Lane 4 AvrM before TEV protease. Lane 5 AvrM after removal of TEV protease. Lane 6 AvrM concentrated sample. Lane 7 avrM+TEV protease. Lane 8 avrM before TEV protease. Lane 9 avrM after removal of TEV protease. Lane 10 avrM concentrated sample. **B** SYPRO® Ruby stain of AvrM EA2 and avrM a3 proteins. Lane 1 Ladder. Lane 2 Blank. Lane 3 AvrM EA2+TEV protease. Lane 4 AvrM EA2 before TEV protease. Lane 5 AvrM EA2 after removal of TEV protease. Lane 6 AvrM EA2 concentrated sample. Lane 7 avrM a3+TEV protease. Lane 8 avrM a3 before TEV protease. Lane 9 avrM a3 after removal of TEV protease. Lane 10 avrM a3 concentrated sample.

As the immobilisation surfaces to be used both exploited the 6xHis-tag on the M protein, the 6xHis-tag on the effectors needed to be completely removed, to ensure all binding to the ligand surface was due to M/AvrM interaction, rather than AvrM/Nickel interaction. An anti-6xHis-tag western blot was performed on AvrM and avrM samples pre- and post-TEV protease treatment, and after the removal of TEV. As can be seen in Figure 5.6, the TEV protease cleaved the 6xHis-tag, causing a size shift in AvrM on SDS-PAGE as seen in Figure 5.6A lanes 2 and 3. Lanes 5 and 6 in Figure 5.6B show that the 6xHis-tag has been completely removed. The bands in lanes 3 and 4 of the western blot are TEV protease, which itself has a 6xHis-tag. TEV protease is identical in size to AvrM and avrM when the 6xHis-tag is cleaved (27 kDa) resulting in a band that would correspond to AvrM and avrM on the western blot.

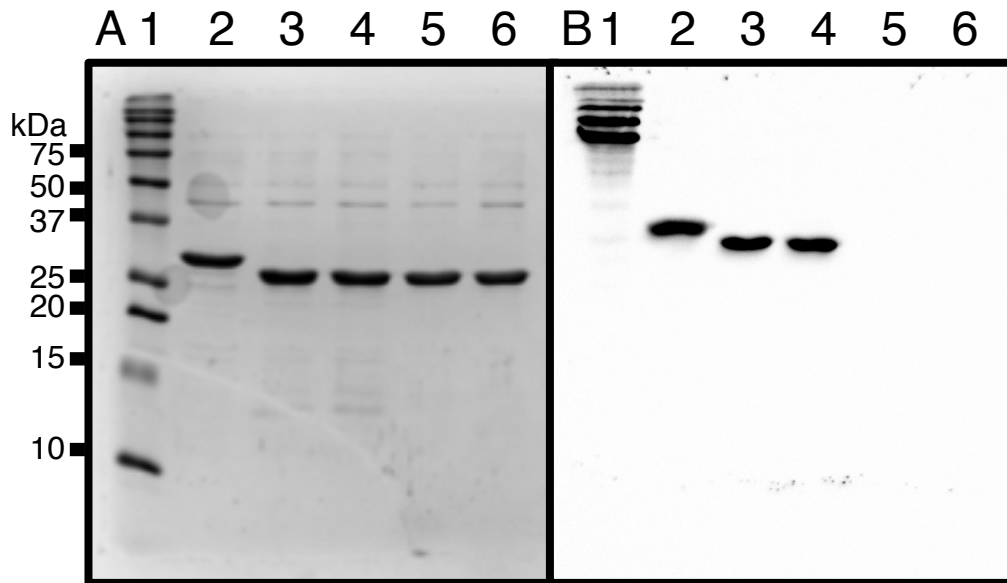


Figure 5.6 Western blot of AvrM and avrM proteins, showing removal of 6xhis-tag. **A** Coomassie stain and **B** Anti-6xHis-tag Western Blot. Lane 1 Ladder. Lane 2 AvrM before addition of TEV protease. Lane 3 AvrM and TEV protease before removal of TEV protease. Lane 4 avrM and TEV protease before removal of TEV protease. Lane 5 AvrM with His-tag removed. Lane 6 avrM with 6xHis-tag removed.

With all proteins now purified and the 6xHis-tag removed the effector proteins, SPR analysis can begin.

## Ni-NTA Immobilisation

To conduct kinetic experiments, it is recommended to immobilise the ligand to an RU ( $R_{Ligand}$ ) that corresponds to an  $R_{max}$  of 100 RU for the interaction between the target ligand and analyte (Karlsson et al., 1991). This can be calculated using the equation below

$$R_{max} = \frac{R_{Ligand} \times Mw_{Analyte} \times Valency_{Ligand}}{Mw_{Ligand}}$$

$$\therefore R_{Ligand} = \frac{R_{max} \times Mw_{Ligand}}{Mw_{Analyte} \times Valency_{Ligand}}$$

where  $R_{max}$  is the maximum response of AvrM binding,  $R_{Ligand}$  is the binding response of the ligand,  $Mw_{Analyte}$  is the molecular mass of the analyte,  $Valency_{Ligand}$  is the number of binding sites and  $Mw_{Ligand}$  is the molecular mass of the ligand. For an  $R_{max}$  of 100 RU for AvrM binding to M, an  $R_{Ligand}$  for M of 294 RU is required, assuming a molecular mass of 147 kDa and 50 kDa for M and AvrM respectively, and a binding stoichiometry of 1:1. The molecular weight of AvrM is listed as 50 kDa due to the assumption that a dimeric AvrM is required to bind to M. This calculation was chosen over two binding sites and a  $Mw_{Analyte}$  of 25 kDa.

First, the Ni-NTA immobilisation method was trialled. A Ni-NTA chip (GE Life sciences) was first conditioned according to the manufacturer's instructions (3 mM EDTA in running buffer (50 mM Tris pH 8.0 150 mM NaCl)). To activate the surface, 0.5 mM NiSO<sub>4</sub> was injected over the sample channel for 1 min at 10  $\mu$ L.min<sup>-1</sup>, followed by injection of 100-400 nM 6xHis-tagged M protein for 1-2 min at 5  $\mu$ L.min<sup>-1</sup>. The average binding of Nickel was 50 RU, and the average binding response of M was 40 RU. A sample sensorgram can be seen in Figure 5.7.

Some baseline drift was observed post M injection, with an average drift in the sample channel of  $\sim -0.08$  RU.s<sup>-1</sup>. The level of M immobilisation to assess the kinetics of

interaction with AvrM was also insufficient, below the required 294 RU. With binding low and baseline drift high, any response to AvrM would be difficult to detect. However, so as to not waste protein, multi-cycle kinetic experiments were still undertaken.

Modifications of the injection times and M concentration were trialled to increase the RU, however neither were sufficient to generate the required 286 RU, nor a sufficiently stable baseline to perform the long injection times required for weak interacting proteins. Modifications to the NTA immobilisation method could be made in the future, perhaps by combining the Ni-NTA interaction with a covalent coupling method, or trying different buffers, temperatures or metal ions. However, due to time constraints, it was decided to assess the viability of the other immobilisation method, the SA-biotin-trisNTA method. Suggested modifications to the NTA method will be discussed further in the future work section.

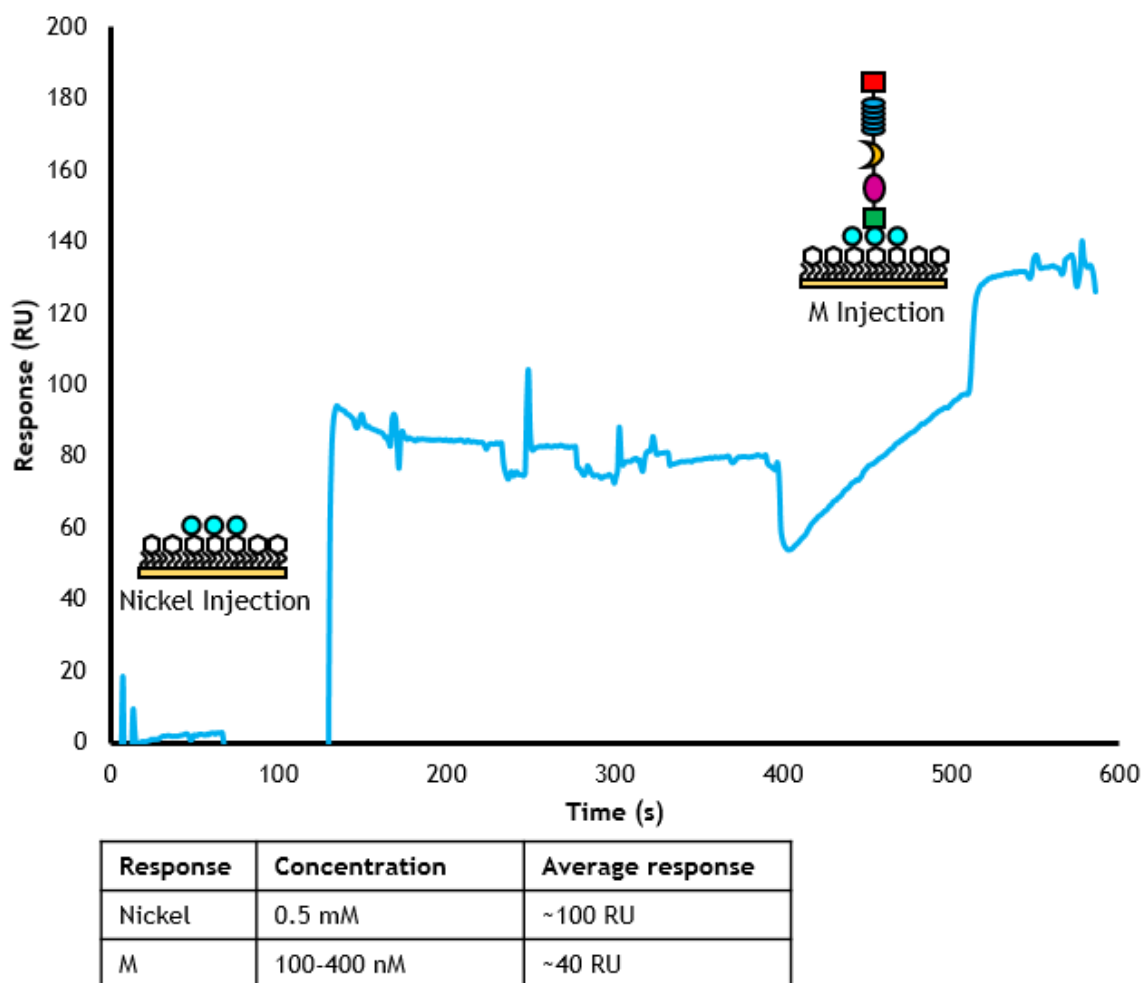


Figure 5.7 Sample sensorgram of the NTA M immobilisation method, shown in blue. Visualisation of each step is shown diagrammatically above the step on the sensorgram, based on Figure 5.4. 0.5mM Nickel was injected over a NTA surfaced preconditioned according to the manufacturer's instructions (3mM EDTA in running buffer). Across the NTA experiments, the average response was 100 RU. After nickel injection, and the various cleaning steps to remove excess nickel, M was injected over the nickel charged surface. The average response across the NTA experiments was 40 RU.

## **SA-biotin-trisNTA Immobilisation**

Streptavidin (SA) chips were pre-conditioned as per manufacturer's instructions, by 3 x 1 min injections of a 50mM NaOH 1M NaCl solution at 50  $\mu\text{L}\cdot\text{min}^{-1}$ . As described by (Reichel et al., 2007), biotin-trisNTA was injected over the conditioned SA chip surface. The surface was saturated by injecting 500 nM of biotin-trisNTA for 5 min at 20  $\mu\text{L}\cdot\text{min}^{-1}$ . This was done to ensure the majority of SA binding sites were occupied, to prevent any binding of the M C-terminal Strep-tag II to SA. Whilst the Strep-tag II is designed to bind to StrepTactin, it still exhibits some affinity for SA (Schmidt et al., 1996). In future experiments, it may be wise to design a construct for M expression and purification with a cleavable Strep-tag II, or attach the Strep-tag II to the N-termini, with the 6xHis-tag.

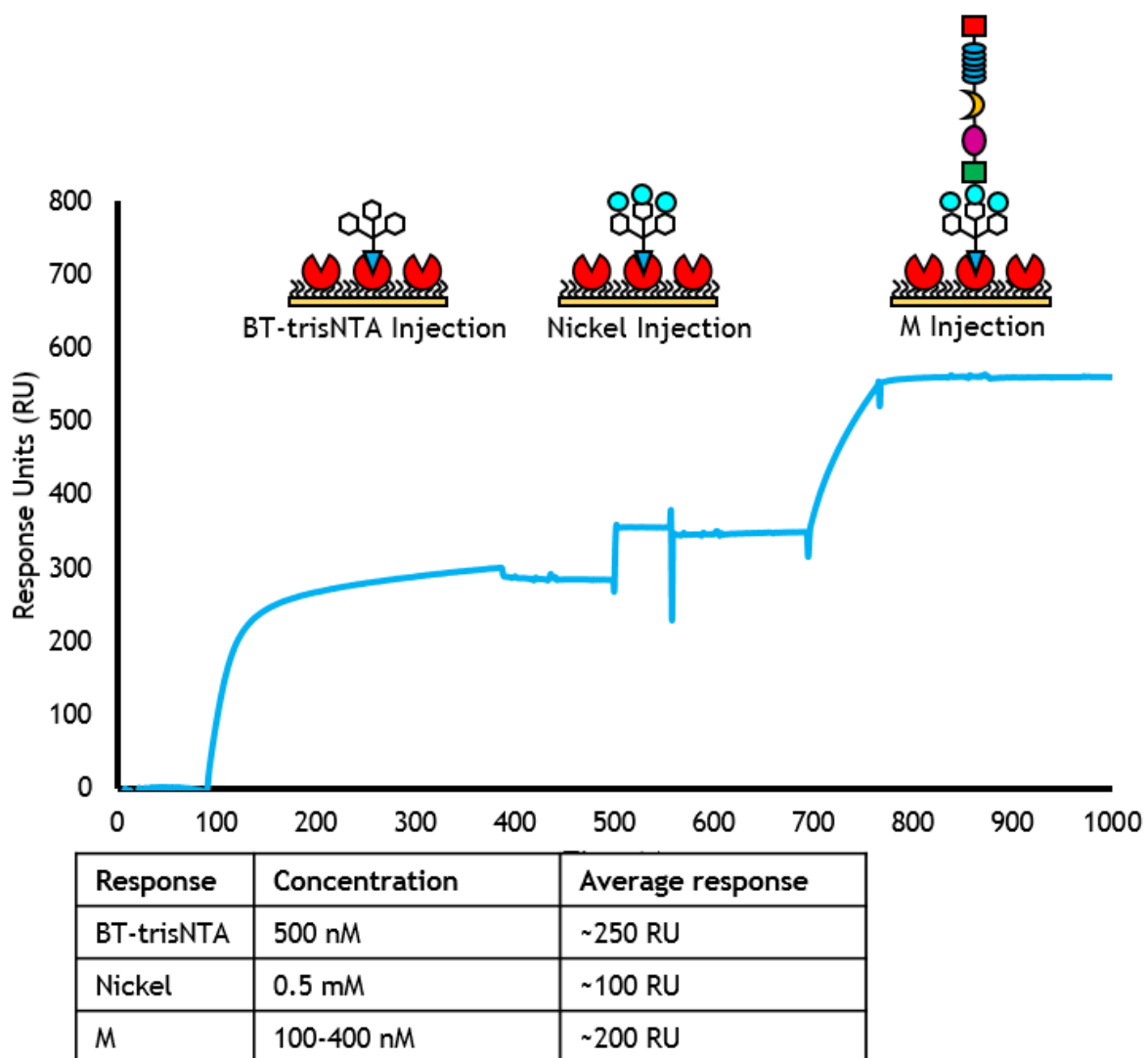


Figure 5.8 Sample sensorgram of the SA-biotin-trisNTA M immobilisation method, shown in blue. Visualisation of each step is shown diagrammatically above the step on the sensorgram. 500nM of biotin-trisNTA was injected over the pre-conditioned SA surface to an average response of 250 RU. Nickel was then injected over the surface, to an average RU of 100. After nickel injection, M was injected over the nickel charged surface. The average response across the SA experiments was 200 RU.

Figure 5.8 shows a sample sensorgram and schematic of M immobilisation to the SA-biotin-trisNTA surface. Biotin-trisNTA bound to the SA surface to ~250 RU across various experiments. Using the equation above; and assuming 1:1 binding of a 6xHis-tagged protein to a tris-NTA moiety, a Mw of 147 kDa for M and 1.39 kDa for biotin-trisNTA; this gives an  $R_{max}$  for M of 20,000 RU. This level is more than sufficient to bind the 294 RU required for an  $R_{max}$  of 100 RU for the interaction between M and AvrM.

After injection of the biotin-trisNTA, nickel was injected over the surface. Nickel binding typically ranged from 50-100 RU across the experiments and produced a very stable baseline in comparison to the NTA surface. After injection of the nickel, M was injected over the surface. The average response for M was ~200 RU, significantly higher than the NTA immobilisation method, however it was also more variable than the NTA method. This was perhaps due to various batches and concentrations of M. The higher RU responses were also coupled with a much more stable baseline, which enabled longer injection times and the potential to conduct titration kinetic experiments. It also meant fewer regeneration steps, which are likely to reduce the activity of the M protein, and possibly influence its ability to bind AvrM.

Figure 5.9 shows the average binding and drift of the two immobilisation methods. The SA method is preferred to the NTA method but may still require some optimisation. Differences between M binding could also be attributed to different co-purified contaminants or breakdown products in the difference M batches, so perhaps a little more refinement in the purification methods is still required. Regardless, full-length M has been successfully immobilised to the SPR surface sufficiently to examine interaction between NLRs and effectors.

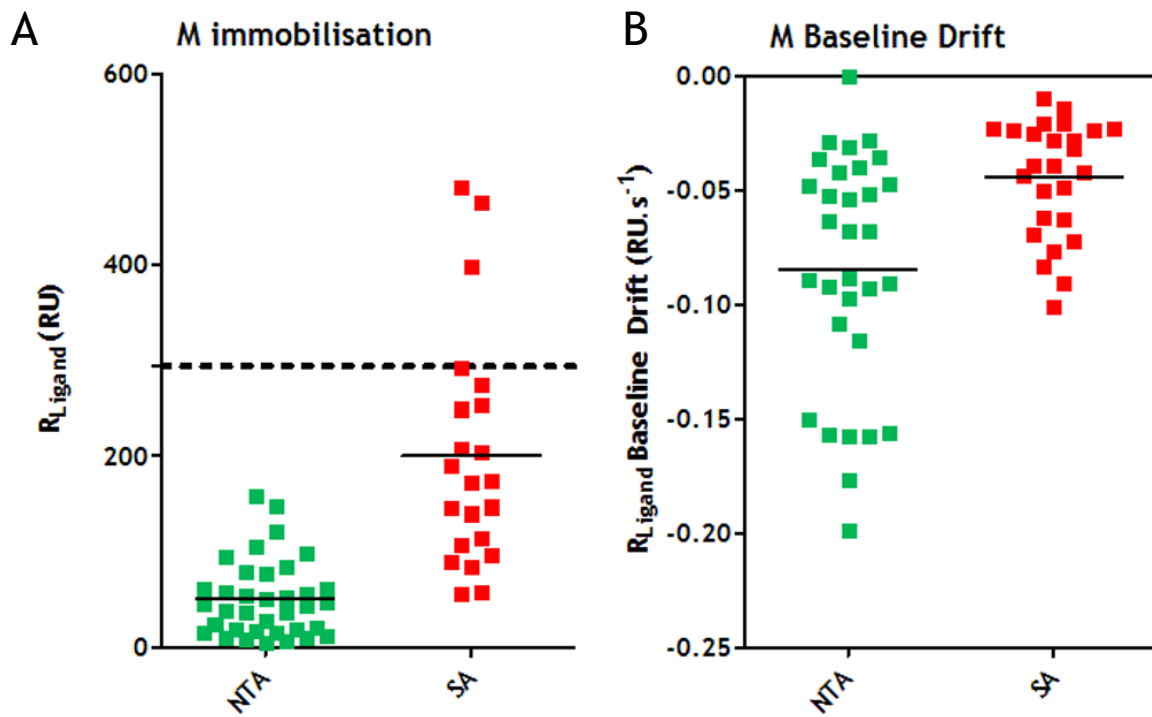


Figure 5.9 Compilation of M binding and drift on both NTA and SA surfaces. A Plots the  $R_{Ligand}$  for each experiment. The dotted line indicates the required RU to achieve an  $R_{max}$  for M/AvrM of 100, the recommended figure for kinetics experiments. B shows baseline drift of the sample channel after M injection. Drift is measured in  $RU \cdot s^{-1}$ .

## **Ni-NTA AvrM experiments**

To assess M and AvrM binding, M was immobilised using the Ni-NTA method. AvrM was then injected over the sample and reference surfaces. Figure 5.10 shows the results of six different sensorgrams. In this experiment different concentrations of AvrM, avrM and a blank injection were flowed over independently immobilised M protein. For each run, 100 nM of 10  $\mu\text{L}$  M protein was injected over the sample surface at 5  $\mu\text{L}\cdot\text{min}^{-1}$  to 40-50 RU. To begin the measuring association, 90  $\mu\text{L}$  of AvrM or avrM or buffer was then injected over both sample and reference surfaces at 30  $\mu\text{L}\cdot\text{min}^{-1}$ , and was followed by injection of 60  $\mu\text{L}$  of running buffer at 30  $\mu\text{L}\cdot\text{min}^{-1}$ . Between runs the surface was regenerated with running buffer containing 1 mM EDTA to remove nickel, M and effector proteins.

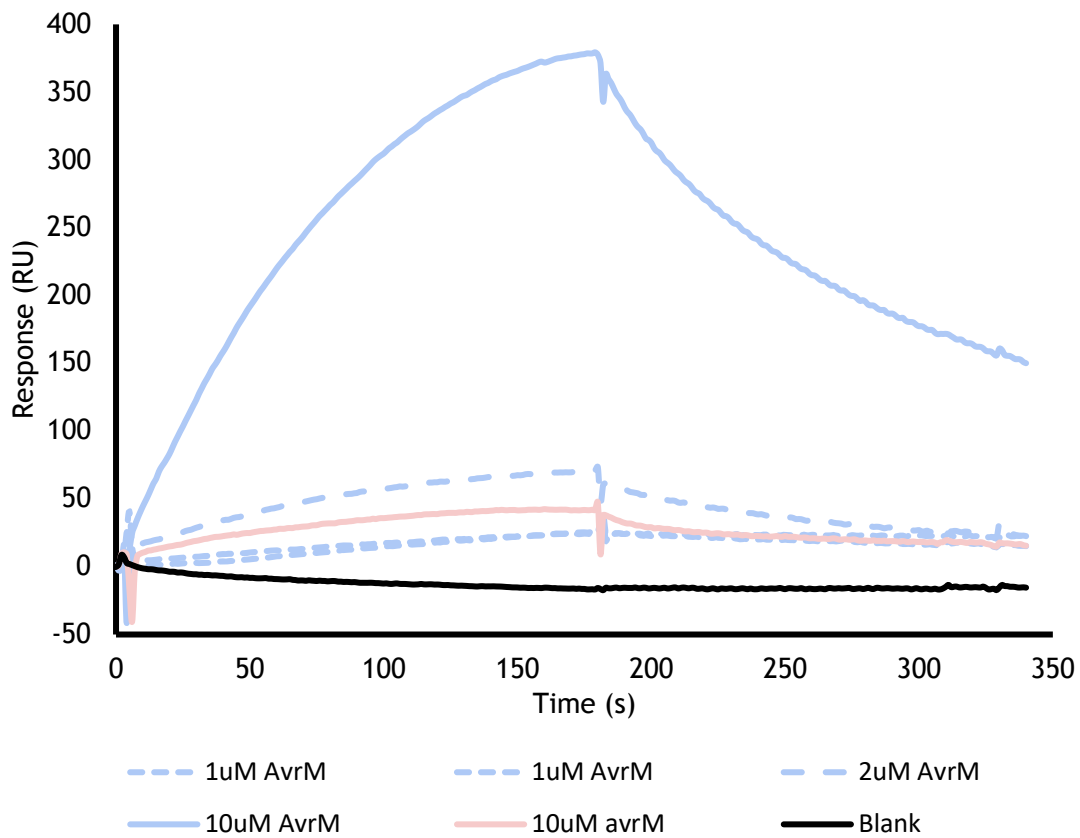


Figure 5.10 Examples of AvrM and avrM sensorgrams. Various AvrM (blue) concentrations injected over M immobilised on an NTA surface. Also included are a blank injection (black) and avrM injection (pink).

Figure 5.10 shows the association and dissociation curves for the effectors, with the point of effector injection set to 0 s, 0 RU. The sensorgrams clearly show that AvrM binds more rapidly than avrM to the M surface, with 10  $\mu$ M AvrM reaching an RU of 384, compared to 41 RU for 10  $\mu$ M avrM. AvrM at a concentration of 2  $\mu$ M was able to generate a higher response (69 RU) than 10  $\mu$ M avrM. To confirm this result, it was also necessary to examine non-specific binding to the reference surface.

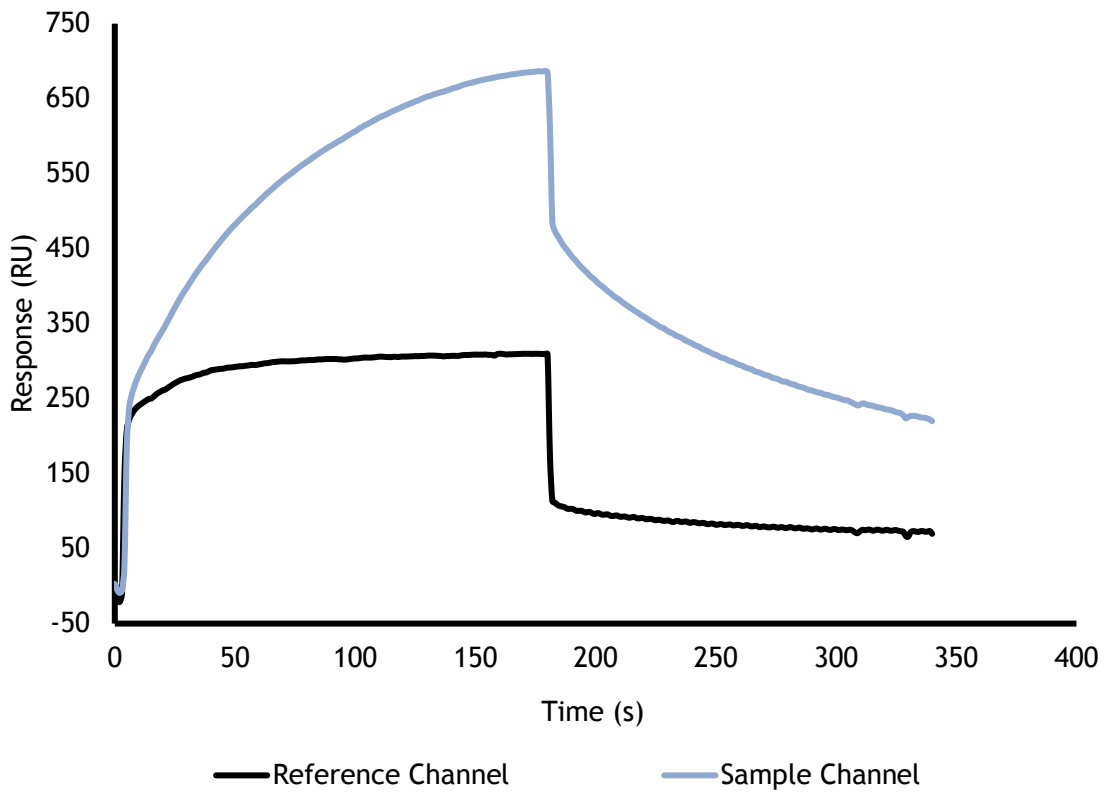


Figure 5.11 Reference channel sensorgram. Reference and Sample channel of 10uM AvrM injection over M immobilised on NTA surface. Black = reference channel, nickel only injection, Blue = sample channel, nickel and M injection.

The reference surface was charged with nickel, but no M was injected over the surface, and was used to account for non-specific binding of AvrM to the sensor chip surface. Figure 5.11 shows the difference in binding of 10  $\mu\text{M}$  AvrM between the reference and sample surfaces. The vertical jumps in RU at 0s and 180s are caused by changes in refractive index of the buffers and samples injected over the surface. There is significantly more interaction between the sample surface, containing M protein, than the reference channel. This suggests the interaction observed is between the M protein and AvrM, although using a different NLR of 6xHis-tagged protein would serve as another robust control. From this result, additional concentrations of AvrM were used to generate kinetic constants for the interaction between M and AvrM.

To derive kinetics of the interaction between M and AvrM, different concentrations of AvrM were injected over immobilised protein. M protein was removed and fresh protein was immobilised to 50-100 RU for each AvrM concentration. Conditions were the same as the experiment as in Figure 5.10, except that the concentration of the M protein injected was 350 nM instead of 100 nM. A range of concentrations were chosen between 1  $\mu\text{M}$  and 10  $\mu\text{M}$  AvrM, however some were excluded due to significant spikes in the curves, likely due to air bubbles introduced during sample preparation.

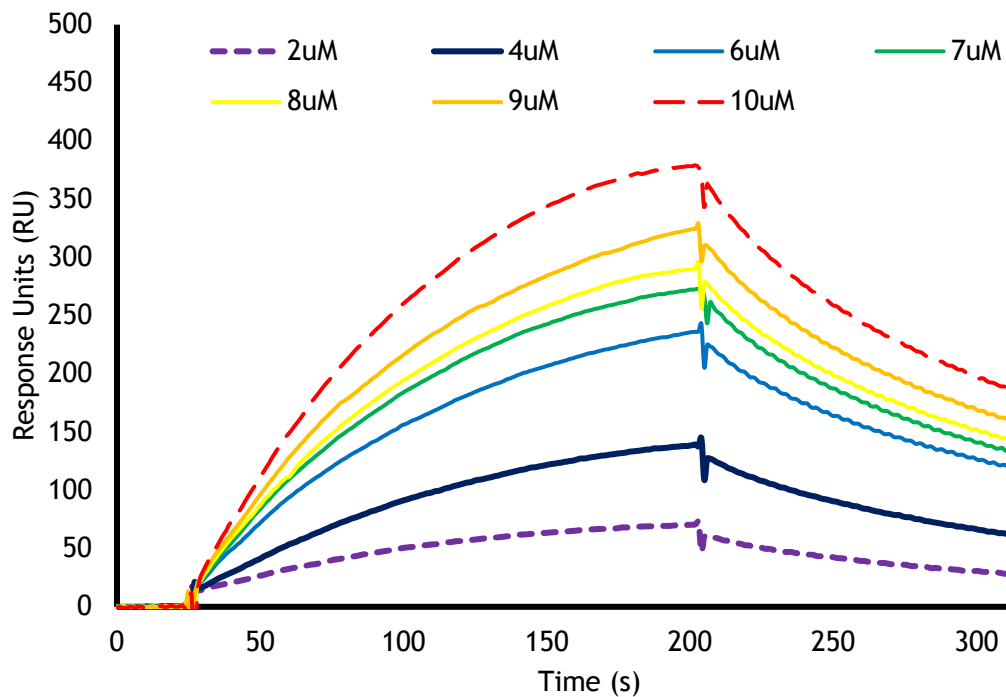


Figure 5.12 Multi-cycle kinetic analysis of the M/AvrM interaction on M immobilised using the NiNTA immobilisation strategy. Surface was regenerated and recharged with new nickel and M between each concentration.

As seen in Figure 5.12, RU increased as AvrM concentration increased. AvrM at a concentration of 2  $\mu\text{M}$  produced RU of 70, similar to the previous run (Figure 5.10), as did 10  $\mu\text{M}$  AvrM (378 RU compared to 384 RU). Using the  $R_{\text{max}}$  formula, a  $R_{\text{ligand}}$  of 100 for M, an  $R_{\text{max}}$  for AvrM of 378 RU (the RU of the highest concentration measured) and assuming 1:1 binding of the AvrM dimer to M monomer, this suggests that either one M protein is binding 11 dimers of AvrM, or that there are some non-specific interactions occurring between the surface of the chip, or other proteins on the chip surface, and AvrM, the latter being the more likely scenario. This is despite the reference channel with no M immobilised showing very little interaction with AvrM, with most change caused by changes in refractive index. Contaminants or aggregated protein on the chip surface may also explain a higher than expected  $R_{\text{max}}$ .

Despite these results, there does appear that there is some difference in binding to M between AvrM and avrM in SPR. Unfortunately, in the Ni-NTA immobilisation system there appears to be significant non-specific binding making it difficult to show that differences in interaction are real and not an artefact. To try and mitigate this non-specific binding, another immobilisation system was also trialled.

## **M and AvrM on SA-biotin-trisNTA surface**

To mitigate some of the non-specific interaction between the M immobilised surface and AvrM, a different immobilisation method was used. Overall, as seen in Figure 5.9, M was immobilised to a higher RU using the SA-biotin-trisNTA immobilisation technique compared to the Ni-NTA technique. Figure 5.13 shows two example sensorgrams of M immobilisation, with a blank injection and an AvrM injection. Each run was done after charging with biotin-trisNTA. To activate the surface, 100  $\mu\text{L}$  of 500 nM biotin-trisNTA diluted in  $\text{H}_2\text{O}$  was injected over the sample surface of each chip at  $20 \mu\text{L}\cdot\text{min}^{-1}$ . As with the Ni-NTA surface preparation, 0.5 mM  $\text{NiSO}_4$  was injected over the sample channel for 1 min at  $10 \mu\text{L}\cdot\text{min}^{-1}$ , followed by 20  $\mu\text{L}$  of 425 nM of M at  $10 \mu\text{L}\cdot\text{min}^{-1}$ . AvrM was then injected over the sample and reference channels. 200  $\mu\text{L}$  of AvrM was injected at  $40 \mu\text{L}\cdot\text{min}^{-1}$ , followed by 200  $\mu\text{L}$  of running buffer at the same flow rate.

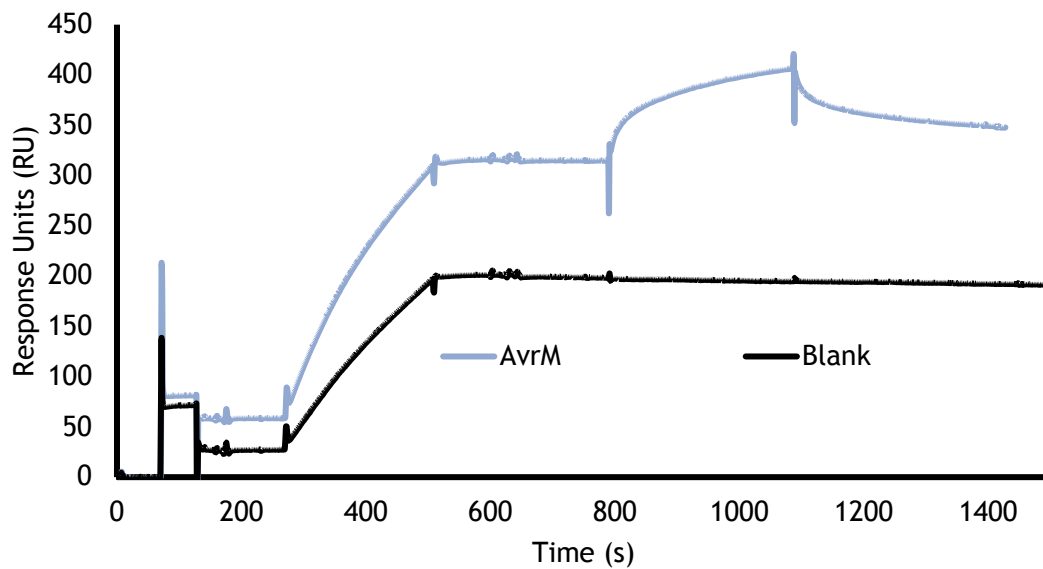


Figure 5.13 Comparison of AvrM (blue) and blank injection (black) sensograms over SA-biotin-trisNTA surface. Nickel injection is seen from 70-140 s, M injection from 270-500 s, AvrM and blank association phase from 800-1100s and dissociation from 1100-1500 s.

To assess if AvrM was binding non-specifically to the reference surface, different concentrations of AvrM were injected over a SA-biotin-trisNTA surface with nickel immobilised, but no M. As a control, 60  $\mu\text{L}$  of buffer at 20  $\mu\text{L}\cdot\text{min}^{-1}$  was injected in the ligand binding step, followed by 200  $\mu\text{L}$  of concentrations of 0  $\mu\text{M}$ , 200  $\mu\text{M}$ , 400  $\mu\text{M}$ , 800  $\mu\text{M}$ , 1600  $\mu\text{M}$  and 3200  $\mu\text{M}$  AvrM at 50  $\mu\text{L}\cdot\text{min}^{-1}$ . Figure 5.14 shows the maximum RU for AvrM during each injection step, with no concentration reaching above 3 RU. This shows that any interactions seen on surfaces with M protein immobilised are likely to be interactions between the M and AvrM, and not nonspecific interactions. Determination of binding kinetics of M and AvrM was then next step, using two different methods, single cycle kinetics and multi-cycle kinetics.

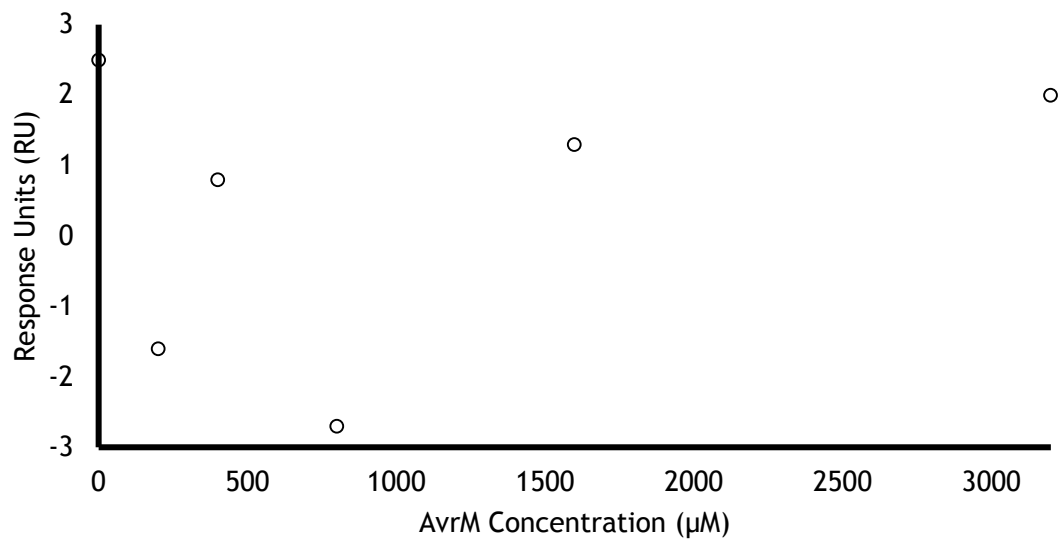


Figure 5.14 Blank surface AvrM injections. Increasing concentrations of AvrM were injected over a SA-biotin-trisNTA charged with nickel, but not M, to measure non-specific binding to the reference surface.

## Multi-cycle kinetics for AvrM interaction with M

For the derivation of kinetics for AvrM interaction with M, a multi-cycle approach was used. In this experiment, different concentrations of AvrM were injected over the same immobilised M surface, with a wash step in between each run to remove excess AvrM. Running buffer was used to wash AvrM from the surface, without dissociating M protein. Washing with EDTA to remove both M and AvrM between each cycle would provide a cleaner surface each time, but to conserve M protein, a gentle wash step to remove as much as AvrM as possible was employed. Figure 5.15 shows two replicates of such kinetics assays. As can be seen from the sensorgrams, RU due to AvrM increased as AvrM concentration increased. A Langmuir 1:1 binding model was fitted to the curves, shown in Appendix 4, with a  $\text{Chi}^2$  of 0.39 for Figure 5.15A and  $\text{Chi}^2$  of 0.678 for Figure 5.15B. The resultant association rate constants ( $k_a$ ), dissociation rate constants ( $k_d$ ) and dissociation constants ( $K_D$ ) for both experiments were comparable.

The association rate constant,  $k_a$ , describes the rate of complex formation i.e. the number of M/AvrM complexes formed per second in a one molar solution of M and AvrM, and has units of  $\text{complexes} \cdot \text{M}^{-1} \cdot \text{s}^{-1}$ . Association rate constants for protein-protein interactions range between  $1 \times 10^3$  to  $1 \times 10^9 \text{ M}^{-1} \cdot \text{s}^{-1}$  (Schreiber et al., 2009).  $k_d$  describes the stability of the complex; the fraction of complexes that decay per second, with a typical range is  $1 \times 10^{-1}$  to  $1 \times 10^{-6}$ . A  $k_d$  of  $1 \times 10^{-2} \text{ s}^{-1}$  means that 1% of complexes decay every second.

M and AvrM have a  $k_a$  of  $2.53 \times 10^3 \pm 99 \text{ M}^{-1} \cdot \text{s}^{-1}$ , and a  $k_d$  of  $5.98 \times 10^{-3} \pm 7.78 \times 10^{-4} \text{ s}^{-1}$ . According to Alsallaq and Zhou (2008) and Schreiber et al. (2009) this interaction is quite weak, well below the association rate constant for protein-antibody interactions ( $1 \times 10^6 \text{ M}^{-1} \cdot \text{s}^{-1}$ ). The dissociation rate constant falls in the middle of the range for protein-protein complexes, with 0.6% of M/AvrM complexes decaying every second. The dissociation constant for the interaction was measured as  $2.37 \times 10^{-6} \pm 3.96 \times 10^{-7} \text{ M}$ , indicative of a weak transient protein-protein interaction (Acuner Ozbabacan et al., 2011).

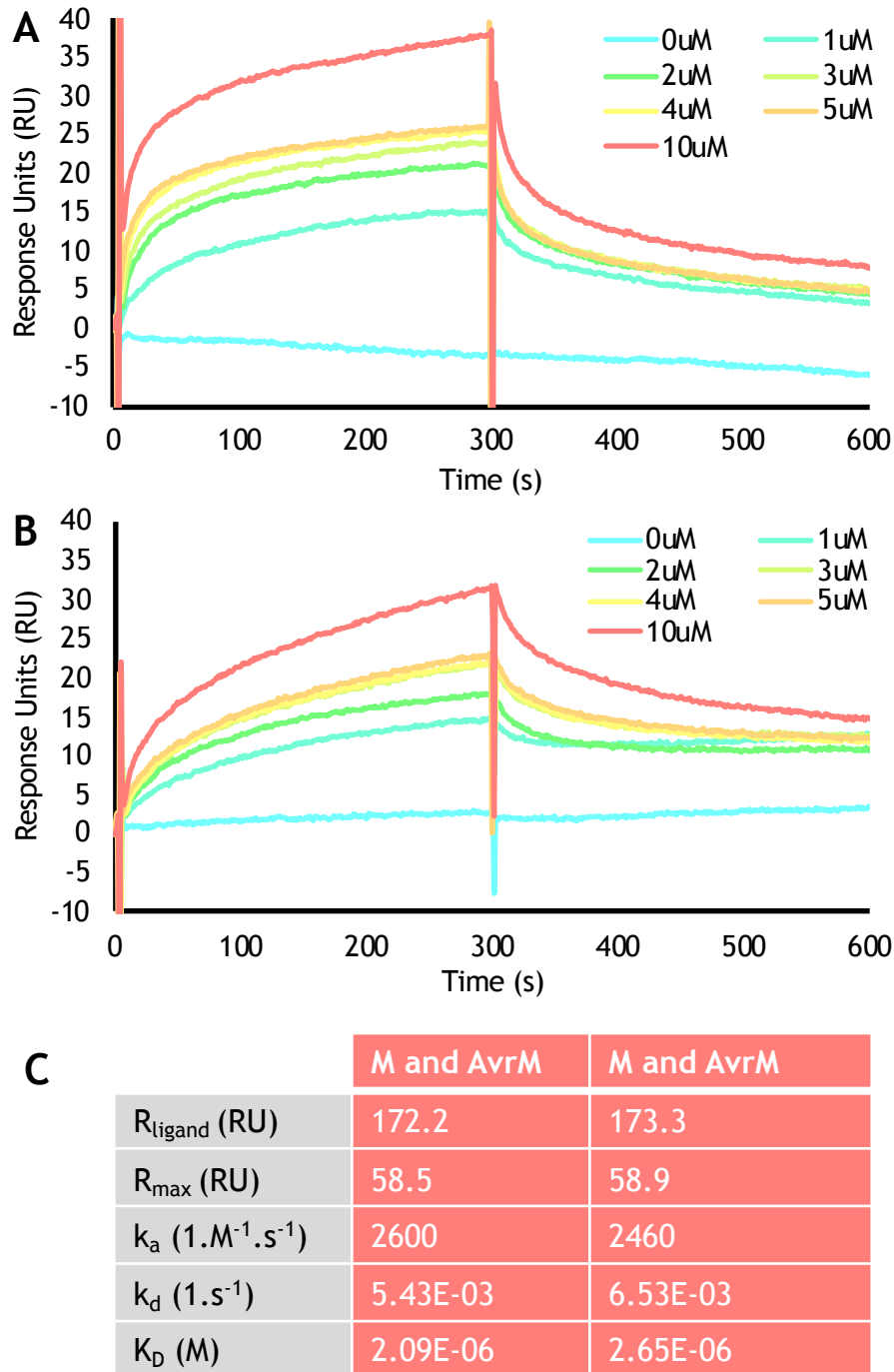


Figure 5.15 Multi-cycle kinetic analysis for AvrM interaction with M. **A** and **B** Duplicate multi-cycle kinetics analysis for AvrM. Sample channel was charged with nickel and M, reference channel with neither. M was immobilised to ~170 RU in each experiment. Increasing concentrations of AvrM were injected over the surface, with short injections of running buffer in between as a gentle regeneration method. Curves were fit to Langmuir 1:1 binding models, and **C** resulting kinetic data were derived from these models.

To further validate these kinetic parameters, a different concentration range of AvrM was injected over an M immobilised surface, as seen in Figure 5.16. In these experiments, more M protein was immobilised, resulting in higher RU than that seen in Figure 5.15. Fitting a Langmuir 1:1 binding model to each of the curves, seen in Appendix 4 Figure 7.12, gave the kinetics of the interaction, comparable to that seen in Figure 5.15C. The measured  $k_a$  was slightly lower, at  $1.65 \times 10^3 \pm 7.7 \text{ M}^{-1} \cdot \text{s}^{-1}$ , as was the  $k_d$ , at  $2.08 \times 10^{-3} \pm 9.90 \times 10^{-5} \text{ s}^{-1}$ . The  $K_D$  was also comparable, at around  $1.27 \times 10^{-6} \pm 4.95 \times 10^{-8} \text{ M}$ . The range of AvrM concentrations in Figure 5.16 are more suitable for deriving kinetic parameters than those presented in Figure 5.15, as they cover a broader range of the  $R_{\text{max}}$ . Having kinetic parameters for the M/AvrM interaction, the next step was to derive the same parameters for the M/avrM interaction.

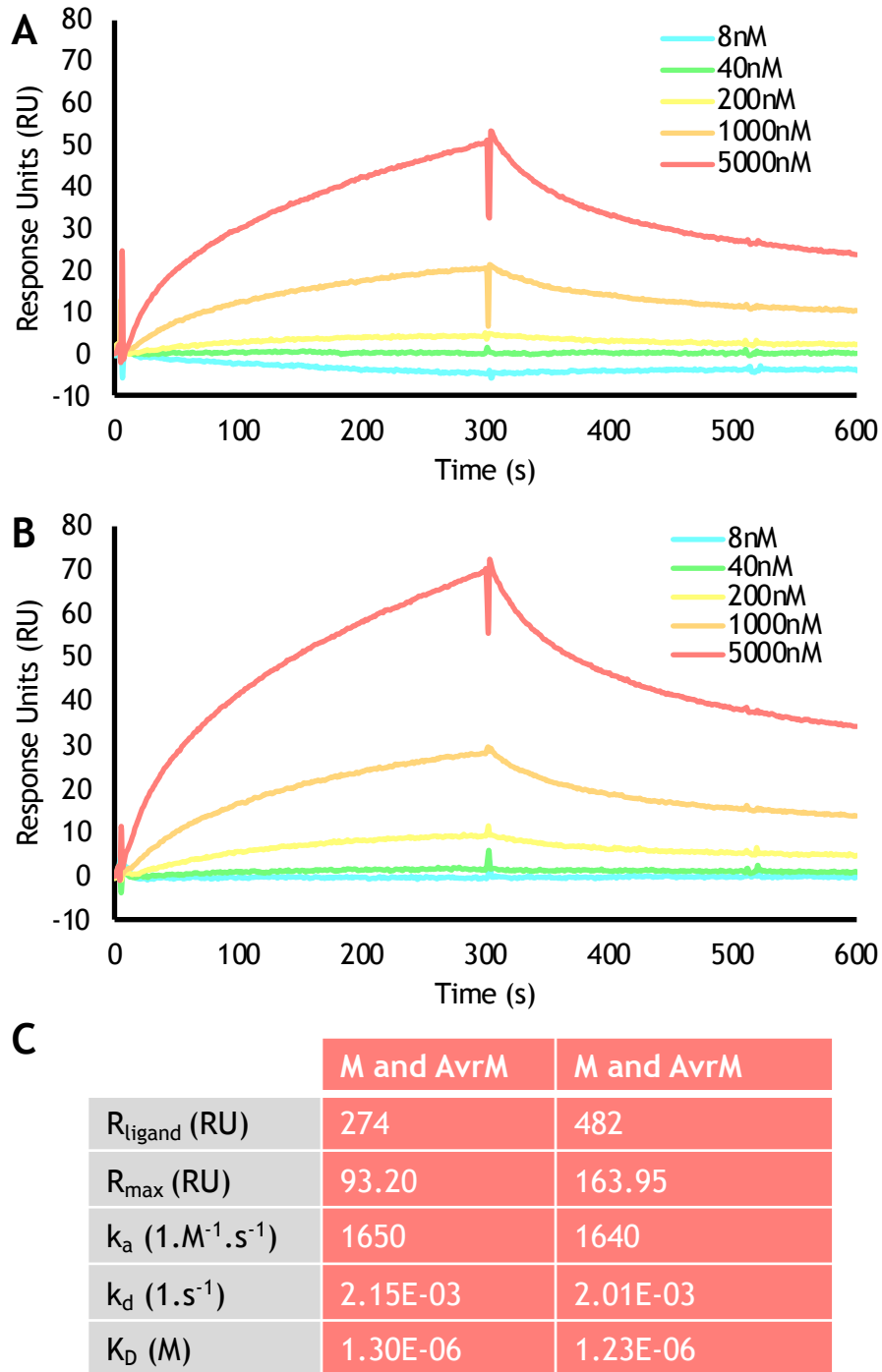
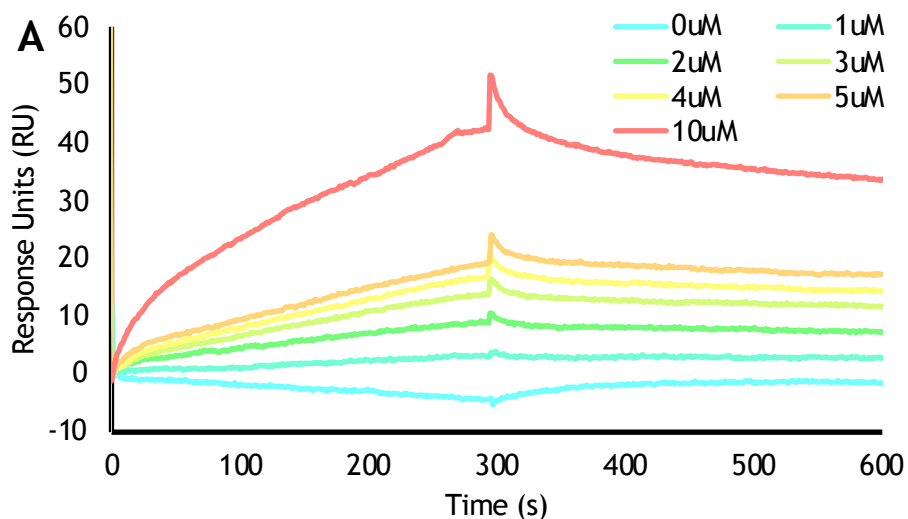


Figure 5.16 Multi-cycle kinetic analysis for AvrM interaction with M. **A** and **B** Duplicate multi-cycle kinetics analysis for AvrM. Sample channel was charged with nickel and M, reference channel with neither. Increasing concentrations of AvrM were injected over immobilised M. Curves cut and shifted using BIAEvaluation software, kinetics derived using BIAEvaluation software.

## **M and avrM Multi-cycle kinetics**

The same approach that was used to derive M/AvrM interaction kinetics was used to derive M/avrM interaction kinetics. Different concentrations of avrM were injected over the same immobilised M surface, with a wash step in between each run to remove excess avrM. Running buffer was used to wash avrM from the surface, without dissociating M protein. M was immobilised to an RU of 146, and concentrations ranging from 1 to 10  $\mu\text{M}$  of avrM were injected over the surface. Flow rates, buffers and injections times were the same as in Figure 5.13.

$k_a$ ,  $k_d$  and  $K_D$  were all calculated for avrM using the same Langmuir 1:1 binding models, seen in Appendix 4, Figure 7.13, and can be seen in Figure 5.17. The  $k_a$  was significantly lower than that for M/AvrM, at  $8.29 \text{ M}^{-1} \cdot \text{s}^{-1}$ , lower than any association rate constant measured for protein-protein interactions (Schreiber et al., 2009). This suggests the interaction between M and avrM is extraordinarily weak, or more likely non-existent. Interestingly, the  $k_d$  measure is comparable to that of the M/AvrM interaction, at  $1.82 \times 10^{-3} \text{ s}^{-1}$ , however the  $K_D$  was lower, at  $2.19 \times 10^{-4} \text{ M}$ . The  $k_d$  and  $K_D$  for the M/avrM complex are likely artefacts, given the association rate is also close to zero.



**B**

	M and avrM
$R_{\text{ligand}}$ (RU)	146.1
$R_{\text{max}}$ (RU)	49.7
$k_a$ ( $1 \cdot M^{-1} \cdot s^{-1}$ )	8.29
$k_d$ ( $1 \cdot s^{-1}$ )	1.82E-03
$K_D$ (M)	2.19E-04

Figure 5.17 Multi-cycle kinetic analysis for avrM interaction with M. **A** Multi-cycle kinetics analysis for AvrM. Sample channel was charged with nickel and M, reference channel with neither. M was immobilised to ~170 RU. Increasing concentrations of avrM were injected over the surface, with short injections of running buffer in between as a gentle regeneration method. Curves were fit to Langmuir 1:1 binding models, and **B** resulting kinetic data was derived from these models.

To assess if avrM was interacting with the SA-biotin-trisNTA surface, different concentrations were injected over a nickel charged surface, with no M injected. As seen in Figure 5.18, avrM appears to bind to the surface more than AvrM, see Figure 5.14. It is likely then that most of the apparent interaction observed between M immobilised surfaces and avrM are artefacts.

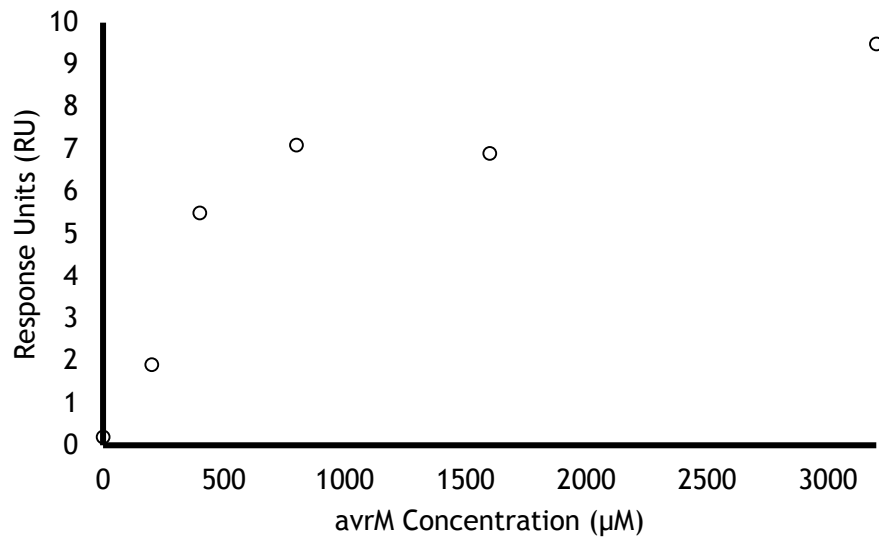


Figure 5.18 avrM interaction with blank surface. Increasing concentrations of avrM were injected over a SA-biotin-trisNTA charged with nickel, but not M, to measure non-specific binding to the reference surface.

## Single cycle kinetics

As well as the multi-cycle kinetics approach, a slightly different method to measure kinetic parameters was also tested. The single cycle kinetics, or kinetic titration method, involves injection of increasing concentrations of the analyte over the same ligand surface, as described in Karlsson et al. (2006). This method was employed as a way to conserve M protein, and to reduce the number of wash steps between effector injections, in the hopes that the M protein would remain more active and stable after repeat experiments.

M was immobilised in the same manner as the multi-cycle kinetic experiments. For AvrM and avrM, concentrations of 1, 2, 3, 4 and 5  $\mu\text{M}$  were injected over the surface in a volume of 200  $\mu\text{L}$  at 40  $\mu\text{L}\cdot\text{min}^{-1}$ , with each concentration followed by 200  $\mu\text{L}$  of running buffer before the next concentration was injected. Curves were analysed and models were fit using the BiaEvaluation software. A modified version of the kinetic model from (Karlsson et al., 2006) was used to fit the curves, with adjustments to the concentration range used, shown in Appendix 5 Figure 7.14. Models fit to the curves in Figure 5.19 can also be seen in Appendix 5.

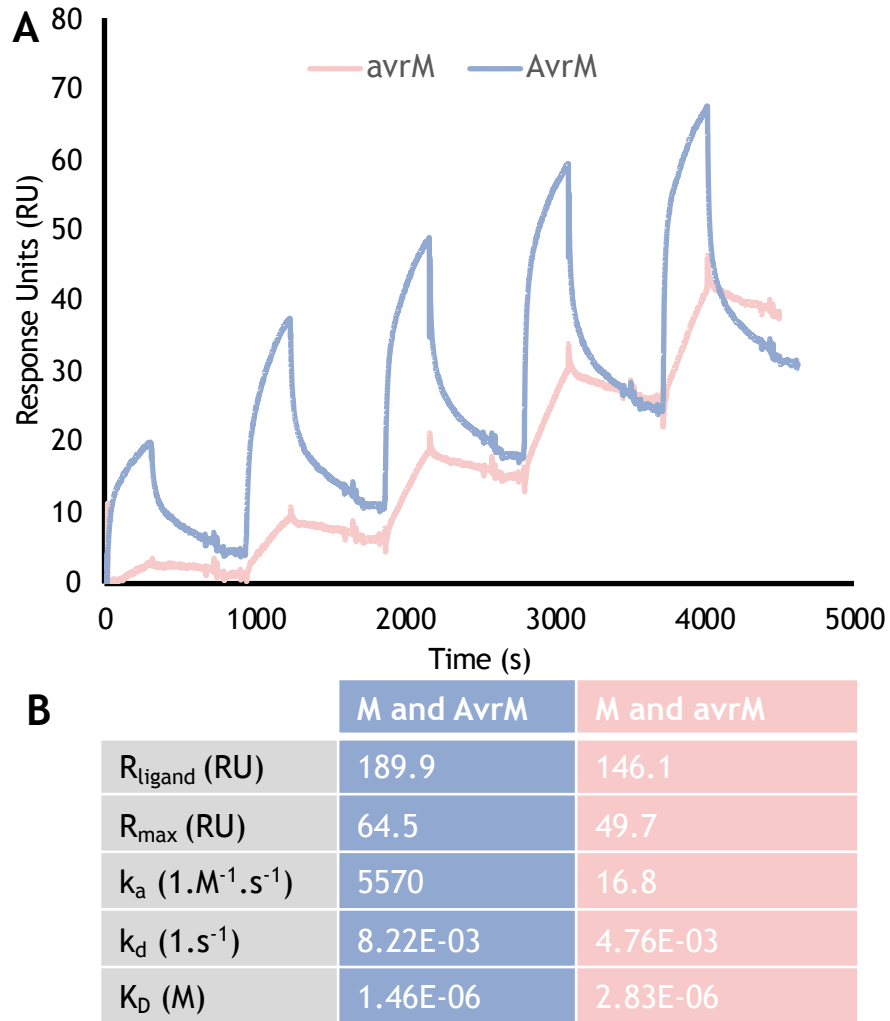


Figure 5.19 Single-cycle kinetic analysis of the interaction of AvrM and avrM with M. **A** Single-cycle kinetics (or titration kinetics) analysis for AvrM and avrM. Sample channel was charged with nickel and M, reference channel with neither. M was immobilised to 190 RU for AvrM and 145 RU for avrM. Increasing concentrations of AvrM and avrM were injected over both surfaces. Curves were fit to a slightly modified (Figure 7.14) Kinetic Titration models, and **B** resulting kinetic data was derived from these models.

The  $k_a$ ,  $k_d$  and  $K_D$  values obtained from the single cycle kinetics experiments were comparable to those obtained from the multi-cycle kinetics for both AvrM and avrM. The  $k_a$  for AvrM interaction with M was measured as  $5.57 \times 10^3 \text{ M}^{-1} \cdot \text{s}^{-1}$ , whilst for avrM was  $16.8 \text{ M}^{-1} \cdot \text{s}^{-1}$ . This is consistent with the M/AvrM complex being a weak transient protein-protein interaction, and the interaction between M and avrM being almost non-existent. The  $k_d$  measured for the M/AvrM interaction was  $8.22 \times 10^{-3} \text{ s}^{-1}$ , and for M/avrM  $4.76 \times 10^{-3} \text{ s}^{-1}$ . As the association rate constant for M/avrM is very low, this is likely non-specific interactions occurring between avrM and the surface. The  $K_D$  value for the M/AvrM interaction is also comparable to the multi-cycle kinetics  $K_D$  value, at  $1.46 \times 10^{-6} \text{ M}$ . From these results, and the multi-cycle kinetics results, it appears that M and AvrM interact in a weak, transient manner, with micromolar affinity, and M and avrM have almost no interaction at all. Next, the effect of mutations on this interaction was observed.

## **AvrM and avrM Mutants**

To assess the binding kinetics of AvrM EA2 and avrM a3, a multi-cycle kinetics approach was used, with a wash step between each effector concentration to remove excess effector. Injection volumes, flow rates and dissociation times were the same as used for AvrM and avrM kinetics experiments, as were the concentrations used. As can be seen in Figure 5.20, for almost every concentration of either AvrM EA2 and avrM a3 injected, the response units exceeded the theoretical  $R_{\max}$  for the interaction between monomeric M and a dimeric effector, assuming a 1:1 binding. The  $R_{\max}$  for an interaction between monomeric and M and monomeric effector would be half the values shown in Figure 5.20.

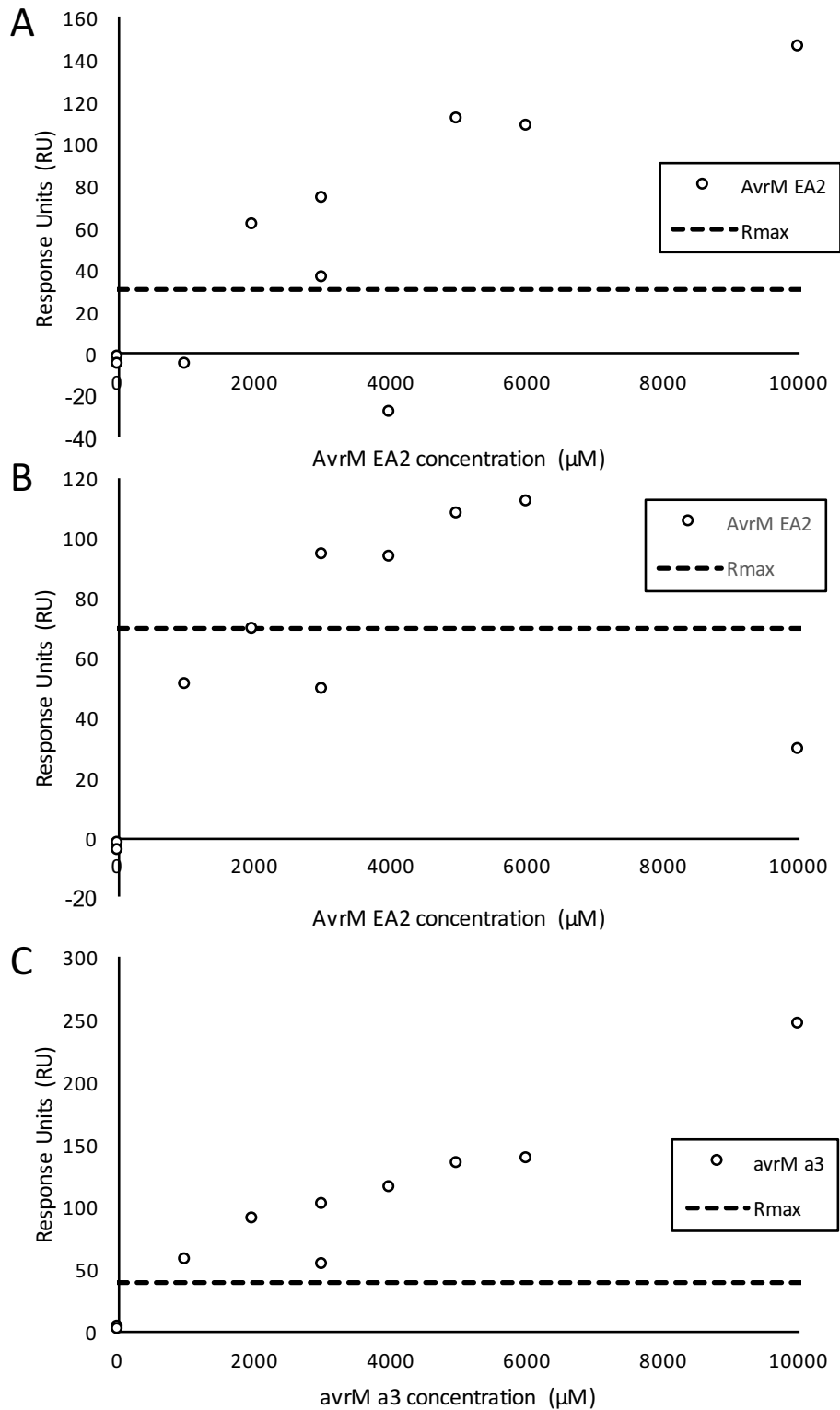


Figure 5.20 Response unit v concentration plots of interaction between M/AvrM EA2 and M/avrM a3. Increasing concentrations of EA2 and a3 were injected over M immobilised by SA-biotin-trisNTA. Effector mutants were injected over the surface at  $40 \mu\text{L}\cdot\text{s}^{-1}$  for  $200 \mu\text{L}$ , with a regeneration step between each concentration to remove excess effector. Dotted lines show the theoretical  $R_{\text{max}}$  for each M ligand RU, assuming an effector dimer and 1:1 binding.

Interestingly, AvrM EA2 gave a similar RU for each concentration despite different M immobilisation between the two experiments, suggesting either binding to the matrix, or significant non-specific binding. It was more likely non-specific binding to the M protein, as the RU shown is the difference between the reference and sample surface. Unfortunately, due to time constraints and resources, it was not possible to optimise the conditions to attempt to reduce non-specific binding for the effector mutants.

## **Discussion**

### **M immobilisation method**

The most important part of any SPR experiment is choosing the appropriate immobilisation chemistry. The most commonly used method of protein immobilisation in SPR experiments is amine coupling, whereby free amines are covalently bound to the carboxymethyl-dextran matrix of the sensor chip (Fischer, 2010). There are other methods of covalent coupling that target other side groups, including carboxyl and sulfhydryl groups. This method is advantageous because any protein can be covalently bound to a carbon dextran surface so long as it has a solvent exposed amine, carboxyl or sulfhydryl group (Arenkov et al., 2000).

Covalent binding can be both advantageous and disadvantageous, depending on the protein immobilised. Covalent binding will ensure minimal baseline drift when conducting experiments, and removing analyte between experiments is almost trivial, as most common regeneration methods will not be able to disrupt the covalent bond between the ligand or analyte. However, if the process of immobilisation or regeneration comprises the ligands activity or structure, it cannot be removed and often the chip will be rendered useless. It was decided that amine coupling, or other covalent coupling methods, were not suitable for M immobilisation. There are a few reasons for this, which are explained below.

For M immobilisation, there were a few considerations that needed to be made, the first being the aim of the experiment. Depending on the experiment type, differing levels of M needed to be bound to the surface, each requiring different injection times and flow rates depending on the effector concentration. Kinetic interaction experiments

required low amounts of ligand binding. Any type of immobilisation surface could have been used for kinetics analysis, however a surface that could be regenerated with fresh ligand was more desirable, as it allowed for variation of ligand concentration without rendering the chip surface unsuitable if too much ligand was immobilised. An affinity capture method rather than a covalent capture method was therefore considered suitable for M immobilisation, as ligands could be removed more easily than covalent immobilisation.

The immobilisation method chosen also depended on injection lengths and dissociation times. Long injections were required for interactions between M and AvrM, as they were slow to dissociate. This meant a strong interaction between the ligand and the surface was required to account for M drift from the surface. As the M/AvrM mutant interaction was likely to be quite transient, a covalent interaction would have been best for this purpose. However, covalent immobilisation surfaces make it more difficult to regenerate the surface, which were required during longer injection times, especially when the ligand was susceptible to activity loss or structural changes. Trying covalent capture could be considered for future experiments, to eliminate the drifting baseline, however rigorous controls would be needed to ensure that M remains active during the immobilisation process.

Another consideration to make was uniform vs random capture (Trilling et al., 2013). Amine coupling (as well as other covalent coupling methods) will covalently bind the ligand to the carboxymethyl-dextran matrix in a multitude of orientations, often at multiple sites, creating a non-uniform surface for the analyte to bind. Uniform capture methods immobilise each ligand in the same orientation, to create a uniform binding surface for the analyte to interact with. This capture orientation is especially important for large protein-protein interactions that have low sensitivity, such as M and AvrM. Whilst it is unknown if any interaction would be observed with a random capture orientation, the amine coupling method may be more suitable for immobilisation of AvrM to the sensor surface.

As amine and other side-chain coupling methods do not discriminate between the ligand and any co-purified proteins or contaminants, samples that are not 100% pure will have other proteins bound to the chip surface as well as the target ligand. Even with the improved M purification methodology outlined in chapter 4, there are still contaminants associated with the purified proteins that could have interfered with interpretation of results. Using a more specific immobilisation system, targeting a protein tag or using an antibody specific to the ligand, is a more suitable method to capture proteins from a non-homogenous sample. Consideration of the above factors was the rationale for choosing the Ni-NTA method and SA-biotin-trisNTA method of capture.

### ***Ni-NTA immobilisation performance***

Ni-NTA immobilisation utilises the interaction between Ni-NTA and 6xHis-tagged proteins. It is a convenient method for immobilisation, as there is often no need for modification of the target ligand if it has been purified by IMAC. M has been purified by IMAC in the past (Williams et al., 2011), and is stable in the buffers used for this interaction. Using SAC purified M protein with a Ni-NTA surface serves as a secondary purification step, as any contaminants, breakdown products and co-purifying proteins will be unlikely to bind to the Ni-NTA surface. Ni-NTA immobilisation also has a uniform capture orientation, and is easy to regenerate, by either EDTA or imidazole. The easy regeneration step is also desirable, as SPR chips are expensive.

The downside of the Ni-NTA immobilisation strategy was the relatively weak binding affinity displayed between the 6xHis-tag and NTA molecule. For the longer injection times likely required for interaction analysis between AvrM and M, the baseline drift and weak binding caused by this weak interaction made it difficult to assess different concentrations of AvrM over the single M immobilised surface. The surface needed to be regenerated between each cycle with new M immobilised each time a new AvrM concentration was to be tested, creating a difference in  $R_{max}$  and other factors. This also consumed more purified M protein than trying a range of different concentrations with the one M immobilised surface.

### ***Streptavidin, biotin-trisNTA performance***

The second method took advantage of one of the strongest known non-covalent interactions known to biochemistry, the interaction between biotin and avidin (Chivers et al., 2011). This method worked similarly to both the Ni-NTA-6xHis-tag and Biotin-SA method, using a biotin-trisNTA conjugate to essentially 'biotinylate' a 6xHis-tag. The interaction between the trisNTA groups and a 6xHis-tag is four orders of magnitude stronger than other Ni chelators (Lata et al., 2005), enabling a much more stable capture. It is also more easily regenerated than a biotinylated protein on a SA surface, as EDTA can disrupt the binding between the 6xHis-tag and trisNTA groups.

Downsides of this setup included more chances for non-specific binding, additional mass on the surface (SA is around 58kDa) and slightly added cost (biotin-trisNTA is expensive). However, it did provide the benefits of uniform capture orientation and easy regeneration, both desirable characteristics for the intended experiments. The stronger binding affinity provided a more stable baseline than the Ni-NTA surface, enabling multiple concentrations of AvrM over a single M surface to be analysed, enabling more data points to be collected from precious stocks of M protein. This method has been used to immobilise proteins for SPR in the past (Reichel et al., 2007).

It was decided that M protein would be immobilised to the surface of the chips rather than the effectors for several reasons. First, and most significant, there was simply not sufficient amounts of M to perform the amount of experiments required to characterise the kinetics of the interaction. Second, the tags on the M protein would make both affinity capture methods difficult, as a tag-removal step would have to be added to the purification procedure. This could have been combated by using a covalent coupling method to immobilise the AvrM and effector proteins to the surface, however this would result in a random orientation on the surface of the chip, not ideal for transient protein-protein interactions. Third, immobilising the effect proteins would mean having to optimise at least five different immobilisation methods, as opposed to one when immobilising M. For these reasons, it was decided to only perform experiments with M immobilised. In future, trying the reverse orientation would be a good test of the kinetics derived from this approach.

## Kinetics of the M/AvrM interaction

Different kinetic experiments all yielded slightly varied, but comparable association and dissociation rate constants, and dissociation constants. Multi-cycle kinetics experiments yielded  $k_a$  values of  $2.53 \times 10^3 \pm 99 \text{ M}^{-1} \cdot \text{s}^{-1}$  (Figure 5.15) and  $1.65 \times 10^3 \pm 7.7 \text{ M}^{-1} \cdot \text{s}^{-1}$  (Figure 5.16), and  $k_d$  values of  $5.98 \times 10^{-3} \pm 7.78 \times 10^{-4} \text{ s}^{-1}$  (Figure 5.15) and  $2.08 \times 10^{-3} \pm 9.90 \times 10^{-5} \text{ s}^{-1}$  (Figure 5.16). The  $K_D$  of the M/AvrM interaction was  $2.37 \times 10^{-6} \pm 3.96 \times 10^{-7} \text{ M}$  (Figure 5.15) and  $1.27 \times 10^{-6} \pm 4.95 \times 10^{-8} \text{ M}$  (Figure 5.16). Single cycle kinetics experiments also produced comparable kinetics data, with a  $k_a$  of  $5.57 \times 10^3 \text{ M}^{-1} \cdot \text{s}^{-1}$ , a  $k_d$  of  $8.22 \times 10^{-3} \text{ s}^{-1}$  and a  $K_D$  of  $1.46 \times 10^{-6} \text{ M}$  (Figure 5.19). The  $k_a$ , the association rate constant, measures the number of M/AvrM complexes formed per molar per second, and is a measure of how quickly the complex forms. The  $k_d$ , the dissociation rate constant, not to be confused with the dissociation constant  $K_D$ , measures the portion of complexes that dissociate per second, and is used to measure how long complexes remain bound together.

With a  $k_a$  of  $\sim 2 \times 10^3 \text{ M}^{-1} \cdot \text{s}^{-1}$ , the M/AvrM interaction is not particularly strong, falling below the 'basal' rate for protein-protein interactions, that is interaction that occurs in the absence of an external biasing force (Schreiber et al., 2009). This low association rate constant could be explained by the activation models presented in chapter 3, which suggest that NLRs need to be in an active conformation in order to bind effectors. In the SPR assays conducted, no extra ATP was added as a means to induce an active form of the NLR, which may have resulted in the low association rate constant. Perhaps upon ATP binding, the association rate constant would increase, or perhaps another external biasing force is required for the interaction of M/AvrM.

The  $k_d$  of the interaction between M/AvrM is harder to put into context of protein-protein interactions, as the dissociation rate constant appears to be often neglected in analysis of protein-ligand binding (Corzo, 2006). With a measured  $k_d$  of  $\sim 4 \times 10^{-3} \text{ s}^{-1}$ , 0.4% of M/AvrM complexes decay every second, corresponding to a half-life of  $\sim 175 \text{ s}$  and a mean life, the average life span of the complex (Corzo, 2006), of  $\sim 250 \text{ s}$ .

The  $K_D$  of  $\sim 1.3 \text{ } \mu\text{M}$  for the interaction between M/AvrM suggests that is a weak, transient interaction. For comparison, the dissociation constant for binding of AVR-

PikD to the HMA domain of the rice NLR Pikp-1 measured by Maqbool et al. (2015) was determined to be 13 nM, two orders of magnitude greater affinity than the M/AvrM interaction. However, the AVR-PikD/Pikp-1-HMA domain interaction is measured between the decoy domain and effector protein, not in context of a full-length NLR, making direct comparisons difficult. It does suggest, as does the low  $k_a$ , in both the context of the equilibrium-switch model, and given that purified M protein is bound with more ADP than ATP, that an active ATP-bound M is required to bind AvrM more strongly. As (Maqbool et al., 2015) did not measure  $k_a$  and  $k_d$  values, the rate of complex formation and half-life cannot be compared.

### **M/avrM interaction**

Comparison of the M/avrM interaction to the M/AvrM interaction shows a faster rate of association between M and AvrM than M and avrM. Multi-cycle kinetics analysis determined the  $k_a$  to be  $8.29 \text{ M}^{-1} \cdot \text{s}^{-1}$ , the  $k_d$   $1.82 \times 10^{-3} \text{ s}^{-1}$  and the  $K_D$   $2.19 \times 10^{-4} \text{ M}$ , whilst single cycle kinetics analysis gave a  $k_a$  of  $16.8 \text{ M}^{-1} \cdot \text{s}^{-1}$ , a  $k_d$  of  $4.76 \times 10^{-3} \text{ s}^{-1}$  and a  $K_D$  of  $2.83 \times 10^{-6} \text{ M}$ . A  $k_a$  of less than  $20 \text{ M}^{-1} \cdot \text{s}^{-1}$  is miniscule, and far below rate constants normally associated with protein-protein interactions (Schreiber et al., 2009), which strongly suggests there is almost no interaction between M and avrM *in vitro*. This data supports the yeast-2-hybrid assays and co-IP work done by Catanzariti et al. (2010), with M interacting with AvrM but not avrM. The  $k_d$  values for the M/avrM interaction are both comparable to the M/AvrM interaction, however are likely the result of non-specific binding to M, due to the low  $k_a$ . The  $K_D$  for the interaction between M/avrM is variable, largely in part to the low  $k_a$  value. Without measuring the  $k_a$  and  $k_d$  of this interaction, the dissociation constant of the two interactions would have appeared very similar, suggesting no difference in binding between AvrM and avrM.

### **M interaction with AvrM and avrM mutants**

AvrM EA2 and avrM a3 mutant proteins bound non-specifically to the M surface, making it impossible to measure the interaction kinetics without optimisation of either the M immobilisation chemistry, or the running conditions. Changes to charged residues on the surface of proteins can often result in changes in pI and stability of the protein, and this may have contributed to the stickiness of the effectors to the M protein or the sensor surface. Mutations in the AvrM EA2 mutant remove two charged

residues from the dimer interact of AvrM, possibly exposing hydrophobic residues to solvent. Mutants in the *avrM* a3 mutant also introduce some hydrophobic residues, which may cause the effector to become 'sticky' (Serebriiskii and Golemis, 2001). Varying the pH and salt concentrations may enable the assessment of binding kinetics for the effectors, however the same conditions would need to be replicated for AvrM and *avrM* for a direct comparison of interaction kinetics. In future experiments, screening a range of pH and salt concentrations, as well as testing some different surface chemistries for non-specific binding, may provide a system for the successful analysis of the interaction of these mutant proteins with M.

### **M complex formation and effector binding?**

The low  $k_a$  of the M/AvrM interaction in comparison to other protein-protein interactions (Schreiber et al., 2009) suggests that, in order to for the interaction to occur more often and more rapidly within the cell, changes must be made to the M protein or AvrM protein. Multiple studies, including those presented in this thesis, have shown that nucleotide binding plays a crucial role in the regulation and activation of NLRs. Studies from other systems shown that oligomerisation plays a crucial role in the signalling complexes (NLRC4 and APAF-1). Given these considerations, Figure 5.21 shows the equilibrium-switch model of activation proposed by Bernoux et al. (2016) and this thesis, with potential protein-protein interactions. From the data in this results chapter, the interaction between an NLR purified from *P. pastoris*, M, and an effector purified from *E. coli*, AvrM, is likely representative of the interaction between an ADP bound M protein and AvrM.

There is a weak transient protein-protein interaction, but upon binding, the half-life of the complex is reasonably long lived. Future studies comparing the  $k_a$  and  $k_d$  of different stages of the model would provide a clear picture of how and when interactions occur. Examining the  $k_a$  and  $k_d$  of the ATP-bound form of M and effectors with the ADP-bound form would clearly demonstrate whether the NLR requires ATP binding first, then effector binding. Study of the  $k_a$  and  $k_d$  of the interaction between two active ATP-bound NLRs, with and without effector present would also be of interest. It would provide details on whether some complexes form pre- or post-

effector binding. Also of interest would be the half-lives of the complexes, and may give an insight into the cycling of signalling, and possibly whether downstream signalling partners are required.

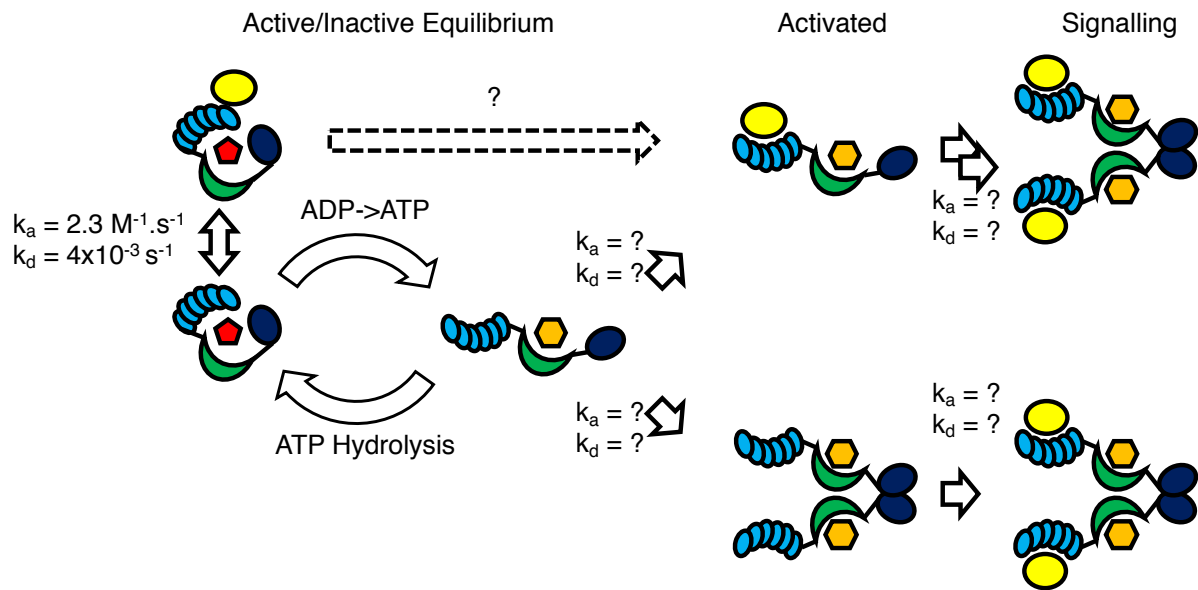


Figure 5.21 Binding constants in the equilibrium-switch model. Arrows indicate transition from one state to the next, with known interaction constants listed,  $k_a$  indicating the association rate constant, and  $k_d$  the dissociation rate constant. Knowing these parameters for other interactions could provide information on how NLRs signal. The red pentagon represents ADP, and the orange hexagon represents ATP. M is presented as three separate shapes, with the multiple cyan blobs representing the LRR domain, the green crescent the NB-ARC domain and the indigo oval the TIR domain. AvrM is represented as a yellow oval.

## Direct binding not so uncommon?

To date, there are few characterised examples of the direct interaction model of NLR activation; these include M and AvrM (Catanzariti et al., 2010), L6 and Avr1567 (Dodds et al., 2006), Pi-ta and AVR-Pita (Jia et al., 2000), and RPP1 and ATR1 (Krasileva et al., 2010). Direct binding of effector and NLR had been reasonably uncommon, with many more instances identified for the decoy/guardee models and the recently characterised integrated-decoy model. Recently more direct binding pairs have been identified. Wheat stem rust Sr50 and the effector AvrSr50 have recently been shown to interact (Chen et al., 2017).

A recent study by Schultink et al. (2017) identified another direct interaction pair; TIR containing NLR ROQ1 from *Nicotiana benthamiana* and effector XopQ from *Xanthomonas* spp. ROQ1 co-immuno-precipitated with XopQ, suggesting direct physical interaction between effector and NLR. ROQ1 was able to provide resistance to *Xanthomonas* expressing XopQ in the host plant, close relative *Nicotiana sylvestris*, and distant relative *Beta vulgaris*.

## Future work

Surface plasmon resonance, and other sensitive protein-protein interaction techniques experiments are not commonly used in the plant innate immunity field. There are many experiments using yeast-2-hybrid assays and co-IPs to measure protein-protein interaction, but to date only one paper (Maqbool et al., 2015) has employed SPR to analyse the interaction between effectors and NLR domains. Yeast-2-hybrid assays and co-IPs are very useful for screening interactions in a large set of candidates, and co-IPs can provide robust interaction data from the native environment, but both techniques are largely qualitative, and can be prone to false-positives and false-negatives (Nguyen and Goodrich, 2006, Bruckner et al., 2009).

Surface plasmon resonance can be used to determine the kinetics of different interactions within the effector NLR interaction, like those seen in Figure 5.21, and how different factors can affect the interaction, such as the addition of different nucleotides, binding partners and changes in the environmental conditions, such as

salinity, pH and temperature. Surface plasmon resonance can also be used to measure the interaction between domains, to address some of the questions posed in chapter 3, and the interaction between the TIR domains of L6 and L7 and the NB-ARC domain.

Surface plasmon resonance can also be applied to “fish” for ligands, by coupling the SPR system with MALDI MS (Zhukov et al., 2004). Through injection of complex pathogen samples over either a target NLR, decoy or guardee, or decoy domain, samples that bind strongly can be identified. These can then be eluted from the surface, and then identified by mass spectrometry. This approach is technically difficult, with purification of the NLR potentially difficult, as well as preparing suitable samples for injection, but still remains a feasible technique to identify binding partners for NLRs and other proteins involved in the pathway. Any protein hits would need to be screened *in planta*, but this method could help to identify unknown effector proteins, especially when combined with robust genetics screens.

## **Microscale thermophoresis to measure protein-protein interactions?**

Microscale Thermophoresis (MST) is a technique, that like SPR, enables the quantification of the interaction between two molecules, by thermophoretic detection of minute changes of the pair in microscopic temperature gradients (Jerabek-Willemsen et al., 2011). MST, also like SPR, requires small amounts of protein, but does not require immobilisation to a sensor surface (Jerabek-Willemsen et al., 2011). MST experiments often require one binding partner to be fluorescently labelled (Baksh et al., 2011), which can potentially complicate the purification process, however interactions can also be assessed without addition of a label by exploiting the intrinsic UV-fluorescence of proteins (Seidel et al., 2012). MST, like SPR, should be sensitive enough to measure NLR/effector interactions, and should be trialled, however like all experiments involving NLRs, would require likely significant optimisation.

## **Conclusions**

Here, a method for measuring the interaction between M and AvrM using SPR is presented, with some refinement required before thorough testing of AvrM and various

AvrM and avrM mutants can be completed. The data obtained indicates that the difference in interaction between AvrM and avrM, and the M protein is due to a faster association rate constant, indicating M binds AvrM more rapidly than it can bind avrM. These 'on' rates are still slow compared to other protein-protein interactions, but likely reflect interactions between inactive NLRs and effectors. It will be interesting to try experiments with the addition of ATP or other NLR activation factors and attempt to induce oligomerisation before effector binding. As ever, difficulty in obtaining M protein is a limiting factor, however this SPR technique does not require much protein, and can readily accommodate additives to probe the interactions of M and AvrM.

## Chapter 6 - General Discussion

The overall aim of the research presented in this thesis was to further probe how plant NLRs are activated and regulated. The nucleotide binding results in chapter three, in conjunction with extensive mutagenesis and *in planta* work presented by Bernoux et al. (2016), led to the formation of a new model for NLR regulation and activation, the equilibrium-switch model. The SAC purification method presented in chapter four enabled full-length flax NLRs to be produced at higher yields and purity, enabling many more biochemical and biophysical studies to be conducted. Chapter five represents the first report of interaction between a full-length NLR protein and its cognate effector protein *in vitro* and in real time.

### Equilibrium-Switch Model for plant NLRs

The equilibrium-switch model for NLR activation presents a shift away from the molecular switch activation model. In the molecular switch model, proposed by Takken et al. (2006) it is hypothesised that a dormant, resting NLR is kept in check by ADP, waiting and ready to be triggered by an effector. Upon activation, the NLR exchanges ADP for ATP, signals HR, then ATP hydrolysis of the ATP to ADP resets the NLR to bind another effector. The equilibrium-switch model has the NLR in a slow cycling equilibrium between an inactive ADP-bound state, and a primed active ATP bound state. Protein in the ATP-bound state is ready to bind and detect effectors, whilst the protein in the ADP-bound state helps keep any autoimmune signalling in check. Upon effector binding, this proportion of ATP-bound protein increases, due either to inhibition of hydrolysis, or an increase in ATP binding, and then is able to proceed to signal HR.

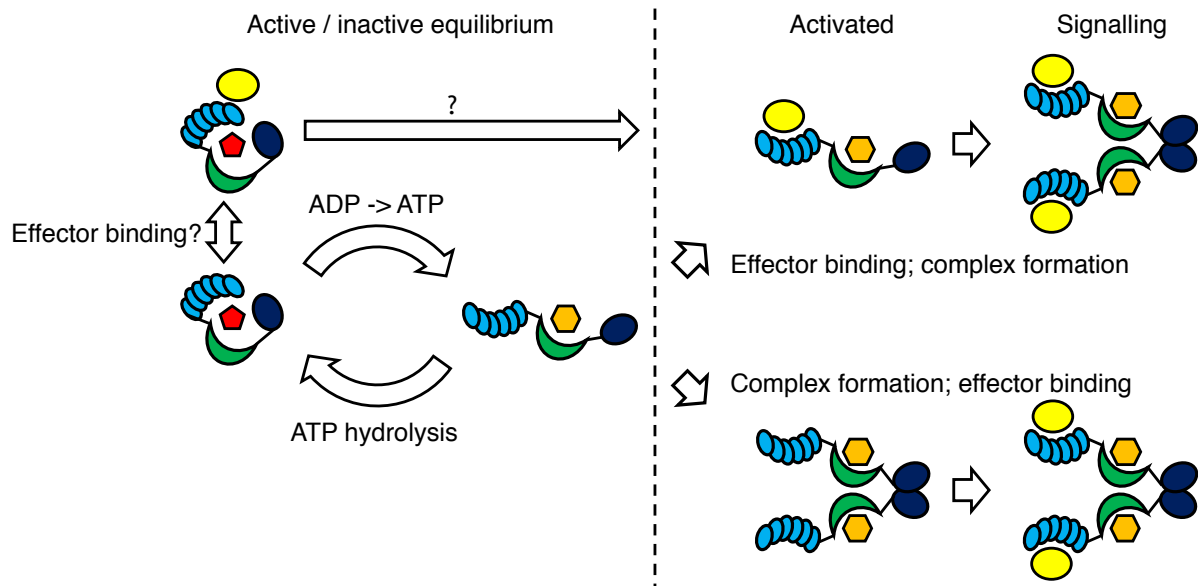


Figure 6.1 Stages and unknowns of the Equilibrium-Switch model of plant NLR activation. Nucleotide exchange and ATP hydrolysis maintain the effector in an active/inactive equilibrium, which can be shifted by effector binding or complex formation. The nucleotide exchange likely occurs before binding of the effector, as shown by weak binding of AvrM to ADP bound M protein. After activation, the NLR may form a complex that can bind effectors and signal HR, or the active NLR may be able to bind effectors, then form a large complex and signal HR. The red pentagon represents ADP and the orange hexagon represents ATP. The NLR is presented as three separate shapes, with the multiple cyan blobs representing the LRR domain, the green crescent the NB-ARC domain and the indigo oval the TIR domain. An effector is represented as a yellow oval.

## **Nucleotide exchange and ATP hydrolysis**

The exchange of nucleotides is a common feature through many different protein classes, with NLRs from mammals requiring nucleotide exchange events for activation (Reubold et al., 2009, Hu et al., 2013), along with GTPases (Rivero et al., 2017) and Motor proteins (Tafoya and Bustamante, 2018). In each case, the regulated, autoinhibited form is bound to ADP, and the active form is bound to ATP. Nucleotide exchange causes large conformational changes, enabling either binding of other proteins, or exposure of catalytic domains of the protein to perform their function. It can be concluded based on the results presented in chapter three that nucleotide exchange is also important for plant NLRs, as NLRs with a reduced affinity for ADP are able to signal HR more strongly, and those more tightly bound to ADP to induce HR at all. Examination of ADP and ATP binding kinetics of full-length NLRs would give more insight into how this nucleotide exchange is regulated, especially when the effector is introduced.

ATP hydrolysis is the other key component of the active/inactive equilibrium. Proteins that rely on nucleotide exchange also often possess ATP hydrolysis activity, and this activity is either used to drive conformational changes to 'reset' the inactive state (Reubold et al., 2009, Hu et al., 2013), or in the case of the motor proteins drive the function of the protein (Tafoya and Bustamante, 2018). ATP hydrolysis activity for full-length NLRs has not been widely reported in the literature, with flax M the only full-length plant NLR protein shown to catalyse hydrolysis as reported by Sornaraj (2013) and de Courcy-Ireland (2015). ATP hydrolysis activity of plant NLRs is thought to play the role of resetting and regulation of the NLR protein. Examination of hydrolysis rates of L6 and L7, in the presence of the effector AvrL567 would provide support for this hypothesis. It is hypothesised that the effectors would stabilise the NLR in an ATP-bound state by inhibition of ATP hydrolysis, by currently unknown mechanisms.

## **What comes first, effector binding or nucleotide exchange?**

One of the unresolved questions of NLR activation models is what comes first, nucleotide exchange or effector binding? Molecular switch models suggest that effector binding facilitates nucleotide exchange (Collier et al., 2011, Takken and

Goverse, 2012). However, evidence presented in this thesis suggests nucleotide exchange may occur first, enabling effector binding. This is demonstrated by preferentially ADP-bound L7's weak association with effector AvrL567 in yeast-2-hybrid assays (Bernoux et al., 2011), and by the lower ADP-bound L6 and L7 FCY/SRR having a strong association with effector AvrL567 (Figure 3.8). These data are consistent with a model whereby ADP-bound NLRs cannot interact with effectors and nucleotide exchange is required for NLR/effector binding. This is further supported by the weak, transient binding of AvrM to M in the SPR studies described in chapter. As the M protein used in the assay was most likely bound to ADP, based on its demonstrated ATP hydrolytic activity ((Sornaraj, 2013), and chapter 4 of this thesis), it had a very weak and transient interaction with AvrM. Inclusion of ATP or forcing the M protein into an ATP-bound state by introducing the MHV mutation, is expected to have a higher affinity of effector binding. In summary, the SPR method of measuring NLR/effector interaction enables further experiments to probe this important question in plant NLR activation.

### **Complex formation; a plant apoptosome?**

The apparent requirement of high order structure formation of TIR domains (Nimma et al., 2017), mammalian NLRs (Hu et al., 2015), and other cell death inducing proteins (Yuan et al., 2011, Cain et al., 2002, Yan et al., 2005) suggests that plant NLRs may also require the formation of large multimeric structures to induce HR. It is a requirement of many plant TIR domains to dimerise in order to induce signalling (Bernoux et al., 2011, Williams et al., 2014, Mestre and Baulcombe, 2006), and perhaps this TIR dimerization is facilitated by the formation of an APAF-1-like ring structure (Zhou et al., 2015). The large structure may also form a platform for other binding partners to interact with the TIR domain.

Another unknown in plant NLR activation is, if this complex does form at all, is it facilitated by binding of effectors, or does nucleotide exchange allow formation of the complex to enable effector binding, with effector binding acting to stabilise the complex? Structural experiments, combined with interaction experiments would provide insights into possible downstream mechanisms.

## **Small GTPases and third party interactors**

Nucleotide exchange and ATP hydrolysis are two of the key steps in regulation of HR, and yet what exactly stimulates nucleotide exchange, and how both nucleotide exchange and ATP hydrolysis are regulated in plant NLRs is not fully understood. The small GTPase protein family have a regulatory mechanism reminiscent of that equilibrium-switch model, with an inactive protein being held in a GDP-bound state and an active protein in a GTP-bound state (Rivero et al., 2017). Three different classes of interactors of small GTPases have been identified, Guanidine nucleotide exchange factors (GEFs), GTPase activating proteins (GAPs) and guanosine nucleotide dissociation inhibitors (GDIs), each with a role in regulating the nucleotide exchange and hydrolysis of these small GTPases. Guanidine nucleotide exchange factors catalyse the exchange of GDP to GTP, GAPs increase GTP hydrolysis and GDIs inhibit exchange of GDP to GTP, each influencing the regulatory state of the GTPase.

Perhaps some effectors and downstream signalling partners may function in similar ways with plant NLRs. An avirulence effector, for example, may act as a 'AEF', or adenine nucleotide exchange factor, activating the NLR by forcing nucleotide exchange. Negative regulators of NLRs may act as 'AAPs', or ATPase activating proteins, enhancing ATPase activity to maintain an ADP-bound state, or as 'ADIs', adenine nucleotide dissociation inhibitors, preventing nucleotide exchange occurring before it is required. How the NLR interacts with other proteins is still unknown but is something that could be probed further with more structural information on NLRs.

## **Still waiting for a structure**

Binding kinetics of the interactions involved in NLR signalling should be accompanied by structural data of the interaction, using cryo-EM or X-ray crystallography techniques. Currently, there still is no reported structure of a full-length plant NLR. A high-resolution crystal or cryoEM structure of a full-length plant NLR would give great insight into interactions between domains of an NLR, as well as conformational changes between an ADP and ATP bound form of the protein.

Using cryo-EM to observe the complex could also provide information on how any complex does form, and inferences could be made on important interfaces and residues involved in the binding of M and AvrM. These interfaces and residues can then be compared to avrM and the mutants that perturb the HR phenotypes of both AvrM and avrM, to provide a clear mechanism for both the action of M/AvrM induced ETI responses, and the direct binding activation mode for NLRs.

## **Direct effector interaction NLRs for robust resistance!**

Plant NLRs have a broad range of pathogen detection mechanisms. Utilisation of all types of NLRs will be important to provide robust resistance to new virulent strains of pathogens. Direct interaction NLRs are better suited to transfer between different plant species than indirect interaction NLRs, as they do not rely on similar guardee and targets within the new host plant and can still retain resistance to their target pathogen effector. A variety of effector detection methods would provide plants a diverse resistance spectra against pathogens, enabling more durable resistance to rapidly diversifying microbes.

## **Conclusion**

There are still many questions to be answered on how plant NLRs function, but this thesis has provided some insight into the regulatory mechanisms involved. The equilibrium-switch model of activation is backed by the nucleotide binding data, and further supported by SPR experiments showing a weak interaction occurs between effector and NLR. This thesis shows that it is possible to produce full-length NLR proteins suitable for biochemical assays to probe function and provides some early evidence of NLR effector interaction *in vitro*.

As more and more NLR genes are identified and cloned, it remains important to properly characterise the proteins produced. Without expression and purification of proteins, particularly full-length proteins, function and interacting partners would be difficult to characterise and identify, and without knowing how the plant innate immune system functions, producing robust resistance in important commercial crops will be even more difficult.

## **Chapter 7 - Appendices**

### **Appendix 1 – Vector Maps and L6 and L7 Site Directed Mutagenesis Gels**

#### **Vectors**

Both L6 and L7 genes were cloned into pP6H3C by Simon Williams (School of Chemistry and Molecular Biosciences, UQ). M was cloned in pPICZA by Pradeep Sornaraj (Sornaraj, 2013). Constructs contain an N-terminal 6xHis-tag and C-terminal Strep-tag II. Sr33 and RUN1 were also cloned in the pP6H3C construct, Sr33 by Adam Bentham (School of Chemistry and Molecular Biosciences, UQ), and RUN1 by members of the Dry lab at CSIRO plant industries.

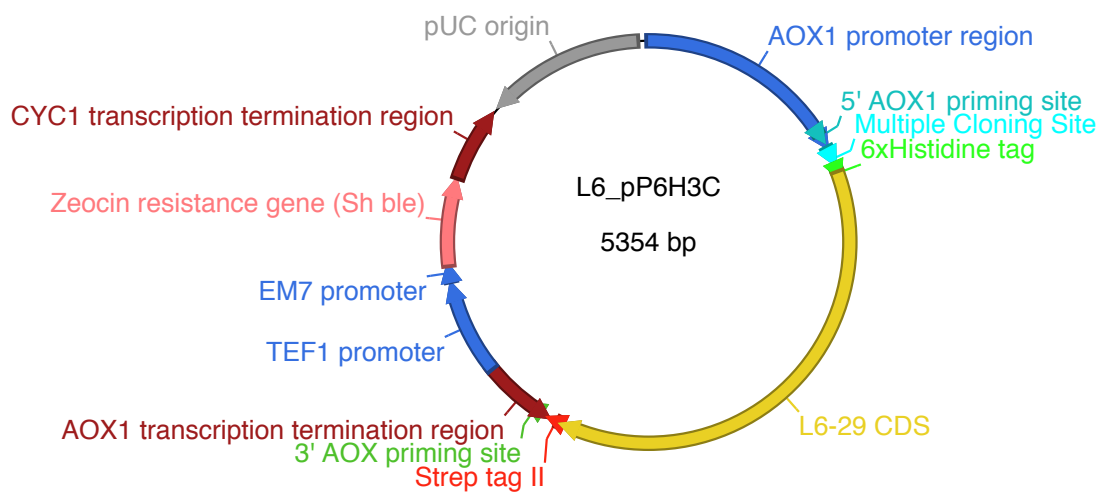


Figure 7.1 The pP6H3C plasmid, used for expression of all constructs in *P. pastoris*. Contains an AOX1 promoter, and N-terminal 6xHis-tag and C-terminal Strep-tag II. For selection, the Zeocin resistance gene is used. In other constructs, the CDS takes the place of the L6 CDS.

## Mutagenesis

Mutations were introduced into the full-length L6 and L7 cDNA in the pP6H3C vector using the Phusion Site Directed Mutagenesis protocol. Primers used contained the desired mutation, and 9-15 base pair extensions flanking either side of the target codon.

Table 1 Mutagenesis primers used to generate mutants in L6 and L7 constructs. Changed codons bolded.

Primer Name	Sequence
L6 FLCY Fw	ACCGATTTCCCTATATCAG <b>TTTCTCTGTTACT</b> TATAAGATTCACACTTTT
L6 FLCY Rv	AAAAGTGTGAATCTTATAG <b>TACAGAGAA</b> ACTGATATAGGAAATCGGT
L7 K271M Fw	ATGGGTGGAATAGGC <b>ATGAC</b> GACCACTGCAAAG
L7 K271M Rv	CTTTGCAGTGGTCGT <b>CATGC</b> CCTATTCCACCCAT
L7 SLRR Fw	ACCGATTTCCCTATATCATT <b>TCTCTCCGTCGC</b> TATAAGATTCACACTTTT
L7 SLRR Rv	AAAAGTGTGAATCTTATAG <b>GCGACGGAGAGA</b> AATGATATAGGAAATCGGT
L6/L7 D541V Fw	AAAATGCAC <b>GTCCA</b> ACTTAGA
L6/L7 D541V Rv	TCTAAGTTG <b>GAC</b> GTGCATTTT
L7 C288R Fw	TCTTGTTTCGAT <b>CGTT</b> GTTGTTTTATT
L7 C288R Rv	AATAAAACAACA <b>ACGAT</b> CGAAACAAGA

**L6 K271M and L7 K271M, L6 MHV and L7 MHV**

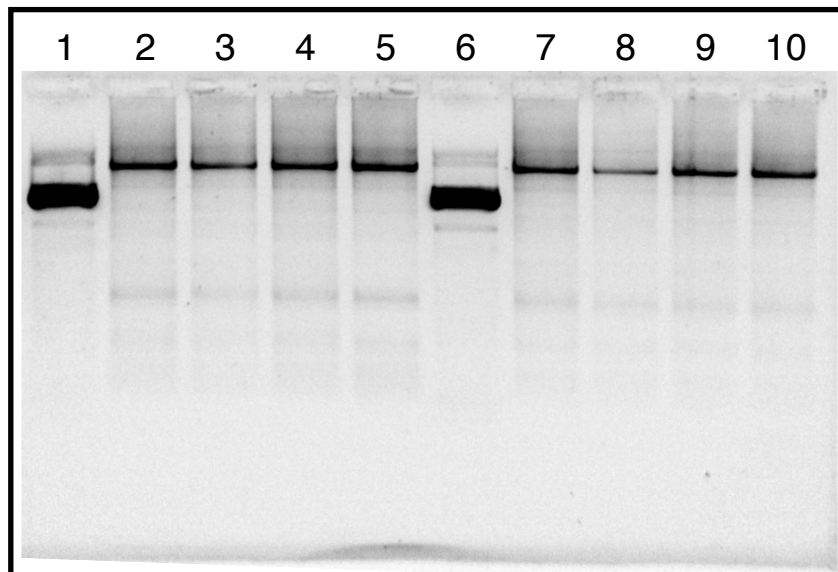


Figure 7.2 Mutagenesis of L6 K271M and L7 K271M. PCR samples after Dpn1 treatment for L6 K271M and L7 K271M. Lane 1 L6 pP6H3C template. Lane 2-5 L6 K271M PCR. Lane 6 L7 pP6H3C template. Lane 7-10 L7 K271M PCR.

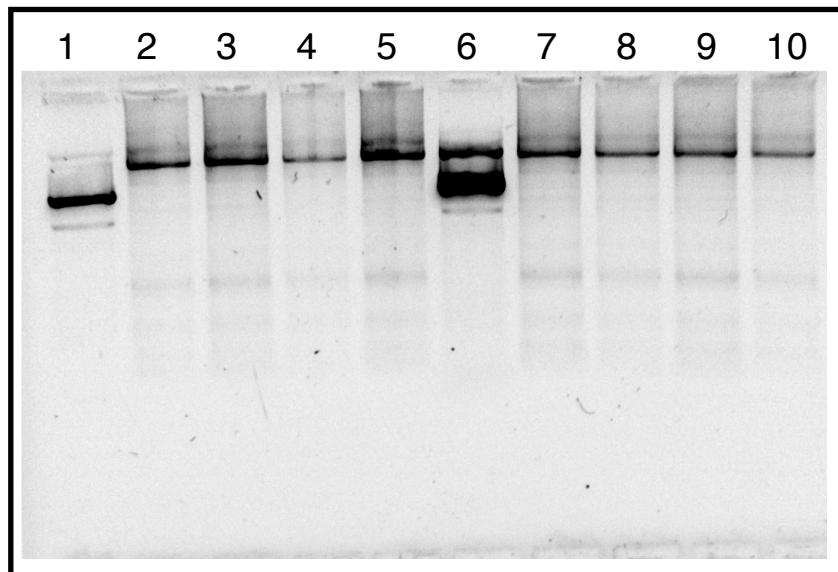


Figure 7.3 Mutagenesis of L6 MHV and L7 MHV. PCR samples after Dpn1 treatment for L6 MHV and L7 MHV. Lane 1. L6 pP6H3C template. Lane 2-5 L6 MHV PCR. Lane 6 L7 pP6H3C template. Lane 7-10 L7 MHV PCR.

Lysine to methionine 271 and aspartate to valine 541 mutations were introduced to the L6 and L7 genes by site directed mutagenesis. Primers used are described in Bernoux et al. (2016). PCR conditions. Mutations confirmed by sequencing (AGRF). Colonies expressing successful changes stored and used for productions of plasmid DNA for *P. pastoris* transformation.

## **L6 SRR/FCY, L7 FCY/SRR**

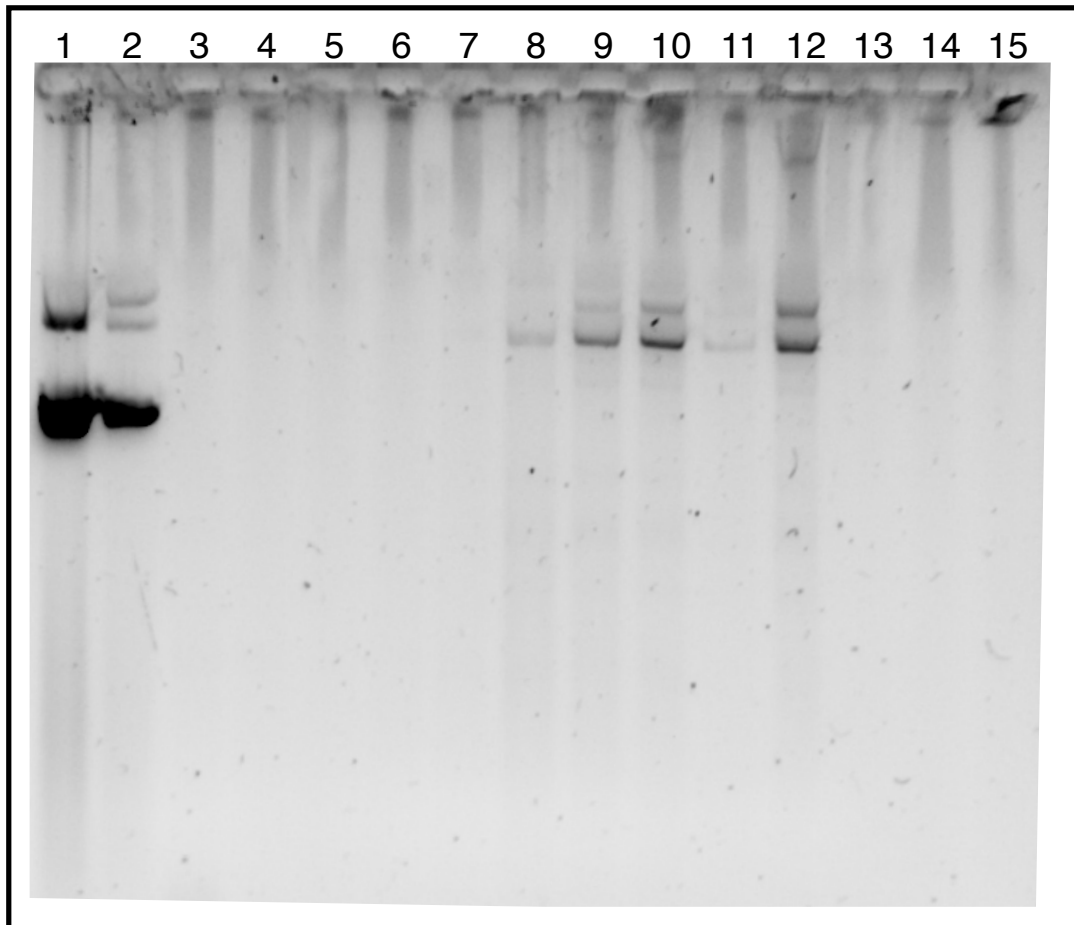


Figure 7.4 Mutagenesis of L6 SRR/FCY and L7 SRR/FCY. PCR samples after Dpn1 treatment for L6 SRR/FCY and L7 FCY/SRR. Lane 1. L6 pP6H3C template. Lane 2 L7 pP6H3C template. Lane 3-8 L6 FCY/SRR PCR. Lane 9-15 L7 SRR/FCY PCR. L6 SRR/FCY 8, and L7 FCY/SRR 9, 10 and 12 sequenced and change confirmed.

Triple mutations introduced in L6 and L7 genes. All three mutations made simultaneously, with primers described in Bernoux et al. (2016). Mutations introduced using primers designed with least changes to the wild type cDNA rather than the direct change from L6 to L7 codons. This approach was used as the direct change was introducing too many changes simultaneously. The least changes approach was much more successful.

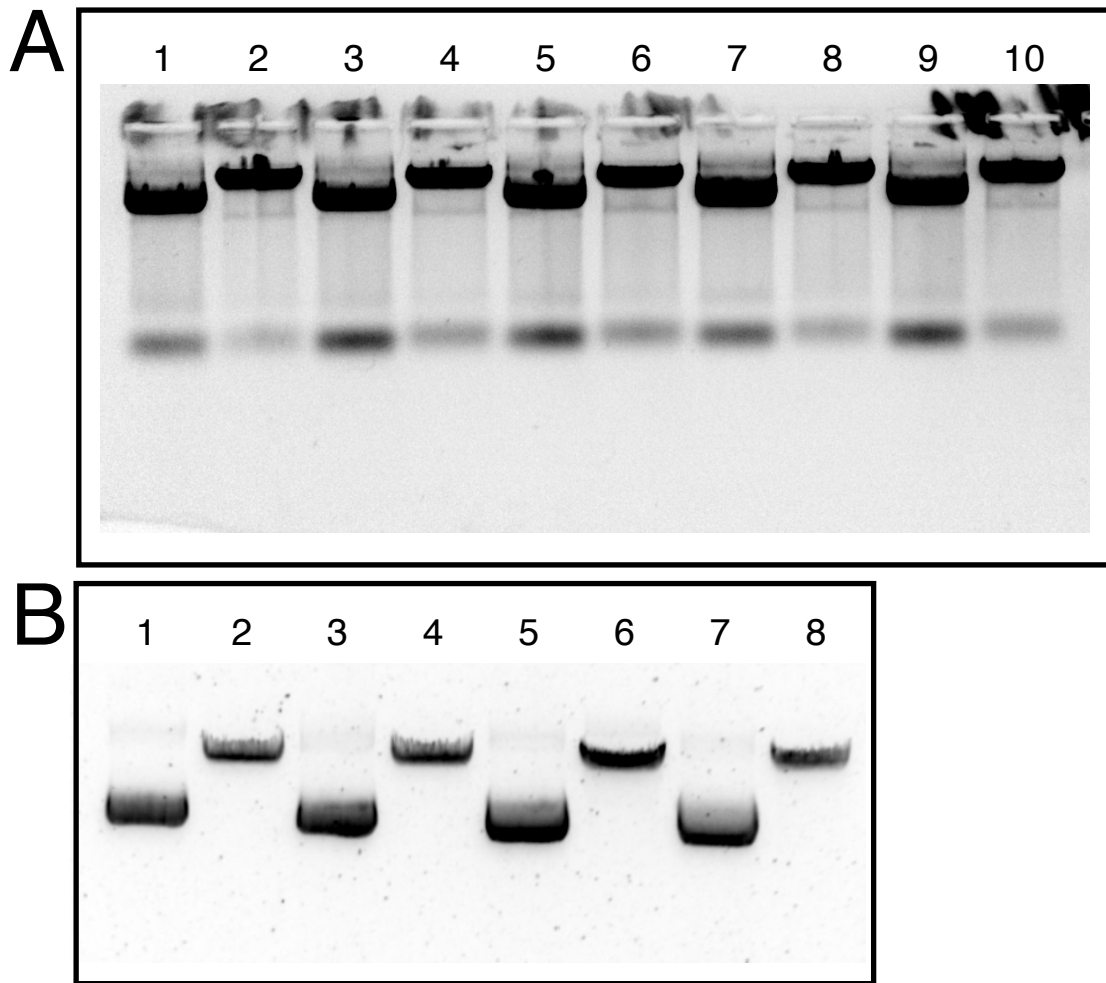


Figure 7.5 Restriction Digests of L6/L7 and mutant plasmids for transformation into *P. pastoris*. Plasmids were digested with Sac1, in Cutsmart™ buffer for 1 h at 37°C. **A** Lane 1 L6 pP6H3C. Lane 2 L6 pP6H3C Sac1 digest. Lane 3 L6 K271M pP6H3C. Lane 4 L6 K271M pP6H3C Sac1 digest. Lane 5 L7 K271M pP6H3C. Lane 6 L7 K271M pP6H3C Sac1 digest. Lane 7 L6 MHV pP6H3C. Lane 8 L6 MHV pP6H3C Sac1 digest. Lane 9 L7 MHV pP6H3C. Lane 10 L7 pP6H3C Sac1 digest. **B** Lane 1 L7 pP6H3C. Lane 2 L7 pP6H3C Sac1 digest. Lane 3 L6 SRR/FCY pP6H3C. Lane 4 L6 SRR/FCY pP6H3C Sac1 digest. Lane 5 L7 FCY/SRR pP6H3C. Lane 6 L7 FCY/SRR pP6H3C Sac1 digest. Lane 7 L7 C288R pP6H3C. Lane 8 L7 C288R pP6H3C Sac1 digest.

## **L7 C288R**

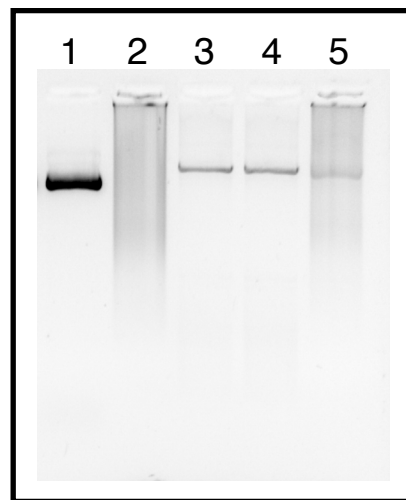


Figure 7.6 Mutagenesis of L7 C288R. PCR samples after Dpn1 treatment for L7 C288R. Lane 1 L7 p6H3C template. Lane 2-5 L7 C288R PCR. L7 C288R 3 and 4 were sequenced and changes were confirmed.

## Appendix 2 – Sample IMAC purification of NLR

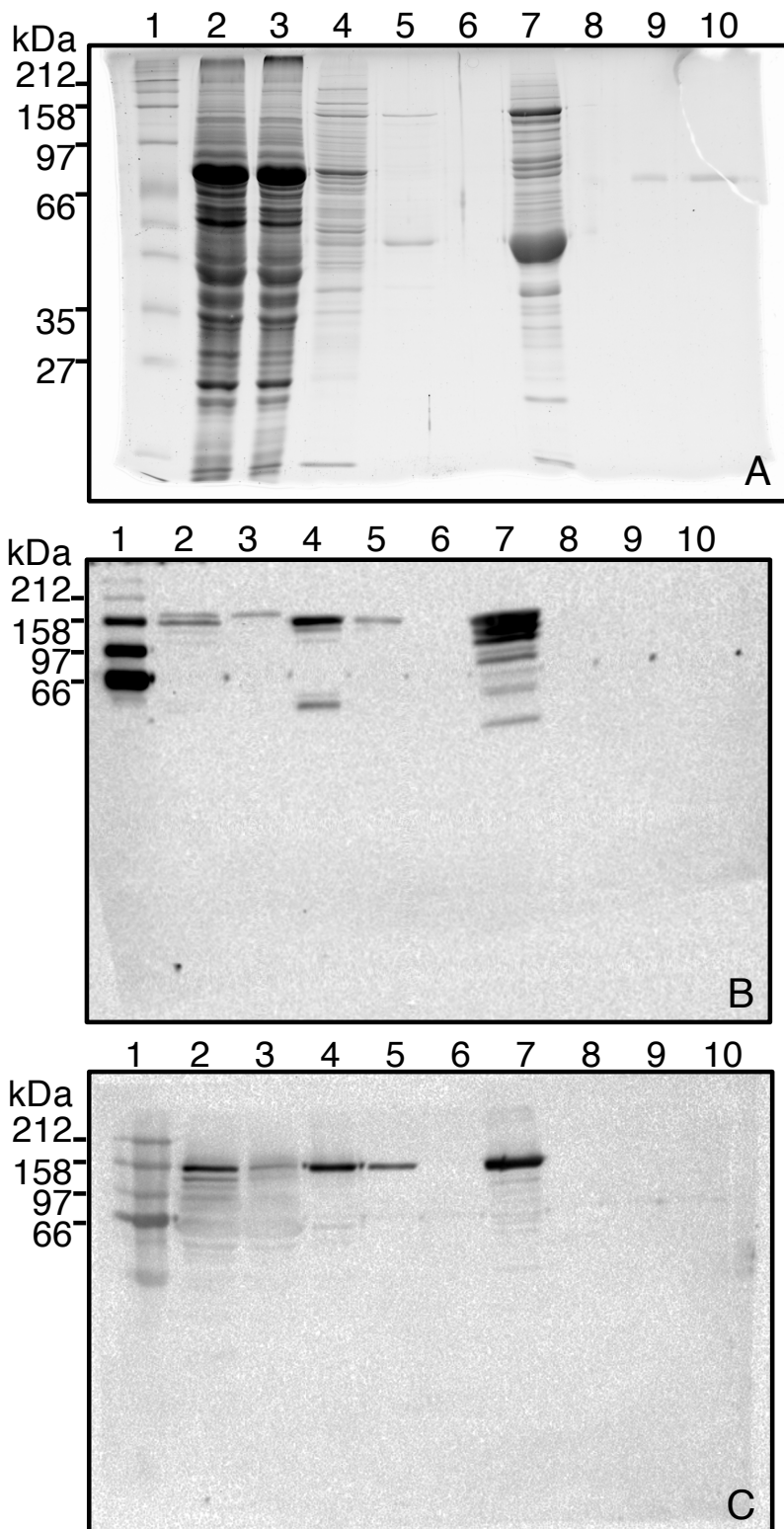


Figure 7.7 Example of a IMAC purified L7 MHV, from crude lysate to concentrated elution fractions. **A** SYPRO® Ruby stain, **B** Anti-6xHis-tag Western Blot and **C** Anti-StrepTag-II Western Blot. Lane 1 Ladder. Lane 2 Crude Lysate. Lane 3 Flow through. Lane 4 Wash fraction (55mM Imidazole). Lane 5

Elution fraction **1** (250mM Imidazole). Lane **6** Elution fraction 2 (250mM Imidazole). Lane **7** Concentrated Elution fractions. Lane **8-10** BSA controls.

### **Appendix 3 – Calculation of Protein Concentration**

To calculate the concentration of full-length NLR in each sample, the use of a sensitive protein stain and BSA standard curve was used. Known amounts of BSA was loaded onto an SDS-PAGE gel, along with the IMAC purified NLR sample. The gel was stained with SYPRO® Ruby stain, imaged using a Chemic-doc (Bio-Rad) and evaluated using Image Lab software (Bio-Rad). Densities for each of the BSA standards were calculated and plotted on a standard curve. The density of the band containing the full-length NLR was calculated in the same way, and using the standard curve, the mass of the band was calculated, allowing calculation of the concentration of NLR in the complex purified protein sample. Figure 7.8 shows an example of the BSA standard curve used.

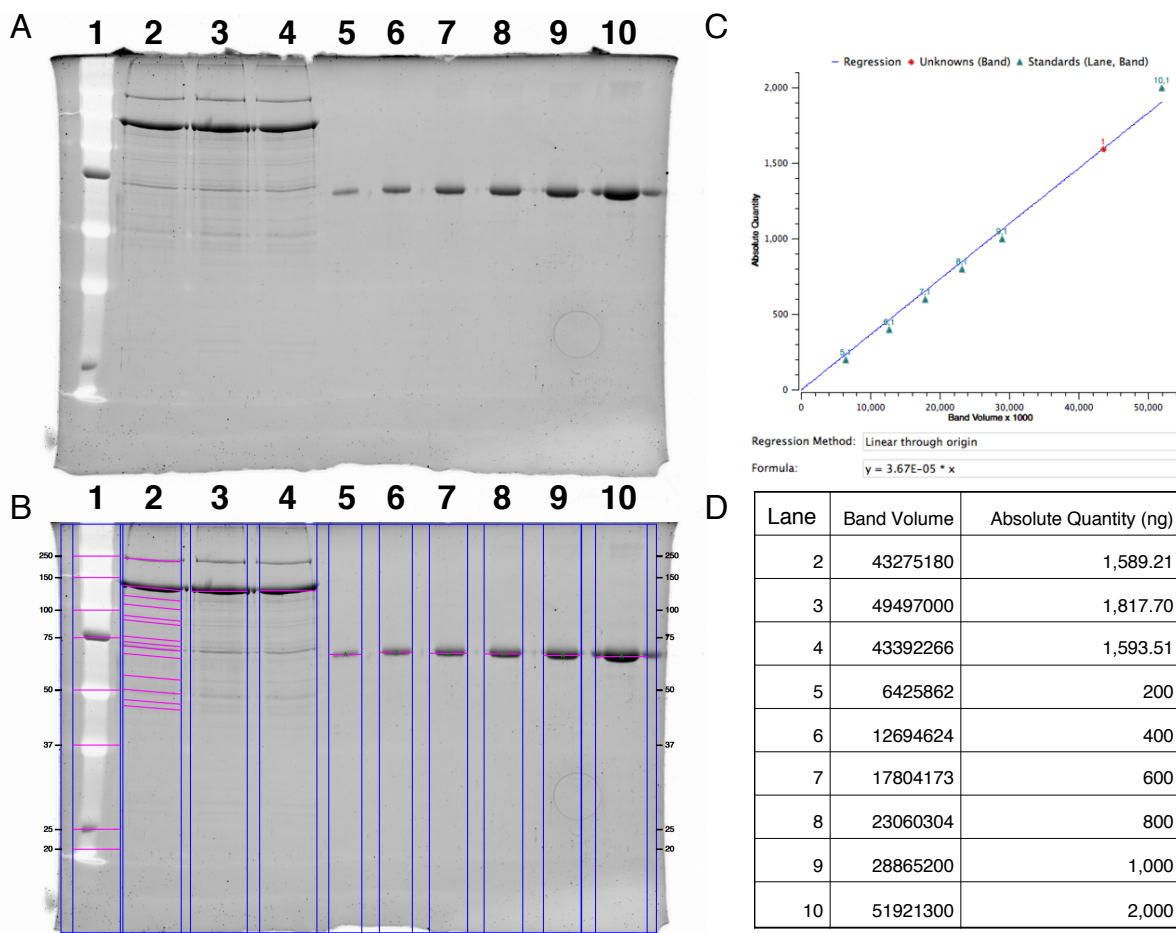


Figure 7.8 Example of protein concentration calculation using SYPRO® Ruby stain and BSA standards. A SYPRO® Ruby stain of SDS-PAGE gel containing Lane 1 Protein Ladder. Lane 2-4 M SAC purified samples in triplicate. Lane 5-10 BSA standards, 200 ng, 400 ng, 600 ng, 800 ng, 1,000 ng and 2,000 ng. B Lane and band analysis using ImageLab software of A. Lane margins in blue, bands in pink. C Standard curve made using quantity one software, using volumes from bands in B. D calculation of quantity of bands in lanes 2, 3 and 4 using standard curve in C. These quantities were average and used to calculate the concentration of M protein.

## Appendix 4 - Purification of Sr33, a CC-containing NLR from *Aegilops tauschii* and RUN1, a TIR-containing NLR from *Muscadinia rotundifolia*

Below are SYPRO® Ruby stains and anti-6xHis-tag and anti-Strep-tag II western blots of purifications of NLRs Sr33 and RUN1.

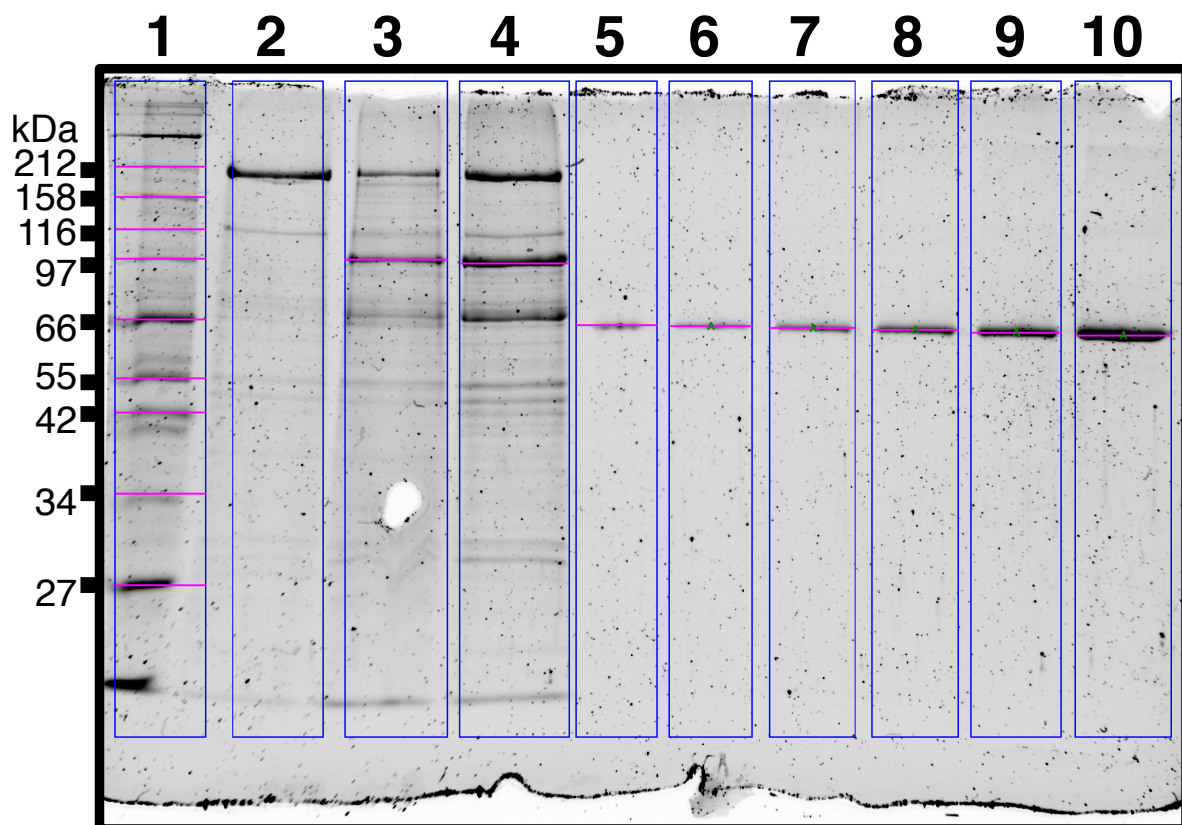


Figure 7.9 RUN1 and Sr33 SYPRO® Ruby Stain. Lane 1 Protein ladder. Lane 2 SAC purified RUN1 sample. Lane 3 Sr33 SAC purified sample. Lane 4 Sr33 SAC purified sample. Lane 5-10 BSA standards, 100 ng, 200 ng, 300 ng, 400 ng, 500 ng and 100 ng. No band was observed for RUN1 sample (expected size 152.35 kDa), whilst bands were observed for Sr33 (indicated in lanes 3 and 4 by a pink band). Sr33 SAC sample from lane 4 was analysed by western blot in Figure 7.10.

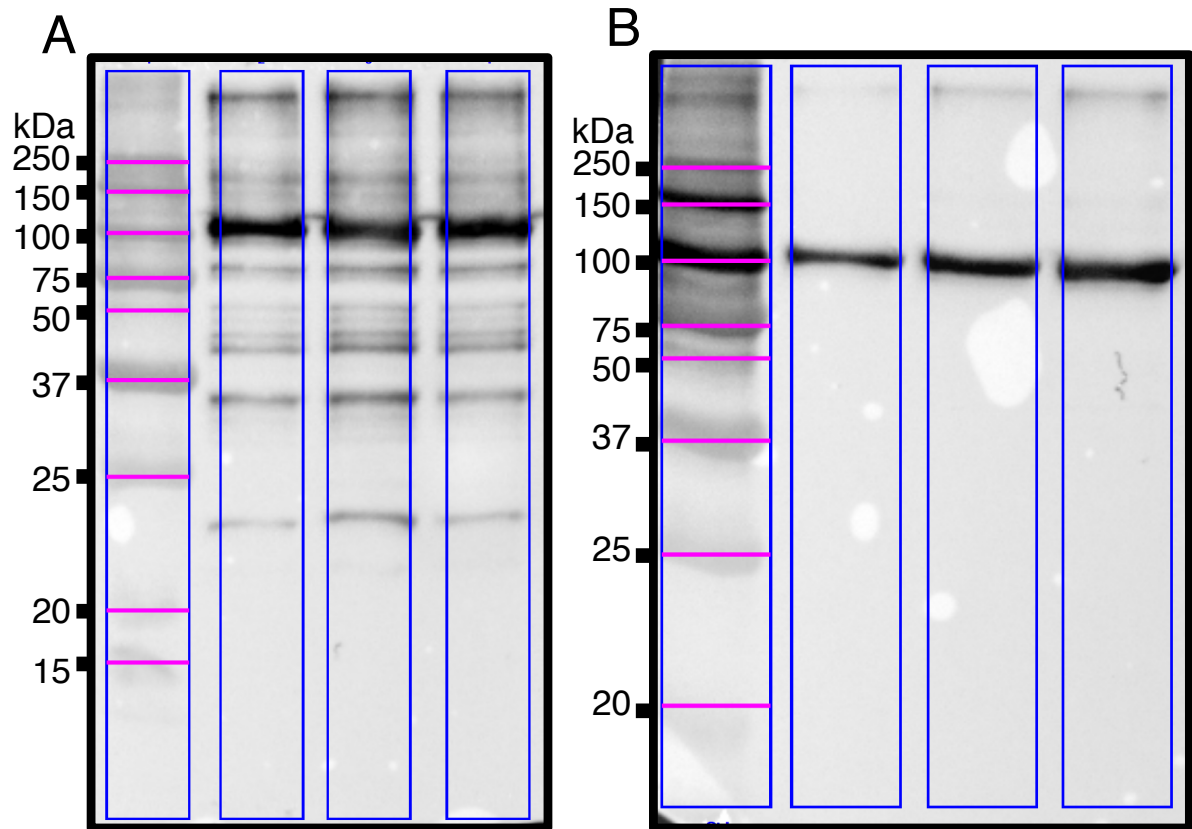


Figure 7.10 Western Blots of Sr33 purification. **A** anti-Strep-tag II western blot. Lane 1 Protein ladder. Lane 2-4 SAC purified Sr33 from Figure 7.9, lane 4. **B** anti-6xHis-tag western blot. Lane 1 protein ladder. Lanes 2-4 SAC purified Sr33 from Figure 7.9, lane 4.

## Appendix 5 - Kinetic models for M/AvrM and M/avrM interactions

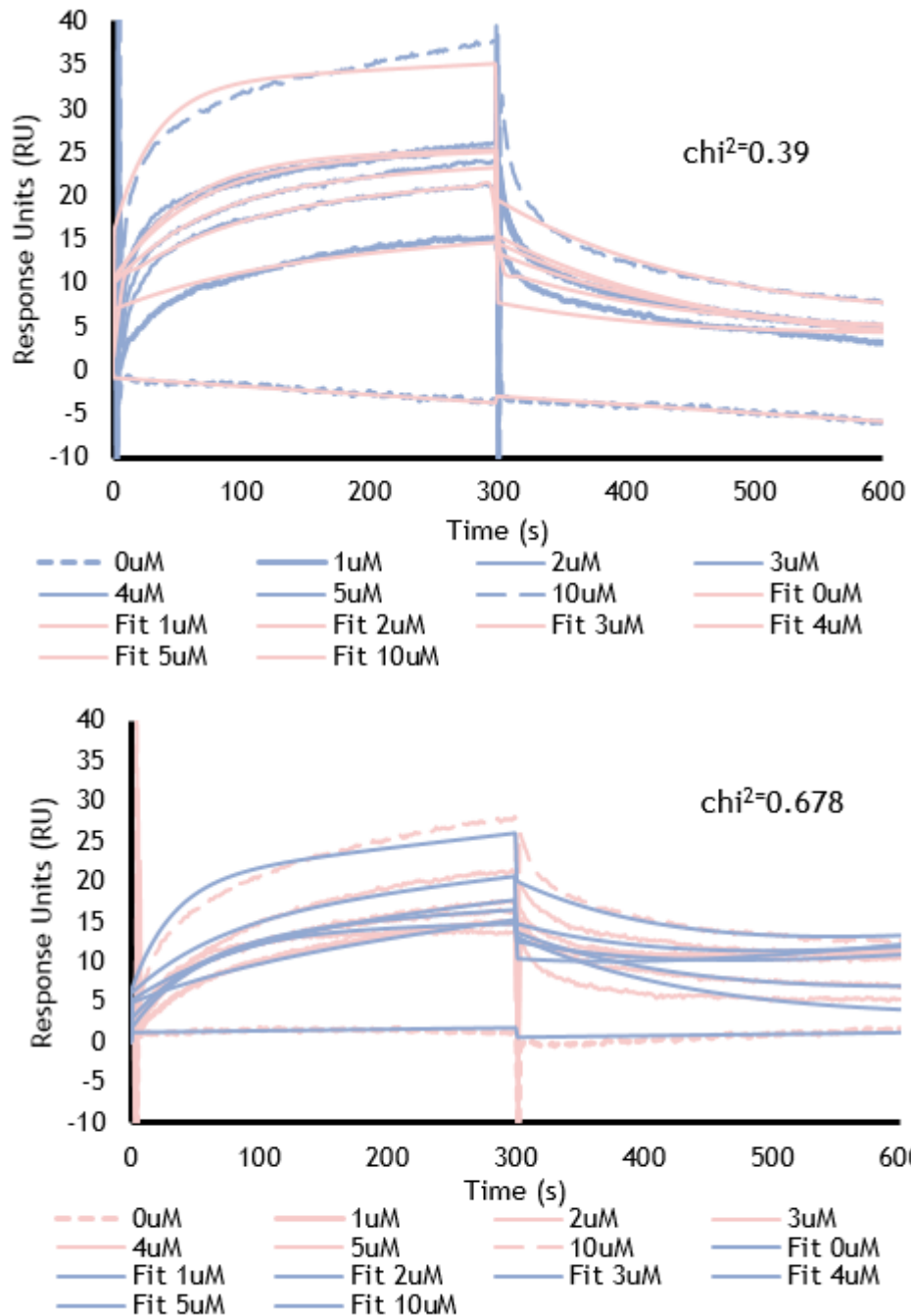


Figure 7.11 Models fit to AvrM binding data from Figure 5.15. Models used were Langmuir 1:1 binding in each instance. Models generated using BiaEval software. Model  $\chi^2$  inset in each plot.

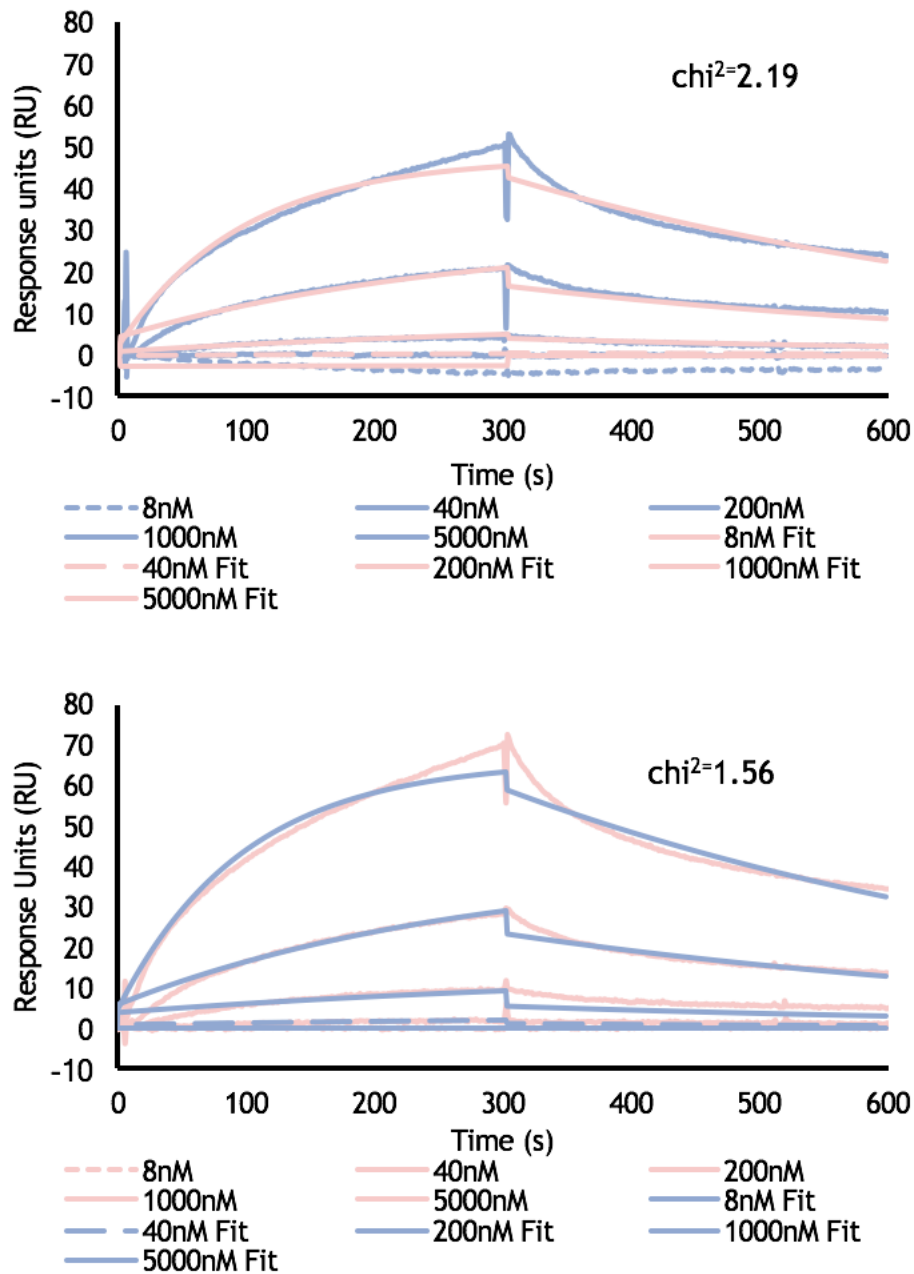


Figure 7.12 Fits on curves from Figure 5.16. A Curves from Figure 5.16A, shown in blue with fits in pink. B curves from Figure 5.16B, shown in pink with fits in blue. Fits are Langmuir 1:1 binding from BiaEval software,  $\chi^2$  values inset in plot.

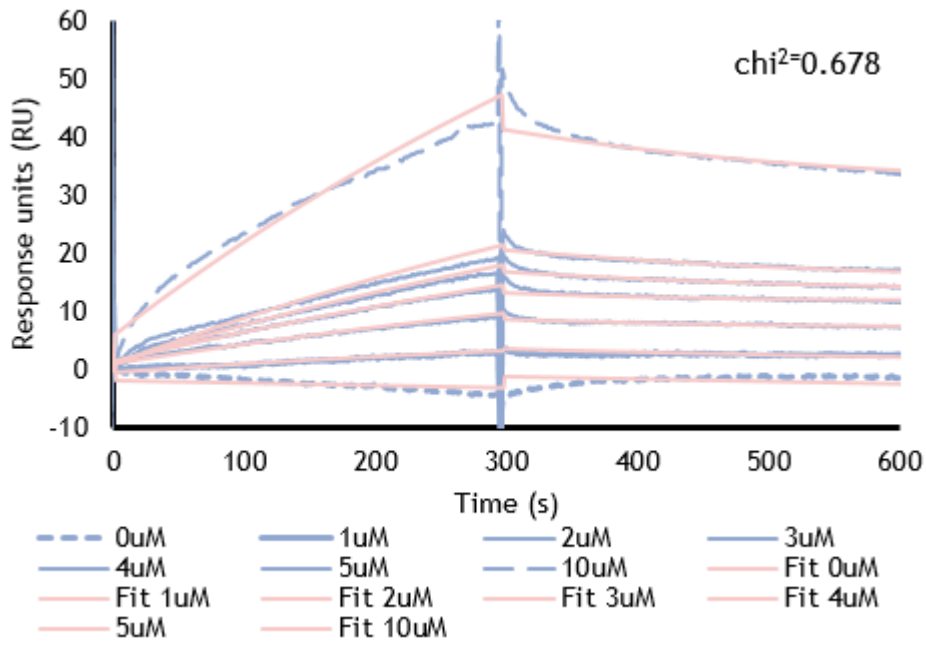


Figure 7.13 Models used to derive kinetic data derived from curves in Figure 5.17. Fits are Langmuir 1:1 binding from BiaEval software, chi<sup>2</sup> values inset in plot.

### Numeric model

---

$$LA + RI1*\$1 + RI2*\$2 + RI3*\$3 + RI4*\$4 + RI5*\$5 + Drift*(t-ton1));$$

$$\$1=(\text{sign}(t-(\text{ton}1))-\text{sign}(t-(\text{ton}1+c\_time)))/2;$$

$$\$2=(\text{sign}(t-(\text{ton}2))-\text{sign}(t-(\text{ton}2+c\_time)))/2;$$

$$\$3=(\text{sign}(t-(\text{ton}3))-\text{sign}(t-(\text{ton}3+c\_time)))/2;$$

$$\$4=(\text{sign}(t-(\text{ton}4))-\text{sign}(t-(\text{ton}4+c\_time)))/2;$$

$$\$5=(\text{sign}(t-(\text{ton}5))-\text{sign}(t-(\text{ton}5+c\_time)))/2;$$

$$\$6=kt*(\$1*conc/(F^4) + \$2*conc/(F^3) + \$3*conc/(F^2) + \$4*conc/(F) + \$5*conc-A); \quad (0.1)$$

$$\$7=ka*L*A - kd*LA;$$

$$A=\$6-\$7|0;$$

$$L=-\$7|Rmax;$$

$$LA=\$7|0;$$

---

L	= ligand
A	= analyte
LA	= complex
kt	= mass transport coefficient
Conc	= highest analyte concentration
F	= dilution factor
c_time	= contact time analyte
ton1	= start time of injection 1
RI1	= refractive index response of injection 1

### Numeric model

---

$$LA + RI1*\$1 + RI2*\$2 + RI3*\$3 + RI4*\$4 + RI5*\$5 + Drift*(t-ton1));$$

$$\$1=(\text{sign}(t-(\text{ton}1))-\text{sign}(t-(\text{ton}1+c\_time)))/2;$$

$$\$2=(\text{sign}(t-(\text{ton}2))-\text{sign}(t-(\text{ton}2+c\_time)))/2;$$

$$\$3=(\text{sign}(t-(\text{ton}3))-\text{sign}(t-(\text{ton}3+c\_time)))/2;$$

$$\$4=(\text{sign}(t-(\text{ton}4))-\text{sign}(t-(\text{ton}4+c\_time)))/2;$$

$$\$5=(\text{sign}(t-(\text{ton}5))-\text{sign}(t-(\text{ton}5+c\_time)))/2;$$

$$\$6=kt*(\$1*(conc*0.2)+\$2*(conc*0.4)+\$3*(conc*0.6)+\$4*(conc*0.8)+\$5*conc-A); \quad (0.1)$$

$$\$7=ka*L*A - kd*LA;$$

$$A=\$6-\$7|0;$$

$$L=-\$7|Rmax;$$

$$LA=\$7|0;$$

---

L	= ligand
A	= analyte
LA	= complex
kt	= mass transport coefficient
Conc	= highest analyte concentration
F	= dilution factor
c_time	= contact time analyte
ton1	= start time of injection 1
RI1	= refractive index response of injection 1

Figure 7.14 Modified model used for single cycle kinetics calculations. The top model shows the original model as described by Karlsson et al. (2006), the second model shows the one used in experiments done in this thesis. The only difference is in line 6, to account for different concentrations of analytes then the Karlsson et al. (2006) model.

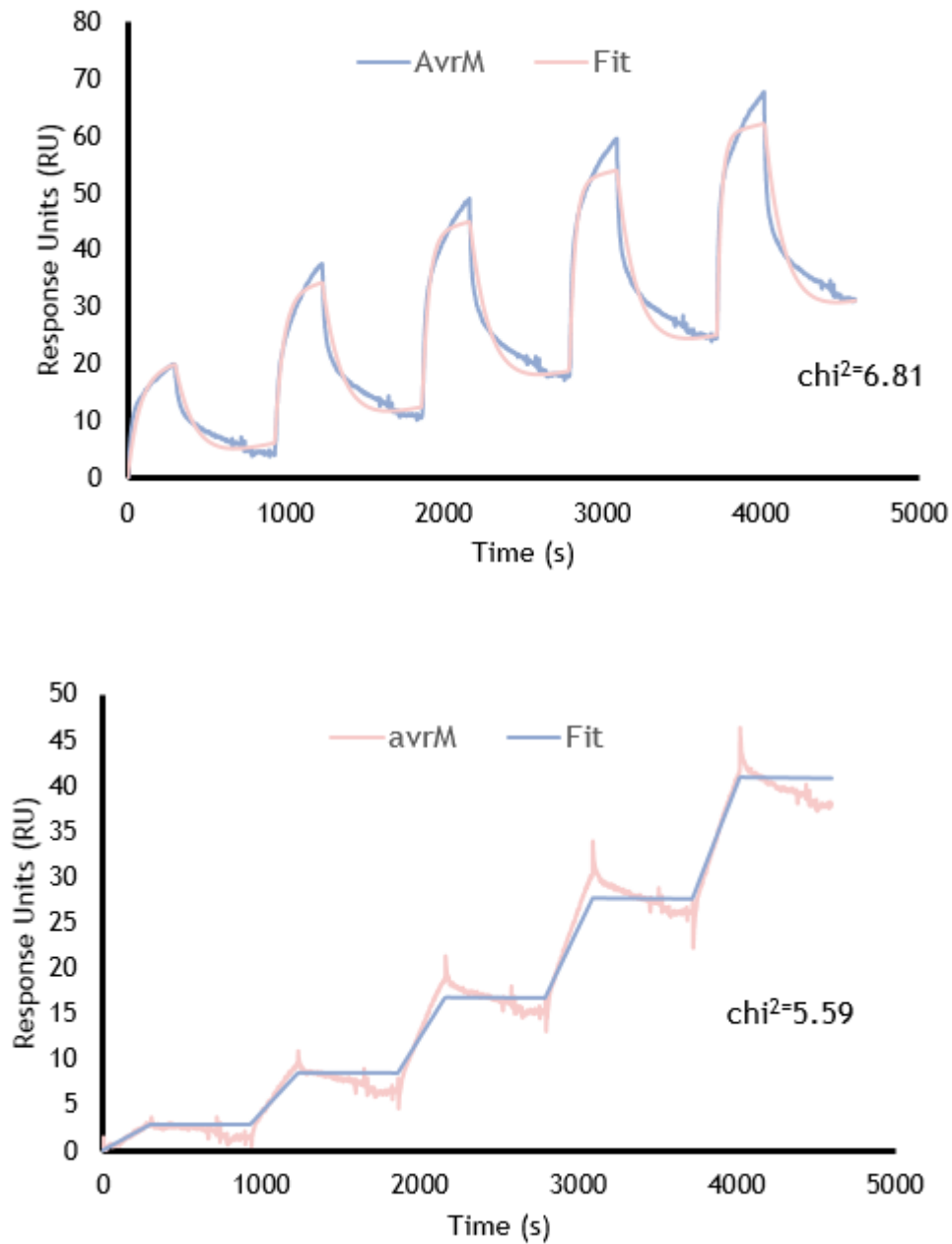


Figure 7.15 Models used to derive kinetic data from AvrM and avrM single-cycle kinetic models. Models used are a variation of the single cycle models described in Karlsson et al. (2006). Chi<sup>2</sup> value inset.

## References

- Acuner Ozbabacan, S. E., Engin, H. B., Gursoy, A. & Keskin, O. 2011. Transient protein-protein interactions. *Protein Engineering Design and Selection*, 24, 635-648.
- Ade, J., Deyoung, B. J., Golstein, C. & Innes, R. W. 2007. Indirect activation of a plant nucleotide binding site-leucine-rich repeat protein by a bacterial protease. *Proceedings of the National Academy of Sciences of the United States of America*, 104, 2531-2536.
- Alsallaq, R. & Zhou, H. X. 2008. Electrostatic rate enhancement and transient complex of protein-protein association. *Proteins*, 71, 320-35.
- Anderson, P. A., Lawrence, G. J., Morrish, B. C., Ayliffe, M. A., Finnegan, E. J. & Ellis, J. G. 1997. Inactivation of the flax rust resistance gene *M* associated with loss of a repeated unit within the leucine-rich repeat coding region. *Plant Cell*, 9, 641-651.
- Arenkov, P., Kukhtin, A., Gemmell, A., Voloshchuk, S., Chupeeva, V. & Mirzabekov, A. 2000. Protein microchips: Use for immunoassay and enzymatic reactions. *Analytical Biochemistry*, 278, 123-131.
- Ashikawa, I., Hayashi, N., Yamane, H., Kanamori, H., Wu, J., Matsumoto, T., Ono, K. & Yano, M. 2008. Two adjacent nucleotide-binding site-leucine-rich repeat class genes are required to confer Pikm-specific rice blast resistance. *Genetics*, 180, 2267-76.
- Baker, N. A., Sept, D., Joseph, S., Holst, M. J. & Mccammon, J. A. 2001. Electrostatics of nanosystems: Application to microtubules and the ribosome. *Proceedings of the National Academy of Sciences of the United States of America*, 98, 10037-10041.
- Baksh, M. M., Kussrow, A. K., Mileni, M., Finn, M. G. & Bornhop, D. J. 2011. Label-free quantification of membrane-ligand interactions using backscattering interferometry. *Nature Biotechnology*, 29, 357-360.
- Barker, C. L., Donald, T., Pauquet, J., Ratnaparkhe, M. B., Bouquet, A., Adam-Blondon, A. F., Thomas, M. R. & Dry, I. 2005. Genetic and physical mapping of the grapevine powdery mildew resistance gene, *RUN1*, using a bacterial artificial chromosome library. *Theoretical and Applied Genetics*, 111, 370-377.
- Belkhadir, Y., Nimchuk, Z., Hubert, D. A., Mackey, D. & Dangl, J. L. 2004. Arabidopsis RIN4 negatively regulates disease resistance mediated by RPS2 and RPM1 downstream or independent of the NDR1 signal modulator and is not required for the virulence functions of bacterial type III effectors AvrRPT2 or AvrRPM1. *Plant Cell*, 16, 2822-2835.
- Bendahmane, A., Farnham, G., Moffett, P. & Baulcombe, D. C. 2002. Constitutive gain-of-function mutants in a nucleotide binding site-leucine rich repeat protein encoded at the *Rx* locus of potato. *Plant Journal*, 32, 195-204.
- Bendahmane, A., Kanyuka, K. & Baulcombe, D. C. 1999. The *Rx* gene from potato controls separate virus resistance and cell death responses. *Plant Cell*, 11, 781-792.
- Bentham, A., Burdett, H., Anderson, P. A., Williams, S. J. & Kobe, B. 2017. Animal NLRs provide structural insights into plant NLR function. *Annals of Botany*, 119, 689-702.
- Bernoux, M., Burdett, H., Williams, S. J., Zhang, X., Chen, C., Newell, K., Lawrence, G. J., Kobe, B., Ellis, J. G., Anderson, P. A. & Dodds, P. N. 2016. Comparative analysis of the flax immune receptors L6 and L7 suggests an equilibrium-based switch activation model. *Plant Cell*, 28, 146-159.
- Bernoux, M., Ve, T., Williams, S. J., Warren, C., Hatters, D., Valkov, E., Zhang, X., Ellis, J. G., Kobe, B. & Dodds, P. N. 2011. Structural and functional analysis of a plant resistance protein TIR domain reveals interfaces for self-association, signaling, and autoregulation. *Cell Host Microbe*, 9, 200-211.
- Bettgenhaeuser, J., Gilbert, B., Ayliffe, M. & Moscou, M. J. 2014. Nonhost resistance to rust pathogens - a continuation of continua. *Frontiers in Plant Science*, 5, 664.
- Bigeard, J., Colcombet, J. & Hirt, H. 2015. Signaling mechanisms in pattern-triggered immunity (PTI). *Molecular Plant*, 8, 521-539.

- Billeter, M., Wagner, G. & Wuthrich, K. 2008. Solution NMR structure determination of proteins revisited. *Journal of Biomolecular NMR*, 42, 155-158.
- Bruckner, A., Polge, C., Lentze, N., Auerbach, D. & Schlattner, U. 2009. Yeast two-hybrid, a powerful tool for systems biology. *International Journal of Molecular Sciences*, 10, 2763-2788.
- Brutus, A., Sicilia, F., Maccone, A., Cervone, F. & De Lorenzo, G. 2010. A domain swap approach reveals a role of the plant wall-associated kinase 1 (WAK1) as a receptor of oligogalacturonides. *Proceedings of the National Academy of Sciences of the United States of America*, 107, 9452-9457.
- Burch-Smith, T. M., Schiff, M., Caplan, J. L., Tsao, J., Czymmek, K. & Dinesh-Kumar, S. P. 2007. A novel role for the TIR domain in association with pathogen-derived elicitors. *PLoS Biology*, 5, 501-514.
- Butt, T. R., Edavettal, S. C., Hall, J. P. & Mattern, M. R. 2005. SUMO fusion technology for difficult-to-express proteins. *Protein Expression and Purification*, 43, 1-9.
- Cain, K., Bratton, S. B. & Cohen, G. M. 2002. The APAF-1 apoptosome: A large caspase-activating complex. *Biochimie*, 84, 203-214.
- Caplan, J. L., Mamillapalli, P., Burch-Smith, T. M., Czymmek, K. & Dinesh-Kumar, S. P. 2008. Chloroplastic protein NRIP1 mediates innate immune receptor recognition of a viral effector. *Cell*, 132, 449-462.
- Casey, L. W., Lavrencic, P., Bentham, A. R., Cesari, S., Ericsson, D. J., Croll, T., Turk, D., Anderson, P. A., Mark, A. E., Dodds, P. N., Mobli, M., Kobe, B. & Williams, S. J. 2016. The CC domain structure from the wheat stem rust resistance protein Sr33 challenges paradigms for dimerization in plant NLR proteins. *Proceedings of the National Academy of Sciences of the United States of America*, 113, 12856-12861.
- Catanzariti, A. M., Dodds, P. N., Lawrence, G. J., Ayliffe, M. A. & Ellis, J. G. 2006. Haustorially expressed secreted proteins from flax rust are highly enriched for avirulence elicitors. *Plant Cell*, 18, 243-256.
- Catanzariti, A. M., Dodds, P. N., Ve, T., Kobe, B., Ellis, J. G. & Staskawicz, B. J. 2010. The AvrM effector from flax rust has a structured C-terminal domain and interacts directly with the M resistance protein. *Molecular Plant-Microbe Interactions*, 23, 49-57.
- Cesari, S., Kanzaki, H., Fujiwara, T., Bernoux, M., Chalvon, V., Kawano, Y., Shimamoto, K., Dodds, P., Terauchi, R. & Kroj, T. 2014. The NB-LRR proteins RGA4 and RGA5 interact functionally and physically to confer disease resistance. *The EMBO Journal*, 33, 1941-1959.
- Cesari, S., Thilliez, G., Ribot, C., Chalvon, V., Michel, C., Jauneau, A., Rivas, S., Alaux, L., Kanzaki, H., Okuyama, Y., Morel, J. B., Fournier, E., Tharreau, D., Terauchi, R. & Kroj, T. 2013. The rice resistance protein pair RGA4/RGA5 recognizes the *Magnaporthe oryzae* effectors AVR-Pia and AVR1-CO39 by direct binding. *Plant Cell*, 25, 1463-1481.
- Chan, S. L., Mukasa, T., Santelli, E., Low, L. Y. & Pascual, J. 2010. The crystal structure of a TIR domain from *Arabidopsis thaliana* reveals a conserved helical region unique to plants. *Protein Science*, 19, 155-161.
- Chen, J., Upadhyaya, N. M., Ortiz, D., Sperschneider, J., Li, F., Bouton, C., Breen, S., Dong, C., Xu, B., Zhang, X., Mago, R., Newell, K., Xia, X., Bernoux, M., Taylor, J. M., Steffenson, B., Jin, Y., Zhang, P., Kanyuka, K., Figueroa, M., Ellis, J. G., Park, R. F. & Dodds, P. N. 2017. Loss of AvrSr50 by somatic exchange in stem rust leads to virulence for Sr50 resistance in wheat. *Science*, 358, 1607-1610.
- Chivers, C. E., Koner, A. L., Lowe, E. D. & Howarth, M. 2011. How the biotin-streptavidin interaction was made even stronger: Investigation via crystallography and a chimaeric tetramer. *Biochemical Journal*, 435, 55-63.
- Choi, H. W. & Klessig, D. F. 2016. DAMPs, MAMPs, and NAMPs in plant innate immunity. *BMC Plant Biology*, 16, 232.

- Collier, S. M., Hamel, L. P. & Moffett, P. 2011. Cell death mediated by the N-terminal domains of a unique and highly conserved class of NB-LRR protein. *Molecular Plant-Microbe Interactions*, 24, 918-931.
- Corzo, J. 2006. Time, the forgotten dimension of ligand binding teaching. *Biochemistry and Molecular Biology Education*, 34, 413-416.
- Couto, D. & Zipfel, C. 2016. Regulation of pattern recognition receptor signalling in plants. *Nature Reviews Immunology*, 16, 537-552.
- Cui, H., Tsuda, K. & Parker, J. E. 2015. Effector-triggered immunity: From pathogen perception to robust defense. *Annual Review of Plant Biology*, 66, 487-511.
- Danot, O. 2015. How 'arm-twisting' by the inducer triggers activation of the MalT transcription factor, a typical signal transduction ATPase with numerous domains (STAND). *Nucleic Acids Research*, 43, 3089-3099.
- De Courcy-Ireland, E. 2015. *Refining the model of plant disease resistance protein activation*. Flinders University.
- De La Fuente Van Bentem, S., Vossen, J. H., De Vries, K. J., Van Wees, S., Tameling, W. I., Dekker, H. L., De Koster, C. G., Haring, M. A., Takken, F. L. & Cornelissen, B. J. 2005. Heat shock protein 90 and its co-chaperone protein phosphatase 5 interact with distinct regions of the tomato I-2 disease resistance protein. *Plant Journal*, 43, 284-298.
- Denoux, C., Galletti, R., Mammarella, N., Gopalan, S., Werck, D., De Lorenzo, G., Ferrari, S., Ausubel, F. M. & Dewdney, J. 2008. Activation of defense response pathways by OGs and Flg22 elicitors in Arabidopsis seedlings. *Molecular Plant*, 1, 423-445.
- Dinesh-Kumar, S. P., Tham, W. H. & Baker, B. J. 2000. Structure-function analysis of the tobacco mosaic virus resistance gene *N*. *Proceedings of the National Academy of Sciences of the United States of America*, 97, 14789-14794.
- Dodds, P. N., Lawrence, G. J., Catanzariti, A. M., Ayliffe, M. A. & Ellis, J. G. 2004. The *Melampsora lini* AvrL567 avirulence genes are expressed in haustoria and their products are recognized inside plant cells. *Plant Cell*, 16, 755-768.
- Dodds, P. N., Lawrence, G. J., Catanzariti, A. M., Teh, T., Wang, C. I., Ayliffe, M. A., Kobe, B. & Ellis, J. G. 2006. Direct protein interaction underlies gene-for-gene specificity and coevolution of the flax resistance genes and flax rust avirulence genes. *Proceedings of the National Academy of Sciences of the United States of America*, 103, 8888-8893.
- Dodds, P. N., Lawrence, G. J. & Ellis, J. G. 2001. Six amino acid changes confined to the leucine-rich repeat beta-strand/beta-turn motif determine the difference between the P and P2 rust resistance specificities in flax. *Plant Cell*, 13, 163-178.
- Dodds, P. N. & Rathjen, J. P. 2010. Plant immunity: Towards an integrated view of plant-pathogen interactions. *Nature Reviews Genetics*, 11, 539-548.
- Ellis, J. G., Lawrence, G. J., Luck, J. E. & Dodds, P. N. 1999. Identification of regions in alleles of the flax rust resistance gene *L* that determine differences in gene-for-gene specificity. *Plant Cell*, 11, 495-506.
- Esposito, D. & Chatterjee, D. K. 2006. Enhancement of soluble protein expression through the use of fusion tags. *Current Opinion in Biotechnology*, 17, 353-358.
- Fenyk, S., Campillo Ade, S., Pohl, E., Hussey, P. J. & Cann, M. J. 2012. A nucleotide phosphatase activity in the nucleotide binding domain of an orphan resistance protein from rice. *Journal of Biological Chemistry*, 287, 4023-4032.
- Fenyk, S., Dixon, C. H., Gittens, W. H., Townsend, P. D., Sharples, G. J., Palsson, L. O., Takken, F. L. & Cann, M. J. 2016. The tomato nucleotide-binding leucine-rich repeat immune receptor I-2 couples DNA-binding to nucleotide-binding domain nucleotide exchange. *Journal of Biological Chemistry*, 291, 1137-1147.
- Fenyk, S., Townsend, P. D., Dixon, C. H., Spies, G. B., Campillo, A. D., Sloopweg, E. J., Westerhof, L. B., Gawehns, F. K. K., Knight, M. R., Sharples, G. J., Goverse, A., Palsson, L. O., Takken, F. L. W. & Cann, M. J. 2015. The potato nucleotide-binding

- leucine-rich repeat (NLR) immune receptor Rx1 is a pathogen-dependent DNA-deforming protein. *Journal of Biological Chemistry*, 290, 24945-24960.
- Fischer, M. J. 2010. Amine coupling through EDC/NHS: A practical approach. *Methods in Molecular Biology*, 627, 55-73.
- Frost, D., Way, H., Howles, P., Luck, J., Manners, J., Hardham, A., Finnegan, J. & Ellis, J. 2004. Tobacco transgenic for the flax rust resistance gene *L* expresses allele-specific activation of defense responses. *Molecular Plant-Microbe Interactions*, 17, 224-232.
- Gabriels, S. H., Vossen, J. H., Ekengren, S. K., Van Ooijen, G., Abd-El-Haliem, A. M., Van Den Berg, G. C., Rainey, D. Y., Martin, G. B., Takken, F. L., De Wit, P. J. & Joosten, M. H. 2007. An NB-LRR protein required for HR signalling mediated by both extra- and intracellular resistance proteins. *Plant Journal*, 50, 14-28.
- Govrin, E. M. & Levine, A. 2000. The hypersensitive response facilitates plant infection by the necrotrophic pathogen *Botrytis cinerea*. *Current Biology*, 10, 751-757.
- Gutierrez, J. R., Balmuth, A. L., Ntoukakis, V., Mucyn, T. S., Gimenez-Ibanez, S., Jones, A. M. E. & Rathjen, J. P. 2010. Prf immune complexes of tomato are oligomeric and contain multiple Pto-like kinases that diversify effector recognition. *Plant Journal*, 61, 507-518.
- Hanson, P. I. & Whiteheart, S. W. 2005. AAA+ proteins: Have engine, will work. *Nature Reviews Molecular Cell Biology*, 6, 519-529.
- Hao, W., Collier, S. M., Moffett, P. & Chai, J. J. 2013. Structural Basis for the Interaction between the Potato Virus X Resistance Protein (Rx) and Its Cofactor Ran GTPase-activating Protein 2 (RanGAP2). *Journal of Biological Chemistry*, 288, 35868-35876.
- Higgins, D. R. & Cregg, J. M. 1998. Introduction to *Pichia pastoris*. In: HIGGINS, D. R. & CREGG, J. M. (eds.) *Pichia Protocols*. Totowa, NJ: Humana Press.
- Houterman, P. M., Ma, L., Van Ooijen, G., De Vroomen, M. J., Cornelissen, B. J. C., Takken, F. L. W. & Rep, M. 2009. The effector protein Avr2 of the xylem-colonizing fungus *Fusarium oxysporum* activates the tomato resistance protein I-2 intracellularly. *Plant Journal*, 58, 970-978.
- Howles, P., Lawrence, G., Finnegan, J., Mcfadden, H., Ayliffe, M., Dodds, P. & Ellis, J. 2005. Autoactive alleles of the flax *L6* rust resistance gene induce non-race-specific rust resistance associated with the hypersensitive response. *Molecular Plant-Microbe Interactions*, 18, 570-582.
- Hu, Z., Yan, C., Liu, P., Huang, Z., Ma, R., Zhang, C., Wang, R., Zhang, Y., Martinon, F., Miao, D., Deng, H., Wang, J., Chang, J. & Chai, J. 2013. Crystal structure of NLRC4 reveals its autoinhibition mechanism. *Science*, 341, 172-5.
- Hu, Z., Zhou, Q., Zhang, C., Fan, S., Cheng, W., Zhao, Y., Shao, F., Wang, H. W., Sui, S. F. & Chai, J. 2015. Structural and biochemical basis for induced self-propagation of NLRC4. *Science*, 350, 399-404.
- Islam, M. R. & Mayo, G. M. E. 1990. A compendium on host genes in flax conferring resistance to flax rust. *Plant Breeding*, 104, 89-100.
- Jacob, F., Vernaldi, S. & Maekawa, T. 2013. Evolution and conservation of plant NLR functions. *Frontiers in Immunology*, 4, 297.
- Jerabek-Willemsen, M., Wienken, C. J., Braun, D., Baaske, P. & Duhr, S. 2011. Molecular interaction studies using microscale thermophoresis. *Assay and Drug Development Technologies*, 9, 342-353.
- Jia, Y., Mcadams, S. A., Bryan, G. T., Hershey, H. P. & Valent, B. 2000. Direct interaction of resistance gene and avirulence gene products confers rice blast resistance. *The EMBO Journal*, 19, 4004-4014.
- Jiang, R. H., Tripathy, S., Govers, F. & Tyler, B. M. 2008. RXLR effector reservoir in two *Phytophthora* species is dominated by a single rapidly evolving superfamily with more than 700 members. *Proceedings of the National Academy of Sciences of the United States of America*, 105, 4874-4879.
- Kale, S. D., Gu, B., Capelluto, D. G. S., Dou, D., Feldman, E., Rumore, A., Arredondo, F. D., Hanlon, R., Fudal, I., Rouxel, T., Lawrence, C. B., Shan, W. & Tyler, B. M. 2010.

- External lipid PI3P mediates entry of eukaryotic pathogen effectors into plant and animal host cells. *Cell*, 142, 284-295.
- Karlsson, R., Katsamba, P. S., Nordin, H., Pol, E. & Myszka, D. G. 2006. Analyzing a kinetic titration series using affinity biosensors. *Analytical Biochemistry*, 349, 136-147.
- Karlsson, R., Michaelsson, A. & Mattsson, L. 1991. Kinetic-Analysis of Monoclonal Antibody-Antigen Interactions with a New Biosensor Based Analytical System. *Journal of Immunological Methods*, 145, 229-240.
- Kim, H. E., Du, F., Fang, M. & Wang, X. 2005. Formation of apoptosome is initiated by cytochrome c-induced dATP hydrolysis and subsequent nucleotide exchange on APAF-1. *Proceedings of the National Academy of Sciences of the United States of America*, 102, 17545-17550.
- Kobe, B. & Kajava, A. V. 2001. The leucine-rich repeat as a protein recognition motif. *Current Opinion in Structural Biology*, 11, 725-732.
- Kong, L., Qiu, X. F., Kang, J. G., Wang, Y., Chen, H., Huang, J., Qiu, M., Zhao, Y., Kong, G. H., Ma, Z. C., Wang, Y., Ye, W. W., Dong, S. M., Ma, W. B. & Wang, Y. C. 2017. A *Phytophthora* effector manipulates host histone acetylation and reprograms defense gene expression to promote infection. *Current Biology*, 27, 981-991.
- Koonin, E. V. & Aravind, L. 2000. The NACHT family - a new group of predicted NTPases implicated in apoptosis and MHC transcription activation. *Trends in Biochemical Sciences*, 25, 223-224.
- Krasileva, K. V., Dahlbeck, D. & Staskawicz, B. J. 2010. Activation of an Arabidopsis resistance protein is specified by the *in planta* association of its leucine-rich repeat domain with the cognate oomycete effector. *Plant Cell*, 22, 2444-2458.
- Kroj, T., Chanclud, E., Michel-Romiti, C., Grand, X. & Morel, J. B. 2016. Integration of decoy domains derived from protein targets of pathogen effectors into plant immune receptors is widespread. *New Phytologist*, 210, 618-626.
- Krol, E., Mentzel, T., Chinchilla, D., Boller, T., Felix, G., Kemmerling, B., Postel, S., Arents, M., Jeworutzki, E., Al-Rasheid, K. A., Becker, D. & Hedrich, R. 2010. Perception of the Arabidopsis danger signal peptide 1 involves the pattern recognition receptor AtPEPR1 and its close homologue AtPEPR2. *Journal of Biological Chemistry*, 285, 13471-13479.
- Laemmli, U. K. 1970. Cleavage of structural proteins during the assembly of the head of bacteriophage T4. *Nature*, 227, 680-685.
- Lata, S., Reichel, A., Brock, R., Tampe, R. & Piehler, J. 2005. High-affinity adaptors for switchable recognition of histidine-tagged proteins. *Journal of the American Chemical Society*, 127, 10205-10215.
- Lawrence, G. J., Finnegan, E. J., Ayliffe, M. A. & Ellis, J. G. 1995. The *L6* gene for flax rust resistance is related to the Arabidopsis bacterial resistance gene *RPS2* and the tobacco viral resistance gene *N*. *Plant Cell*, 7, 1195-1206.
- Le Roux, C., Huet, G., Jauneau, A., Camborde, L., Tremousaygue, D., Kraut, A., Zhou, B., Levailant, M., Adachi, H., Yoshioka, H., Raffaele, S., Berthome, R., Coute, Y., Parker, J. E. & Deslandes, L. 2015. A receptor pair with an integrated decoy converts pathogen disabling of transcription factors to immunity. *Cell*, 161, 1074-1088.
- Li, B., Meng, X., Shan, L. & He, P. 2016. Transcriptional regulation of pattern-triggered immunity in plants. *Cell Host Microbe*, 19, 641-650.
- Li, X., Mooney, P., Zheng, S., Booth, C. R., Braunfeld, M. B., Gubbens, S., Agard, D. A. & Cheng, Y. 2013. Electron counting and beam-induced motion correction enable near-atomic-resolution single-particle cryo-EM. *Nature Methods*, 10, 584-590.
- Liedberg, B., Nylander, C. & Lundstrom, I. 1983. Surface-plasmon resonance for gas-detection and biosensing. *Sensors and Actuators*, 4, 299-304.
- Liu, Z., Zhang, Z., Faris, J. D., Oliver, R. P., Syme, R., McDonald, M. C., McDonald, B. A., Solomon, P. S., Lu, S., Shelver, W. L., Xu, S. & Friesen, T. L. 2012. The cysteine rich necrotrophic effector SnTox1 produced by *Stagonospora nodorum* triggers susceptibility of wheat lines harboring Snn1. *PLoS Pathogens*, 8, e1002467.

- Ma, L. S., Houterman, P. M., Gawehns, F., Cao, L. X., Sillo, F., Richter, H., Clavijo-Ortiz, M. J., Schmidt, S. M., Boeren, S., Vervoort, J., Cornelissen, B. J. C., Rep, M. & Takken, F. L. W. 2015. The AVR2-SIX5 gene pair is required to activate I-2-mediated immunity in tomato. *New Phytologist*, 208, 507-518.
- Maekawa, T., Cheng, W., Spiridon, L. N., Toller, A., Lukasik, E., Saijo, Y., Liu, P., Shen, Q. H., Micluta, M. A., Somssich, I. E., Takken, F. L. W., Petrescu, A. J., Chai, J. & Schulze-Lefert, P. 2011. Coiled-coil domain-dependent homodimerization of intracellular barley immune receptors defines a minimal functional module for triggering cell death. *Cell Host Microbe*, 9, 187-199.
- Maqbool, A., Saitoh, H., Franceschetti, M., Stevenson, C. E., Uemura, A., Kanzaki, H., Kamoun, S., Terauchi, R. & Banfield, M. J. 2015. Structural basis of pathogen recognition by an integrated HMA domain in a plant NLR immune receptor. *Elife*, 4.
- Mcpherson, A. & Gavira, J. A. 2014. Introduction to protein crystallization. *Acta Crystallographica Section F-Structural Biology Communications*, 70, 2-20.
- Meng, X. & Zhang, S. 2013. MAPK cascades in plant disease resistance signaling. *Annual Review of Phytopathology*, 51, 245-266.
- Mes, J. J., Van Doorn, A. A., Wijbrandi, J., Simons, G., Cornelissen, B. J. & Haring, M. A. 2000. Expression of the Fusarium resistance gene *I-2* colocalizes with the site of fungal containment. *Plant Journal*, 23, 183-193.
- Mestre, P. & Baulcombe, D. C. 2006. Elicitor-mediated oligomerization of the tobacco N disease resistance protein. *Plant Cell*, 18, 491-501.
- Meyers, B. C. 2003. Genome-Wide Analysis of NBS-LRR-Encoding Genes in Arabidopsis. *The Plant Cell Online*, 15, 809-834.
- Meyers, B. C., Dickerman, A. W., Michelmore, R. W., Sivaramakrishnan, S., Sobral, B. W. & Young, N. D. 1999. Plant disease resistance genes encode members of an ancient and diverse protein family within the nucleotide-binding superfamily. *Plant Journal*, 20, 317-332.
- Meyers, B. C., Kaushik, S. & Nandety, R. S. 2005. Evolving disease resistance genes. *Current Opinion in Plant Biology*, 8, 129-134.
- Michael Weaver, L., Swiderski, M. R., Li, Y. & Jones, J. D. 2006. The *Arabidopsis thaliana* TIR-NB-LRR R-protein, RPP1A; protein localization and constitutive activation of defence by truncated alleles in tobacco and Arabidopsis. *Plant Journal*, 47, 829-840.
- Miller, J. M. & Enemark, E. J. 2016. Fundamental characteristics of AAA+ protein family structure and function. *Archaea*, 2016, 9294307.
- Mindrinos, M., Katagiri, F., Yu, G. L. & Ausubel, F. M. 1994. The *A. thaliana* disease resistance gene RPS2 encodes a protein containing a nucleotide-binding site and leucine-rich repeats. *Cell*, 78, 1089-99.
- Miya, A., Albert, P., Shinya, T., Desaki, Y., Ichimura, K., Shirasu, K., Narusaka, Y., Kawakami, N., Kaku, H. & Shibuya, N. 2007. CERK1, a LysM receptor kinase, is essential for chitin elicitor signaling in Arabidopsis. *Proceedings of the National Academy of Sciences of the United States of America*, 104, 19613-19618.
- Moffett, P., Farnham, G., Peart, J. & Baulcombe, D. C. 2002. Interaction between domains of a plant NBS-LRR protein in disease resistance-related cell death. *The EMBO Journal*, 21, 4511-4519.
- Morel, J. B. & Dangl, J. L. 1997. The hypersensitive response and the induction of cell death in plants. *Cell Death and Differentiation*, 4, 671-683.
- Mucyn, T. S., Clemente, A., Andriotis, V. M. E., Balmuth, A. L., Oldroyd, G. E. D., Staskawicz, B. J. & Rathjen, J. P. 2006. The tomato NBARC-LRR protein Prf interacts with Pto kinase in vivo to regulate specific plant immunity. *Plant Cell*, 18, 2792-2806.
- Mucyn, T. S., Wu, A. J., Balmuth, A. L., Arasteh, J. M. & Rathjen, J. P. 2009. Regulation of tomato Prf by Pto-like protein kinases. *Molecular Plant-Microbe Interactions*, 22, 391-401.

- Narusaka, M., Shirasu, K., Noutoshi, Y., Kubo, Y., Shiraishi, T., Iwabuchi, M. & Narusaka, Y. 2009. *RRS1* and *RPS4* provide a dual resistance-gene system against fungal and bacterial pathogens. *Plant Journal*, 60, 218-226.
- Newman, M. A., Sundelin, T., Nielsen, J. T. & Erbs, G. 2013. MAMP (microbe-associated molecular pattern) triggered immunity in plants. *Frontiers in Plant Science*, 4, 139.
- Nguyen, T. N. & Goodrich, J. A. 2006. Protein-protein interaction assays: Eliminating false positive interactions. *Nature Methods*, 3, 135-139.
- Nimma, S., Ve, T., Williams, S. J. & Kobe, B. 2017. Towards the structure of the TIR-domain signalosome. *Current Opinion in Structural Biology*, 43, 122-130.
- Ntoukakis, V., Balmuth, A. L., Mucyn, T. S., Gutierrez, J. R., Jones, A. M. E. & Rathjen, J. P. 2013. The tomato Prf complex is a molecular trap for bacterial effectors based on Pto transphosphorylation. *PLoS Pathogens*, 9, e1003123.
- Padmanabhan, M. S., Ma, S., Burch-Smith, T. M., Czymmek, K., Huijser, P. & Dinesh-Kumar, S. P. 2013. Novel positive regulatory role for the SPL6 transcription factor in the N TIR-NB-LRR receptor-mediated plant innate immunity. *PLoS Pathogens*, 9, e1003235.
- Periyannan, S., Moore, J., Ayliffe, M., Bansal, U., Wang, X., Huang, L., Deal, K., Luo, M., Kong, X., Bariana, H., Mago, R., Mcintosh, R., Dodds, P., Dvorak, J. & Lagudah, E. 2013. The gene *Sr33*, an ortholog of barley MLA genes, encodes resistance to wheat stem rust race Ug99. *Science*, 341, 786-788.
- Petre, B., Lorrain, C., Saunders, D. G. O., Win, J., Sklenar, J., Duplessis, S. & Kamoun, S. 2016. Rust fungal effectors mimic host transit peptides to translocate into chloroplasts. *Cellular Microbiology*, 18, 453-465.
- Phillips, G. N., Jr. 1997. Structure and dynamics of green fluorescent protein. *Current Opinion in Structural Biology*, 7, 821-827.
- Qi, D., Deyoung, B. J. & Innes, R. W. 2012. Structure-function analysis of the coiled-coil and leucine-rich repeat domains of the RPS5 disease resistance protein. *Plant Physiology*, 158, 1819-1832.
- Qi, S., Pang, Y., Hu, Q., Liu, Q., Li, H., Zhou, Y., He, T., Liang, Q., Liu, Y., Yuan, X., Luo, G., Li, H., Wang, J., Yan, N. & Shi, Y. 2010. Crystal structure of the *Caenorhabditis elegans* apoptosome reveals an octameric assembly of CED-4. *Cell*, 141, 446-457.
- Rahman, M. 2016. *Molecular basis of recognition of rust effectors by the M flax resistance protein*. Flinders University.
- Ravensdale, M., Bernoux, M., Ve, T., Kobe, B., Thrall, P. H., Ellis, J. G. & Dodds, P. N. 2012. Intramolecular interaction influences binding of the flax L5 and L6 resistance proteins to their AvrL567 ligands. *PLoS Pathogens*, 8, e1003004.
- Rehmany, A. P., Gordon, A., Rose, L. E., Allen, R. L., Armstrong, M. R., Whisson, S. C., Kamoun, S., Tyler, B. M., Birch, P. R. & Beynon, J. L. 2005. Differential recognition of highly divergent downy mildew avirulence gene alleles by *RPP1* resistance genes from two Arabidopsis lines. *Plant Cell*, 17, 1839-1850.
- Reichel, A., Schaible, D., Al Furoukh, N., Cohen, M., Schreiber, G. & Piehler, J. 2007. Noncovalent, site-specific biotinylation of histidine-tagged proteins. *Analytical Chemistry*, 79, 8590-8600.
- Reubold, T. F., Wohlgemuth, S. & Eschenburg, S. 2009. A new model for the transition of APAF-1 from inactive monomer to caspase-activating apoptosome. *Journal of Biological Chemistry*, 284, 32717-32724.
- Reubold, T. F., Wohlgemuth, S. & Eschenburg, S. 2011. Crystal structure of full-length APAF-1: How the death signal is relayed in the mitochondrial pathway of apoptosis. *Structure*, 19, 1074-1083.
- Rich, R. L. & Myszka, D. G. 2007. Higher-throughput, label-free, real-time molecular interaction analysis. *Analytical Biochemistry*, 361, 1-6.
- Ridout, C. J., Skamnioti, P., Porritt, O., Sacristan, S., Jones, J. D. & Brown, J. K. 2006. Multiple avirulence paralogues in cereal powdery mildew fungi may contribute to parasite fitness and defeat of plant resistance. *Plant Cell*, 18, 2402-2414.

- Riedl, S. J., Li, W., Chao, Y., Schwarzenbacher, R. & Shi, Y. 2005. Structure of the apoptotic protease-activating factor 1 bound to ADP. *Nature*, 434, 926-933.
- Rivero, C., Traubenik, S., Zanetti, M. E. & Blanco, F. A. 2017. Small GTPases in plant biotic interactions. *Small GTPases*, 1-11.
- Roden, J., Eardley, L., Hotson, A., Cao, Y. & Mudgett, M. B. 2004. Characterization of the Xanthomonas AvrXv4 effector, a SUMO protease translocated into plant cells. *Molecular Plant-Microbe Interactions*, 17, 633-643.
- Ron, M. & Avni, A. 2004. The receptor for the fungal elicitor ethylene-inducing xylanase is a member of a resistance-like gene family in tomato. *Plant Cell*, 16, 1604-1615.
- Sacco, M. A., Mansoor, S. & Moffett, P. 2007. A RanGAP protein physically interacts with the NB-LRR protein Rx, and is required for Rx-mediated viral resistance. *Plant Journal*, 52, 82-93.
- Sambrook, J., Fritsch, E. F. & Maniatis, T. 1989. *Molecular cloning: A laboratory manual*, Cold Spring Harbor, NY, Cold Spring Harbor Laboratory Press.
- Sarris, P. F., Duxbury, Z., Huh, S. U., Ma, Y., Segonzac, C., Sklenar, J., Derbyshire, P., Cevik, V., Rallapalli, G., Saucet, S. B., Wirthmueller, L., Menke, F. L. H., Sohn, K. H. & Jones, J. D. G. 2015. A plant immune receptor detects pathogen effectors that target WRKY transcription factors. *Cell*, 161, 1089-1100.
- Schmidt, S. A., Williams, S. J., Wang, C. I., Sornaraj, P., James, B., Kobe, B., Dodds, P. N., Ellis, J. G. & Anderson, P. A. 2007. Purification of the M flax-rust resistance protein expressed in *Pichia pastoris*. *Plant Journal*, 50, 1107-1117.
- Schmidt, T. G., Koepke, J., Frank, R. & Skerra, A. 1996. Molecular interaction between the Strep-tag affinity peptide and its cognate target, streptavidin. *Journal of Molecular Biology*, 255, 753-766.
- Schreiber, G., Haran, G. & Zhou, H. X. 2009. Fundamental aspects of protein-protein association kinetics. *Chemical Reviews*, 109, 839-860.
- Schreiber, K. J., Benthams, A., Williams, S. J., Kobe, B. & Staskawicz, B. J. 2016. Multiple domain associations within the Arabidopsis immune receptor RPP1 regulate the activation of programmed cell death. *PLoS Pathogens*, 12, e1005769.
- Schultink, A., Qi, T., Lee, A., Steinbrenner, A. D. & Staskawicz, B. 2017. Roq1 mediates recognition of the Xanthomonas and Pseudomonas effector proteins XopQ and HopQ1. *Plant Journal*, 92, 787-795.
- Seddon, A. M., Curnow, P. & Booth, P. J. 2004. Membrane proteins, lipids and detergents: Not just a soap opera. *Biochimica et Biophysica Acta*, 1666, 105-117.
- Seidel, S. A., Wienken, C. J., Geissler, S., Jerabek-Willemsen, M., Duhr, S., Reiter, A., Trauner, D., Braun, D. & Baaske, P. 2012. Label-free microscale thermophoresis discriminates sites and affinity of protein-ligand binding. *Angewandte Chemie International Edition in English*, 51, 10656-10659.
- Selin, C., De Kievit, T. R., Belmonte, M. F. & Fernando, W. G. 2016. Elucidating the role of effectors in plant-fungal interactions: Progress and challenges. *Frontiers in Microbiology*, 7, 600.
- Serebriiskii, I. G. & Golemis, E. A. 2001. Two-hybrid system and false positives: Approaches to detection and elimination. In: MACDONALD, P. N. (ed.) *Two-Hybrid Systems*. Totowa, NJ: Humana Press.
- Seybold, H., Trempel, F., Ranf, S., Scheel, D., Romeis, T. & Lee, J. 2014. Ca<sup>2+</sup> signalling in plant immune response: From pattern recognition receptors to Ca<sup>2+</sup> decoding mechanisms. *New Phytologist*, 204, 782-790.
- Shen, Q. H. & Schulze-Lefert, P. 2007. Rumble in the nuclear jungle: Compartmentalization, trafficking, and nuclear action of plant immune receptors. *The EMBO Journal*, 26, 4293-4301.
- Slootweg, E. J., Spiridon, L. N., Roosien, J., Butterbach, P., Pomp, R., Westerhof, L., Wilbers, R., Bakker, E., Bakker, J., Petrescu, A. J., Smant, G. & Govers, A. 2013. Structural determinants at the interface of the ARC2 and leucine-rich repeat domains

- control the activation of the plant immune receptors Rx1 and Gpa2. *Plant Physiology*, 162, 1510-1528.
- Sornaraj, P. 2013. *Activation of the M flax-rust resistance protein*. Flinders University.
- Steinbrenner, A. D., Goritschnig, S. & Staskawicz, B. J. 2015. Recognition and activation domains contribute to allele-specific responses of an Arabidopsis NLR receptor to an oomycete effector protein. *PLoS Pathogens*, 11, e1004665.
- Studier, F. W. 2005. Protein production by auto-induction in high density shaking cultures. *Protein Expression and Purification*, 41, 207-234.
- Sueldo, D. J., Shimels, M., Spiridon, L. N., Caldararu, O., Petrescu, A. J., Joosten, M. H. & Tameling, W. I. 2015. Random mutagenesis of the nucleotide-binding domain of NRC1 (NB-LRR required for Hypersensitive Response-Associated Cell Death-1), a downstream signalling nucleotide-binding, leucine-rich repeat (NB-LRR) protein, identifies gain-of-function mutations in the nucleotide-binding pocket. *New Phytologist*, 208, 210-223.
- Swiderski, M. R., Birker, D. & Jones, J. D. 2009. The TIR domain of TIR-NB-LRR resistance proteins is a signaling domain involved in cell death induction. *Molecular Plant-Microbe Interactions*, 22, 157-165.
- Szabo, A., Stolz, L. & Granzow, R. 1995. Surface-plasmon resonance and its use in biomolecular interaction analysis (BIA). *Current Opinion in Structural Biology*, 5, 699-705.
- Tafoya, S. & Bustamante, C. 2018. Molecular switch-like regulation in motor proteins. *Philosophical transactions of the Royal Society of London. Series B, Biological Sciences*, 373.
- Takemoto, D., Rafiqi, M., Hurley, U., Lawrence, G. J., Bernoux, M., Hardham, A. R., Ellis, J. G., Dodds, P. N. & Jones, D. A. 2012. N-terminal motifs in some plant disease resistance proteins function in membrane attachment and contribute to disease resistance. *Molecular Plant-Microbe Interactions*, 25, 379-392.
- Takken, F. L. W., Albrecht, M. & Tameling, W. I. 2006. Resistance proteins: Molecular switches of plant defence. *Current Opinion in Plant Biology*, 9, 383-390.
- Takken, F. L. W. & Govere, A. 2012. How to build a pathogen detector: Structural basis of NB-LRR function. *Current Opinion in Plant Biology*, 15, 375-384.
- Tameling, W. I., Elzinga, S. D., Darmin, P. S., Vossen, J. H., Takken, F. L., Haring, M. A. & Cornelissen, B. J. 2002. The tomato R gene products I-2 and MI-1 are functional ATP binding proteins with ATPase activity. *Plant Cell*, 14, 2929-2939.
- Tameling, W. I. L., Vossen, J. H., Albrecht, M., Lengauer, T., Berden, J. A., Haring, M. A., Cornelissen, B. J. C. & Takken, F. L. W. 2006. Mutations in the NB-ARC domain of I-2 that impair ATP hydrolysis cause autoactivation. *Plant Physiology*, 140, 1233-1245.
- Tang, C., Schwieters, C. D. & Clore, G. M. 2007. Open-to-closed transition in apo maltose-binding protein observed by paramagnetic NMR. *Nature*, 449, 1078-1082.
- Tao, Y., Yuan, F., Leister, R. T., Ausubel, F. M. & Katagiri, F. 2000. Mutational analysis of the Arabidopsis nucleotide binding site-leucine-rich repeat resistance gene *RPS2*. *Plant Cell*, 12, 2541-2554.
- Thompson, R. F., Walker, M., Siebert, C. A., Muench, S. P. & Ranson, N. A. 2016. An introduction to sample preparation and imaging by cryo-electron microscopy for structural biology. *Methods*, 100, 3-15.
- Towbin, H., Staehelin, T. & Gordon, J. 1979. Electrophoretic transfer of proteins from polyacrylamide gels to nitrocellulose sheets - procedure and some applications. *Proceedings of the National Academy of Sciences of the United States of America*, 76, 4350-4354.
- Trilling, A. K., Harmsen, M. M., Ruigrok, V. J., Zuilhof, H. & Beekwilder, J. 2013. The effect of uniform capture molecule orientation on biosensor sensitivity: Dependence on analyte properties. *Biosensors and Bioelectronics*, 40, 219-226.

- Ueda, H., Yamaguchi, Y. & Sano, H. 2006. Direct interaction between the tobacco mosaic virus helicase domain and the ATP-bound resistance protein, N factor during the hypersensitive response in tobacco plants. *Plant Molecular Biology*, 61, 31-45.
- Van Ooijen, G., Mayr, G., Kasiem, M. M. A., Albrecht, M., Cornelissen, B. J. C. & Takken, F. L. W. 2008. Structure-function analysis of the NB-ARC domain of plant disease resistance proteins. *Journal of Experimental Botany*, 59, 1383-1397.
- Ve, T., Williams, S. J., Catanzariti, A. M., Rafiqi, M., Rahman, M., Ellis, J. G., Hardham, A. R., Jones, D. A., Anderson, P. A., Dodds, P. N. & Kobe, B. 2013. Structures of the flax-rust effector AvrM reveal insights into the molecular basis of plant-cell entry and effector-triggered immunity. *Proceedings of the National Academy of Sciences of the United States of America*, 110, 17594-17599.
- Ve, T., Williams, S. J. & Kobe, B. 2015. Structure and function of Toll/Interleukin-1 receptor/resistance protein (TIR) domains. *Apoptosis*, 20, 250-261.
- Ve, T., Williams, S. J., Stamp, A., Valkov, E., Dodds, P. N., Anderson, P. A. & Kobe, B. 2011a. Crystallization and x-ray diffraction analysis of the C-terminal domain of the flax rust effector protein AvrM. *Acta Crystallographica Section F-Structural Biology Communications*, 67, 1603-1607.
- Ve, T., Williams, S. J., Valkov, E., Ellis, J. G., Dodds, P. N. & Kobe, B. 2011b. Crystallization, x-ray diffraction analysis and preliminary structure determination of the TIR domain from the flax resistance protein L6. *Acta Crystallographica Section F-Structural Biology Communications*, 67, 237-240.
- Wagner, S., Stuttmann, J., Rietz, S., Guerois, R., Brunstein, E., Bautor, J., Niefind, K. & Parker, J. E. 2013. Structural basis for signaling by exclusive EDS1 heteromeric complexes with SAG101 or PAD4 in plant innate immunity. *Cell Host Microbe*, 14, 619-630.
- Wan, L., Zhang, X., Williams, S. J., Ve, T., Bernoux, M., Sohn, K. H., Jones, J. D., Dodds, P. N. & Kobe, B. 2013. Crystallization and preliminary x-ray diffraction analyses of the TIR domains of three TIR-NB-LRR proteins that are involved in disease resistance in *Arabidopsis thaliana*. *Acta Crystallographica Section F-Structural Biology Communications*, 69, 1275-1280.
- Wang, C. I., Guncar, G., Forwood, J. K., Teh, T., Catanzariti, A. M., Lawrence, G. J., Loughlin, F. E., Mackay, J. P., Schirra, H. J., Anderson, P. A., Ellis, J. G., Dodds, P. N. & Kobe, B. 2007. Crystal structures of flax rust avirulence proteins AvrL567-A and -D reveal details of the structural basis for flax disease resistance specificity. *Plant Cell*, 19, 2898-2912.
- Wang, G. F., Ji, J. B., Ei-Kasmi, F., Dangl, J. L., Johal, G. & Balint-Kurti, P. J. 2015. Molecular and Functional Analyses of a Maize Autoactive NB-LRR Protein Identify Precise Structural Requirements for Activity. *PLoS Pathogens*, 11, e1004674.
- Whitham, S., Dineshkumar, S. P., Choi, D., Hehl, R., Corr, C. & Baker, B. 1994. The product of the tobacco mosaic-virus resistance gene-N - similarity to Toll and the Interleukin-1 receptor. *Cell*, 78, 1101-1115.
- Wiermer, M., Feys, B. J. & Parker, J. E. 2005. Plant immunity: The EDS1 regulatory node. *Current Opinion in Plant Biology*, 8, 383-389.
- Williams, S. J. 2010. *Molecular insight into the activation of a plant disease resistance protein*. Doctor of Philosophy Flinders University.
- Williams, S. J., Sohn, K. H., Wan, L., Bernoux, M., Sarris, P. F., Segonzac, C., Ve, T., Ma, Y., Saucet, S. B., Ericsson, D. J., Casey, L. W., Lonhienne, T., Winzor, D. J., Zhang, X., Coerd, A., Parker, J. E., Dodds, P. N., Kobe, B. & Jones, J. D. 2014. Structural basis for assembly and function of a heterodimeric plant immune receptor. *Science*, 344, 299-303.
- Williams, S. J., Sornaraj, P., Decourcy-Ireland, E., Menz, R. I., Kobe, B., Ellis, J. G., Dodds, P. N. & Anderson, P. A. 2011. An autoactive mutant of the M flax rust resistance protein has a preference for binding ATP, whereas wild-type M protein binds ADP. *Molecular Plant-Microbe Interactions*, 24, 897-906.

- Williams, S. J., Yin, L., Foley, G., Casey, L. W., Outram, M. A., Ericsson, D. J., Lu, J., Boden, M., Dry, I. B. & Kobe, B. 2016. Structure and function of the TIR domain from the grape NLR protein RPV1. *Frontiers in Plant Science*, 7, 1850.
- Willmann, R., Lajunen, H. M., Erbs, G., Newman, M. A., Kolb, D., Tsuda, K., Katagiri, F., Fliegmann, J., Bono, J. J., Cullimore, J. V., Jehle, A. K., Gotz, F., Kulik, A., Molinaro, A., Lipka, V., Gust, A. A. & Nurnberger, T. 2011. Arabidopsis lysin-motif proteins LYM1 LYM3 CERK1 mediate bacterial peptidoglycan sensing and immunity to bacterial infection. *Proceedings of the National Academy of Sciences of the United States of America*, 108, 19824-19829.
- Wulff, B. B., Heese, A., Tomlinson-Buhot, L., Jones, D. A., De La Pena, M. & Jones, J. D. 2009. The major specificity-determining amino acids of the tomato Cf-9 disease resistance protein are at hypervariable solvent-exposed positions in the central leucine-rich repeats. *Molecular Plant-Microbe Interactions*, 22, 1203-1213.
- Yamaguchi, Y., Huffaker, A., Bryan, A. C., Tax, F. E. & Ryan, C. A. 2010. PEPR2 is a second receptor for the Pep1 and Pep2 peptides and contributes to defense responses in Arabidopsis. *Plant Cell*, 22, 508-522.
- Yan, N., Chai, J. J., Lee, E. S., Gu, L. C., Liu, Q., He, J. Q., Wu, J. W., Kokel, D., Li, H. L., Hao, Q., Xue, D. & Shi, Y. G. 2005. Structure of the CED-4-CED-9 complex provides insights into programmed cell death in *Caenorhabditis elegans*. *Nature*, 437, 831-837.
- Yoshida, K., Saitoh, H., Fujisawa, S., Kanzaki, H., Matsumura, H., Yoshida, K., Tosa, Y., Chuma, I., Takano, Y., Win, J., Kamoun, S. & Terauchi, R. 2009. Association genetics reveals three novel avirulence genes from the rice blast fungal pathogen *Magnaporthe oryzae*. *Plant Cell*, 21, 1573-1591.
- Yuan, S., Yu, X., Topf, M., Dorstyn, L., Kumar, S., Ludtke, S. J. & Akey, C. W. 2011. Structure of the Drosophila apoptosome at 6.9 Å resolution. *Structure*, 19, 128-140.
- Zhang, L., Chen, S., Ruan, J., Wu, J., Tong, A. B., Yin, Q., Li, Y., David, L., Lu, A., Wang, W. L., Marks, C., Ouyang, Q., Zhang, X., Mao, Y. & Wu, H. 2015. Cryo-EM structure of the activated NAIIP2-NLRC4 inflammasome reveals nucleated polymerization. *Science*, 350, 404-9.
- Zhang, L., Du, L. Q. & Poovaiah, B. W. 2014. Calcium signaling and biotic defense responses in plants. *Plant Signaling & Behavior*, 9, e973818.
- Zhang, X. X., Bernoux, M., Benthams, A. R., Newman, T. E., Ve, T., Casey, L. W., Raaymakers, T. M., Hu, J., Croll, T. I., Schreiber, K. J., Staskawicz, B. J., Anderson, P. A., Sohn, K. H., Williams, S. J., Dodds, P. N. & Kobe, B. 2017. Multiple functional self-association interfaces in plant TIR domains. *Proceedings of the National Academy of Sciences of the United States of America*, 114, E2046-E2052.
- Zhou, M., Li, Y., Hu, Q., Bai, X. C., Huang, W., Yan, C., Scheres, S. H. & Shi, Y. 2015. Atomic structure of the apoptosome: Mechanism of cytochrome c- and dATP-mediated activation of APAF-1. *Genes & Development*, 29, 2349-2361.
- Zhukov, A., Schürenberg, M., Jansson, Ö., Areskoug, D. & Buijs, J. 2004. Integration of surface plasmon resonance with mass spectrometry: Automated ligand fishing and sample preparation for MALDI MS using a Biacore 3000 biosensor. *Journal of Biomolecular Techniques*, 15, 112-119.
- Zipfel, C. 2014. Plant pattern-recognition receptors. *Trends in Immunology*, 35, 345-351.